Chitosan/Alginate Polyelectrolyte Complexes (PECs) for Bioactive Peptide (BAP) Delivery

Yoni Atma

Submitted in accordance with the requirements for the degree of
Doctor of Philosophy

School Food Science and Nutrition
The University of Leeds

July 2025

The candidate confirms that the work submitted is his own, except where work which has formed part of jointly-authored publications has been included. The contribution of the candidate and the other authors to this work has been explicitly indicated below. The candidate confirms that appropriate credit has been given within the thesis where reference has been made to the work of others. Details of the jointly-authored publications and the contributions of the candidate and the other authors to the work are outlined on pages iv and v.

This copy has been supplied on the understanding that it is copyright material and that no quotation from the thesis may be published without proper acknowledgement.

The right of Yoni Atma to be identified as Author of this work has been asserted by his in accordance with the Copyright, Designs and Patents Act 1988.

© 2025 The University of Leeds and Yoni Atma

Further details of the jointly-authored publications and the contributions of the candidate and the other authors to the work are included below:

Chapter 2

Atma, Y., Murray, B.S., Sadeghpour, A., Goycoolea, F.M. 2024. Encapsulation of short-chain bioactive peptides (BAPs) for gastrointestinal delivery: a review. *Food & Function*, 15, 3959-3979.

Chapter 3

Atma, Y., Sadeghpour, A., Murray, B.S., Goycoolea, F.M. 2025. Chitosan-alginate polyelectrolyte complexes for encapsulation of low molecular weight fish bioactive peptides. *Food Hydrocolloids*, 160, 110789.

Details of authorship contributions:

1. Encapsulation of short-chain bioactive peptides (BAPs) for gastrointestinal delivery: a review.

Yoni Atma: conceptualization, writing – original draft, visualization; Brent S Murray: conceptualization, writing – review and editing, supervision; Amin Sadeghpour: writing – review and editing, supervision; Francisco M. Goycoolea: conceptualization, writing – review and editing, supervision

2. Chitosan-alginate polyelectrolyte complexes for encapsulation of low molecular weight fish bioactive peptides.

Yoni Atma: Writing – original draft, Visualization, Investigation, Funding acquisition, Formal analysis, Data curation, Conceptualization.

Amin Sadeghpour: Writing – review & editing, Writing – original draft, Visualization, Validation, Supervision, Software, Methodology, Investigation, Formal analysis, Conceptualization.

Brent S. Murray: Writing – review & editing, Writing – original draft, Visualization, Validation, Supervision, Project administration, Methodology, Formal analysis, Conceptualization.

Francisco M. Goycoolea: Writing – review & editing, Writing – original draft, Visualization, Validation, Supervision, Project administration, Methodology, Formal analysis, Conceptualization

List of accepted conference abstracts:

Poster Presentations:

Atma, Y., Sadeghpour, A., Murray, B.S., Goycoolea, F.M. 2023. Tailored design of chitosan-alginate self-assembled electrostatic macromolecular aggregates for encapsulation of low molecular weight bioactive peptides. *UK Colloids 2023*. Liverpool, UK.

Atma, Y., Sadeghpour, A., Murray, B.S., Goycoolea, F.M. 2023. Short fish peptides encapsulation by polyelectrolyte complexes (PECs) based on biopolymers. *3rd Food Chemistry Conference.* Dresden, Germany.

Atma, Y., Murray, B.S., Sadeghpour, A., Goycoolea, F.M. 2024. ACE inhibitor fish bioactive peptides (BAPs) and preparation their vehicles. *10th Food Science and Nutrition PhD Conference.* Leeds, UK.

Atma, Y., Sadeghpour, A., Murray, B.S., Goycoolea, F.M. 2024. Alginate/chitosan electrostatic self-assembled for oral delivery bioactive peptides (BAPs). *SoftComp/EUSMI Annual Meeting 2024*. Lyon, France.

Atma, Y., Murray, B.S., Sadeghpour, A., Goycoolea, F.M. 2024. Fish peptides encapsulation via electrostatic interaction chitosan/alginate. *13th International Colloids Conference*. Sitges-Barcelona, Spain.

Oral Presentations:

Atma, Y., Sadeghpour, A., Murray, B.S., Goycoolea, F.M. 2023. Purification antihypertensive fish peptides and preparation their vehicles based on biopolymers. *9th Food Science and Nutrition PhD Conference*. Leeds, UK (5MT).

Atma, Y., Sadeghpour, A., Murray, B.S., Goycoolea, F.M. 2024. Tailored design of polyelectrolyte complexes (PECs) for encapsulation of low molecular weight bioactive peptides (BAPs). *19th Food Colloids Conference*. Thessaloniki, Greece.

Atma, Y., Sadeghpour, A., Murray, B.S., Goycoolea, F.M. 2025. In vitro digestion and release of bioactive peptides from chitosan-alginate polyelectrolyte complexes. *22nd Gum and Stabiliser for the Food Industry Conference*. Wageningen, Netherlands.

Received travel grant, supports, and award:

Travel Grant:

The SoftComp/EUSMI Annual Meeting 2024. May 21 – 24, Valpre Hotel, Lyon, France.

Travel Supports:

Discover Material (DMA) Conference 2023. September 13 – 14, Edgbaston Park Hotel and Conference Centre, Birmingham, UK.

Rising Stars in Materials Science Workshop 2023. January 12 – 13, Royce Hub Building, Manchester, UK.

Award:

Faculty of Environment Partnership Awards. Winner for Faculty Group Award 2023, given by The Faculty of Environment and Leeds University Union.

Acknowledgements

I would like to express my sincere gratitude to the supervisory committee: Prof. Brent S. Murray, Dr. Amin Sadeghpour, and Prof. Francisco M. Goycoolea (for his supervision during my first and 2nd years of study) for their invaluable guidance and insightful feedback throughout the four years of my doctoral study. Their patience, dedication, and high standards have shaped this thesis and the research outcomes.

My deepest appreciation goes to examiner committee: Dr. Evi Paximada and Professor Gordon Morris for the constructive feedback and positive discussion, which have contributed to the improvement of my thesis.

I have been blessed with a scholarship from the Indonesian Education Scholarship (BPI), provided by the Ministry of Education, Research, and Technology of Indonesia in collaboration with the Indonesian Endowment Fund for Education (LPDP). This scholarship supports my PhD studies and provides allowances for me and my family during our time in the UK.

I am profoundly grateful for the assistance provided by the school technician team: Neil, Natalie, Miles, Joanna, Graham, Sara, Ian, and school admin Gita, Jenna, George, Katelyn, and Catherine. Their assistance contributed significantly to the smooth progress of my research and academic activities. I also appreciate working on SLS analysis with Johan and Dan (Bragg Centre), TEM analysis with Zabeada (LEMAS), and INFOGEST chemicals with Taskin. I thank those warmly welcomed me as I began my doctoral program: lecturers in the School of Food Science and Nutrition, the journal club and the lab. meeting members, and all my fellow PhD colleagues.

Special thanks to Indonesian communities in Leeds: Kibar Leeds, PPI Leeds, BPI Leeds, Curdis Leeds, and Indonesian residencies, i.e. Holborn Shay Street Housing, for togetherness and for making the distance between Leeds and Indonesia feel so near.

With all my heart, I want to thank my mother because I genuinely believe her prayer is behind every achievement. Thank you also to my younger brother, Yovan, and the entire Basri family for their support, to my beloved wife, Eka Mulyani Asra, who has walked with me through every step of my PhD journey, shared the responsibilities and happiness to our children: Dzaka and Delisha.

Finally, I dedicate this thesis in loving memory of my elder brother: Yovisol Ardha, and my father-in-law: Yusra who sadly did not live to see until I complete this.

Leeds, July 2025

ABSTRACT

Short bioactive peptides (BAPs) have gained significant traction given their potential health benefits, particularly, to aid in mitigating hypertension and diabetes. Hence, their potential application as functional food ingredients, supplements, or nutraceuticals, has been recognised, though not yet realised. However, BAPs are highly susceptible to degradation and instability when considering aspects of the product development process, and the most critical concern remains their susceptibility to hydrolysis in the gastrointestinal tract during digestion that compromises their bioaccessibility and bioavailability. One promising strategy to address this limitation is to encapsulate BAPs in a suitable encapsulation vehicle.

Polyelectrolyte complexes (PECs) obtained by electrostatic self-assembly of oppositely charged chitosan (CS) and alginate (ALG) represent a simple to prepare, sustainable and versatile biopolymer platform for bioactive compounds association and oral delivery. CS+ALG PECs protect against acid, salt hydrolysis, and proteases degradation. However, key underpinning factors such as the role of charge ratio (n^-/n^+) that can contribute to the PEC formation, stability and delivery, need further investigation.

This thesis focuses on studying CS+ALG PECs for the gastrointestinal delivery of BAPs derived from fish, with emphasis in understanding the role of the complexation charge ratio (n^-/n^+). The CS (M_w 111 kDa, degree of acetylation 10%) and two distinct ALG (M_w 21 kDa; M/G 1.4, and M_w 8 kDa; M/G 5.1), were selected to prepare PECs at varying (n^-/n^+). Then their biophysical characteristics were investigated using dynamic light scattering (DLS), small angle X-ray scattering (SAXS), and microviscosimetry measurements. The selected PECs (based on size/R_h and stability/ζ-potential) were then loaded with the BAPs, and the encapsulation efficiency was quantified using HPLC-UV. To examine the stability of unloaded (blank) and BAP-loaded PECs during digestion, simulated gastric and intestinal fluids were prepared following the INFOGEST protocol. The results show that PECs with n^-/n^+= 0.5 are more stable, and resilient against gastric fluids but not intestinal.

In summary, it was found that via setting the n^-/n^+, BAP encapsulation efficiency (EE) and PEC stability were increased. In addition, the PECs protect the BAPs from proteases (pepsin, trypsin, chymotrypsin) degradation, and preserve the activity of BAPs during *in vitro* static digestion, demonstrating their potential for incorporation into functional food formulations.

TABLE OF CONTENTS

Further details of the jointly-authored publications iv
Details of authorship contributions v
List of accepted conference abstracts vi
Received travel grant, supports, and award: vii
Acknowledgements viii
ABSTRACT x
TABLE OF CONTENTS xi
LIST OF TABLES xv
LIST OF FIGURES xvi
LIST OF ABBREVIATIONS xx
CHAPTER 1 GENERAL INTRODUCTION 1
1.1 Overall Research Aims 3
1.2. Molecular Structure of Chitosan and Alginate 5
1.2.1 Chemical structure of chitosan (CS) and alginate (ALG) 6
1.2.2 PECs based on chitosan (CS)/alginate (ALG) 12
1.3.3 Previous examples of encapsulation via CS + ALG PECs 17
1.3 General Overview of BAP Stability During Gastrointestinal Digestion 18
1.3.1. BAPs in salivary, gastric, and intestinal fluids 18
1.4 The Special Significance of Fish BAPs 19
1.4.1 Fish BAPs as antihypertensive agent via angiotensin converting enzyme (ACE) inhibition 20
1.5 Principle of The Various Characterisation Techniques Used in This Thesis 22
1.5.1 Dynamic light scattering (DLS) and ζ-potential 22
1.5.2 High performance liquid chromatography (HPLC) 26
1.5.3 Small angle X-ray scattering (SAXS) 30
1.5.4 Transmission electron microscopy (TEM) 32
1.5.5 Fourier-transform infrared (FTIR) spectroscopy 35
1.5.6 Density and viscosity 35
1.5.7 *In vitro* gastric and intestinal digestion 36
1.6 Outline of The Thesis 37
1.7 References 39

CHAPTER 2 LITERATURE REVIEW: STATE-OF-THE-ART RESEARCH ON ENCAPSULATION OF SHORT-CHAIN BAPs 50
2.1 Introduction 50
2.2 Types of Short-chain BAPs 53
2.3 Types of Carrier Particles for Encapsulation and Their Preparation 55
2.3.1 Nanoencapsulation 56
2.3.1.1 Nanoparticles (NPs) 56
2.3.1.2 Liposomes 60
2.3.2 Microencapsulation 62
2.3.2.1 Microgel particles 62
2.3.2.2 Microfibers 63
2. 4. Key characteristics of delivery vehicles 65
2.4.1 Association/entrapment efficiency (EE) 65
2.4.2 Size, surface properties and shape (morphology) 68
2.4.3 Stability, release, absorption/permeability, and bioactivity of encapsulated BAPs .. 70
2.4.4 Cytotoxicity 76
2.5. Summary - Gastrointestinal Delivery Vehicles for BAPs: Challenges and Opportunities . 77
2.6 References 81
CHAPTER 3 DEVELOPMENT AND CHARACTERISATION OF CHITOSAN-ALGINATE POLYELECTROLYTE COMPLEXES (PECs) FOR ENCAPSULATION BAPs DERIVED FROM FISH 90
3. 1. Introduction 90
3. 2. Materials and Methods 92
3. 2.1 Materials 92
3. 2.2 BAP isolation from protein extract 93
3. 2.3 Preparation and calibration of the ALG and CS stock solutions 93
3.2.4 Molar charge ratio (n^-/n^+) calculation 95
3.2.5 Formation of polyelectrolyte complex (PEC) 96
3.2.6 Encapsulation efficiency (EE) 96
3.2.7 Analysis of viscosity 97
3.2.8 The release (R) of BAPs 97
3.2.9 Measurements of PEC particle sizes 98
3. 2.10 Small angle X-ray scattering (SAXS) 99
3. 2.11 Transmission electron microscopy (TEM) 99
3. 2.12 Statistical analysis 99

3.3 Results and Discussion 99
3.3.1 Fish BAPs fractionation and identification 99
3.3.2 Physical properties of CS + ALG PECs 102
3.3.3 Physical properties of CS + ALG PECs loaded with BAPs 108
3.3.4 Microscopic evidence of morphology of PECs loaded with BAPs 111
3.3.5 Studies of BAP release from PECs due to pH change 112
3. 4. Conclusions 114
3.5 References 114
CHAPTER 4 CHITOSAN-ALGINATE PECs LOADED WITH FISH BAPs: AN IN VITRO DIGESTION STUDY 119
4.1 Introduction 119
4.2 Materials and Methods 121
4.2.1 Materials 121
4.2.2 Methods 122
4.2.2.1 Preparation ALG, CS and polyelectrolyte complexes (PECs) loaded and unloaded with fish BAPs 122
4.2.2.2 Stability PECs 122
4.2.2.3 Gastric and intestinal fluids preparation 123
4.2.2.4 In vitro static digestion and release study 124
4.2.2.5 In vitro enzymatic stability of fish BAPs 125
4.2.2.6 Fourier transform infrared spectroscopy (FT-IR) 125
4.2.2.7 Ultra-high-performance liquid chromatography (UHPLC) 126
4.2.2.8 Hydrodynamic radius (Rh), ζ-potential, and polydispersity index (PDI) 126
4.2.2.9 In vitro angiotensin converting enzyme (ACE) inhibition assay 126
4.2.3 Statistical analysis 127
4.3 Results and Discussion 127
4.3.2 CS+ALG polyelectrolyte complexes (PECs) and interaction with BAPs 127
4.3.3 Stability of CS+ALG PECs with BAPs 129
4.3.3.1 Incubation at different pH 129
4.3.3. In vitro digestion 132
4.3.4 Bioactivity 138
4.3.4.1 Bioactivity after release 138
4.3.5 Enzymatic stability BAPs 140
4.4 Conclusion 144

4.5 References 144
CHAPTER 5 GENERAL DISCUSSION 149
5.1 Introduction 149
5.2 Comparison of Encapsulation Efficiency (EE) with Similar Studies 153
5.3 Cumulative Release BAPs from PECs 154
5.4 Size and Stability PECs During Digestion 155
5.5 References 156
CHAPTER 6 CONCLUSIONS AND POTENTIAL FUTURE WORK 158
6.1 Conclusions 158
6.2 Potential Future Work 158
APPENDICES 160

LIST OF TABLES

Table 1.1 Documented CS + ALG PECs for encapsulation of bioactive compounds. 17

Table 2.1. Short-chain BAPs encapsulated for gastrointestinal delivery..... 54

Table 2.2. Encapsulation agents, encapsulation methods, encapsulation efficiency (EE), sizes, and kinetic releases for short-chain BAPs 75

Table 2.3. Other essential attributes on encapsulation of BAPs 80

Table 3.1. Comparison of measured properties of CS + ALG21 PECs with and without BAP loading. n^-/n^+ = molar charge ratio; R_h hydrodynamic radius; ζ = zeta potential; PDI = polydispersity index; EE = encapsulation efficiency. 108

Table 4.1 Volume and concentration stock solutions for gastric and intestinal fluids 123

Table 4.2. The ionic strength of salts on the gastric fluid 124

Table 4.3. The ionic strength of salts on the intestinal fluid 124

Table 5.1 EE of BAPs and other bio-active payloads with CS+ALG PEC compared with other studies 153

Table A1. Measured values of the viscosities (η) of supernatants of PEC preparations, used for calculation (via eq. (6) in the text) of the hydrodynamic radii (R_h) of the PECs from the diffusion coefficients (*D*) of the PECs measured via DLS. Values are shown for the two different combinations of CS + ALG8 and CS + ALG21 at the different molar charge ratios n^-/n^+. 161

LIST OF FIGURES

Figure 1.1. Chemical structure of a representative chitosan stretch of and degree of polymerisation (n+2), and a schematic representation of a chitosan chain using the standardised carbohydrate symbol nomenclature of chitosan. Chitosan sequences are comprised by deacetylated β-(1→4)-linked 2-amino-D-glucose (glucosamine/GlcN) (half-filled squares, D residues) and acetylated β-(1→4)-linked 2-acetamido-D-glucose (N-acetylglucosamine/GlcNAc) residues (filled squares, A residues). The sequences diagrams depict chitosans' structural variation regarding the degree of acetylation, pattern of acetylation (random, blockwise or alternating) and degree of polymerisation (n+2). 7

Figure 1.2. Chemical structure of a representative alginate polymer stretch, and a schematic representation of an alginate block co-polymer structure using the standardised carbohydrate symbol nomenclature. Alginate is comprised by L-guluronic (orange circles, G residues) and M-mannuronic (green circles, M residues) which are arranged in a block co-polymeric structure of poly-guluronate (G-block), poly-mannuronate (M-block) and an alternate pattern of poly-mannuronate-guluronate (MG-block), as depicted for a hypothetical sequence. 10

Figure 1.3. Schematic PEC formation from two oppositely charged polyelectrolytes (PEs) ... 12

Figure 1.4. Two models of PEC structure 14

Figure 1.5. Schematic of PECs formation from cationic and anionic PE at excess and equal n^-/n^+ 15

Figure 1.6 Mechanism of blood pressure increasing by the role of ACE enzyme (top) and blood pressure decreasing by ACE inhibitor (bottom) 21

Figure 1.7. Schematic of DLS instrumentation 24

Figure 1.8. A model and diagram for electrical double layer. 25

Figure 1.9. Diagram a modern liquid chromatography. 27

Figure 1.10. Schematic HPLC systems 28

Figure 1.11. Correlation between incident X-ray, scattered angle (θ), and scattering vector (q). 31

Figure 1.12. SAXS compartment. 32

Figure 1.13. Signals generated when high energy beam of electrons interacts with thin sample or specimen. 33

Figure 1.14. Schematic diagram of transmission electron microscopy (TEM) 34

Figure 2.1. The percentage of BAPs (as ACE and DPP-IV inhibitors) from food origins collected according to "high bioactivities" as mentioned on previous paragraph. 51

Figure 2.2 Multilevel pie chart describing important aspects of developing encapsulated BAPs as ingredients of food supplements, nutraceuticals, and functional food. 53

Figure 2.3. Illustration of the three techniques for BAP encapsulations via ionic gelation/coacervation. 58

Figure 2.4. An illustration of the approach for encapsulation BAPs using double emulsions + solvent evaporation. 61

Figure 2.5. Size distribution of NPs and MPs based on biopolymers as delivery vehicles for short-chain BAPs. 65

Figure 2.6. The illustration describes the role of encapsulation of BAP during digestion 71

Figure. 3.1 Standard curves for unfiltered solution density (ρ) versus concentration (C): CS (orange); ALG21 (blue); ALG8 (purple), with the corresponding linear regression lines. 95

Figure. 3.2. Cartoon of complex formation with or without BAPs (a); schematic illustration of preparation of PECs (b). 96

Figure 3.3 Chromatograms of standard curves for synthetic LKPNM (a), synthetic LKP (b), and chromatogram UF fraction (≤ 3kDa) fish BAPs calculated from area under the curves (AUC) (c). 100

Figure. 3.4. The magnitude of the net charge |N| on single molecules of the polymers and the BAPs as a function of pH. Left hand ordinate: |N| (+ve) for CS (red short, dashed line); |N| (-ve) for ALG21 (blue short, dashed line); |N| (-ve) for ALG8 (magenta short, dashed line). Right hand ordinate: |N| for the LKPNM or LKP BAPs. (Calculation explained in the text). The vertical dashed line indicates the pH (5.5) of PEC formation. 101

Figure. 3.5 Hydrodynamic radius (R_h) and ζ-potential of unloaded PECs as a function of molar charge ratio n^-/n^+ at a total polymer concentration of 2 mg mL^{-1}. Shading on the round shape in figure indicating biopolymers constructing the PECs. Red dominant meaning excess CS, blue and magenta dominant indicating excess ALG21 and ALG8 respectively. ... 103

Figure. 3. 6. Measured PEC sizes via SLS (R_g, cyan) and DLS (R_h, light yellow) for the CS + ALG21 systems at n^-/n^+ = 0.5 and 10, both loaded and unloaded with BAPs. (Bars with different letters are values that are statistically different from one another, at $p < 0.05$) ... 105

Figure. 3.7. Viscosity (η) of the supernatants of centrifuged CS + ALG mixtures as a function of the original mass fraction of ALG (f) in the systems for (a) CS + ALG 8 kDa and (b) CS + ALG 21 kDa at 25 °C. The dashed lines in (a) and (b) are the theoretical η of the biopolymer mixtures assuming simple additivity of the η of the pure components. (Thus, η at f = 0 and 1 are the values of CS and ALG stock solutions at 2 mg mL^{-1}, respectively). Figures (c) and (d) show the % difference of the measured η from the additive line for CS + ALG8 and CS + ALG21, respectively. 106

Figure. 3.8. Small-angle X-ray scattering (SAXS) patterns (a) and corresponding Kratky plots (b) are presented for 2 mg mL^{-1} CS, ALG, and their PECs at two different n^-/n^+ molar charge ratios. The Kratky plots demonstrate swollen chain behaviour for pure polyelectrolytes, whereas Gaussian and collapsed chains/clustered structures are observed for PECs of ALG8 and ALG21, respectively. The scattering profiles were acquired at 85 mM NaCl and 25 °C. The horizontal dashed lines in Kratky plots provide a guide for the Gaussian (random coil) chain behaviour at low q values. 107

Figure. 3.9. The signed molar charge ratio $-(n^-/n^+)$ for the CS + ALG21 PECs calculated excluding (back full curve) and including (red dashed curve) the contribution of charges from

encapsulated BAPs as a function of the volume of 2 mg mL^{-1} stock ALG21 solution added into the system. The horizontal dashed line indicates $n^-/n^+ = 1$, i.e., overall charge compensation of the systems. 109

Figure. 3.10. Ratio between freshly prepared and re-suspended values of R_h, ζ, and PDI of both loaded and unloaded CS + ALG21 PECs, at $n^-/n^+ = 0.5$ and 10. 110

Figure. 3.11. Viscosity (η) at 25 °C of the supernatants of centrifuged CS + ALG21 mixtures as a function of the original mass fraction of ALG21 (*f*) in the system. The dashed curve represents the data for the unloaded system, taken from **Fig. 7b.** The red squares indicate the η values for the PECs loaded with BAPs, the black diamonds correspond to unloaded (but re-suspended) PECs. 111

Figure. 3.12. TEM analysis of PECs for CS + ALG21 at $n^-/n^+ = 0.5$ after loading with fish BAPs. 112

Figure. 3. 13. The % release of BAPs from CS + ALG21 PECs for $n^-/n^+ = 0.5$ (excess CS) and $n^-/n^+ = 10$ (excess ALG21) after 3 h at 37 °C at pH 3.0 and pH 6.8. Bars with different letters are statistically different from one another, at $p < 0.05$..... 113

Figure 4.1. FT-IR spectra of freeze-dried CS, ALG, CS+ALG PEC ($n^-/n^+ = 0.5$, excess CS), CS+ALG PEC ($n^-/n^+ = 10$, excess ALG), and BAPs (**a**); and CS+ALG PEC ($n^-/n^+ = 0.5$) loaded with BAPs (**b**). 128

Figure 4.2. Hydrodynamic radius (R_h) (black), ζ-potential (red), and PDI (blue) of CS+ALG PECs ($n^-/n^+ = 10$, circles; and $n^-/n^+ = 0.5$, boxes) loaded with BAP (filled symbols, left panels) (a), or unloaded (open symbols, right panels) (b), during incubation at different pH conditions (as per central legends: uncontrolled, 4, 5, and 6) and varying time intervals. .. 131

Figure 4.3 Evolution of BAPs release (%R) (a), R_h (b), and ζ-potential (c) of loaded PECs during *in vitro* digestion, and relative release (% release with enzymes:% release without enzymes) (d), as well as relative R_h (R_h with enzymes:R_h without enzymes) (e). The excess CS systems ($n^-/n^+ = 0.5$) are shown by open (black boxes) symbols and the excess ALG system ($n^-/n^+ = 10$) are shown by filled (red circles) symbols both throughout. Note that the corresponding charges on the constituent molecules at the gastric and intestinal digestion conditions are as follows: Gastric (SGF), pH 3 (green): CS600+, ALG-30, FP (fish BAPs) +1.1. The intestinal (SIF), pH 7, (sky blue): CS50+, ALG-120, FP+1.0. 133

Figure 4.4. The bioactivity ACE inhibition with time of BAPs upon release during gastric (top) and intestinal (bottom) digestion with enzymes (left) and without enzymes (right) of CS + ALG PECs of excess CS ($n^-/n^+ = 0.5$) PEC and excess ALG ($n^-/n^+ = 10$) PEC. The bioactivity assay was performed on both BAP-loaded (filled symbols) and unloaded (open symbols) PECs. . 139

Figure 4.5 Residual BAPs in % (initial loaded concentration 1 mg mL^{-1} = 100%) in CS+ALG PECs taken at the beginning (0 min), and after 120 min of incubation in gastric fluid compared with their encapsulation efficiency 140

Figure 4.6. Residual fish BAP (initial loaded concentration = 1 mg mL^{-1}) after incubated with pepsin (2000 U mL^{-1} at pH 3), trypsin (100 U mL^{-1} at pH 7), chymotrypsin (25 U mL^{-1} at pH 7) quantified with HPLC at different time interval. 141

Figure 4.7. ACE inhibition of free fish BAPs (concentration 1 mg mL^{-1}), captopril (0.1 mM), BAPs after loaded into ALG + CS and BAPs release from ALG + CS after 120 min incubation in gastric and intestinal fluids. 142

Figure 4.8 Schematic illustration showing the proposed structure of PEC and the released BAP after digestion..... 151

Figure 5.1 Schematic framework of this thesis 151

Figure 5.2 schematic hydrolysis of LKPNM and LKP by trypsin and chymotrypsin via in silico analysis 152

Figure 5.3 Cumulative release (%) of fish BAPs from CS+ALG PECs at gastrointestinal fluids with enzymes (a) and without enzymes (b) 155

Fig. A1. a) The experimental (circles) and fitted (lines) static light scattering of PECs for CS + ALG21 with and without fish peptide (FP) at different charge ratios. b) The distribution of radius of gyration of PEC obtained from the fitting of experimental data using the spherical particles model. 162

Fig A2. Hydrodynamic radius (R_h) of ALG+CS, loaded (filled symbols) and unloaded (open symbols) with excess CS (n^-/n^+ 0.5) (black) and excess ALG (n^-/n^+ 10) (red), measured during gastric fluid (top) and during intestinal fluid (bottom) with enzymes (left) and without enzymes (right). 163

Fig. A3. ζ-potential of ALG+CS, loaded (filled symbols) and unloaded (open symbols) with excess CS (n^-/n^+ 0.5) (black) and excess ALG (n^-/n^+ 10) (red), measured during gastric fluid (top) and during intestinal fluid (bottom) with enzymes (left) and without enzymes (right). 164

Fig. A4. Polydispersity indexes (PDI) of PECs ALG+CS, loaded (filled symbols) and unloaded (open symbols) with excess CS (n^-/n^+ 0.5) (black) and excess ALG (n^-/n^+ 10) (/(red), measured during gastric fluid (top) and during intestinal fluid (bottom) with enzymes (left) and without enzymes (right). 165

Fig. A5. Size distribution after gastric and intestinal simulation digestion (without enzymes) of loaded polyelectrolyte complexes (PECs) ($n^-/n^+ \approx 0.5$ excess CS (a) and $n^-/n^+ \approx 10$ excess ALG (b). 166

Fig. A6. Percentage of fish BAPs release from PECs during gastric (top) and intestinal (bottom) static digestion with enzyme (left) and without enzymes (right). 166

Fig. A7. Standard curve generated from chromatographic analysis of fish-derived BAPs, plotting concentration against area under the curve (AUC) 167

LIST OF ABBREVIATIONS

ACE = Angiotensin converting enzyme

ACN = Acetonitrile

ALG = Alginate

ALG8 = Alginate 8 kDa

ALG21 = Alginate 21 kDa

AP = Apical

AUC = Area under the curve

BAP(s) = Bioactive peptide(s)

BL = Basolateral

Caco-2 = Colonic carcinoma cells-2

CCD = Charge-coupled device

CCK-8 = Cell counting kit-8

CD = Cyclodextrin

CLSM = Confocal laser scanning microscopy

CS = Chitosan

CS111 = Chitosan 111 kDa

CS+ALG PEC(s) = Chitosan-alginate polyelectrolyte complex(es)

CS/α-CD-TPP = Chitosan- α- cyclodextrin-tripolyphosphate

CS/SBE-β-CD-TPP= Chitosan-sulphobutyl ether-β-cyclodextrin-tripolyphosphate

DAD = Diode array detector

DD/DA = Degree of deacetylation/degree of acetylation

DED = Direct electron detector

DLS = Dynamic light scattering

DMEM = Dulbecco's modified eagle medium

DMSO = Dimethyl sulfoxide

DNA = Deoxyribonucleic acid

DP = Degree polymerisation

DPP-IV = Dipeptidyl Peptidase IV

DPPC = 1,2-dipalmitoyl-sn-glycero-3-phosphocholine

ECG = Epigallocatechin gallat

EDL = Electrical double layer

EE = Encapsulation efficiency/entrapment efficiency

EFSA = European food safety authority

EM = Electron microscopy

EPC = Egg phosphatidylcholine

FAP = *N-[3-(2-furyl)acryloyl]-L-phenylalanyl*

FAPGG = *N-[3-(2-furyl)acryloyl]-L-phenylalanylglycylglycine*

FDA = Food and Drug Administration

FIR = Far Infrared

FNC = Flush nano-complexation

FPH = Fish protein hydrolysates

FPLC = Flush performance liquid chromatography

FSP = Fish sarcoplasmic protein

FTIR = Fourier transform infrared

G block = Guluronic block

GDS = Gastric digestion simulator

GI = Gastrointestinal

GM Block = Guluronic-mannuronic block

GRAS = Generally Recognized as Safe

GSH = Glutamyl-L-cysteinyl-glycine (glutathione)

HA = Hyaluronic acid

HBBS = Hanks' balanced salt solution

HepG2 = Hepatocellular G2 (human liver cancer cell line)

HFIP = Hexafluoro-2-propanol

HHL = Hippuryl-L-histidyl-L-leucine

HMWC = High molecular weight chitosan

HPA = Hippuric acid

HPLC = High performance liquid chromatography

IBD = Inflammatory bowel disease

IC_{50} = Half maximal inhibitory concentration

ICE6 = Intestinal epithelioid cell line No. 6

INFOGEST = International network on food digestion

Is = Ionic strength

kDa = Kilodalton

LC-MS = Liquid chromatography mass spectroscopy

LKP = Leucine-Lysin-Proline

LKPNM = Leucine-Lysin-Proline-Asparagine-Methionine

LMWC = Low molecular weight chitosan

MF = Microfibre

MIR = Mid Infrared

M/G = Mannuronic-guluronic ratio

MLV = Multilamellar vehicles

MMWC = Medium molecular weight chitosan

M3-PALS = Mixed mode measurement - phase analysis light scattering

MMP-2 = Matrix metalloproteinase-2

M_n = The number-average molar mass

MP = Micropartilce

MTS = 3-(4,5-dimethylthiazol-2-yl)-5-(3- carboxymethoxyphenyl)-2-(4-sulfophenyl)-2Htetrazolium

MTT = 3-(4,5-dimethylthiazol-2-yl)-2,5-diphenyl-2H-tetrazolium bromide

M_w = Molecular weight

M_{wa} = The weight-average molar mass

M_w $ALG_{(mon)}$ = Molecular weight alginate (monomer)

M_w $CS_{(mon)}$ = Molecular weight chitosan (monomer)

mRNA = Messenger ribonucleic acid

MWCO = Molecular weight cut off

NF = Nanofiltration

NIR = Near infrared

NP = Nanoparticle

NP-HLPC = Normal phase - High performance liquid chromatography

n^-/n^+ = Molar charge ratio

O-CMCS = O-carboxymethyl chitosan

O/W = Oil in water

PCS = Photon correlation spectroscopy

PE(s) = Polyelectrolyte(s)

PEC(s) = Polyelectrolyte complex(es)

PEGDA = Poly(ethylene glycol) diacrylate

PBS = Phosphate buffer saline

PDDF = Pair distance distribution function

PDI = Polydispersity index

pI = pH isoelectric

pKa = Acid dissociation constant

PLA = Poly(lactic-acid)

PLGA = Poly(lactic-co-glycolic acid)

PSD = Particle size distribution

PVA = Poly(vinyl alcohol)

R or %R = Release or % release

Rel%R = Relative release

RelR_h = Relative hydrodynamic radius

R_h = Hydrodynamic radius

RI = Refractive index

RP-HPLC = Reverse phase - High performance liquid chromatography

RT = Retention time

SA = Sodium alginate

SAL-O-CMCS = Sodium alginate- O-carboxymethyl chitosan

SANS = Small angle neutron scattering

SAXS = Small angle X-ray scattering

SBE = Sulphobutyl ether

SEC = size-exclusion chromatography

SEM = Scanning electron microscopy

SGF = Simulated gastric fluid

SIF = Simulated intestinal fluid

SLP = S-layer protein

SLS = Static light scattering

TEM = Transmission electron microscopy

TFA = Trifluoro acetic acid

TNF-a = Tumor necrosis factor-alpha

THF = Tetrahydrofuran

TPP = Tripolyphosphate

UV-Vis = Ultraviolet-Visible

UF = Ultrafiltration

UHPLC = Ultra high-performance liquid chromatography

WAXS = Wide angle X-ray scattering

W/O = Water-in-Oil

W/O/W = Water-in-Oil-in-Water

WPI = Whey protein isolate

WST-1 = Water-soluble tetrazolium salt

CHAPTER 1
GENERAL INTRODUCTION

Public awareness of the quality of life, health, and well-being has significantly increased. This is indicated by the rising market demand for food supplements, nutraceuticals, and functional foods (Du et al., 2024, Vignesh et al., 2024, Maria Leena et al., 2020, Luo and Wang, 2014). The application of synthetic bioactive for health-promoting product ingredients has decreased, with a noticeable shift to natural alternatives. Among the natural components that can promote human health and prevent diseases are the bioactive peptides (BAPs). The terminology of bioactive peptides was first introduced by Tsuru et al. (1976), who studied bradykinin (a nonapeptide), which has a role in various physiological processes. A decade later, Rabbani et al. (1986) and Sharma and Ortwerth (1987) published papers about the purification and characterization of BAPs. However, the sources of BAPs were derived from precursors initially found in the human body. Meisel et al. (1989) were the first to report the production and isolation of BAPs from bovine casein via *in vivo* digestion. By the 2010s, studies about BAPs have increased gradually, including exploring the sources (natural sources, especially food or food processing by-products), production, fractionation, purification, and characterization (Sánchez and Vázquez, 2017). Currently, more than 5,112 BAPs have been identified and stored on the BIOPEP-UWM database platform (Minkiewicz et al., 2019; Awaniak et al. 2024).

BAPs' *in vitro* activity is rarely confirmed by *in vivo* studies (Fleury et al., 2022, Sato, 2022, Lee et al., 2007, Miguel et al., 2006). This has been attributed to BAP's susceptibility to physiological enzymes like proteases and peptidases absent in the former (Pei et al., 2022, Xu et al., 2019, Segura-Campos et al., 2011). Although the hydrolysis of parent protein or polypeptides can generate BAPs with higher bioactivities, in some cases, the bioactivity declined (Sutantawong et al., 2024, Udenigwe and Fogliano, 2017, Boutrou et al., 2015) or it is called uncontrollable bioactivity. Therefore, several approaches have been examined to prevent BAPs from undesirable hydrolysis and degradation; one of them is via the encapsulation strategy (Mirzapour-Kouhdasht et al., 2023, Aguilar-Toala et al., 2022). There are some advantages offered by encapsulation that other approaches are missing. For instance, by protecting BAPs with encapsulation, we do not need to modify the original

structure of BAPs. The encapsulation creates a shield that avoids direct physical interaction BAPs with unfavourable surrounding environments. In addition, a broad range of materials is available, and some are versatile depending on the concept and purpose of encapsulation (Sharma et al., 2024, Brown et al., 2019, Wandrey et al., 2010).

The concept of BAP encapsulation is inherently linked to the advent of encapsulation of therapeutic proteins and peptides a few decades ago, such as insulin or human growth hormones, which were used to protect them from early degradation and enhance bioavailability via controlled release in the target sites (Noorbatcha et al., 2018, Maciel et al., 2017). Studies on encapsulation of therapeutic proteins or polypeptides have been conducted since the 1970s when this was first published (Patel and Ryman, 1976) for insulin. Meanwhile, BAP encapsulation only started around ten years ago with a study by Li et al. (2015) for encapsulation of bioactive salmon protein hydrolysate.

Some encapsulation systems have been successful to increase the bioaccessibility and bioavailability of bioactive protein or protein hydrolysates (Moreira et al., 2021, Batista et al., 2018, Mohan et al., 2015, Colletier et al., 2002). They include liposomes, solid lipid nanoparticles, microgel particles, emulsions, or a combination of two encapsulation techniques (Perry and McClements, 2020, McClements, 2018). However, the encapsulation of BAPs might not be the same as for other protein and peptides. The BAPs mostly have effective bioactivities in the shorter sequences or small peptides, consisting of less than 20 amino acids or molecular weight (M_w) less than 3 kDa. The short BAPs may be more challenging in regard to the capability of the wall materials to associate them effectively during the entrapment process, also known as encapsulation efficiency or entrapment efficiency (EE). Also, it might be difficult to prevent their release throughout storage, as well as avoiding their fast release in physiological fluids. For example, in cases during the process of encapsulation, where the BAPs might tend to dissolve with the water/liquid phase rather than being retained with the carrier matrix (BAPs are mostly hydrophilic), which also called leaching effect or due to insufficient binding affinity with encapsulant materials, these could lead to very low EE (Bicak et al., 2021, Parmentier et al., 2011, Trapani et al., 2010). Moreover, the fast release of BAPs might depend on the type of the systems, wall materials, and release medium environment (pH, ionic strength, temperature). For polymeric colloidal particles, BAPs can diffuse when they have smaller sizes than the pores of encapsulant particles (Perez-Perez et al., 2024). Therefore, it is important to ensure that the pore size is small. If not, it should be ensured

that the interaction of BAPs with the coating matrix is strong enough and only changes under specific environmental factors at the target sites (McClements, 2017).

Concerning quality and purity requirements and potential of translation of encapsulated BAPs intended as ingredients of functional foods, nutraceuticals, or food supplement formulation, all materials and BAPs should be food grade approved. Also, their gastrointestinal stability and biodegradability are important variables. Other relevant assets might include mucoadhesive capacity, sustainability of production, low cost, green chemistry compliance and natural abundance or availability (da Silva et al., 2024, Zabot et al., 2022, Zhu, 2017). Despite these requirements, it is surprising that most of the systems so far addressed in research studies, have been formulated using non-food grade components and required considerable preparation time (Zhang et al., 2021, Brown et al., 2019, McClements, 2018, Batista et al., 2018). Simple, quick, adaptable, and cost-effective techniques are key elements to make encapsulation strategies feasible for industrial application. This work was motivated by the need to addressing some of the above current challenges, ultimately seeking to contribute to gain understanding of the key parameters that determine the properties and performance of these systems.

1.1 Overall Research Aims

In the present thesis, the trends in current studies on encapsulation of short-chain BAPs have been critically analysed. A new strategy of BAPs encapsulation, based on the electrostatic self-assembly of oppositely charged polysaccharides, which is simple and adaptable for industrial applications, has been developed. Finally, the appropriateness for oral delivery of prototyped formulations, has been examined via simulated gastrointestinal digestion. Many food-grade wall materials for encapsulation are labile in the gastric and intestinal environment. For instance, protein, lipid or carbohydrate-based polymers can be digested by enzymes in the human gastrointestinal tract, which leads to the premature release of the bioactive payload. Several techniques of encapsulation using mucoadhesive polymers have been studied. However, most of these are time-consuming, include synthetic components, or do not give high encapsulation or entrapment efficiency (EE) (Yermak et al., 2022, Kruk and Winnicka, 2022, Du et al., 2019, Bicak et al., 2021, Trapani et al., 2010).

Polyelectrolyte complexes (PECs) are easy and straightforward to prepare as encapsulation systems. Cationic chitosan (CS) and anionic alginate (ALG) have been used for foods, drugs, and biomaterials as wall materials. CS and ALG are not expected to be digested in human saliva, gastric, and intestinal tracts (Kipkoech, 2023, Houghton et al., 2015, Odunsi et al., 2010). Some studies found that combining these natural polymers prevented short and low M_w peptides from inopportune leaching and release (Wang et al., 2024, Auwal et al., 2024). However, the preparation of PECs for the encapsulation is still not optimised; for example, the majority was only by mixing specific concentration ratios instead of considering initial charges or not setting their charge ratio (n^-/n^+) precisely before loading with BAPs. The molar charge ratio (n^-/n^+) is one of the most important parameters influencing PEC formation (Holkar et al., 2021, Wu et al., 2020, Kulkarni et al., 2016). This thesis has examined carefully the effect of n^-/n^+ on PEC properties. The features of PECs that have been characterised in this thesis include sizes and stability using dynamic light scattering (DLS), complexation with small angle-X scattering (SAXS). In addition, electron microscopy (EM) was performed to confirm the sizes and polydispersity based on DLS measurement. Encapsulation or entrapment efficiency (EE) and release study were quantified via high-performance liquid chromatography (HPLC). Moreover, this thesis also tested the performance of CS+ALG PECs during storage and during in vitro simulation digestion and the corresponding bioactivity of the BAPs measured.

The values of $n^-/n^+ \approx 1$ may produce smaller and more compact PEC particles due to stronger ionic interaction but with lower stability because of the compensation of equal charges (Shovsky et al., 2009, Kulkarni et al., 2016). Excess CS or excess ALG create larger PECs due to weak Coulombic interaction, allowing more space, but with better PEC stability as a function of excess charges or repulsion force with the medium or between the PEC particles. Reducing the M_w of wall materials should diminish the sizes of PECs (Ferreira et al., 2020, Sæther et al., 2008). Higher M_w of encapsulant materials might increase encapsulation efficiency (EE) (Sæther et al., 2008).

During digestion, changes in pH and ionic strength may disrupt the ionic interaction of BAPs with the wall material, triggering the release of BAPs into the medium. The bioactivity of BAPs before and after encapsulation (release) should not change unless excess CS and ALG affect bioactivity as well.

1.2. Molecular Structure of Chitosan and Alginate

The term chitosan (CS) refers to a family of natural polymers derived from the partial deacetylation of chitin. Chitin is a linear aminopolysaccharide that constitutes the structure of the exoskeleton of a large number of arthropods, molluscs, fish, fungi, yeasts, bacteria, and microalgae (Brück et al., 2010). At the industrial scale, chitin is obtained from waste of commercial marine processing industries such as shrimps, crabs, lobster, and squids (Brück et al., 2010). An estimated 10^{10} – 10^{12} kg per year of chitin is produced from marine sources (Dhillon et al., 2013). Although most chitosan used for pharmaceutical and food industries is extracted from marine crustaceans (Ngasotter et al., 2023, Hamed et al., 2016), it is also found in insects and certain fungi (Nwe et al., 2010) Moreover, it had started to be produced from microbial sources (Joseph et al., 2021, Knezevic-Jugovic et al., 2011). Chitin and cellulose are among the most abundant biopolymers on earth. However, insolubility in water and most organic solvents and poor processability are the limiting factors that have prevented a wider use of chitin (Guarnieri et al., 2022). Fortunately, deacetylation of chitin generates chitosan, which is soluble in aqueous acidic conditions. Deacetylation enhances chitin biocompatibility, biodegradability, and versatility (Islam et al., 2016, Qun and Ajun, 2006). Given its material and biological properties, CS has been applied in foods, food packaging, cosmetics, biomaterials, medical devices, dentistry, textiles, water treatment, agriculture, aquaculture, pharma, biotechnology and other sectors. In the pharmaceutical field, CS has been used for encapsulation of drugs and various active ingredients (Ferreira et al., 2020, Goycoolea et al., 2012, Alonso et al., 2008).

Alginate (ALG) describes yet another family of polysaccharides that occurs naturally in brown multicellular seaweeds (class Phaeophyceae) and are secreted by few bacterial species such as *Pseudomonas aeruginosa* and *Azotobacter vineladii* (Bertagnolli et al., 2014). Commercial ALG is mostly extracted from cell-wall brown seaweed as the soluble sodium alginate salt. On average, brown seaweeds contain 40% dry matter of alginate, with the production reaching more than 230,000 tons annually derived from approximately 85,000 tons of their parent origin (Bertagnolli et al., 2014). ALG is one of the most versatile and valuable biopolymers applied in diverse food, pharmaceutical, and cosmetic sectors. ALG is approved as food additive hydrocolloid by FDA and many other agencies worldwide. It is used to control the structure and physicochemical properties of foods, namely as a thickening and

gelling agent, stabilizers, emulsifiers, and fat substitute (Guo et al., 2020). ALG has also been used as natural edible coatings (Tabassum and Khan, 2020) and biodegradable films (Ehsani et al., 2020). In biomedical and pharmaceutical sectors, ALG has roles as a biodegradable scaffold and wound dressing materials (tissue engineering) and drug delivery agent, as well as taste marker and suspending agent. There have been much research on developing ALG as an encapsulation material for enzymes, proteins and polypeptides (Zhang et al., 2016).

1.2.1 Chemical structure of chitosan (CS) and alginate (ALG)

CS is a structural analogue of cellulose, differing only on a hydroxyl (OH) group at carbon 2 (C-2) replaced with amino or acetamido groups depending on the degree of deacetylation (DD). CS is a copolymer consisting of β-(1→4)-2- amino-D-glucose (glucosamine/GlcN) or deacetylated residue (D), and β-(1→4)-2-acetamido-D-glucose (N-acetylglucosamine/GlcNAc) or acetylated residue (A) units (Peniche et al., 2008). **Figure 1.1** shows the structure of CS and its variations.

The identity of chitosan is given by the degree (DA) and pattern of acetylation (PA), degree of polymerisation (DP, given by the M_w and the average molar mass per residue), and distribution of the M_w. Depending on sources and production techniques, the DA of CS ranges from ~2 to ~45 %; CS is obtained when chitin is deacetylated to a degree (DD) of ~50% (Rinaudo, 2006), but at least ~85% deacetylation is required for good solubility of CS. Based on DA, CS is categorized as high DA -low DD- (25 – 45%) and low DA -high DD- (<25%) (Dinculescu et al., 2024, Joseph et al., 2021).

The DA, expressed as a percentage (DA %), or as a fraction (from 0 to 1.0) (FA), is given by the molar fraction of GlcNAc (A) to the total (A+D), from Equation 1.1:

$$DA\ (\%) = \frac{A}{A+D} \times 100 \qquad (1.1)$$

Either DA or DD (=100 – DA) are used indistinctly in the literature to refer to the same parameter.

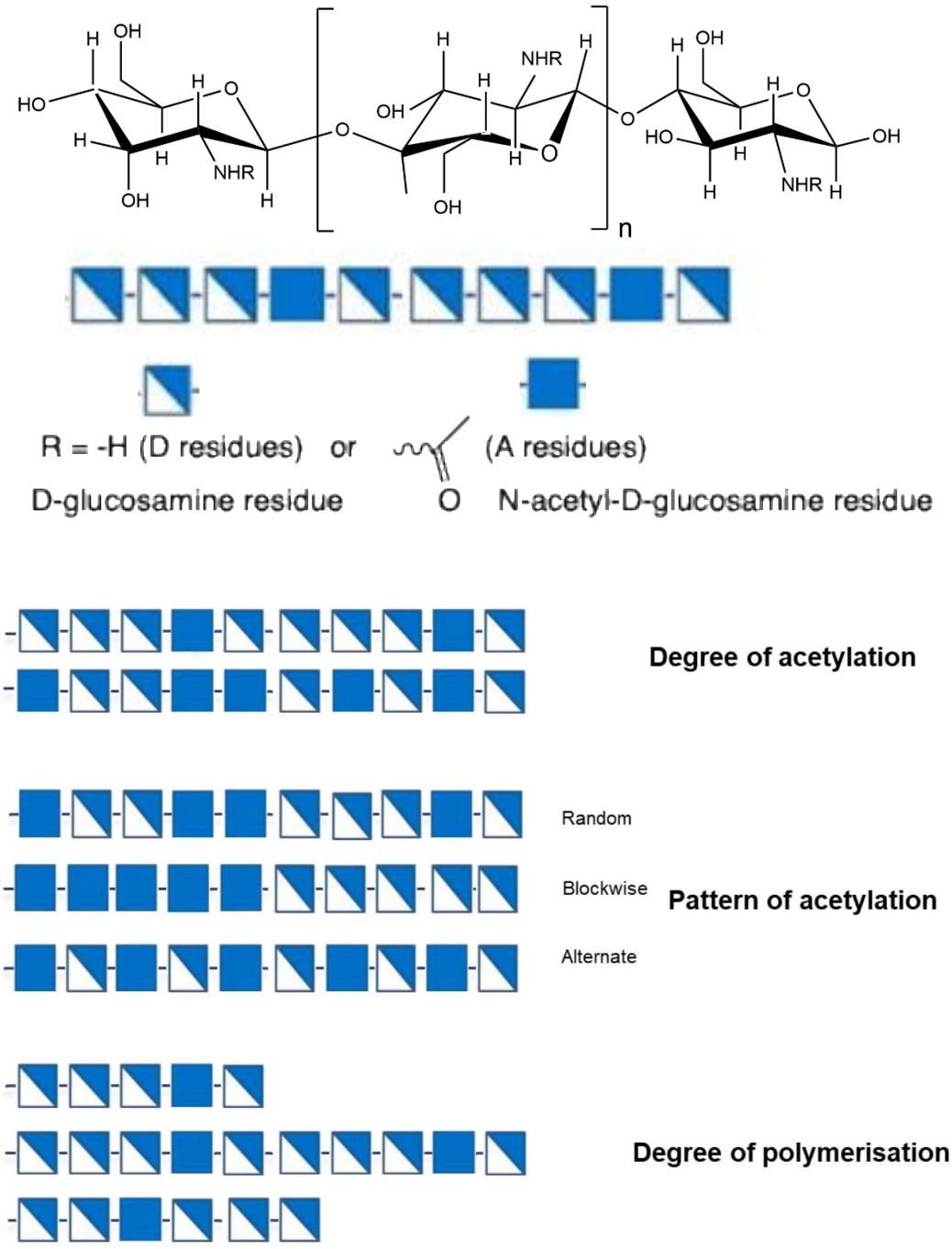


Figure 1.1. Chemical structure of a representative chitosan and degree of polymerisation (n+2), and a schematic representation of a chitosan chain using the standardised carbohydrate symbol nomenclature of chitosan. Chitosan sequences are comprised by deacetylated β-(1→4)-linked 2-amino-D-glucose (glucosamine/GlcN) (half-filled squares, D residues) and acetylated β-(1→4)-linked 2-acetamido-D-glucose (N-acetylglucosamine/GlcNAc) residues (filled squares, A residues). The sequences diagrams depict chitosans' structural variation regarding the degree of acetylation, pattern of acetylation (random, blockwise or alternating) and degree of polymerisation (n+2).

The PA, in turn, is defined by a statistical parameter that considers the frequency of occurrence for neighbouring A and D residues, as determined by ^{13}C NMR spectroscopy applying diad (or triad) analysis of the probabilities that two A groups are adjacent to each other and the probability that one residue A has a D neighbour (Weinhold et al., 2009). Commercial chemically produced chitosans obtained by heterogenous thermoalkaline deacetylation of chitin have recently been found to have a non-random regular pattern with A residues overrepresented every third position (Hellmann et al., 2024). For many decades, it was thought that these chitosans had a random PA. A new generation of chitosans with blockwise PAs has been recently developed using enzymatic processes, and it has uncovered the great importance of the role of the PA in dictating the physicochemical and biological properties of chitosan (Sreekumar et al., 2022). Despite this, the PA is hardly characterised in studies with CS.

The amino groups from D residues become fully protonated at pH below 4, thus making CS a cationic polyelectrolyte. Some literature stated that CS is protonated upon dissolution in the aqueous acidic medium at pH < 6.5 (pK_a of amin group ≈ 6.5) (Yadav et al., 2023, Ding et al., 2019), but a study mentioned that at pH 5.2, an unstable structure is generated (Bakshi et al., 2020). At pH 6.5, the size, aggregation, and phase separation arise. The CS loses its solubility in very weak acid solutions at pH 7 or above (Bakshi et al., 2020).

The molecular weight (M_w) of CS is determined by the number of the constituent monosaccharides units per polymer molecule (degree of polymerisation) and the average molar mass. In statistical terms, the weight-average molar mass (M_{wa}) and the number-average molar mass (M_n) are the parameters used to characterise the M_W distribution and its polydispersity given by the parameter Đ (=M_{wa}/M_n). CS´s M_w can vary over a wide range of values, typically between ~10 – ~700 kDa, when characterised by SEC-MALS-dRI (Roman-Doval et al., 2023; Goycoolea et al., 2016). Although values of up to ~2000 kDa have been documented (Mourya et al., 2011), these might be overestimated by the characterisation method. Reducing the M_w of CS has been performed using chemical hydrolysis and enzymatic degradation (with lysozyme or chitosanase) approaches (Alonso et al., 2008). Some of these treatments introduce chemical modifications, for example at the reducing end.

When classified according to their M_w, CS is grouped into low molecular weight chitosan (LM_WC), M_w < 150 kDa; medium molecular weight chitosan (MM_WC), M_w 150 – 700 kDa; and high molecular weight chitosan (HM_WC), M_w > 700 kDa (Roman-Doval et al., 2023). These M_W depend on the preparation process and source origins (Mania et al., 2023). LM_WC has a higher solubility than medium and higher M_w CS, bringing better potential for food and medicinal applications, but the thermostability of LM_WC is smaller than MM_WC and HM_WC. Lowering the M_w of CS also reduces their viscosity but increases the permeability (Aranaz et al., 2021, Qandil et al., 2018). Altogether, DA, PA and M_W are the essential structural features that dictate the physicochemical (e.g., viscosity, gel forming capacity, nanoparticles and nanofibers formation) and biological properties of CS and determine their specific applications (Goncalves et al., 2021).

Chitosan can also be derivatised by multiple chemical synthesis routes, leading to a wide range of chemical derivatives whose properties are the subject of intensive research. Three types of reactive functional groups in CS may allow them to be modified chemically, including an amino or acetamido group and primary and secondary OH groups at C-2, C-3, and C-6. CS modification is intended use to improve their functional properties (Aranaz et al., 2021).

The complete and diligent analytical characterization of CS and the main structural parameters (DA, M_W and PA) using appropriate and validated analytical tools is fundamental to understanding its material properties and biological activities. The variation in these parameters accounts for the vast structural diversity of chitosan and determines its physicochemical, material and biological properties, hence, the performance and applications in different sectors (Sreekumar et al., 2022; Goncalves et al., 2021).

Alginate (ALG) or sodium alginate $[C_6H_7O_6Na]_m$ with an average value of molar mass (per monosaccharide) structural unit of 198.11 g/mol (or ~198 Da) is composed of two conformational isomer residues, namely β-D-mannuronic acid (M) and α-L-guluronic acid (G). In ALG polymers, M and G are homogeneously or heterogeneously distributed and linked via 1-4 glycosidic bonds. The ALG with repeating unit two or more G residue is named a G-block, while the M-block is repeating unit two or more M residue. G and M repeating and alternately bonded are termed GM/MG-block (Draget and Taylor, 2011). **Figure 1.2** depicts the structure of ALG showing the three different type of block patterns. The proportion of these two acid residues on the ALG chain is called the M/G ratio. The M and G compositions depend on the sources and affect the physicochemical properties of ALG (George and Abraham, 2006, Augst et al., 2006). For instance, ALG with a high G ratio are more rigid, but when the G ratio is lower, the ALG become more elastic (Bojorges et al., 2023, Abasalizadeh et al., 2020). Moreover, ALG with high M block has higher water solubility than those ALG with higher G blocks (Barbu et al., 2021).

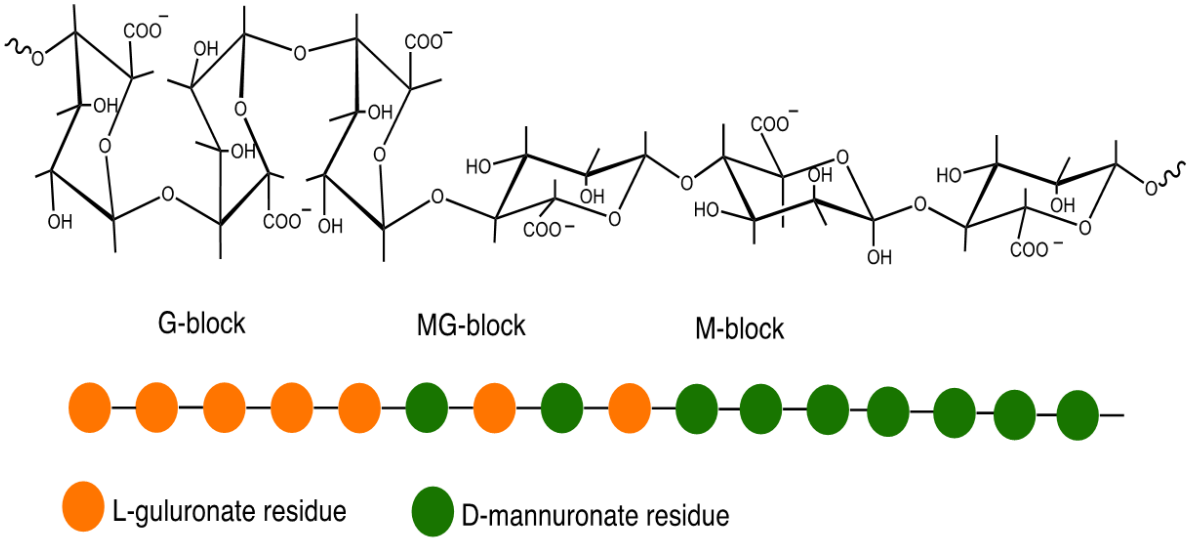


Figure 1.2. Chemical structure of a representative alginate polymer stretch, and a schematic representation of an alginate block co-polymer structure using the standardised carbohydrate symbol nomenclature. Alginate is comprised by L-guluronic (orange circles, G residues) and M-mannuronic (green circles, M residues) which are arranged in a block co-polymeric structure of poly-guluronate (G-block), poly-mannuronate (M-block) and an alternate pattern of poly-mannuronate-guluronate (MG-block), as depicted for a hypothetical sequence.

The solubility of ALG is influenced by several factors, including pH, ALG´s M_w, and the presence of salts. ALG is generally water soluble, and the solubility increases by increasing pH due to deprotonation of carboxyl groups, thus resulting in a negatively charged polyanionic structure. ALG become less soluble at low pH as it approaches its pK_a, namely 3.38 for the M residue and 3.65 for the G residue. Under specific conditions of low pH, ALG tends to make a gel (Potaś et al., 2020, Roopa and Bhattacharya, 2008, Smidsrød, 1970). According to Zhao et al. (2022), The M_w of ALG ranged from ~32 – ~200 kDa, but hydrolysis enabled the reduction of their M_w (Zhao et al., 2022, Ahmad Raus et al., 2021). M_w affects the viscosity; low M_w gives lower viscosity. In the case of Ca^{2+} addition into the sodium ALG solution, divalent cations (*e.g.*, Ca^{2+}, Ba^{2+}) replace some monovalent ions (Na^{+}) to form calcium ALG gel (Zdiri et al., 2022, Hu et al., 2022, Pravinata et al., 2016). This is the result of a specific binding via chelation of the divalent cations to homopolyguluronate (G-blocks) stretches in ALG caused by structural features of the G-blocks. This was explained with the so-called “egg-box” binding model, based on the linkage conformation (di-axial) between the guluronate (G) residues (Grant et al., 1973). Despite some refinements since its original proposal, this model persists for more than five decades. ALG ionic gelation with Ca^{2+} can be controlled under two main methods: the diffusion method and the internal setting method. Both have been harnessed in numerous applications in foods and other fields (Nordgard and Draget, 2021).

ALG at low concentrations of monovalent salts, such as NaCl or KCl, has a good solubility. However, when the salt concentration is too high, the solubility is reduced due to aggregates forming and gel formation (Chen et al., 2006, Zhang et al., 2001).

Based on M/G ratios, ALG is divided into two groups: high M/G ratios (>1), with high contents of M blocks (low G blocks), and low M/G ratios (<1), with low contents of M blocks (high G blocks). ALG with a high M/G ratio has good elasticity and provides soft gels due to M blocks composition, while the low M/G ratio of ALG provides ALG with strong and rigid gels (Bojorges et al., 2023, Zhang et al., 2021).

ALG can be categorised according to their sources: marine algae ALG and bacterial ALG. Marine algae ALG is the most common form of commercial ALG (generally extracted from brown seaweeds). In addition, Rahman et al. (2024) have classified the ALG according to their sources and process of extraction; this includes sodium ALG, calcium ALG, alginic acid,

macrocystis ALG, laminaria ALG, sargassum ALG and durvillaea ALG. First, sodium ALG (Na-ALG) is the dominant form of ALG. It is produced from kelp (Laminariales order) and is treated with ethanol during its precipitation stage. Na-ALG may also be obtained from calcium ALG (Ca-ALG) or alginic acid precipitate via sodium carbonate (Na_2CO_3) addition during the purification stage. Secondly, the Ca-ALG obtained via precipitation extracted sodium ALG using calcium chloride ($CaCl_2$). The Ca-ALG form a gel when Ca^{2+} ions react with carboxyl groups of ALG. The third one is alginic acid, usually found in minor quantities during extraction; the alginic acid may be treated further (purification) to become Na-ALG or Ca-ALG. The remaining types of ALG are based on the name of species of brown seaweeds such as macrocystis, laminaria, sargassum, and durvillaea ALG, which are extracted from *Macrocystis pyrifera*, *Laminaria* spp., *Sargassum* spp, and *Durvillaea* spp, respectively (Bojorges et al., 2023, Peteiro, 2018).

1.2.2 PECs based on chitosan (CS)/alginate (ALG)

PECs are formed via electrostatic (Coulombic) forces between at least two macromolecules with opposite charges (**Figure 1.3**). This may accidentally also lead to other interactions, either inter or intramolecular interactions, *e.g*. via another electrostatic, hydrogen, hydrophobic, Van der Waals forces or dipole-dipole association (Luo and Wang, 2014). In the case of PEC of CS+ALG, the electrostatic interaction occurs between carboxylate (COO^-) moieties on ALG with protonated amine (NH_3^+) on CS (Li et al., 2009).

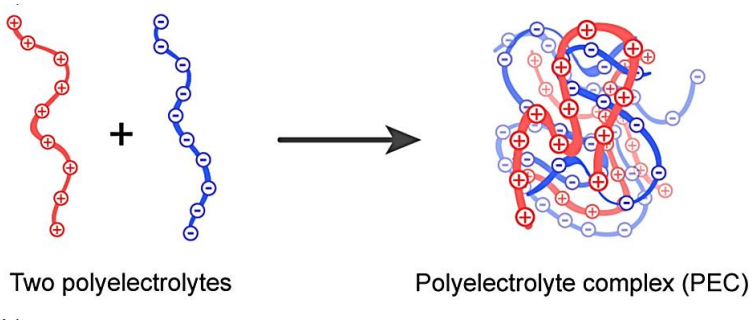


Figure 1.3. Schematic PEC formation from two oppositely charged polyelectrolytes (PEs) (Herrera et al., 2023).

PEC formation is divided into three stages: primary complex formation, secondary complex arrangement, and inter-complex aggregation. The primary complex formation occurs immediately when oppositely charged PE solutions are mixed; an ionic or electrostatic

interaction is the driving force of this complexation. The formation process during this stage is extremely fast, around 5 μs (Bourganis et al., 2017) or even less (Kulkarni et al., 2016). Wu et al. (2020) have suggested that this step is an instantaneous formation causing random (primary) complex formation with significant distortion on the configuration of polymer chains. The second stage is secondary complex formation, which is formed by the self-assembly and development of existing linkages intra-complex involving the arrangement of new bonds such as hydrophobic interaction, hydrogen, and electrostatic bonds. This stage is a slower process, about an hour (Kulkarni et al., 2016), where thermodynamic rearrangement, correction of the distortion of polymer chains, and PE redistribution to obtain conformation closer to equilibrium occur during this point. Then, the final stage of PEC formation is an aggregation of secondary complexes, which is predominantly due to hydrophobic interactions and leading to the formation of larger complexes. There are three complex aggregate models: entanglement, order networks, and large fibril aggregate structures (Wu et al., 2020, Kulkarni et al., 2016). In a solution, these larger complexes (complex coacervates) cause turbid or cloudy suspension and, under certain conditions, create two-phase systems or phase-separation, i.e. supernatant liquid and precipitated PECs (Dias and Stokke, 2014).

There are two models of PEC structure: 1) lattice-like or ladder-like structure and 2) scrambled egg structure (Sim et al., 2024, Kulkarni et al., 2016) as illustrated in **Figure 1.4**. The alignment of charge brings to neutralization in a lattice-like model. However, it is not due to various mismatches from structural (charge spacing and distributions) or differences in polymer flexibility. The scrambled eggs are made from flexible polymers, and because of all the charges on the molecules, they are not accessible for electrostatic interactions for steric reasons (Sim et al., 2024, Kulkarni et al., 2016, Pergushov et al., 2012). The CS + ALG PECs do not adapt regular rod-like or toroidal morphologies (Vold et al., 2006, Schatz et al., 2004, Rinaudo et al., 1993).

In general, PEC formation is controlled by intrinsic and extrinsic variables. The intrinsic variables include type of structure of the polymers or polyelectrolytes (PE's) and their M_w. The extrinsic variables include polymer or PE concentrations, n^-/n^+, pH, ionic strength, and mixing mode. Regarding intrinsic variables, various types of PEs are found naturally or chemically synthesised with different densities, shapes, and compositions. For example, strong PEs are

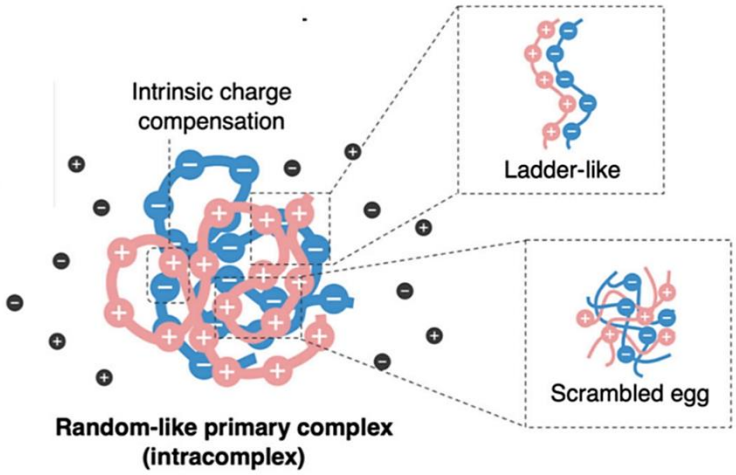


Figure 1.4. Two models of PEC structure (Sim et al., 2024).

mostly pH-independent charge, like poly-(vinyl sulphate), which tends to build aggregation with the counterparts compared to weak PEs (pH-dependent charge) like most natural polymers. Some PEs have linear structures but also branched and crosslinked structures, in the form of composition, they have homopolymers and copolymers. In general, PE's with higher M_w produce larger PECs. Higher M_w PE's have longer chains, which tend to become more interwoven or interconnected during complex formation. These can lead to increased crosslinking, resulting in denser and more entangled complexes, ultimately contributing to a larger overall structure. A study also found that when two oppositely charged PE's with essentially different M_w or degree polymerisation (DP) (around 30) are mixed, they could fabricate the most stable PECs (Wu et al., 2020), but this also depends on the medium conditions (n^-/n^+, pH, and ionic strength) which will be discussed later. Compared with single biopolymer, CS + ALG PECs exhibit lower swelling and better structural strength and mechanical stability. For instance, upon immersion in a simulated body fluid (pH 7.4), the diameter of CS samples increased 40.2% compared to CS + ALG PECs. The CS + ALG exhibits the Young's modulus of 8.167 MPa and a compressive yield strength of 0.467 MPa, compared to 2.567 MPa and 0.125 MPa for pure chitosan (Li et al., 2005). The binding ability of CS to ALG is increased by lowering the M_w of the CS and lowering the DA of the CS (George and Abraham, 2006, Li et al., 2009).

Regarding extrinsic variables, the preparation mode has an extreme impact on PEC formation. Higher concentration of PEs contributes to a bigger size of PECs due to the distance or space between PEs in solution becoming closer or diminished. In addition, with higher

concentration, the charge compensation becomes more pronounced because of more counter ions, which finally contributes to rapid charge neutralization. The effect of n^-/n^+ on the formation of PECs indicates that when n^-/n^+ is closer to 1, more reversible aggregation occurs. It is because of complete charge compensation and leads to the neutralization causing destabilization. Thus, secondary aggregation and macroscopic flocculation are developed. In contrast, as $n^-/n^+ >> 1$ OR $<< 1$, smaller PECs will be created. The charge from excess PE's gives more PEC particle repulsion. **Figure 1.5**. illustrates the complexation of PECs from two oppositely charged PEs when $n^-/n^+ \approx 1$ or $>> 1$ or $<< 1$. pH is another variable that can affect PEC formations, where the charges on both polymers will depend on how close the pH is to the pK_a or pI of the polymers.

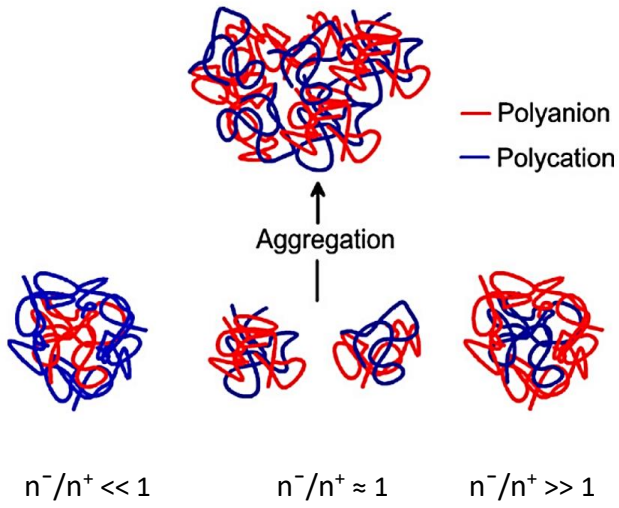


Figure 1.5. Schematic of PECs formation from cationic and anionic PE at excess and equal n^-/n^+ (Sæther et al. (2008), with slight modification)

Ionic strength also significantly impacts PEC formation. Increasing ionic strength may reduce the size of PECs due to chain flexibility (Delair, 2011). However, an ionic strength that is too high (i.e., 1.5 M) can lead to precipitation (Berger et al., 2004, Costalat et al., 2014). Kulkarni et al. (2016) stated that increasing salt concentration supports the coagulation of primary PECs to become enormous secondary PECs. However, on the other hand, the PE's shell of the PEC aggregates shrinks to a smaller one. A study using NaCl, KCl, and LiCl showed that increasing the concentration from 0 to 0.5 M escalated the size from <~90 nm to ~400

nm; however, the size dropped sharply to become soluble complexes when the salt concentration increased again due to flexibility of PE's chains (Kulkarni et al., 2016).

Lastly, the mixing mode also contributes to the PEC fabrication. Jet/flash nano complexation (FNC) or one-shot mixing gave more miniature, uniform, and better stability PECs than colloid titration (Wu et al., 2020, Qiao et al., 2018). PEs with less charge or deficient concentration should be added to the one in excess PEs to prevent aggregate formation (Yilmaz et al., 2019). However, this order of mixing applies to colloidal titration, while rapid one-shot mixing was insensitive to the order of addition (Schatz et al., 2004).

Luo and Wang (2014) studied PEC formation specifically from CS + ALG. According to their results, PECs size is determined by polymer concentrations, M_w, charge ratio (n^-/n^+ or n^+/n^-), and the process of fabrication. Smaller PEC particles were achieved at lower concentrations and lower M_w. Smaller PECs were also obtained when one of the PE's was in excess concentration or deviation from charge stoichiometry. When $n^-/n^+ \sim 1$, smaller PECs were generated initially, although these later tended to aggregate and sediment, due to charge neutralization. This precipitate could be broken up to reduce the size of the PECs again. Of course, PEC also depended on the pH of medium and ionic strength, since these factors alter the strength of the electrostatic interactions. This is in agreement with a study by Sæther et al. (2008), who investigated the effect of net charge ratio, M_w, DA of CS, guluronic acid (G) composition of ALG, mixing order, pH, speed of homogenization to the characteristics (sizes and shapes) and stability of PEC CS + ALG, as well as with finding of Yilmaz et al. (2019), who examined the influence of n^-/n^+ and mixing order on the CS + ALG PEC formation and characteristics. The results showed that the net n^-/n^+ and M_w were the most significant variables that affected the sizes and stability of PEC. However, changing the DA for CS and M/G ratio for ALG did not significantly alter the PEC properties. They were using a colloidal titration mixing technique, with CS M_w ~47 kDa – ~400 kDa (DA ~2 – ~61%) and ALG M_w ~41 – ~219 kDa (M/G ratio ~0.45 – ~1.17). The smallest PEC was indeed derived from low M_w CS and ALG. PECs with excess CS have smaller segments with spherical and round shapes, but in PECs with excess ALG, aggregates and agglomerates were observed. Higher homogenizer speed lowers the size of PECs. During incubation at pH 3 until 6.4, diameter PECs were almost constant; pH 6.4 to 6.7 increased sharply and at pH 7, they became 50x bigger than at pH ~6. The largest diameter of PEC was produced when n^-/n^+ was ~1 (stoichiometric point), > ~6 µm. Increasing

the ionic strength to 0.15 M, PEC with less reproducible structures and low stability were obtained (Saether et al. 2008). In the study by Yilmaz et al. (2019), the pH of formation was kept constant at 4. The ALG and CS M_w were ~200 kDa and ~100 kDa respectively. The mixing technique was by colloidal titration, and the PECs were characterized after ~3-5 h incubation and stirring. The dependence of sizes on the n^-/n^+ was confirmed Kulkarni et al., (2016) review and Sæther et al. (2008) results, where non-stoichiometry conditions (whether excess CS or ALG) generate smaller and steady PECs. The addition of ALG into the CS solution produced smaller and more stable PECs than the addition of CS into the ALG solution. Both mixing orders created distorted spherical shapes. CS + ALG PEC fabrication mainly uses a one-stage mixing process. There are two approaches in the one-stage mixing technique, namely colloidal titration (dropwise) and one-shot mixing. The additional process after PEC formation also have been applied, and it is impacting the PEC characteristics; for example, the CS + ALG PECs morphology was affected by freeze drying process, where this treatment made they lose the spherical shape, with instead a rough surface (Luo and Wang, 2014).

1.3.3 Previous examples of encapsulation via CS + ALG PECs

Table 1.1 Documented CS + ALG PECs for encapsulation of bioactive compounds.

Systems	Bioactive Compounds	References
CS + ALG	Ovalbumin (M_w ~ 44 kDa)	Cegnar et al. (2011)
	Doxorubicin (DOX) (M_w ~0.5 kDa)	Park et al. (2019)
	Rhodamine 6G (R6G) (M_w ~0.5 kDa)	Park et al. (2019)
	Sodium diclofenac (DFs) (M_w ~0.3 kDa)	Nikolova et al. (2021)
CS + ALG + tripolyphosphate (TPP)	Insulin (M_w ≈5.8 kDa)	Goycoolea et al. (2009)
	Stone fish BAPs (~0.8 kDa)	Auwal et al. (2024)
CS + ALG + calcium (Ca^{2+})	Insulin (M_w ~5.8 kDa)	Sarmento et al. (2007)
	Lysozyme (M_w ~14.3 kDa)	Wu et al. (2018)
	Rice bran BAPs (~1 kDa)	Liu et al. (2025)

Previous studies (**Table 1.1**) have used CS + ALG complexes as encapsulation agents, but many have also incorporated synthetic crosslinkers or gelation inducers during formation. Sarmento et al. (2007) used Calcium (Ca^{2+}), Goycoolea et al. (2009) and Auwal et al. (2024) using tripolyphosphate (TPP), both for encapsulation of insulin, and later to encapsulate BAPs derived from stone fish. CS + ALG complexes crosslinked with Ca^{2+} as a co-crosslinking agent,

to encapsulate lysozyme (Wu et al., 2018) and BAPs derived from rice bran (Liu et al., 2025). Only few studies have focused on plain CS + ALG for PECs (i.e., without any other counterions added) to encapsulate bioactive compounds. For instance, Cegnar et al. (2011), Park et al. (2019) and Nikolova et al. (2021) examined the encapsulation of ovalbumin, doxorubicin (DOX) and rhodamine 6G (R6G) (a fluorescent dye), and diclofenac sodium (DFs) respectively. Even when these preceding studies have used well characterised CS and ALG samples in regard to M_W, neither further characterisation has been provided (*e.g.*, CS´s DA or ALG´s M/G ratio) nor the role of the n^-/n^+ on the PECs formation and encapsulation efficiency, have been thoroughly investigated. These studies and the prevailing gaps of understanding, serve as background for BAPs encapsulation in this thesis.

1.3 General Overview of BAP Stability During Gastrointestinal Digestion

1.3.1. BAPs in salivary, gastric, and intestinal fluids

Previous reports mainly examined the stability of BAPs during simulated gastric and intestinal hydrolysis and ignored the salivary part. It is generally accepted that BAPs are stable when they pass across the oral cavity because salivary glands do not secrete proteases but amylase (ptyalin) and lingual lipase (Alpers, 2003, Hamosh and Scow, 1973). Even though whole human saliva may contain a few proteolytic enzymes, all of them are secreted from white blood cells and oral microbiota (Banerjee et al., 2022) and less information can be found concerning proteases produced by salivary glands and present in human saliva, and protein or polypeptide digestion in human saliva is poorly understood.

Pepsin, trypsin, chymotrypsin, carboxypeptidases, and peptidases can hydrolyse BAPs in gastric and intestinal tracts. Some BAPs appear unstable to these enzymes. For instance, the angiotensin-converting enzyme (ACE) BAPs inhibitor Tyr-Lys-Val-Pro-Gln-Leu (YKVPQL) was partially hydrolysed by pancreatin to become YKVP, then their ACE inhibition declined (Maeno et al., 1996). Also, other ACE inhibitors, YAEERYPIL and RADHPFL, were susceptible to proteolytic degradation after incubation with pepsin and pancreatic extract, and the bioactivity reduced significantly after digestion (Miguel et al., 2006). The most recent study analysed 66 different BAPs which were mapped as having 134 cleaving sites, including 13 in

the N-terminal and 48 at the C-terminal. The average M_w of unstable BAPs is 0.79 kDa, and the average chain length ≈7 amino acids (Ahmed et al., 2022).

As part of intestinal protease digestion, the brush border peptidases are also active against tri, tetra, and peptides of up to ten amino acid long. Brush border peptidases can cleave the peptides both internally (endopeptidases) and externally (exopeptidases). Lacroix et al. (2017) demonstrated 5 BAP sequences, namely LKPTPEGDL, IPIQY, LPYPY, WR, and IPI, were degraded by peptidases on the Caco-2 cell surface. The antidiabetic BAP, IPI, was the most sensitive to enzymatic hydrolysis, while dipeptide WR was the most stable. The BAP LPYPY degraded into PYPY, PYP, YPY, LP, PY, YP, and Y found in the apical side; however, only YPY, LP, YP and Y were identified in the basolateral side. The resultant bioactivity was initially reduced by 52% against DPP-IV, then became only 33%. IPIQY hydrolysed into IPIQ, IPI, IQY, IP, and PI detected on the apical side, whilst IPI, IQY, IP, and PI were discovered on the basolateral side. In this case, the bioactivity was weakened by around half.

1.4 The Special Significance of Fish BAPs

Both saltwater and freshwater fish, significantly contribute to BAP research innovation and production. Some studies categorised the source according to their environment, e.g., warm and cold-water fish. Fish contains ~15 – ~30% of protein (Ullah et al., 2022) with high essential amino acid content. In addition, a by-product from fish processing industries, especially head, skin, bone, or viscera, contain on average 30% and even more protein, but disposed of as a waste. The bioactivities of fish derived BAPs encompass antihypertensive, antioxidant, antiproliferative and anti-inflammatory, antimicrobial, immunomodulatory, and antidiabetic effects. Moreover, these bioactivities are dependent on the process of production (Ghalamara et al., 2024, Najafian and Babji, 2012, Gómez-Guillén et al., 2011).

Fish BAP production is mostly via enzymatic hydrolysis to produce fish protein hydrolysates (FPH). Enzymes that have been used for FPH production include thermolysin, alcalase, pepsin, trypsin, chymotrypsin, pancreatin, flavourzyme, pronase, neutrase, papain, bromelain, orientase, cryotin F, protease N, and protease A (Ghalamara et al., 2024; Ortizo et al., 2023, Ishak and Sarbon, 2017; Ahmed et al., 2022). Most research has tried to optimise FPH production via setting the hydrolysis conditions such as pH, temperature, time, or enzyme activity. Separation, fractionation, and purification are required to improve specific activity.

Separation, fractionation, and purification techniques generally use membranes (Ortizo et al., 2023, Halim et al., 2016). Separation is carried out with nanofiltration (NF) membranes to concentrate the hydrolysates or using membrane ultrafiltration (UF) with a molecular weight cut off (MWCO) typically 20 – 100 kDa to separate hydrolysed, and non-hydrolysed protein and the proteolytic enzymes. Fractionation usually uses UF membranes with MWCO ≈ 4 – 8 kDa to collect specific hydrolysate fractions or to enrich particular M_w hydrolysates. Purification is conducted with gel filtration or flash performance liquid chromatography (FPLC) to typically obtain short-chain fish BAPs ($M_w \leq 3$ kDa). UF membranes with MWCO 3 kDa are also available to purify low M_w fish BAPs ≤ 3 kDa from the higher M_w (> 3 kDa). Multiple studies have identified the sequences of purified BAPs using liquid chromatography-mass spectroscopy (LC-MS) (Wang et al., 2024, Gao et al., 2021, Ishak and Sarbon, 2017).

1.4.1 Fish BAPs as antihypertensive agent via angiotensin converting enzyme (ACE) inhibition

Hypertension is a severe cardiovascular disease that, according with data of the World Health Organisation, affects ~1.3 billion of adult populations globally; ~80% of the affected people live in low and middle-income countries, and ~46% of them do not know they suffer from this condition (WHO, 2023). Therefore, hypertension has been regarded a “silent killer”. Numerous antihypertensive BAPs have been identified from fish muscle and by-products, with capacity to inhibit the activity of angiotensin converting enzyme (ACE). ACE is an enzyme that has a crucial role in converting angiotensin I into angiotensin II and bradykinin into inactive fragments causing vasoconstriction and thus increasing blood pressure (**Figure 1.6**).

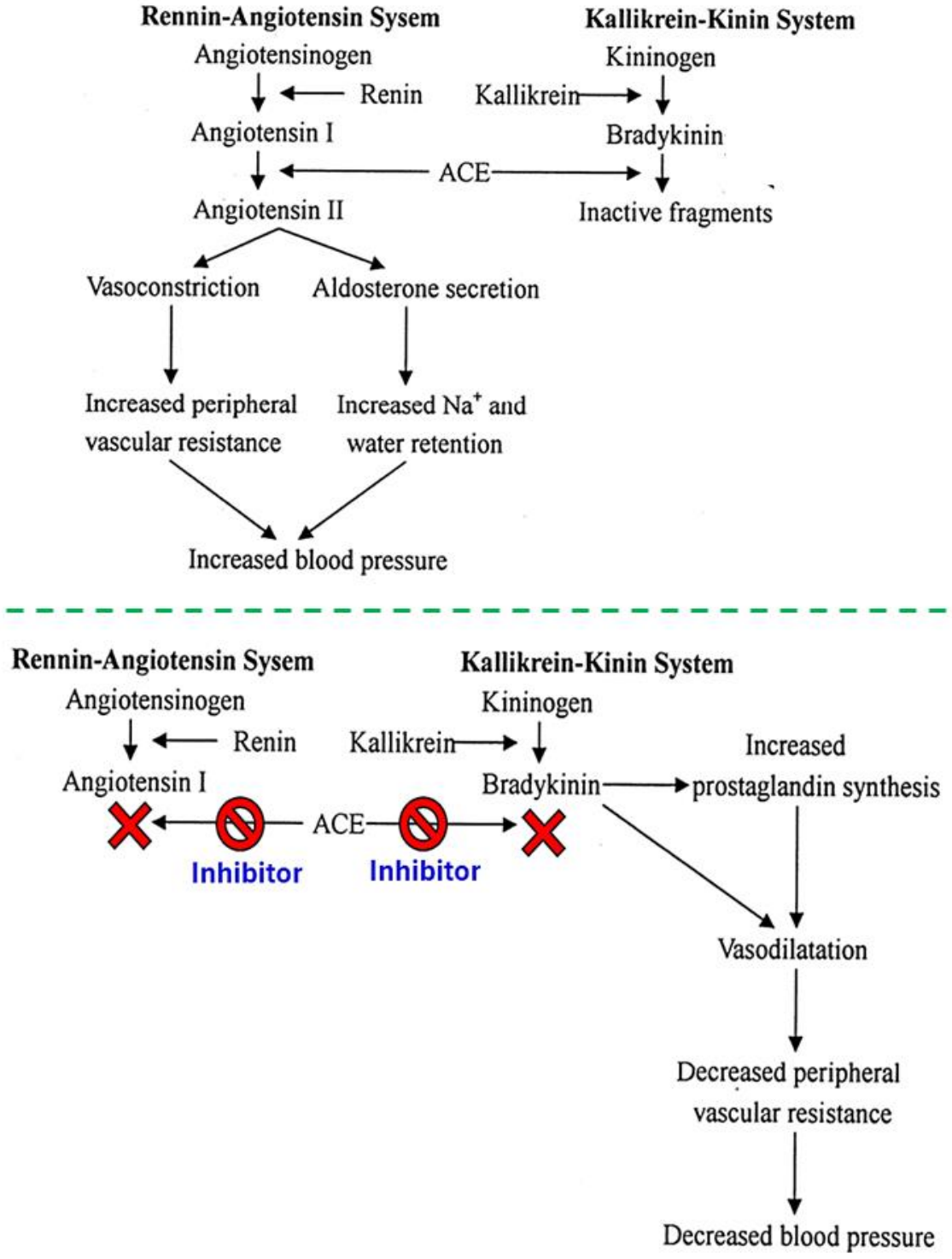


Figure 1.6 Mechanism of blood pressure increasing by the role of ACE enzyme (top) and blood pressure decreasing by ACE inhibitor (bottom) (Li et al., 2004 with modifications).

High ACE inhibition bioactivity of BAPs has been derived from striped snakehead (Channa striata) , pacific cod (*Gadus macrocephalus*) (Himaya et al., 2012), skipjack (*Katsuwonus pelamis*), Alaska pollock (*Theragra chalcogramma*), bonito fish (*Sarda spp*.), marine cobia (*Rachycentron canadum*) skin, catfish (*Clarias batrachus*), and tilapia (*Oreochromis niloticus*) (Lin et al., 2019, Toopcham et al., 2015, Ghassem et al., 2012, Byun and Kim, 2001, Fujita et al., 2000). Among them, bonito fish is among the species that produces the strongest ACE inhibitory activity. The sequences derived from bonito fish with ACE inhibitory activity include LKPNM, LKP, IY, IKP, IWHHT, and IWH (Xue et al., 2021). The presence of aliphatic amino acids like leucine (L) and methionine (M) increases the ACE inhibitory activity (Ghassem et al., 2011, Nasri et al., 2013). Furthermore, the BAPs with hydrophobic amino acids, especially proline (P), showed a correlation to the ACE inhibition activity (Hou et al., 2023, Zhang et al., 2020).

Measuring the bioactivity of BAPs as ACE inhibitors can be conducted via *in vitro* or *in vivo* studies. *In vitro* methods are simple and effective, and they offer an alternative to the use of animals as experimental models. Also, they entail fewer variables which may interfere with the assays. The synthetic substrates for *in vitro* ACE inhibition are *N-hippuryl-L-histidyl-L-leucine* (HHL) and *N-[3-(2-furyl)acryloyl]-L-phenylalanylglycylglycine* (FAPGG). Conversion of HHL and FAPGG by ACE results in the formation of *hippuric acid* (HPA) (Cushman and Cheung, 1971) and *furanacryloyl-L-phenylalanine (FAP)* (Murray et al., 2004, Anzenbacherova et al., 2001), respectively. All the substrates and products can be detected at ultraviolet (UV) wavelengths and measured via spectroscopy or chromatography methods. Many studies have used HHL because it has various reference options and is well-documented. In addition, it costs 50% less and up to 25 times less than FAPGG and angiotensin I, respectively (Ben Henda et al., 2013).

1.5 Principle of The Various Characterisation Techniques Used in This Thesis

1.5.1 Dynamic light scattering (DLS) and ζ-potential

DLS, photon correlation spectroscopy (PCS), or quasi-elastic light scattering, is a powerful technique for measuring the diffusion coefficient of macromolecules or particles in a liquid suspension, which can then be linked to their hydrodynamic size (hydrodynamic

radius, R_h). Colloidal particles in suspension are not stationary but diffuse randomly due to Brownian motion (*i.e.*, due to collisions with neighbouring solvent molecules). Hence, when a monochromatic laser beam of light encounters a solution containing particles, the radiated light will scatter in all directions, and its intensity fluctuates due to constructive/destructive interference derived from the scattering phenomena. The net intensity of the scattered light fluctuates more rapidly for the smaller particles due to their faster movement. An autocorrelator quantifies the intensity fluctuations of the scattered light with time (Stetefeld et al., 2016). Stokes-Einstein equation and the correlation function can be related to the translational diffusion coefficient (D) of the particles (Stetefeld et al., 2016, Pusey, 1974). D in turn can be related to R_h via the Stokes-Einstein equation and define the terms (R_h=particle size, η=viscosity of the surrounding fluid, k= the Boltzmann constant= 1.380649×10^{-23} J K^{-1}, T=temperature). Obviously, if the actual particles one not spherical, then the calculated R_h may not reflect the actual particle dimensions.

The Malvern Zetasizer® is a popular DLS instrument with 4 mW He-Ne laser λ 633 nm. The measurement is employed at a 90° standard angle or 173° backscatter angle detector. Detection at backscatter (173°) can neglect the scattering contribution from the rotational diffusion effect that might be observed in autocorrelation profiles. In addition, backscatter can minimize multiple scattering of light by more concentrated samples since light does not travel through the entire sample in the cuvette (Bhattacharjee, 2016, Amin et al., 2014).

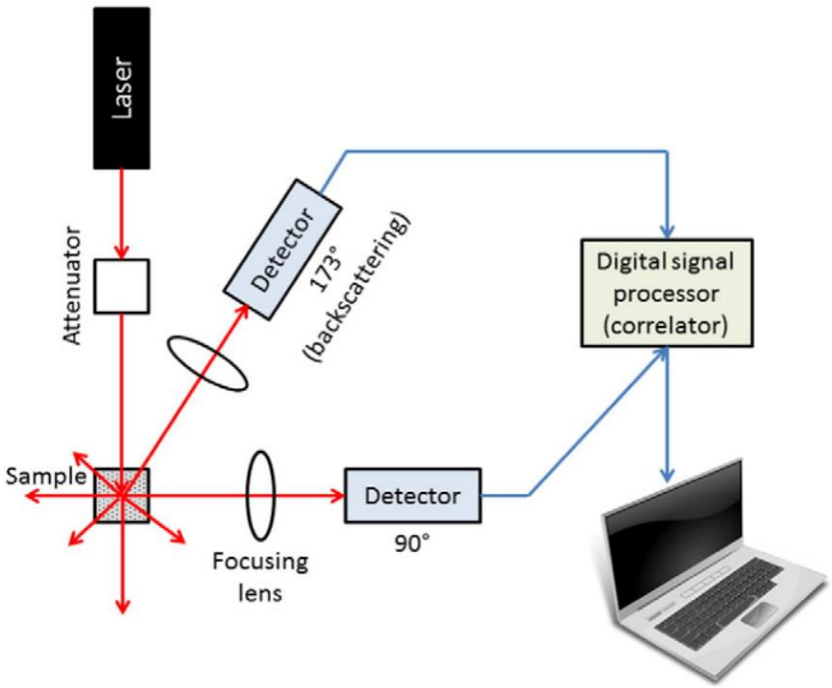


Figure 1.7. Schematic of DLS instrumentation (Bhattacharjee, 2016).

Regarding sample concentration, high concentration results in multi-scattering, where scattered light from one particle interacts with others before reaching the detector and loses intensity. On the contrary, samples that are too dilute do not guarantee enough scattered light to analyse (Bhattacharjee, 2016).

The ζ-potential is an important parameter that can help to predict the colloidal stability of the particles. The net electrical charge at the surface of particles conferred by the presence of ionised groups and counterions. The distribution of counterions near a highly charged surface develops into two regions: inner and outer layers (Kaszuba et al., 2010). These two regions are also called electrical double layer (EDL) (Montes Ruiz-Cabello et al., 2014). The inner layer contains ions with a charge opposite to the particle. This layer is closer to the particle's surface, also called the Stern layer, and comprises firmly associated ions. At the same time, the outer layer consists of the same and opposite charge ions because of the electrostatic field of the charged particles. This layer, also known as the diffuse layer, comprises weakly associated ions (cations and anions) that move together with the particle. The charge composition in the diffuse layer is dynamic and varies, influenced by factors such as pH, ionic strength, and concentration (Bhattacharjee, 2016). **Figure 1.8** illustrates the

schematic EDL of a dispersed particle. The ζ-potential is the electrostatic potential at the slipping plane, within this plane the ions move into the particle.

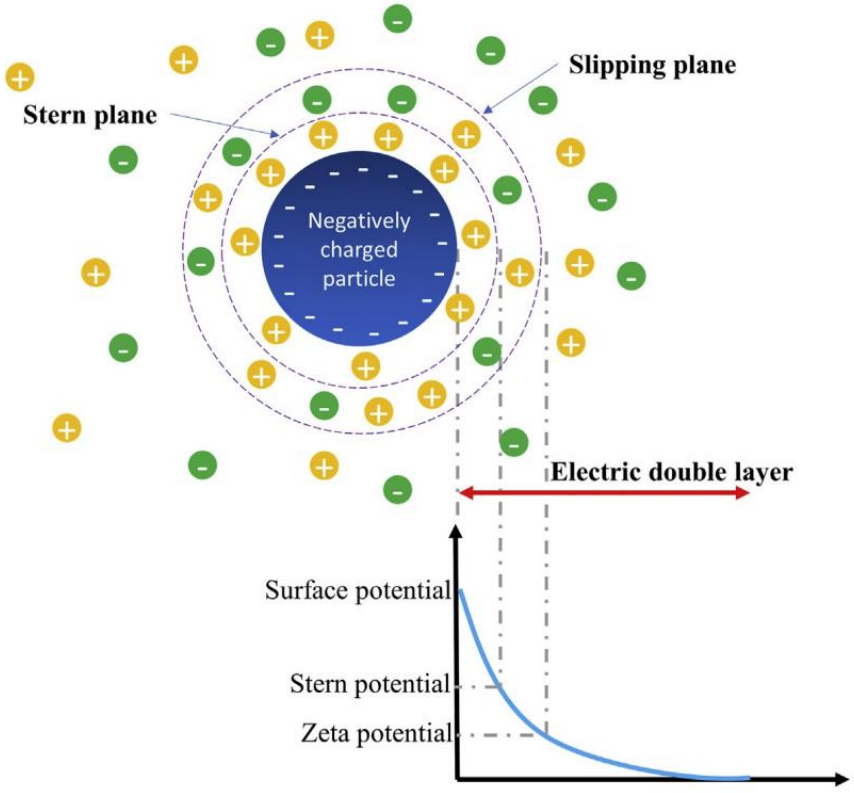


Figure 1.8. A model and diagram for electrical double layer (Feng et al., 2020).

ζ-potential cannot be measured directly. It is deduced from the electrophoretic mobility measured under an applied electric field. The electrophoretic mobility (μe) is calculated as:

$$\mu_e = \frac{V}{E} \qquad (1.2)$$

Where, v = particle velocity (μm/s), and E = electric field (volt/cm).

Then, Henry's equation used to quantify ζ-potential as explain on the below formula:

$$\mu_e = \frac{2\,\varepsilon_T \varepsilon_0\, \zeta\, f(ka)}{3\eta} \qquad (1.3)$$

Where, ε_T is relative permittivity/dielectric constant, ε_0 = permittivity of vacuum, ζ is ζ-potential, f(ka) is Henry's function, and η is viscosity at experimental temperature.

In cases where the thickness of the EDL smaller than size of the particles, the Henry equation becomes Helmholtz-Smalouchowski equation where the value of f(ka) is taken as 1.5. When the thickness EDL is more significant compared to particle (for smaller particles, < 100 nm), f(ka) = 1, and Henry's equation is modified into Huckel equation. Each equation is described below:

Helmholtz-Smalouchowski equation:

$$\mu_e = \frac{\varepsilon_T \varepsilon_0 \zeta}{\eta} \qquad (1.4)$$

Huckel equation:

$$\mu_e = \frac{2\,\varepsilon_T \varepsilon_0 \zeta}{3\eta} \qquad (1.5)$$

An instrument frequently used for ζ-potential measurement is electrophoretic light scattering, using mixed-mode phase analysis light scattering (M3-PALS). This technique is used with DLS from Malvern Zetasizer, where a disposable plastic (polycarbonate) cuvette with capillary gold plate copper electrodes and a bent capillary tube to hold around 0.75 mL sample solution is used. During the instrumentation, initially, the laser beam is split into two directions, one towards the sample and the other one used as a reference. Later, these two beams are optically mixed to determine the Doppler shift, which then deduces particle velocity (V) (Feng et al., 2020, Bhattacharjee, 2016, Patel and Agrawal, 2011).

1.5.2 High performance liquid chromatography (HPLC)

Chromatography is a technique of separating components in a mixture based on the distribution of components between the two phases, the stationary phase in the form of solid or liquid and the mobile phase in the form of liquid or gas, known as liquid or gas chromatography, respectively. There are two types of liquid chromatography: planar (paper and thin layer) chromatography and column chromatography. Column chromatography uses a column (cylindrical glass or plastic tube) to separate components in a mixture, equipped with a faucet or output section under the column to control the liquid flow (mobile phase). Longer and narrower columns enhance resolution and separation. Regarding the separation mode, column chromatography was grouped into gel filtration, ion exchange, and affinity chromatography. Gel filtration is separating molecules based on their molecular sizes using porous gel/media as a stationary phase. It is also known as size-exclusion chromatography

(SEC). Ion-exchange chromatography separates the molecules based on their charge, where an ionic molecule (cationic or anionic) covalently binds with the resin as a stationary phase. Affinity chromatography is separation based on interaction specific between the stationary phase and the molecules in the mobile phase, like the interaction between ligands with protein, DNA, hormone, or antibody with antigen (Ismail and Nielsen, 2010).

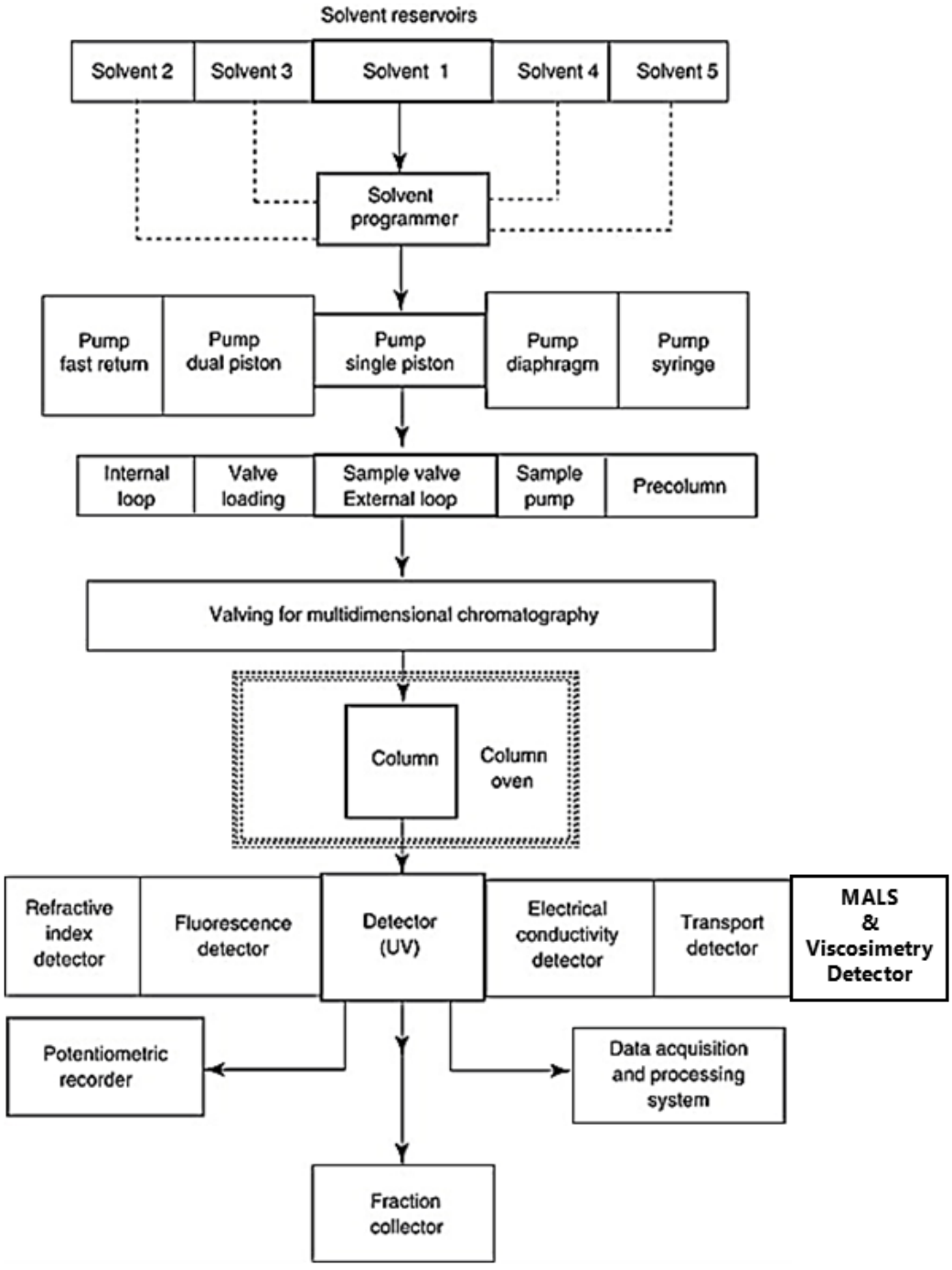


Figure 1.9. Diagram a modern liquid chromatography (Scott, 2005).

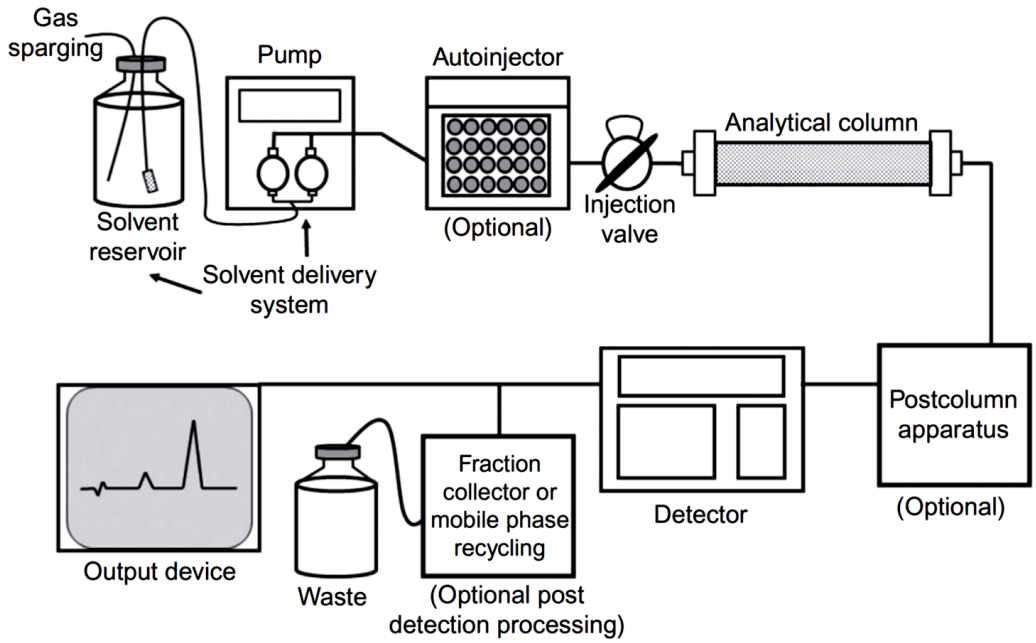


Figure 1.10. Schematic HPLC systems (LaCourse and LaCourse, 2017).

High-performance liquid chromatography (HPLC) as shown in **Figure 1.10** is fundamentally a cutting-edge development of column chromatography. The stationary phase is generally a solid chemical bound or trapped in a column, and the liquid phase is a solvent that can manipulated by setting the compositions. In simple understanding, HPLC is distinguished from the predecessor liquid chromatography by solvent dripping, which used to drip through the column under gravity but is now propelled through high pressure. In HPLC, samples are compressed into columns with heat or temperature settings (oven), and the surface area of sample particles is increased to obtain high-performance separation. It offers less destructive analysis, and the analytical process can be performed at room temperature (LaCourse and LaCourse, 2017, Reuhs and Rounds, 2010). In addition, the HPLC can be used for non-volatile and volatile compounds with good solubility (Cohen et al., 2012).

In relation to the type of mobile and stationary phases, the HPLC is divided into normal-phase HPLC (NP-HPLC) and reverse-phase HPLC (RP-HPLC). The NP-HPLC uses polar stationary and non-polar mobile phases such as hexane, while the RP-HPLC uses non-polar stationary and polar mobile phases. The most popular stationary phase of RP-HPLC is C18 or $[CH_2]_{17}CH_3$. However, there are several options for the stationary phase here starting from low polarity, including C8 ($[CH_2]_7CH_3$), C4 ($[CH_2]_3CH_3$), CH_3, C≡N, and phenyl group bounds in the

silica particle. The silica particles are primarily spherical, but irregular shapes are also available, with particle sizes ranging from around 3 – 10 µm (Lozano-Sánchez et al., 2018, Reuhs and Rounds, 2010). RP-HPLC is ideal for separating samples of M_w <2 kDa or small proteins and peptides (Jadhao et al., 2022) but not ideal for heterogeneous compounds that are very hydrophobic or too hydrophilic, inorganic ions, or stereoisomers. The mobile phase in RP-HPLC is water or water + polar organic solvents. The organic solvents should be water miscible, low ultraviolet (UV) detectability, low viscosity, and non-reactive. Some examples of polar organic solvents starting for higher polarity are CH_3OH (methanol), CH_3CN (acetonitrile), and tetrahydrofuran (THF). Lowering the polarity of the mobile phase should increase their elution power. Molecules with higher polarity have lower retention time (RT), and vice versa; compounds with low polarity or high hydrophobicity have longer RT. The compounds with longer and saturated chains also have higher RT (Lozano-Sánchez et al., 2018, Reuhs and Rounds, 2010).

In case of poor separation, the mixture of components is eluted and come out together, and then the chromatogram of HPLC will show broad peaks rather than sharp peaks. This phenomenon is also called the band broadening or broadening effect. This condition results in the inaccurate quantification of particular components after separation, which may be caused by unsuitable mobile phase solvent components or the age of the column. The Van Deemter Equation explains the broadening effect as a function of several factors described by the equation below:

$$H = A + (B/u) + (C \times u) \qquad (1.6)$$

Where H = broadening effect (refers to the height equivalent to a theoretical plate, which the lower value of H the better performance of the column), A = multipath/eddy diffusion, B = longitudinal diffusion, C = mass transfer, and u = linear flow rate. Multipath or Eddy diffusion (A) is when the same molecules follow different paths when passed through packed bed stationary particles. Molecules with the shortest path would move through the column quickly; on the contrary, molecules with the longest path would slowly move through the column. This difference in the time set of molecules reaching the detector or elution time will get a broadened peak. Longitudinal diffusion (B) is a situation where a set of molecules experiences diffusion from tightly compact particles (more concentrated) to less compact particles (less concentrated particles) when passing through the column. Longitudinal

diffusion increases with the flow rate reduction (u): mass transfer (C) or stationary phase mass transfer caused by the nonuniformity surface area of stationary particles. Increasing porosity of stationary phase particles leads to slower movement of molecules in the column, causing significant discrepancies with other molecules. This situation is escalating as the flow rate increases. Several approaches are possible to minimize band broadening. For instance, multiphase diffusion should be minimal if a packed column, smaller, uniform size, and distribution of stationary particles were selected. In addition, the longitudinal diffusion may be reduced by setting an optimal flow rate (not too high or too low), appropriate column length, and minimal column with a small diameter. Furthermore, the mass transfer might diminish by choosing smaller stationary particles, heating the column, which can keep uniform porosity bound, and manipulating the flow rates to become not too high (Lozano-Sánchez et al., 2018).

1.5.3 Small angle X-ray scattering (SAXS)

When a well-collimated beam of X-rays radiation incident on a given material sample, most of the incident radiation is transmitted through the sample. A fraction of the radiation interacts with sample and is scattered at an angle $\theta > 0$, while a fraction of the energy is transferred between the sample and the incident beam. A detector is used to measure the scattering intensity (I) as a function of θ, which is expressed as a scattering vector (q) -see below-(**Figure 1.11)**. In contrast to light scattering that works at angles in the range of 30 – 135°, in SAXS technique the measurements are recorded at very small angle (<10°). Importantly, in X-ray scattering, the contrast is due to differences in electron density, and not due to an increment in refractive index in light scattering. SAXS can be used to determine the structure of nanoparticles (Apostolidis et al., 2023) in terms of average size, shapes, porosity, orientation, internal structure, and crystallinity (Schnablegger and Singh, 2013). SAXS can resolve the particle or structure size ranging from 1 – 100 nm. The resolution of SAXS experiment can be extended by measuring at a smaller (ultra SAXS) or larger angle (wide-angle) of X-ray diffraction. The latter, also known as wide-angle X-scattering (WAXS), is capable of measuring an atomic resolution of 0.1 – 1 nm (Han et al., 2024).

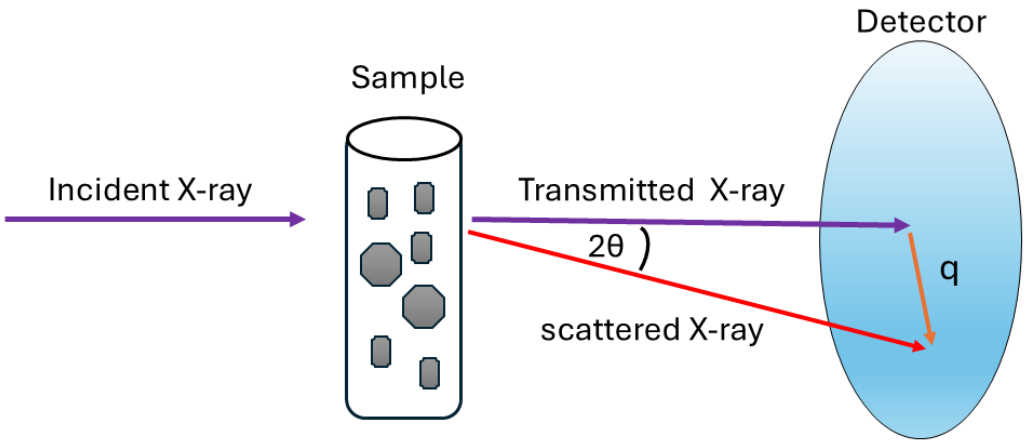


Figure 1.11. Correlation between incident X-ray, scattered angle (θ), and scattering vector (q) (adopted from Skou et al. 2014).

Generally, the SAXS instrument consists of several components, including an X-ray source, collimator systems, sample stage, beam stop, and detector. The collimator function directs and shapes the X-ray beam to focus to the sample and prevents scattering from other parts of the beam except the sample. When the scattered waves constructively interfere, the angle between the incident and scattered beam is assumed equal to 2θ. The magnitude of the *q* scattering vector can be quantified based on an equation derived from Bragg Law theory. Equations 1.7 and 1.8 below explain the correlation between Bragg's Law and *q*. The scattering intensity *I* expressed as a function of *q,* once the relevant calibration, corrections, normalisations and data substructions are applied, they enable to analysing the data against the appropriate structural models to obtain physically meaningful structural parameters. For instance, the radius of gyration (Rg) can be derived via the Guinier plot, or the degree of compactness via the Kratky plot (Schnablegger and Singh, 2013, Porod, 1982).

Bragg's Law:

$n\lambda = 2d \sin\theta$ (1.7)

Where, n is diffraction order, λ is wavelength of incident X-ray, *d* is spacing between crystal plane, θ is diffraction angle. Because $d = \frac{2\pi}{q}$, and for first order diffraction n=1. The scattering vector (q) formula is:

$q = \frac{4\pi}{\lambda} . \sin\theta$ (1.8)

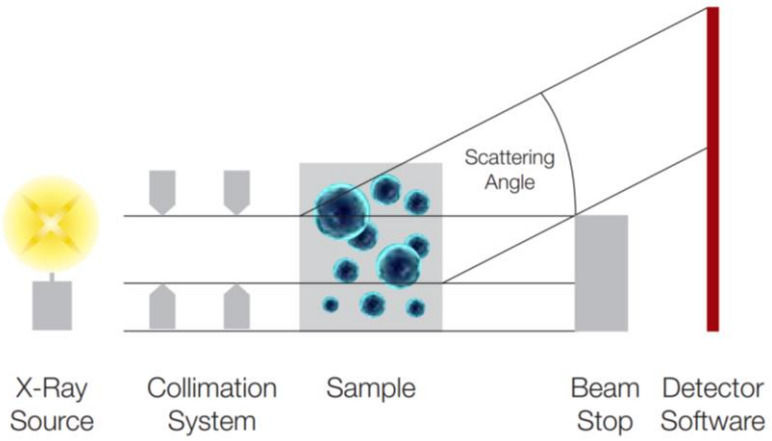


Figure 1.12. SAXS compartment (Schnablegger and Singh, 2013).

1.5.4 Transmission electron microscopy (TEM)

TEM can be used to image structures well below 1 µm in size. In this thesis, TEM was performed to investigate the size and morphology of selected CS + ALG PECs. TEM uses beams of highly energetic electrons to create images after interacting with material or specimen. The electrons that hit the material are scattered, absorbed, transmitted, diffracted, or unaffected. Hence, in TEM, the scattered (forward scattering: elastic and inelastic) and transmitted electrons are then focused by the lens to create a magnified image projected from the material. **Figure 1.12** illustrates the signal generated from the interaction of a high-energy beam of electrons with a thin specimen material. The TEM uses a vacuum system for the instrumentation because oxygen also allows electrons to scatter and even oxidize (Klang et al., 2012, Egerton, 2005). This means that samples are effectively dehydrated, and this can generate artefacts.

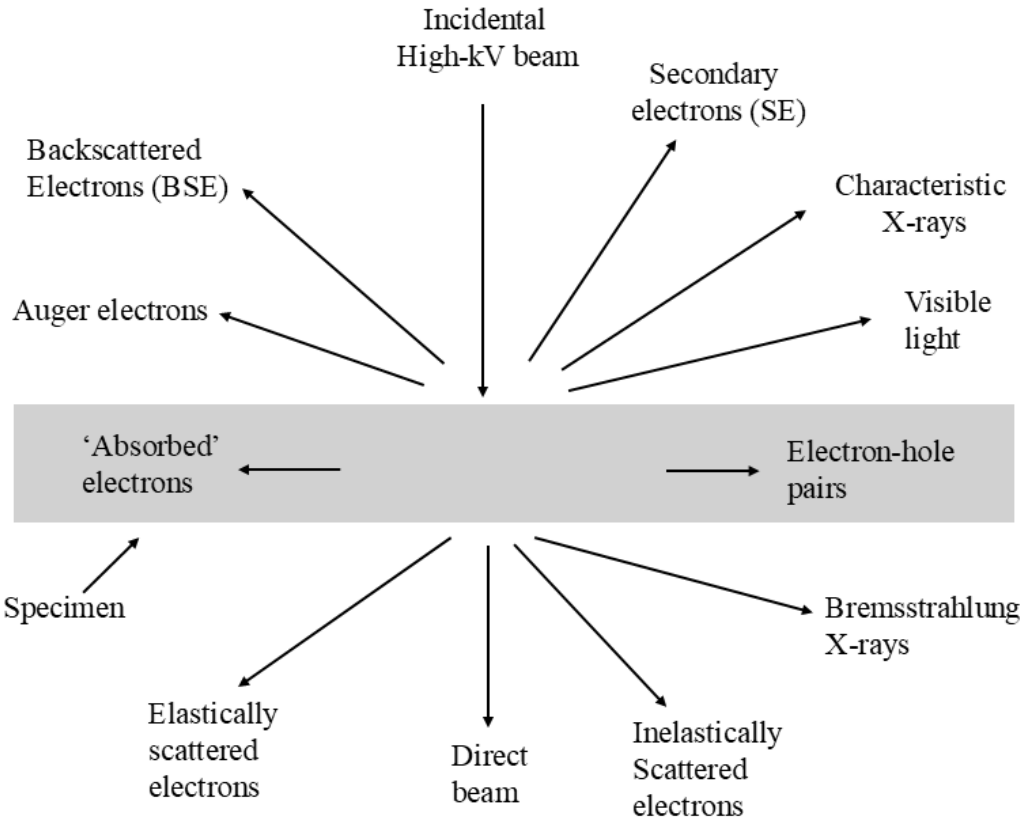


Figure 1.13. Signals generated when high energy beam of electrons interacts with thin sample or specimen (adopted from Williams and Carter, 2009).

Figure 1.13 illustrates the essential components of a modern TEM instrument. The electrons in TEM can be detected in several ways, including fluorescent screens, photographic film, CCD (charge-coupled device) cameras, and DEDs (direct electron detectors) (Egerton, 2005). The CCD camera is currently the most widely used to acquire TEM images, and it is a multi-step process based on photon generation by the scintillator when electrons come. After that, the photon travels down to the optical fibres, and the CDD chip reads the signal (Inkson, 2016, Fan and Ellisman, 1993).

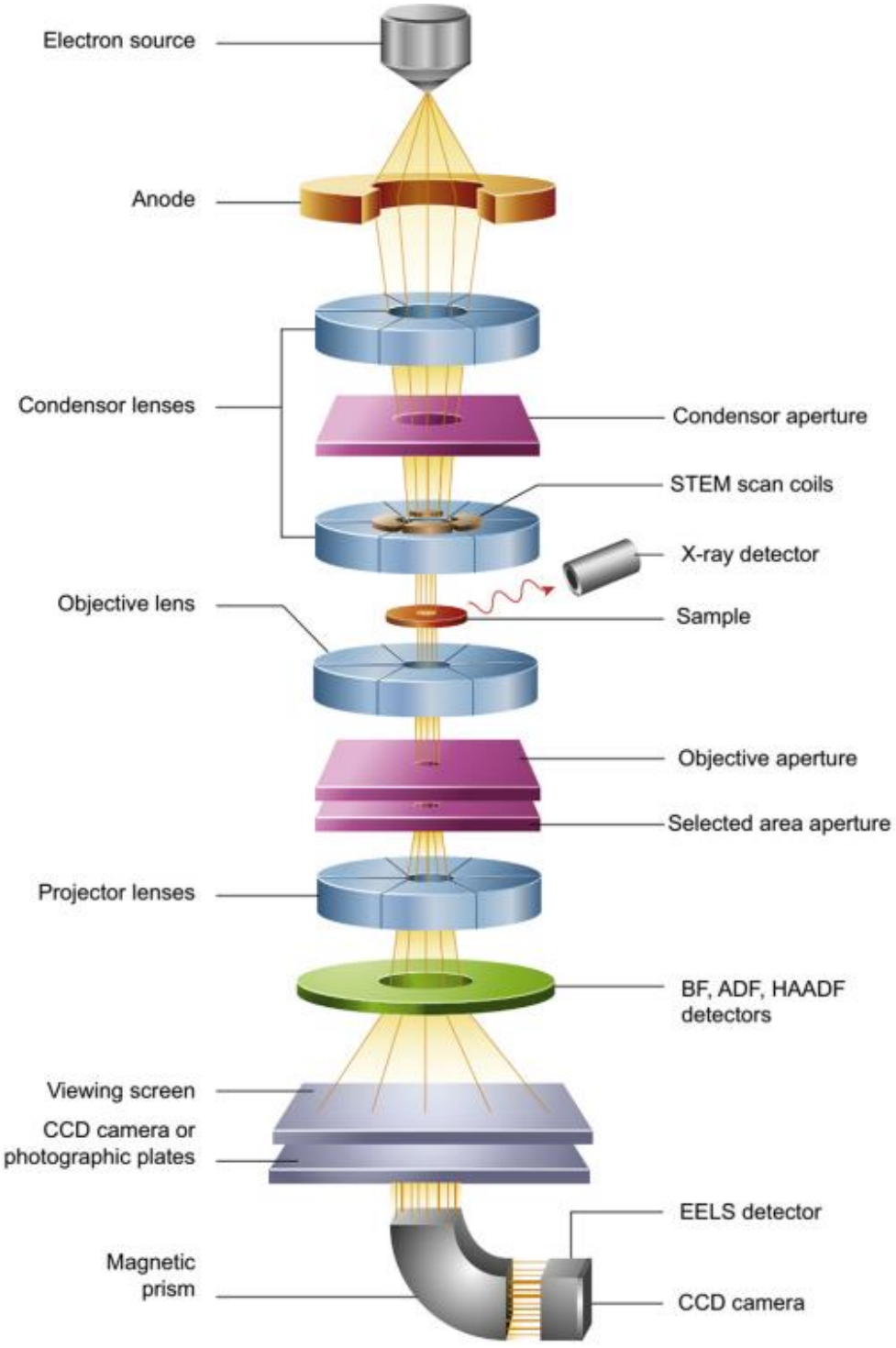


Figure 1.14. Schematic diagram of transmission electron microscopy (TEM) (Yadav et al., 2022).

1.5.5 Fourier-transform infrared (FTIR) spectroscopy

Infrared spectroscopy studies the interaction between matter and infrared (IR) radiation. Matter absorbs specific energy levels corresponding to different vibrational frequencies. Generally, there are two vibration modes of the covalent bond in the molecules: stretching (symmetric and asymmetric) and bending (scissoring, wagging, rocking, and twisting) vibrations. The molecules' bonds absorb a certain amount of energy to induce those vibrations that correspond to the wavelength found in the IR range. The IR radiation is divided into near IR (NIR), mid-IR (MIR), and far IR (FIR). FT-IR is a specific type of infrared (IR) spectrometer that measures the spectrum of light (light intensity) as function of the reciprocal of the wavelength, called wavenumber ($\bar{\nu}$) which is commonly expressed in reciprocal centimetres (cm^{-1}) (Smith, 2011).

The bands in an FT-IR spectrum, either in transmittance or absorption, are not linearly proportional to the concentration; therefore, they are not used for quantitative analysis but for the fingerprint of a compound or qualitative analysis. The band position in an FT-IR spectrum uniquely correlates with molecular structures; hence, it can be used to identify and compare unknown samples with the references (Smith, 2011). FT-IR can also be used for material identification, contamination, polymer modification, or complexation (Shukla, 2025). It has also been used to determine the degree of acetylation of chitin and chitosan (Brugnerotto et al., 2001).

1.5.6 Density and viscosity

In this thesis the density of the samples was measured via a modern digital density meter with a Y-oscillator as a sensor. It is a standard U-tube sensor that bends and moves up and down, and the setup allows precise temperature regulation via Peltier elements. This type of density meter sensor is very sensitive and allows exact measurement due to counter mass, which can reduce parasitic resonance (external oscillations). According to Fitzgerald (2000), the U-tube oscillates at its fundamental frequency related to the system mass. The correlation between oscillation frequency, volume of sample, and density is explained by the formula below:

$$\tau = 2\pi \frac{\sqrt{\rho V + m}}{C} \qquad (1.9)$$

Where τ is oscillation period, ρ is sample density, v = cell volume, m= cell mass, and c=spring constant. Then, according to the above formulation, the correlation between density of a fluid-filled and corresponding oscillation period simplified to become:

$$\rho = \tau^2 - H/G \qquad (1.10)$$

H and G are instrument constants, $G = \frac{4\pi^2 V}{C}$, and $H = \frac{4\pi^2 m}{C}$

Dynamic viscosity (η) is defined as the ratio of shear stress (σ) to shear rate ($\dot{\gamma}$). The unit for dynamic viscosity is Pascal-seconds (Pa·s) or measured in centipoise (cP) for low-viscosity liquids (Kulicke and Clasen, 2004). This study measured the viscosity of supernatants after complexation to estimate the degree of complexation and dissociation (release) between CS, ALG, and fish BAPs. The viscosity measurement was performed with a micro-viscometer (μ-VISC). Micro-viscometer is a viscometer on a chip device that uses a rectangular slit flow technique. This microfluidic viscometer drives fluid along a narrow rectangular microchannel at a controlled flow rate. The shear stress is calculated from pressure drop (measured with sensors along the channel) and shear rate derived from velocity profile (inside the rectangular slit) to determine fluid viscosity. The advantages of a micro-viscometer include a minimum amount of sample (≈ 100 μL), the detection of a wide range viscosity (1 – 3500 cP), and wide temperature setting (18 – 40 ^{o}C), as well as quick testing time (< 1 min) (Zidar et al., 2020).

1.5.7 *In vitro* gastric and intestinal digestion

In vitro digestion models are frequently used to simulate human digestion since in vivo and human studies are incredibly costly, time-consuming, and ethically challenging. However, various in vitro models lacked consistency in the methodologies to represent human digestion conditions. For instance, they used different types of enzymes and sources, enzyme activity and ratio, pH, digestion time, salt compositions, and temperature. Consequently, these bring inconsistency and highly variable digestion results. Thanks to previous studies that tried to introduce and harmonise a standard static in vitro digestion protocol that is physiologically relevant to human digestion (Egger et al., 2016, Minekus et al., 2014). Besides providing a reproducible method, the protocol, also known as INFOGEST, is an abbreviate for International Network on Food Digestion and has been widely applicable, easy to implement, and cost-reducing. The current protocol (INFOGEST 2.0) has been updated and outlined detailed variables of each digestion parameter during gastric and intestinal simulation by eliminating

inconsistency (enzyme, salts, temperature, pH, time, etc.) and guiding the experiment's procedure (Brodkorb et al., 2019).

1.6 Outline of The Thesis

The thesis is organised in a total of six chapters, the contents of which are described next.

Chapter 1 General introduction.

Chapter 1 is a general introduction to bioactive peptides (BAPs), the polyelectrolyte complexes (PECs) based on chitosan (CS) and alginate (ALG), and their applications for BAPs encapsulation. Also, the fundamental principles of the major techniques used to characterize such systems are described.

Chapter 2 Literature review: state of the art research on encapsulation short BAPs.

This chapter reviews critically and discusses the state of art on encapsulation of short-chain BAPs, most of which have sequences of less than ten amino acids and entail particular challenges for their oral delivery. The different encapsulation approaches and delivery vehicles are addressed, namely nanoparticles or microparticles, along with wall materials. The characteristics of delivery vehicles upon BAPs loading, such as average size, stability, encapsulation efficiency (EE), morphology, permeability, cytotoxicity, and BAPs release and bioactivity, have also been reviewed and examined critically, particularly for the methods. The last section of this chapter delves into the pros and cons of those delivery vehicles for BAPs, as well as future challenges and opportunities in developing encapsulation technology for food, nutraceutical, and supplement applications. A paper has been published based on this review Chapter: *Atma, Y., Murray, B.S., Sadeghpour, A., Goycoolea, F.M. 2024. Encapsulation of short-chain bioactive peptides (BAPs) for gastrointestinal delivery: a review. Food & Function, 15, 3959-3979.*

Chapter 3 Development and characterisation of chitosan-alginate polyelectrolyte complexes (PECs) for encapsulation peptide derived from fish.

Chapter 3 entitled “Development and characterisation of chitosan-alginate polyelectrolyte complexes (PECs) for encapsulation peptide derived from fish” investigates the

formation and application of PECs formed from chitosan (CS) and alginate (ALG) for encapsulation of BAPs. The BAPs are fish origin with short sequences (less than ten amino acids). The purification of BAPs was conducted using a UF membrane. PECs were then prepared precisely (including density measurement after filtration) according to the n^-/n^+ calculation, followed by their characterization using DLS for size and polydispersity, M3-PALS for ζ-potential and stability, SAXS, and viscosity measurements to probe the structure and extent of complexation, respectively. The selected PECs were then loaded with fish BAPs, and the encapsulation efficiency (EE) and BAP release at gastric or intestinal pH were quantified using HPLC-UV. The characteristics of PECs before and after loading were also compared. In addition, selected loaded PEC of $n^-/n^+ < 1.0$ (excess CS) were also examined by TEM imaging to probe their morphology. A paper has been published based on the contents of this Chapter: *Atma, Y., Sadeghpour, A., Murray, B.S., Goycoolea, F.M. 2025. Chitosan-alginate polyelectrolyte complexes for encapsulation of low molecular weight fish bioactive peptides. Food Hydrocolloids, 160, 110789.*

Chapter 4 Chitosan-alginate PECs loaded with fish BAPs: an in vitro digestion study.

This chapter focuses on CS + ALG PECs loaded with BAPs. The in vitro release profile of BAP during *in vitro* gastric and intestinal digestion is examined. The static digestion simulation was conducted according with the INFOGEST protocol, and the characteristics of the PECs were compared in conditions between when added with enzymes (proteases + salts) or without them (i.e., only salts). The stability during storage at room temperature were also studied via FT-IR spectroscopy, DLS and M3-PALS. Release of fish BAPs was identified via HPLC-UV, and bioactivity confirmed via inhibition of angiotensin-converting enzyme (ACE). The manuscript is also presented in the format of a publication draft encompassed by all its sections.

Chapter 5 General discussion.

This chapter is a general discussion of the main results of this thesis and highlights the various results and how it has contributed to the various knowledge gaps.

Chapter 6 Conclusion and possible future work.

1.7 References

Abasalizadeh, F., Moghaddam, S. V., Alizadeh, E., Akbari, E., Kashani, E., Fazljou, S. M. B., Torbati, M. & Akbarzadeh, A. 2020. Alginate-based hydrogels as drug delivery vehicles in cancer treatment and their applications in wound dressing and 3D bioprinting. *J. Biol. Eng.* 14**,** 1-22.

Aguilar-Toala, J. E., Quintanar-Guerrero, D., Liceaga, A. M. & Zambrano-Zaragoza, M. L. 2022. Encapsulation of bioactive peptides: a strategy to improve the stability, protect the nutraceutical bioactivity and support their food applications. *RSC Adv.* 12**,** 6449-6458.

Ahmad Raus, R., Wan Nawawi, W. M. F. & Nasaruddin, R. R. 2021. Alginate and alginate composites for biomedical applications. *Asian J. Pharm. Sci.* 16**,** 280-306.

Ahmed, T., Juhász, A., Bose, U., Shiferaw Terefe, N. & Colgrave, M. L. 2024. Research trends in production, separation, and identification of bioactive peptides from fungi – A critical review. *J. Funct. Food.* 119**,** 106343.

Alonso, M. J. Goycoolea, F. M., Higuera-Ciapara I. 2008. Chitosan-polysaccharide blended nanoparticles for controlled drug delivery. *In:* Neves, N. M., Mano, J. F., Gomes, M. E., Marques, A. P. & Azevedo, H. S. (eds.) *Natural-based polymers for biomedical applications.* Cambridge, UK: Woadhead Publishing Ltd.

Alpers, D. H. 2003. Digestion, Absorption, and Metabolism. *In:* Caballero, B., Finglas, P. & Toldra, F. (eds.) *Encyclopedia of Food Sciences and Nutrition.* 2nd ed. San Diego, California, USA: Academic Press.

Amin, S., Barnett, G. V., Pathak, J. A., Roberts, C. J. & Sarangapani, P. S. 2014. Protein aggregation, particle formation, characterization & rheology. *Curr. Opin. Colloid Interface Sci.,* 19**,** 438-449.

Anzenbacherova, E., Anzenbacher, P., Macek, K. & Kvetina, J. 2001. Determination of enzyme (angiotensin convertase) inhibitors based on enzymatic reaction followed by HPLC. *J. Pharm. Biomed. Anal.,* 24**,** 1151-1156.

Apostolidis, E., Stergiou, A., Kioupis, D., Sadeghpour, A., Paximada, P., Kakali, G. & Mandala, I. 2023. Production of nanoparticles from resistant starch via a simple three-step physical treatment. *Food Hydrocolloids.* 137**,** 108412.

Aranaz, I., Alcantara, A. R., Civera, M. C., Arias, C., Elorza, B., Heras Caballero, A. & Acosta, N. 2021. Chitosan: An Overview of Its Properties and Applications. *Polymers (Basel).* 13**,** 1-27.

Augst, A. D., Kong, H. J. & Mooney, D. J. 2006. Alginate hydrogels as biomaterials. *Macromol. Biosci.* 6**,** 623-33.

Auwal, S. M., Ghanisma, S. B. M. & Saari, N. 2024. Improved systolic blood pressure (SBP)-lowering effect of stone fish-derived angiotensin-I converting enzyme (ACE)-inhibitory peptide entrapped in chitosan-coated alginate nanocomposites. *Food Bioscience.* 60**,** 104349.

Awaniak, A., Minkiewicz, P., Darewicz, M. 2024. BIOPEP-UM database - present and future. *Current Opinion in Food Science*. 55, 101108.

Bakshi, P. S., Selvakumar, D., Kadirvelu, K. & Kumar, N. S. 2020. Chitosan as an environment friendly biomaterial - a review on recent modifications and applications. *Int. J. Biol. Macromol.* 150**,** 1072-1083.

Banerjee, P., Adhikary, K., Chatterjee, A., Sarkar, R., Bagchi, D., Ghosh, N. & Das, A. 2022. Digestion and gut microbiome. *In:* Bagchi, D. & Ohia, S. E. (eds.) *Nutrition and Functional Foods in Boosting Digestion, Metabolism and Immune Health.* London, UK: Academic Press.

Barbu, A., Neamtu, B., Zahan, M., Iancu, G. M., Bacila, C. & Miresan, V. 2021. Current Trends in Advanced Alginate-Based Wound Dressings for Chronic Wounds. *J. Pers. Med.* 11**,** 1-20.

Batista, P., Castro, P. M., Madureira, A. R., Sarmento, B. & Pintado, M. 2018. Recent insights in the use of nanocarriers for the oral delivery of bioactive proteins and peptides. *Peptides.* 101**,** 112-123.

Ben Henda, Y., Labidi, A., Arnaudin, I., Bridiau, N., Delatouche, R., Maugard, T., Piot, J. M., Sannier, F., Thiery, V. & Bordenave-Juchereau, S. 2013. Measuring angiotensin-I converting enzyme inhibitory activity by micro plate assays: comparison using marine cryptides and tentative threshold determinations with captopril and losartan. *J. Agric. Food Chem.* 61**,** 10685-90.

Berger, J., Reist, M., Mayer, J. M., Felt, O. & Gurny, R. 2004. Structure and interactions in chitosan hydrogels formed by complexation or aggregation for biomedical applications. *Eur. J. Pharm. Biopharm.* 57**,** 35-52.

Bertagnolli, C., Espindola, A. P., Kleinubing, S. J., Tasic, L. & Da Silva, M. G. 2014. Sargassum filipendula alginate from Brazil: seasonal influence and characteristics. *Carbohydr. Polym.* 111**,** 619-23.

Bhattacharjee, S. 2016. DLS and zeta potential - What they are and what they are not? *J. Control Release.* 235**,** 337-351.

Bicak, B., Budama-Kilinc, Y., Kecel-Gunduz, S., Zorlud, T. & Akman, G. 2021. Peptide based nano-drug candidate for cancer treatment: preparation, characterization, in vitro and in silico evaluation. *J. Mol. Struct.* 1240**,** 130573.

Bojorges, H., López-Rubio, A., Martínez-Abad, A. & Fabra, M. J. 2023. Overview of alginate extraction processes: Impact on alginate molecular structure and techno-functional properties. *Trends in Food Science & Technology.* 140**,** 104142.

Bourganis, V., Karamanidou, T., Kammona, O. & Kiparissides, C. 2017. Polyelectrolyte Complexes as Prospective Carriers for the Oral Delivery of Protein Therapeutics. *Eur. J. Pharm. Biopharm.* 111**,** 44-60.

Boutrou, R., Henry, G. & Sanchez-Rivera, L. 2015. On the trail of milk bioactive peptides in human and animal intestinal tracts during digestion: A review. *Dairy Science & Technology.* 95**,** 815-829.

Brodkorb, A., Egger, L., Alminger, M., Alvito, P., Assuncao, R., Ballance, S., Bohn, T., Bourlieu-Lacanal, C., Boutrou, R., Carriere, F., Clemente, A., Corredig, M., Dupont, D., Dufour, C., Edwards, C., Golding, M., Karakaya, S., Kirkhus, B., Le Feunteun, S., Lesmes, U., Macierzanka, A., Mackie, A. R., Martins, C., Marze, S., McClements, D. J., Menard, O., Minekus, M., Portmann, R., Santos, C. N., Souchon, I., Singh, R. P., Vegarud, G. E., Wickham, M. S. J., Weitschies, W. & Recio, I. 2019. INFOGEST static in vitro simulation of gastrointestinal food digestion. *Nat. Protoc.* 14**,** 991-1014.

Brown, T. D., Whitehead, K. A. & Mitragotri, S. 2019. Materials for oral delivery of proteins and peptides. *Nat. Rev. Mater.* 5**,** 127-148.

Brück, W. M., Slater, J. W. & Carney, B. F. 2010. Chitin and Chitosan from Marine Organisms. *In:* KIM, S.-K. (ed.) *Chitin, Chitosan, Oligosaccharides and Their Derivatives.* 1st Edition ed. Boca Raton: CRC Press.

Brugnerotto, J., Lizardi, J., Goycoolea, F. M., Arguèelles-Monal, W., Desbrieáres, J. & Rinaudo, M. 2001. An infrared investigation in relation with chitin and chitosan characterization. *Polymer,* 42**,** 3569-3580.

Byun, H. G. & Kim, S. K. 2001. Purification and characterization of angiotensin I converting enzyme (ACE) inhibitory peptides from Alaska pollack (*Theragra chalcogramma*) skin. *Process Biochem.,* 36**,** 1155–1162.

Cegnar, M., Miklavzin, A. & Kerc, J. 2011. Freeze-Drying and Release Characteristics of Polyelectrolyte Nanocarriers for the Mucosal Delivery of Ovalbumin. *Acta. Chim. Slov.,* 58**,** 241–250.

Chen, K. L., Mylon, S. E. & Menachem, E. 2006. Aggregation Kinetics of Alginate-Coated Hematite Nanoparticles in Monovalent and Divalent Electrolytes. *Environ. Sci. Technol.* 40**,** 1516-1523.

Cohen, R. D., Liu, Y. & Gong, X. 2012. Analysis of volatile bases by high performance liquid chromatography with aerosol-based detection. *J. Chromatogr. A,* 1229**,** 172-9.

Colletier, J. P., Chaize, B., Winterhalter, M. & Fournie, D. 2002. Protein encapsulation in liposomes: efficiency depends on interactions between protein and phospholipid bilayer. *BMC Biotechnology,* 2**,** 1-8.

Costalat, M., David, L. & Delair, T. 2014. Reversible controlled assembly of chitosan and dextran sulfate: a new method for nanoparticle elaboration. *Carbohydr. Polym.,* 102**,** 717-26.

Cushman, D. W. & Cheung, H. S. 1971. Spectrophotometric assay and properties of the angiotensin-converting enzyme of rabbit lung. *Biochem. Pharmacol.,* 20**,** 1637-1648.

Da Silva, N. G., Colodi, F. G., Pedrão, M. R. & Celligoi, M. a. P. C. 2024. Encapsulating Biosurfactants in Biopolymers for Innovative Applications in the Food Industry. *ACS Food Science & Technology,* 4**,** 2528-2549.

Delair, T. 2011. Colloidal polyelectrolyte complexes of chitosan and dextran sulfate towards versatile nanocarriers of bioactive molecules. *Eur. J. Pharm. Biopharm.,* 78**,** 10-8.

Dhillon, G. S., Kaur, S., Brar, S. K. & Verma, M. 2013. Green synthesis approach: extraction of chitosan from fungus mycelia. *Crit. Rev. Biotechnol.,* 33**,** 379-403.

Dias, R. S. & Stokke, B. T. 2014. Polyelectrolyte Complexes. *In:* M., V. P., Bayraktar, O. & Pico, G. A. (eds.) *Polyelectrolytes: Thermodynamics and Rheology.* Cham, Switzerland: Springer.

Dinculescu, D. D., Apetroaei, M. R., Gijiu, C. L., Anton, M., Enache, L., Schroder, V., Isopescu, R. & Rau, I. 2024. Simultaneous Optimization of Deacetylation Degree and Molar Mass of Chitosan from Shrimp Waste. *Polymers (Basel),* 16**,** 170.

Ding, L., Huang, Y., Cai, X. & Wang, S. 2019. Impact of pH, ionic strength and chitosan charge density on chitosan/casein complexation and phase behavior *Carbohydrate Polymers,* 208**,** 133-141.

Draget, K. I. & Taylor, C. 2011. Chemical, physical and biological properties of alginates and their biomedical implications. *Food Hydrocolloids,* 25**,** 251-256.

Du, C., Gong, H., Zhao, H. & Wang, P. 2024. Recent progress in the preparation of bioactive peptides using simulated gastrointestinal digestion processes. *Food Chem.,* 453**,** 139587.

Du, Z., Liu, J., Zhang, T., Yu, Y., Zhang, Y., Zhai, J., Huang, H., Wei, S., Ding, L. & Liu, B. 2019. A study on the preparation of chitosan-tripolyphosphate nanoparticles and its entrapment mechanism for egg white derived peptides. *Food Chem.,* 286**,** 530-536.

Egerton, R. F. 2005. *Physical Principles of Electron Microscopy: An Introduction to TEM, SEM, and AEM,* NY, USA, Springer.

Egger, L., Ménard, O., Delgado-Andrade, C., Alvito, P., Assunção, R., Balance, S., Barberá, R., Brodkorb, A., Cattenoz, T., Clemente, A., Comi, I., Dupont, D., Garcia-Llatas, G., Lagarda, M. J., Le Feunteun, S., Janssenduijghuijsen, L., Karakaya, S., Lesmes, U., Mackie, A. R., Martins, C., Meynier, A., Miralles, B., Murray, B. S., Pihlanto, A., Picariello, G., Santos, C. N., Simsek, S., Recio, I., Rigby, N., Rioux, L.-E., Stoffers, H., Tavares, A., Tavares, L., Turgeon, S., Ulleberg, E. K., Vegarud, G. E., Vergères, G. & Portmann, R. 2016. The harmonized INFOGEST in vitro digestion method: From knowledge to action. *Food Res. Int.,* 88**,** 217-225.

Ehsani, A., Hashemi, M., Afshari, A., Aminzare, M., Raeisi, M. & Zeinali, T. 2020. Effect of different types of active biodegradable films containing lactoperoxidase system or sage essential oil on the shelf life of fish burger during refrigerated storage. *LWT - Food Science and Technology,* 117**,** 108633.

Fan, G. Y. & Ellisman, M. H. 1993. High-sensitivity lens-coupled slow-scan CCD camera for transmission electron microscopy. *Ultramicroscopy.,* 52**,** 21-29.

Feng, Y., Kilker, S. R. & Lee, Y. 2020. Surface charge (zeta-potential) of nanoencapsulated food ingredients. *In:* JAFARI, S. M. (ed.) *Characterization of Nanoencapsulated Food Ingredients.* London, UK: Academic Press.

Ferreira, L. M. B., Dos Santos, A. M., Boni, F. I., Dos Santos, K. C., Robusti, L. M. G., De Souza, M. P. C., Ferreira, N. N., Carvalho, S. G., Cardoso, V. M. O., Chorilli, M., Cury, B. S. F., De Godoi, D. R. M. & Gremiao, M. P. D. 2020. Design of chitosan-based particle systems: A review of the physicochemical foundations for tailored properties. *Carbohydr. Polym.,* 250**,** 116968.

Fitzgerald, D. 2000. Technical Assessment of the Anton Paar DMA5000 density meter. St Asaph, UK: H & D Fitzgerald Ltd.

Fleury, L., Deracinois, B., Dugardin, C., Nongonierma, A. B., Fitzgerald, R. J., Flahaut, C., Cudennec, B. & Ravallec, R. 2022. In Vivo and In Vitro Comparison of the DPP-IV Inhibitory Potential of Food Proteins from Different Origins after Gastrointestinal Digestion. *Int. J. Mol. Sci.,* 23.

Fujita, H., Yokoyama, K. & Yoshikawa, M. 2000. Classification and antihypertensive activity of angiotensin I-converting enzyme inhibitory peptides derived from food proteins. *J. Food Sci.,* 65**,** 564-569.

Gao, R., Yu, Q., Shen, Y., Chu, Q., Chen, G., Fen, S., Yang, M., Yuan, L., McClements, D. J. & Sun, Q. 2021. Production, bioactive properties, and potential applications of fish protein hydrolysates: Developments and challenges. *Trends Food Sci. Technol.,* 110**,** 687-699.

George, M. & Abraham, T. E. 2006. Polyionic hydrocolloids for the intestinal delivery of protein drugs: alginate and chitosan--a review. *J. Control Release,* 114**,** 1-14.

Ghalamara, S., Brazinha, C., Silva, S. & Pintado, M. 2024. Valorization of Fish Processing by-Products: Biological and Functional Properties of Bioactive Peptides. *Current Food Science and Technology Reports,* 2**,** 393-409.

Ghassem, M., Arihara, K. & Babji, A. S. 2012. Isolation, purification and characterisation of angiotensin I-converting enzyme-inhibitory peptides derived from catfish (*Clarias batrachus*) muscle protein thermolysin hydrolysates. *Int. J. Food Sci. Tech.,* 47**,** 2444-2451.

Ghassem, M., Arihara, K., Babji, A. S., Said, M. & Ibrahim, S. 2011. Purification and identification of ACE inhibitory peptides from Haruan (*Channa striatus*) myofibrillar protein hydrolysate using HPLC–ESI-TOF MS/MS. *Food Chem.,* 129**,** 1770-1777.

Gómez-Guillén, M. C., Giménez, B., López-Caballero, M. E. & Montero, M. P. 2011. Functional and bioactive properties of collagen and gelatin from alternative sources: A review. *Food Hydrocolloids,* 25**,** 1813-1827.

Goncalves, C., Ferreira, N. & Lourenco, L. 2021. Production of low molecular weight chitosan and chitooligosaccharides (COS): A review. *Polymers (Basel),* 13**,** 2466.

Goycoolea, F. M., Lollo, G., Remunan-Lopez, C., Quaglia, F. & Alonso, M. J. 2009. Chitosan-alginate blended nanoparticles as carriers for the transmucosal delivery of macromolecules *Biomacromolecules,* 10**,** 1736–1743.

Goycoolea, F. M., Valle-Gallego, A., Stefani, R., Menchicchi, B., David, L., Rochas, C., Santander-Ortega, M. J. & Alonso, M. J. 2012. Chitosan-based nanocapsules: physical characterization, stability in biological media and capsaicin encapsulation. *Colloid and Polymer Science,* 290**,** 1423-1434.

Goycoolea, F.M., Brunel, F., Gueddari, N.E.E., Coggiola, A., Lollo, G., Moerschbacher, B.M., Remuñán-López, C., Delair, T., Domard, A. and Alonso, M.J. 2016. Physical properties and stability of soft gelled chitosan-based nanoparticles. *Macromolecular Bioscience* 16, 1873-1882.

Grant, G. T., Morris, E. R., Rees, D. A., Smith, P. J. C. & Thom, D. 1973. Biological interaction between polysaccharides and divalent cations: the egg-box model. *FEBS Lett.,* 32**,** 195-198.

Guarnieri, A., Triunfo, M., Scieuzo, C., Ianniciello, D., Tafi, E., Hahn, T., Zibek, S., Salvia, R., De Bonis, A. & Falabella, P. 2022. Antimicrobial properties of chitosan from different developmental stages of the bioconverter insect Hermetia illucens. *Sci. Rep.,* 12**,** 8084.

Guo, X., Wang, Y., Qin, Y., Shen, P. & Peng, Q. 2020. Structures, properties and application of alginic acid: A review. *Int. J. Biol. Macromol.,* 162**,** 618-628.

Halim, N. R. A., Yusof, H. M. & Sarbon, N. M. 2016. Functional and bioactive properties of fish protein hydolysates and peptides: A comprehensive review. *Trends in Food Science & Technology,* 51**,** 24-33.

Hamed, I., Özogul, F. & Regenstein, J. M. 2016. Industrial applications of crustacean by-products (chitin, chitosan, and chitooligosaccharides): A review. *Trends in Food Science & Technology,* 48**,** 40-50.

Hamosh, M. & Scow, R. O. 1973. Lingual Lipase and Its Role in the Digestion of Dietary Lipid. *The Journal of Clinical Investigation,* 52**,** 88-95.

Han, Q., Verissimo, N. V. P., Bryant, S. J., Martin, A. V., Huang, Y., Pereira, J. F. B., Santos-Ebinuma, V. C., Zhai, J., Bryant, G., Drummond, C. J. & Greaves, T. L. 2024. Scattering approaches to unravel protein solution behaviors in ionic liquids and deep eutectic solvents: From basic principles to recent developments. *Adv. Colloid Interface Sci.,* 331**,** 103242.

Hellmann, M. J., Gillet, D., Trombotto, S., Raetz, S., Moerschbacher, B. M. & Cord-Landwehr, S. 2024. Heterogeneously deacetylated chitosans possess an unexpected regular pattern favoring acetylation at every third position. *Nat. Commun.,* 15**,** 6695.

Herrera, S. E., Agazzi, M. L., Apuzzo, E., Cortez, M. L., Marmisolle, W. A., Tagliazucchi, M. & Azzaroni, O. 2023. Polyelectrolyte-multivalent molecule complexes: physicochemical properties and applications. *Soft Matter,* 19**,** 2013-2041.

Himaya, S. W. A., Ngo, D.-H., Ryu, B. & Kim, S.-K. 2012. An active peptide purified from gastrointestinal enzyme hydrolysate of Pacific cod skin gelatin attenuates angiotensin-1 converting enzyme (ACE) activity and cellular oxidative stress *Food Chem.,* 132**,** 1872-1882.

Holkar, A., Toledo, J. & Srivastava, S. 2021. Structure of nanoparticle-polyelectrolyte complexes: Effects of polyelectrolyte characteristics and charge ratio. *AIChE Journal,* 67**,** 1-10.

Hou, Y., Chitrakar, B., Mao, K., Wang, K., Gu, X., Gao, J., Zhang, Q., Bekhit, A. E.-D. A. & Sang, Y. 2023. Bioactivity of collagen peptides derived from commercial animals: In silico investigation. *LWT - Food Science and Technology,* 187**,** 115381.

Houghton, D., Wilcox, M. D., Chater, P. I., Brownlee, I. A., Seal, C. J. & Pearson, J. P. 2015. Biological activity of alginate and its effect on pancreatic lipase inhibition as a potential treatment for obesity. *Food Hydrocolloids,* 49**,** 18-24.

Hu, C., Lu, W., Sun, C., Zhao, Y., Zhang, Y. & Fang, Y. 2022. Gelation behavior and mechanism of alginate with calcium: Dependence on monovalent counterions. *Carbohydr. Polym.,* 294**,** 119788.

Inkson, B. J. 2016. Scanning electron microscopy (SEM) and transmission electron microscopy (TEM) for materials characterization. *In:* Hubschen, G., Altpeter, I., Tschuncky, R. & Herrmann, H.-G. (eds.) *Materials Characterization Using Nondestructive Evaluation (NDE) Methods.* Duxford, UK: Woodhead Publishing.

Ishak, N. H. & Sarbon, N. M. 2017. A Review of Protein Hydrolysates and Bioactive Peptides Deriving from Wastes Generated by Fish Processing. *Food and Bioprocess Technology,* 11**,** 2-16.

Islam, S., Bhuiyan, M. a. R. & Islam, M. N. 2016. Chitin and Chitosan: Structure, Properties and Applications in Biomedical Engineering. *Journal of Polymers and the Environment,* 25**,** 854-866.

Ismail, B. & Nielsen, S. S. 2010. Basic Principles of Chromatography. *In:* NielsenI, S. S. (ed.) *Food Analysis.* New York, USA: Springer

Jadhao, A. S., Ambhore, D. P. & Biyani, K. R. 2022. Importance of RP-HPLC in Analytical Method Development: A Review. *IJARSCT,* 2**,** 345-351.

Joseph, S. M., Krishnamoorthy, S., Paranthaman, R., Moses, J. A. & Anandharamakrishnan, C. 2021. A review on source-specific chemistry, functionality, and applications of chitin and chitosan. *Carbohydrate Polymer Technologies and Applications,* 2**,** 100036.

Kaszuba, M., Corbett, J., Watson, F. M. & Jones, A. 2010. High-concentration zeta potential measurements using light-scattering techniques. *Philos. Trans A Math. Phys. Eng. Sci.,* 368**,** 4439-51.

Kipkoech, C. 2023. Beyond Proteins—Edible Insects as a Source of Dietary Fiber. *Polysaccharides,* 4**,** 116-128.

Klang, V., Matsko, N. B., Valenta, C. & Hofer, F. 2012. Electron microscopy of nanoemulsions: an essential tool for characterisation and stability assessment. *Micron.,* 43**,** 85-103.

Knezevic-Jugovic, Z., Petronijevic, Z. & Smelcerovi, A. 2011. Chitin and Chitosan from Microorganisms. *In:* KIM, S.-K. (ed.) *Chitin, Chitosan, Oligosaccharides and Their Derivatives.* Boca Raton: CRC Press.

Kruk, K. & Winnicka, K. 2022. Alginates Combined with Natural Polymers as Valuable Drug Delivery Platforms. *Mar. Drugs,* 21**,** 11.

Kulicke, W. M. & Clasen, C. 2004. *Viscosimetry of Polymers and Polyelectrolytes* Heidelberg, Germany, Springer Berlin.

Kulkarni, A. D., Vanjari, Y. H., Sancheti, K. H., Patel, H. M., Belgamwar, V. S., Surana, S. J. & Pardeshi, C. V. 2016. Polyelectrolyte complexes: mechanisms, critical experimental aspects, and applications. *Artif. Cells Nanomed. Biotechnol.,* 44**,** 1615-25.

Lacourse, M. E. & Lacourse, W. R. 2017. General instrumentation in HPLC *In:* Fanali, S. F., Haddad, P. R., Poole, C. F. & Riekkola, M.-L. (eds.) *Liquid Chromatography: Fundamentals and Instrumentation.* 2 ed. Amsterdam, Netherlands: Elsevier.

Lacroix, I. M. E., Chen, X. M., Kitts, D. D. & Li-Chan, E. C. Y. 2017. Investigation into the bioavailability of milk protein-derived peptides with dipeptidyl-peptidase IV inhibitory activity using Caco-2 cell monolayers. *Food Funct.,* 8**,** 701-709.

Lee, Y. M., Skurk, T., Hennig, M. & Hauner, H. 2007. Effect of a milk drink supplemented with whey peptides on blood pressure in patients with mild hypertension. *Eur. J. Nutr.,* 46**,** 21-7.

Li, G.-H., Le, G.-W., Shi, Y.-H. & Shrestha, S. 2004. Angiotensin I–converting enzyme inhibitory peptides derived from food proteins and their physiological and pharmacological effects. *Nutrition Research,* 24**,** 469-486.

Li, X., Xie, H., Lin, J., Xie, W. & Ma, X. 2009. Characterization and biodegradation of chitosan–alginate polyelectrolyte complexes. *Polymer Degradation and Stability.,* 94**,** 1-6.

Li, Z., Paulson, A. T. & Gill, T. A. 2015. Encapsulation of bioactive salmon protein hydrolysates with chitosan-coated liposomes. *Journal of Functional Foods.,* 19**,** 733-743.

Lin, Y. H., Chen, C. A., Tsai, J. S. & Chen, G. W. 2019. Preparation and identification of novel antihypertensive peptides from the in vitro gastrointestinal digestion of marine cobia skin hydrolysates. *Nutrients,* 11**,** 1351.

Liu, X., Liu, L., Huang, F., Meng, Y., Chen, Y., Wang, J., Wang, S., Luo, Y., Li, J. & Liang, Y. 2025. pH-sensitive chitosan/sodium alginate/calcium chloride hydrogel beads for potential oral delivery of rice bran bioactive peptides. *Food Chem.,* 470**,** 142618.

Lozano-Sánchez, J., Borrás-Linares, I., Sass-Kiss, A. & Segura-Carretero, A. 2018. Chromatographic Technique: High-Performance Liquid Chromatography (HPLC). *In:* Sun, D.-W. (ed.) *Modern Techniques for Food Authentication.* London, UK: Academic Press.

Luo, Y. & Wang, Q. 2014. Recent development of chitosan-based polyelectrolyte complexes with natural polysaccharides for drug delivery. *Int. J. Biol. Macromol.,* 64**,** 353-67.

Maciel, V. B. V., Yoshida, C. M. P., Pereira, S., Goycoolea, F. M. & Franco, T. T. 2017. Electrostatic self-assembled chitosan-pectin nano- and microparticles for insulin delivery. *Molecules,* 22**,** 1707.

Maeno, M., Yamamoto, N. & Takano, T. 1996. Identifiication of an Antihypertensive Peptide from Casein Hydrolysate Produced by a Proteinase from lactobacillus helveticus CP790. *J. Dairy Sci.,* 79**,** 1316-1321.

Mania, S., Banach-Kopec, A., Staszczyk, K., Kulesza, J., Augustin, E. & Tylingo, R. 2023. An influence of molecular weight, deacetylation degree of chitosan xerogels on their antimicrobial activity and cytotoxicity. Comparison of chitosan materials obtained using lactic acid and CO(2) saturation. *Carbohydr. Res.,* 534**,** 108973.

Maria Leena, M., Mahalakshmi, L., Moses, J. A. & Anandharamakrishnan, C. 2020. Nanoencapsulation of nutraceutical ingredients. *In:* PAL, K., Banerjee, I., Sarkar, P., Kim, D., Deng, W.-P., Dubey, N. K. & Majumder, K. (eds.) *Biopolymer-Based Formulations.* Amsterdam, Netherlands Elsevier.

McClements, D. J. 2017. The future of food colloids: Next-generation nanoparticle delivery systems. *Current Opinion in Colloid & Interface Science,* 28**,** 7-14.

McClements, D. J. 2018. Encapsulation, protection, and delivery of bioactive proteins and peptides using nanoparticle and microparticle systems: A review. *Adv Colloid Interface Sci,* 253**,** 1-22.

Meisel, H., Frister, H. & Sehlimme, E. 1989. Biologically active peptides in milk proteins. *Zeitschrift fur. Ernahrungswissenschaft,* 28**,** 267-278.

Miguel, M., Aleixandre, M. A., Ramos, M. & Lopez-Fandino, R. 2006. Effect of Simulated Gastrointestinal Digestion on the Antihypertensive Properties of ACE-Inhibitory Peptides Derived from Ovalbumin. *J. Agric. Food Chem.,* 54**,** 726−731.

Minekus, M., Alminger, M., Alvito, P., Ballance, S., Bohn, T., Bourlieu, C., Carriere, F., Boutrou, R., Corredig, M., Dupont, D., Dufour, C., Egger, L., Golding, M., Karakaya, S., Kirkhus, B., Le Feunteun, S., Lesmes, U., Macierzanka, A., Mackie, A., Marze, S., McClements, D. J., Menard,

O., Recio, I., Santos, C. N., Singh, R. P., Vegarud, G. E., Wickham, M. S., Weitschies, W. & Brodkorb, A. 2014. A standardised static in vitro digestion method suitable for food - an international consensus. *Food Funct.,* 5**,** 1113-24.

Minkiewicz, P., Iwaniak, A. & Darewicz, M. 2019. BIOPEP-UWM Database of Bioactive Peptides: Current Opportunities. *Int. J. Mol. Sci.,* 20**,** 5978.

Mirzapour-Kouhdasht, A., McClements, D. J., Taghizadeh, M. S., Niazi, A. & Garcia-Vaquero, M. 2023. Strategies for oral delivery of bioactive peptides with focus on debittering and masking. *NPJ Sci. Food.,* 7**,** 22.

Mohan, A., Rajendran, S. R. C. K., He, Q. S., Bazinet, L. & Udenigwe, C. C. 2015. Encapsulation of food protein hydrolysates and peptides: a review. *RSC Advances.,* 5**,** 79270-79278.

Montes Ruiz-Cabello, F. J., Trefalt, G., Maroni, P. & Borkovec, M. 2014. Electric double-layer potentials and surface regulation properties measured by colloidal-probe atomic force microscopy. *Phys. Rev. E Stat. Nonlin. Soft Matter Phys.,* 90**,** 012301.

Moreira, A., Lawson, D., Onyekuru, L., Dziemidowicz, K., Angkawinitwong, U., Costa, P. F., Radacsi, N. & Williams, G. R. 2021. Protein encapsulation by electrospinning and electrospraying. *J Control Release,* 329**,** 1172-1197.

Mourya, V. K., Inamdar, N. N. & Choudhari, Y. M. 2011. Chitooligosaccharides: Synthesis, characterization and applications. *Polymer Science Series A,* 53**,** 583-612.

Murray, B. A., Walsh, D. J. & Fitzgerald, R. J. 2004. Modification of the furanacryloyl-L-phenylalanylglycylglycine assay for determination of angiotensin-I-converting enzyme inhibitory activity. *J. Biochem. Biophys. Methods,* 59**,** 127-37.

Najafian, L. & Babji, A. S. 2012. A review of fish-derived antioxidant and antimicrobial peptides: their production, assessment, and applications. *Peptides,* 33**,** 178-85.

Nasri, R., Younes, I., Jridi, M., Trigui, M., Bougatef, A., Nedjar-Arroume, N., Dhulster, P., Nasri, M. & Karra-Châabouni, M. 2013. ACE inhibitory and antioxidative activities of Goby (Zosterissessor ophiocephalus) fish protein hydrolysates: Effect on meat lipid oxidation. *Food Research International,* 54**,** 552-561.

Ngasotter, S., Xavier, K. a. M., Meitei, M. M., Waikhom, D., Madhulika, Pathak, J. & Singh, S. K. 2023. Crustacean shell waste derived chitin and chitin nanomaterials for application in agriculture, food, and health – A review. *Carbohydrate Polymer Technologies and Applications,* 6**,** 100349.

Nikolova, D., Simeonov, M., Tzachev, C., Apostolov, A., Christov, L. & Vassileva, E. 2021. Polyelectrolyte complexes of chitosan and sodium alginate as a drug delivery system for diclofenac sodium. *Polymer International,* 71**,** 668-678.

Noorbatcha, I. A., Jaswir, I. & Ahmad, H. 2018. Nano-encapsulation of Proteins and Peptides. *Current Nanomaterials,* 2**,** 76-83.

Nordgard, C. T. & Draget, K. I. 2021. Alginates. *In:* Phillips, G. O. & Williams, P. A. (eds.) *Handbook of Hydrocolloids (Third Edition).* Woodhead Publishing.

Nwe, N., Furuike, T. & Tamura, H. 2010. Chitin and Chitosan from Terrestrial Organisms. *In:* Kim, S.-K. (ed.) *Chitin, Chitosan, Oligosaccharides and Their Derivatives: Biological Activities and Applications.* Boca Raton: CRC Press.

Odunsi, S. T., Vazquez-Roque, M. I., Camilleri, M., Papathanasopoulos, A., Clark, M. M., Wodrich, L., Lempke, M., Mckinzie, S., Ryks, M., Burton, D. & Zinsmeister, A. R. 2010. Effect of alginate on satiation, appetite, gastric function, and selected gut satiety hormones in overweight and obesity. *Obesity (Silver Spring),* 18**,** 1579-84.

Ortizo, R. G. G., Sharma, V., Tsai, M.-L., Wang, J.-X., Sun, P.-P., Nargotra, P., Kuo, C.-H., Chen, C.-W. & Dong, C.-D. 2023. Extraction of Novel Bioactive Peptides from Fish Protein Hydrolysates by Enzymatic Reactions. *Applied Sciences,* 13**,** 5768.

Park, J. W., Park, K. H. & Seo, S. 2019. Natural polyelectrolyte complex-based pH-dependent delivery carriers using alginate and chitosan. *Journal of Applied Polymer Science,* 136**,** 48143.

Parmentier, J., Thewes, B., Gropp, F. & Fricker, G. 2011. Oral peptide delivery by tetraether lipid liposomes. *Int. J. Pharm.* 415**,** 150-157.

Patel, H. M. & Ryman, B. E. 1976. Oral administration of insulin by encapsulation within liposomes. *FEBS Lett.,* 62**,** 60-3.

Patel, V. R. & Agrawal, Y. K. 2011. Nanosuspension: An approach to enhance solubility of drugs. *J. Adv. Pharm. Technol. Res.,* 2**,** 81-7.

Pei, J., Gao, X., Pan, D., Hua, Y., He, J., Liu, Z. & Dang, Y. 2022. Advances in the stability challenges of bioactive peptides and improvement strategies. *Curr. Res. Food Sci.,* 5**,** 2162-2170.

Peniche, C., Argüelles-Monal, W. & Goycoolea, F. M. 2008. Chitin and Chitosan: Major Sources, Properties and Applications. *In:* Belgacem, M. N. & Gandini, A. (eds.) *Monomers, Polymers and Composites from Renewable Resources.* Amsterdam, The Netherlands Elsevier Science.

Perez-Perez, V., Jimenez-Martinez, C., Gonzalez-Escobar, J. L. & Corzo-Rios, L. J. 2024. Exploring the impact of encapsulation on the stability and bioactivity of peptides extracted from botanical sources: trends and opportunities. *Front. Chem.,* 12**,** 1423500.

Pergushov, D. V., Muller, A. H. & Schacher, F. H. 2012. Micellar interpolyelectrolyte complexes. *Chem. Soc. Rev.,* 41**,** 6888-901.

Perry, S. L. & McClements, D. J. 2020. Recent Advances in Encapsulation, Protection, and Oral Delivery of Bioactive Proteins and Peptides using Colloidal Systems. *Molecules,* 25**,** 1-26.

Peteiro, C. 2018. Alginate Production from Marine Macroalgae, with Emphasis on Kelp Farming. *In:* Rehm, B. H. A. & Moradali, M. F. (eds.) *Alginates and Their Biomedical Applications.* Singapore: Springer.

Porod, G. 1982. Small Angle X-Scattering: General Theory. *In:* Glatter, O. & Kratky, O. (eds.) *Small Angle X-Scattering.* London: Academic Press.

Potaś, J., Szymańska, E. & Winnicka, K. 2020. Challenges in developing of chitosan – Based polyelectrolyte complexes as a platform for mucosal and skin drug delivery. *European Polymer Journal,* 140**,** 110020.

Pravinata, L., Akhtar, M., Bentley, P. J., Mahatnirunkul, T. & Murray, B. S. 2016. Preparation of alginate microgels in a simple one step process via the Leeds Jet Homogenizer. *Food Hydrocolloid.,* 61**,** 77-84.

Pusey, P. N. 1974. Macromolecular Diffusion. *In:* Cummins, H. Z. & Pike, E. R. (eds.) *Photon Correlation and Light Beating Spectroscopy: NATO Advanced Study Institutes Series.* Boston, MA: Springer.

Qandil, A. M., Marjic, T. J., Al-Taanic, B. M., Khaledd, A. H. & Badwan, A. A. 2018. Depolymerization of HMW into a predicted LMW chitosan and determination of the degree of deacetylation to guarantee its quality for research use. *J. Excipients and Food Chem.,* 9**,** 1-13.

Qiao, D., Liu, L., Chen, Y., Xue, C., Gao, Q., Mao, H. Q., Leong, K. W. & Chen, Y. 2018. Potency of a Scalable Nanoparticulate Subunit Vaccine. *Nano Lett.,* 18**,** 3007-3016.

Qun, G. & Ajun, W. 2006. Effects of molecular weight, degree of acetylation and ionic strength on surface tension of chitosan in dilute solution. *Carbohydrate Polymers.,* 64**,** 29-36.

Rabbani, S. A., Mitchell, J., Roy, D. R., Kremer, R., Bennett, H. P. J. & Goltzman, D. 1986. Purification of Peptides with Parathyroid Hormone-Like Bioactivity from Human and Rat Malignancies Associated with Hypercalcemia. *Endocrinology.,* 118**,** 1200-1210.

Rahman, M. M., Shahid, M. A., Hossain, M. T., Sheikh, M. S., Rahman, M. S., Uddin, N., Rahim, A., Khan, R. A. & Hossain, I. 2024. Sources, extractions, and applications of alginate: a review. *Discover Applied Sciences,* 6**,** 443.

Reuhs, B. L. & Rounds, M. A. 2010. High-Performance Liquid Chromatography. *In:* Nielsen, S. S. (ed.) *Food Analysis.* New York, USA: Springer.

Rinaudo, M. 2006. Chitin and chitosan: Properties and applications. *Progress in Polymer Science,* 31**,** 603-632.

Rinaudo, M., Milas, M. & Le Dung, P. 1993. Characterization of chitosan. Influence of ionic strength and degree of acetylation on chain expansion. *Int. J. Biol. Macromol.,* 15**,** 281-285.

Roman-Doval, R., Torres-Arellanes, S. P., Tenorio-Barajas, A. Y., Gomez-Sanchez, A. & Valencia-Lazcano, A. A. 2023. Chitosan: Properties and Its Application in Agriculture in Context of Molecular Weight. *Polymers (Basel).,* 15**,** 2867.

Roopa, B. S. & Bhattacharya, S. 2008. Alginate gels: I. Characterization of textural attributes. *Journal of Food Engineering,* 85**,** 123-131.

Sæther, H. V., Holme, H. K., Maurstad, G., Smidsrød, O. & Stokke, B. T. 2008. Polyelectrolyte complex formation using alginate and chitosan. *Carbohydrate Polymers,* 74**,** 813-821.

Sánchez, A. & Vázquez, A. 2017. Bioactive peptides: A review. *Food Quality and Safety,* 1**,** 29-46.

Sarmento, B., Ribeiro, A., Veiga, F., Sampaio, P., Neufeld, R. & Ferreira, D. 2007. Alginate/Chitosan nanoparticles are effective for oral insulin delivery. *Pharmaceutical Research,* 24**,** 2198-2206.

Sato, K. 2022. Metabolic Fate and Bioavailability of Food-Derived Peptides: Are Normal Peptides Passed through the Intestinal Layer To Exert Biological Effects via Proposed Mechanisms? *J. Agric. Food Chem.,* 70**,** 1461-1466.

Schatz, C., Domard, A., Viton, C., Pichot, C. & Delair, T. 2004. Versatile and efficient formation of colloids of biopolymer-based polyelectrolyte complexes. *Biomacromolecules,* 5**,** 1882–1892.

Schnablegger, H. & Singh, Y. 2013. *The SAXS Guide: Getting acquainted with the principles,* Graz, Austria, Anton Paar GmbH.

Scott, R. P. W. 2005. Instrumentation. *In:* Worsfold, P., Poole, C. & Townshend, A. (eds.) *Encyclopedia of Analytical Science.* Amsterdam, Netherlands: Elsevier.

Segura-Campos, M., Chel-Guerrero, L., Betancur-Ancona, D. & Hernandez-Escalante, V. M. 2011. Bioavailability of Bioactive Peptides. *Food Reviews International,* 27**,** 213-226.

Sharma, K. K. & Ortwerth, B. J. 1987. Purification and characterization of an aminopeptidase from bovine cornea. *Experimental Eye Research,* 45**,** 117-126.

Sharma, R., Kumar, S., Malviya, R., Prajapati, B. G., Puri, D., Limmatvapirat, S. & Sriamornsak, P. 2024. Recent advances in biopolymer-based mucoadhesive drug delivery systems for oral application. *Journal of Drug Delivery Science and Technology,* 91**,** 105227.

Shovsky, A., Varga, I., Makuska, R. & Claesson, P. M. 2009. Formation and stability of water-soluble, molecular polyelectrolyte complexes: effects of charge density, mixing ratio, and polyelectrolyte concentration. *Langmuir,* 25**,** 6113-21.

Shukla, U. 2025. Fourier transform infrared spectroscopy: A power full method for creating fingerprint of molecules of nanomaterials. *Journal of Molecular Structure,* 1322**,** 140454.

Sim, B., Chang, J. J., Lin, Q., Wong, J. H. M., Ow, V., Leow, Y., Wong, Y. J., Boo, Y. J., Goh, R. & Loh, X. J. 2024. Hydrogels Based on Polyelectrolyte Complexes: Underlying Principles and Biomedical Applications. *Biomacromolecules,* 25**,** 7563-7580.

Skou, S., Gillillan, R.E., Ando, N. 2014. Synchrotron-based small-angle X-ray scattering of proteins in solution. *Nature Protocol.,* 9(7)**:** 1727-1739.

Smidsrød, O. 1970. Solution properties of alginate. *Carbohyd. Res.,* 13**,** 359-372.

Smith, B. C. 2011. *Fundamentals of Fourier Transform Infrared Spectroscopy,* Boca Raton, CRC Press.

Sreekumar, S., Wattjes, J., Niehues, A., Mengoni, T., Mendes, A. C., Morris, E. R., Goycoolea, F. M. & Moerschbacher, B. M. 2022. Biotechnologically produced chitosans with nonrandom acetylation patterns differ from conventional chitosans in properties and activities. *Nat. Commun.,* 13**,** 7125.

Stetefeld, J., Mckenna, S. A. & Patel, T. R. 2016. Dynamic light scattering: a practical guide and applications in biomedical sciences. *Biophys. Rev.,* 8**,** 409-427.

Sutantawong, S., Kim, B. J., Kuhfeld, R. F., Qu, Y. & Dallas, D. C. 2024. Release of bioactive peptides from whey proteins across digestion in adult humans and a static in vitro digestion model. *J. Funct. Foods,* 122**,** 106540.

Tabassum, N. & Khan, M. A. 2020. Modified atmosphere packaging of fresh-cut papaya using alginate based edible coating: Quality evaluation and shelf life study. *Scientia Horticulturae,* 259**,** 108853.

Toopcham, T., Roytrakul, S. & Yongsawatdigul, J. 2015. Characterization and identification of angiotensin I-converting enzyme (ACE) inhibitory peptides derived from tilapia using Virgibacillus halodenitrificans SK1-3-7 proteinases. *Journal of Functional Foods,* 14**,** 435-444.

Trapani, A., Lopedota, A., Franco, M., Cioffi, N., Ieva, E., Garcia-Fuentes, M. & Alonso, M. J. 2010. A comparative study of chitosan and chitosan/cyclodextrin nanoparticles as potential carriers for the oral delivery of small peptides. *Eur. J. Pharm. Biopharm.* 75**,** 26-32.

Tsuru, H., Ishikawa, N. & Shigei, T. 1976. Responsiveness of Isolated Dog Veins to Bradykinin and other Bioactive Peptides: Distribution of Sensitivity to Bradykinin and Possible Correlation with Genesis of the Venous System. *Blood Vessels,* 13**,** 238-248.

Udenigwe, C. C. & Fogliano, V. 2017. Food matrix interaction and bioavailability of bioactive peptides: Two faces of the same coin? *Journal of Functional Foods,* 35**,** 9-12.

Ullah, M. R., Rahman, M. A., Haque, M. N., Sharker, M. R., Islam, M. M. & Alam, M. A. 2022. Nutritional profiling of some selected commercially important freshwater and marine water fishes of Bangladesh. *Heliyon,* 8**,** e10825.

Vignesh, A., Amal, T. C., Sarvalingam, A. & Vasanth, K. 2024. A review on the influence of nutraceuticals and functional foods on health. *Food Chemistry Advances.,* 5**,** 100749.

Vold, I. M. N., Kristiansen, K. A. & Christensen, B. E. 2006. A Study of the Chain Stiffness and Extension of Alginates, in Vitro Epimerized Alginates, and Periodate-Oxidized Alginates Using Size-Exclusion Chromatography Combined with Light Scattering and Viscosity Detectors. *Biomacromolecules.,* 7**,** 2136-2146.

Wandrey, C., Bartkowiak, A. & Harding, S. E. 2010. Materials for Encapsulation. *In:* Zuidam, N. J. & Nedovic, V. (eds.) *Encapsulation Technologies for Active Food Ingredients and Food Processing.* 1 ed. New York, USA: Springer

Wang, Q., Dong, X., Castaneda-Reyes, E. D., Wu, Y., Zhang, S., Wu, Z., Wang, Z., Dai, L., Xu, B. & Xu, F. 2024. Chitosan and sodium alginate nanocarrier system: Controlling the release of rapeseed-derived peptides and improving their therapeutic efficiency of anti-diabetes. *Int. J. Biol. Macromol.,* 265**,** 130713.

Weinhold, M. X., Sauvageau, J. C. M., Kumirska, J. & Thöming, J. 2009. Studies on acetylation patterns of different chitosan preparations. *Carbohydrate Polymers,* 78**,** 678-684.

W. H. O. 2023. *Hypertension* [Online]. Available: *https://www.who.int/news-room/fact-sheets/detail/hypertension* [Accessed May 2025].

Williams, D. B. & Carter, C. B. 2009. *Transmission Electron Microscopy: A Textbook for Materials Science,* New York, NY, Springer.

Wu, D., Zhu, L., Li, Y., Zhang, X., Xu, S., Yang, G. & Delair, T. 2020. Chitosan-based Colloidal Polyelectrolyte Complexes for Drug Delivery: A Review. *Carbohydr. Polym.,* 238**,** 116126.

Wu, T., Li, Y., Shen, N., Yuan, C. & Hu, Y. 2018. Preparation and characterization of calcium alginate-chitosan complexes loaded with lysozyme. *Journal of Food Engineering,* 233**,** 109-116.

Xu, Q., Hong, H., Wu, J. & Yan, X. 2019. Bioavailability of bioactive peptides derived from food proteins across the intestinal epithelial membrane: A review. *Trends in Food Science & Technology,* 86**,** 399-411.

Xue, L., Yin, R., Howell, K. & Zhang, P. 2021. Activity and bioavailability of food protein-derived angiotensin-I-converting enzyme-inhibitory peptides. *Compr. Rev. Food Sci. Food Saf.,* 20**,** 1150-1187.

Yadav, H. M., Shinde, S. K., Kim, D. Y., Chavan, T. P., Thorat, N. D., Ramesh, S. & Bathula, C. D. 2022. Metal oxide-based composites: synthesis and characterization. *In:* Delekar, S. D. (ed.) *Advances in Metal Oxides and Their Composites for Emerging Applications.* Amsterdam, Netherlands: Elsevier.

Yadav, M., Kaushik, B., Rao, G. K., Srivastava, C. M. & Vaya, D. 2023. Advances and challenges in the use of chitosan and its derivatives in biomedical fields: a review. *Carbohydrate Polymer Technologies and Applications* 5**,** 100323.

Yermak, I. M., Davydova, V. N. & Volod'ko, A. V. 2022. Mucoadhesive Marine Polysaccharides. *Mar Drugs,* 20**,** 522.

Yilmaz, T., Maldonado, L., Turasan, H. & Kokini, J. 2019. Thermodynamic mechanism of particulation of sodium alginate and chitosan polyelectrolyte complexes as a function of charge ratio and order of addition. *Journal of Food Engineering,* 254**,** 42-50.

Zabot, G. L., Schaefer Rodrigues, F., Polano Ody, L., Vinicius Tres, M., Herrera, E., Palacin, H., Cordova-Ramos, J. S., Best, I. & Olivera-Montenegro, L. 2022. Encapsulation of Bioactive Compounds for Food and Agricultural Applications. *Polymers (Basel),* 14**,** 4194.

Zdiri, K., Cayla, A., Elamri, A., Erard, A. & Salaun, F. 2022. Alginate-Based Bio-Composites and Their Potential Applications. *J. Funct. Biomater,* 13**,** 117.

Zhang, H., Cheng, J. & Ao, Q. 2021. Preparation of Alginate-Based Biomaterials and Their Applications in Biomedicine. *Mar. Drugs,* 19**,** 264.

Zhang, H., Wang, H., Wang, J., Guo, R. & Zhang, Q. 2001. The Effect of Ionic Strength on the Viscosity of Sodium Alginate Solution. *Polym. Adv. Technol.,* 12**,** 740-745.

Zhang, P., Chang, C., Liu, H., Li, B., Yan, Q. & Jiang, Z. 2020. Identification of novel angiotensin I-converting enzyme (ACE) inhibitory peptides from wheat gluten hydrolysate by the protease of Pseudomonas aeruginosa. *J. Funct. Foods.,* 65**,** 103751.

Zhang, Z., Zhang, R., Zou, L. & McClements, D. J. 2016. Protein encapsulation in alginate hydrogel beads: Effect of pH on microgel stability, protein retention and protein release. *Food Hydrocolloids,* 58**,** 308-315.

Zhao, C., Latif, A., Williams, K. J. & Tirella, A. 2022. The characterization of molecular weight distribution and aggregation by asymmetrical flow field-flow fractionation of unmodified and oxidized alginate. *Reactive and Functional Polymers,* 175**,** 105292.

Zhu, F. 2017. Encapsulation and delivery of food ingredients using starch based systems. *Food Chem.,* 229**,** 542-552.

Zidar M., Rozman, P., Belko-Parkel K., Ravnik, M. 2020. Control of viscosity in biopharmaceutical protein formulations. *Journal of Colloid and Interface Science.* 508: 308-317.

CHAPTER 2
LITERATURE REVIEW: STATE-OF-THE-ART RESEARCH ON ENCAPSULATION OF SHORT-CHAIN BAPs

2.1 Introduction

Short-chain bioactive peptides (BAPs) are peptides consisting of several amino acids (di- until oligopeptides) which have the potential to promote human health and disease prevention. Over sixty peptides have been authorised in Europe, Japan, and the United States. In addition, in the active clinical development stage, more than 170 and around 260 have been tested in human clinical trials (Wang et al., 2022, Lau and Dunn, 2018). Foods are the most potential basis of BAPs. They have antihypertensive and antidiabetic activities, demonstrating the ability to inhibit angiotensin-converting enzyme (ACE) and dipeptidyl peptidase IV (DPP-IV). A study mentioned that combining anti-ACE or anti-DPP-IV with synthetic drugs shows a synergistic effect, further enhancing their therapeutic effectiveness (Han et al., 2019).

The therapeutic potential of BAPs is shown via their bioactivities. A detailed analysis, in which categorised by obtained data, that the “high” bioactivities, which are considered via their IC_{50} (standard half-maximal inhibitory concentration), are < 10 µM for ACE inhibition and <50 µM for DPP-IV inhibition (**Figure 2.1**). It is according to the review on BAPs from diverse food origins, including animal-based products (Cao et al., 2020, Miguel et al., 2006, Miguel et al., 2008, Sangsawad et al., 2018a, Sangsawad et al., 2018b, Sangsawad et al., 2017), plant-based proteins (Yang et al., 2003, Chen et al., 2013, Gu and Wu, 2013, Marczak et al., 2003, S Vallabha and Tiku, 2013, Wang et al., 2015, Wu et al., 2008b, Yang et al., 2011), fish (Byun and Kim, 2001, Fujita et al., 2000, Balti et al., 2015, Balti et al., 2010, Fahmi et al., 2004, Ghassem et al., 2012, Ghassem et al., 2011, Harnedy-Rothwell et al., 2020, Intarasirisawat et al., 2013, Lee et al., 2011, Li-Chan et al., 2012, Lin et al., 2019, Liu et al., 2016, Ngo et al., 2016, So et al., 2016, Wu et al., 2008a), microalgae (Lin et al., 2018, Lu et al., 2011, Montone et al., 2018, Xie et al., 2018), milk (Contreras et al., 2009, Lacroix and Li-Chan, 2014, Lacroix et al., 2016, Mao et al., 2007, Nongonierma et al., 2019, Nongonierma and FitzGerald, 2014, Shanmugam et al., 2021, Silveira et al., 2013, Uenishi et al., 2012, Yamada et al., 2015, Yan et al., 2019), and mushrooms (Geng et al., 2016).

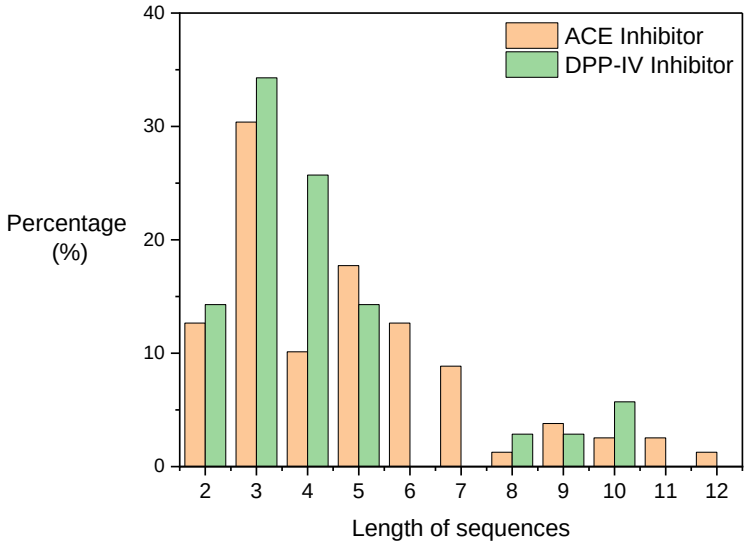


Figure 2.1. The percentage of BAPs (as ACE and DPP-IV inhibitors) from food origins collected according to "high bioactivities"

Figure 2.1 shows that the BAPs with three amino acid sequences have the highest bioactivities. Skrzypczak et al., (2017) mentioned that peptides with 2-10 amino acids are short-chain BAPs, while Cerrato et al., (2022) only adopt those consisting of 2-4 amino acid residues as short-chain BAPs. It is generally accepted that peptide absorption is most efficient as an amino acid or di- or tripeptides (Bhutia and Ganapathy, 2018, Shen and Matsui, 2019). **Figure 2.1** clearly shows that food-based BAPs with the greatest bioactivities seem to have sequences < 10 amino acids.

Some of the latest published reviews have investigated the encapsulation of BAPs. For example, Mirzapour-Kouhdasht et al., (2023) emphasized improving the palatability of BAPs by encapsulation. Berraquero-Garcia et al., (2023) reviews spray-drying and electrospraying techniques for encapsulation of BAPs. Then, Aguilar-Toala et al., (2022) presented approaches to BAP encapsulations and provided an extensive analysis of some methods for protecting the bioactivity of bioactive proteins and peptides. They included a summary of the encapsulation process for bioactive proteins and peptides. Moreover, a review from McClements, (2018) addressed the nanoparticle and microparticle carriers for proteins and peptides, studying challenges for their oral delivery. Despite these comprehensive and timely reviews, none focus on low M_w or short-chain BAPs. While the low M_w or short chain BAPs

entail exceptional obstacles associated with their entrapment/loading in different types of systems, as discussed later in this Chapter (section 2.4), a simple example suffices to this well at the start. A study by O'Neill et al., (2015a) encapsulated a pentapeptide and a dipeptide in similar vehicles. However, it indicated that the dipeptide had lower encapsulation efficiency (EE) and higher release rate, 3 times and 10 times, respectively. Moreover, the amino acid tryptophan (Trp/W) shows an encapsulation efficiency of around 1.25 to 1.5 times lower. It releases ≈1.3 times more than the dipeptide alanine-tryptophan (Ala-Trp/AW), even though both amino acid and the dipeptide have equal charge trends across different pH levels. Hence, the M_w of BAPs has a pivotal effect on encapsulation efficiency and release, as mentioned in Chapter 1 and discussed in this Chapter.

Regarding gastrointestinal stability, it is a crucial prerequisite of BAPs to accelerate the full realisation of their development as bioactive components in functional foods, nutraceuticals, and food supplements. However, the digestion process via proteases in the stomach, intestinal lumen, and intestinal brush border leads to the degradation of BAPs intact sequences and mainly decreases their oral bioaccessibility and bioavailability, as presented in both *in vitro* and *in vivo* studies (Miguel et al., 2008, Lacroix et al., 2017, Basirico et al., 2015, Fernández-Musoles et al., 2013). To overcome this limitation of BAPs, which are vulnerable to protease hydrolysis, encapsulation helps to preserve their structural integrity until they reach the desired site of adsorption in the intestinal epithelium. **Figure 2.2** represents the principal elements and various factors that need to be considered for BAPs and their encapsulation to build innovative functional food ingredients and supplements. The scope of this chapter is to critically analyse the recently published literature on BAP encapsulations and identify existing gaps of knowledge and the important research features that underpin their potential applications in foods.

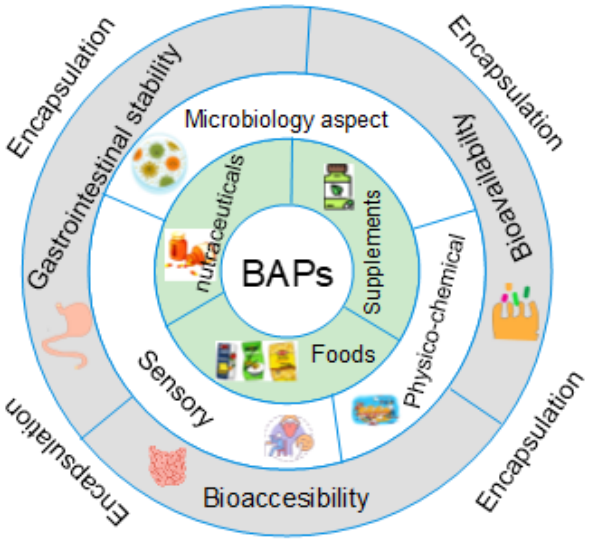


Figure 2.2 Multilevel pie chart describing important aspects of developing encapsulated BAPs as ingredients of food supplements, nutraceuticals, and functional food.

2.2 Types of Short-chain BAPs

Since 2010, several studies have addressed BAP encapsulation for gastrointestinal delivery, and this Chapter concentrates on this period (i.e., 2010 onwards). These were focused on di-, tri-, tetra- and up to undecapeptides of molecular weight (M_w) ranging from 273.5 to 1493.7 Da (g/mol). Encapsulation of BAPs from different sources with proven bioactivities like antioxidant, antihypertensive, antiproliferative, anti-inflammatory, hypocholesterolemic, anxiolytic, anticancer and absorption permeation enhancers have been reported. The summary of research on the encapsulation of BAPs, covering a range of M_w, sequence, and their biological activities, is presented in **Table 2.1.**

The research studies in **Table 2.1** are according to both naturally and synthetic-derived BAPs, with many being purified synthetic peptides, but several were also derived from food origins. The hexapeptide RLSFNP and tripeptide IPP were obtained from lactoglobulin and casein (Nakamura et al., 1995), respectively; the tripeptide LKP was extracted from bonito fish (Fujita and Yoshikawa, 1999), and pentapeptide VLPVP was expressed in milk by engineered recombinant *E. coli* (Liu et al., 2007). The tetrapeptide LQPE was generated from milk casein hydrolysis using a commercialized product of mixture proteases (Neutrase)®(Jiang et al., 2021). The decapeptide YLGYLEQLLR (α-casozepine) is derived from the hydrolysis of whey protein via bovine trypsin (Miclo et al., 2001). Then, using bioprocessing technology, the

glutathione (ɣ-glutamyl-cysteinyl glycine, GSH) or ECG is produced using *Saccharomyces cerevisiae* and *Candida utilis* (Li et al., 2004). In addition, the tripeptide KPV is a hormone (alpha-melanocyte-stimulating) naturally found in the human body. Meanwhile, the octapeptide FCFWKTCT (octreotide) is a synthetic somatostatin with a cyclic structure (Parmentier et al., 2011). Regardless of the exhibited potent biological effect, however, when administered orally, the absolute bioavailability of short peptides and BAPs was negligible (<~1%) due to the degradation and fast elimination (Zhou and Po, 1991, Fjellestad-Paulsen et al., 1993). Colloidal carriers have been applied to improve their pharmacokinetics (Martins et al., 2007). Notable, only a relatively small quantity of short-chain BAPs (amino acids <20) has been appointed for encapsulation studies for gastrointestinal tract delivery. These span a wide range of diversity in terms of their biological sources, methods of production, size and structure, as discussed further on.

Table 2.1. Short-chain BAPs encapsulated for gastrointestinal delivery

Type BAPs	Sequence*	Molar mass (g/mol)	Bioactivities**	Ref.
Dipeptide	AW	275.3	NR	(Stephansen et al., 2014)
	FW	351.4	NR	(O'Neill et al., 2015a, O'Neill et al., 2015b)
	IPP	352.4	Antihypertensive ACE Inhibitor	(Danish et al., 2017)
	LKP	356.5	Antihypertensive ACE Inhibitor	(Danish et al., 2017)
Tripeptide	ECG	307.3	Antioxidant	(Trapani et al., 2010)
	KPV	342.4	Anti-inflammatory	(Laroui et al., 2010, Xiao et al., 2017)
	YKT	410.5	Anticancer	(Bicak et al., 2021)
Tetrapeptide	LQPE	485.5	Hypocholesterole-mic	(Jiang et al., 2021)
Pentapeptide	LWMRF	751.9	NR	(O'Neill et al., 2015a, O'Neill et al., 2015b)
	VLPVP	523.6	Antihypertensive ACE Inhibitor	(Huang et al., 2017)
Hexapeptide	RLSFNP	732.8	Antihypertensive ACE Inhibitor	(Zhang et al., 2019)
Octapeptide	FCFWKTCT	1035.2	Antiproliferative	(Parmentier et al., 2011)
Decapeptide	YLGYLEQLLR	1267.4	Anxiolytic	(Batista et al., 2021)
Undecapeptide	GRKKRRQRRRP	1493.7	Permeation enhancer	(Chen et al., 2017)

**Amino acids single letter code key*: A=alanine; C=cysteine; E=glutamic acid; F=phenylalanine; G=glycine; I=isoleucine; K=lysine; L=leucine; M=methionine; N=asparagine; P=proline; Q=glutamine; R=arginine; S=serine; T=threonine; V=valine; W=tryptophan; Y=tyrosine.
***NR*=not reported

The tripeptides LKP and IPP, pentapeptide VLPVP, and hexapeptide RLSFNP have been documented as angiotensin-converting enzyme (ACE) inhibitors for antihypertensive. (Danish et al., 2017, Huang et al., 2017, Zhang et al., 2019) An anxiolytic activity was shown by decapeptide YLGYLEQLLR (α-casozepine) (Batista et al., 2021). The oxidative damage affected by the reactive oxygen species (ROS) free radicals which circulate in the body was prevented by the GSH (peptide ECG) (Trapani et al., 2010). While antiproliferative activity is provided by octapeptide FCFWKTCT (octreotide) via suppressing endocrine and exocrine secretion by the pancreas (Parmentier et al., 2011). Regarding their possible applications, in most circumstances, they must be absorbed into the systemic circulation system and reach their target sites before finally displaying the bioactive effects (Cao et al., 2020, Fernández-Musoles et al., 2013). To this objective, encapsulation has been recognized as one of the approaches that provide BAPs protection against degradation in the gastrointestinal tracts, control their release in an intact form at the action sites, and enhance their absorption, thus improving their bioaccessibility and bioavailability. In addition, other encapsulated BAPs cover anti-inflammatory tripeptide KPV and hypocholesterolemic tetrapeptide LQPE. The KPV has been documented as having anti-inflammatory activity by inhibiting the synthesis of proinflammatory cytokine, which is naturally secreted into the colon. For this reason, this tripeptide has been investigated as a therapeutic peptide for extensive intestine infection treatment, specifically inflammatory-related bowel diseases (IBD) (Dalmasso et al., 2008, Kannengiesser et al., 2008). The LQPE shows the capacity to reduce micellar cholesterol solubility and influence the enzymes and protein expression associated with cholesterol absorption in the epithelial cells of the small intestine (Jiang et al., 2020), where this tetrapeptide should be released in its complete sequences.

2.3 Types of Carrier Particles for Encapsulation and Their Preparation

A comprehensive review on colloidal nano- and microparticle carriers for therapeutic peptide encapsulation has been published elsewhere (Martins et al., 2007, Aguilar-Toala et al., 2022, McClements, 2018). Several approaches have attempted to entrap peptides, such as via complexation, conjugation, crystallization, or self-assembly through chemical or physical additions (Kommineni et al., 2023). A variety of delivery vehicles have been tailored for encapsulation, preservation and release of short-chain BAPs (hereafter simply referred to as 'BAPs'). Overall, there are two approaches to loading the BAPs into these structures: (i) in situ

loading or the internal method, which means the loading carried out during the particle formation, and (ii) pro-loading or the external method, where the loading is executed after particle formation. Method (i) usually requires mixing the BAP with encapsulant wall materials to some extent, which may determine the size and structure of the carrier vehicle, and the BAPs could simply diffuse into the system. Method (ii) typically comprises depositing a suspension of wall materials (the preformed vehicles) in some sort of solution of the BAPs. For the latter, it could also affect some change in the vehicle's size and structure if it aims to swell or shrinkage in the BAP solution. Indeed, the size of the carrier agents can be used to classify types of delivery vehicles.

2.3.1 Nanoencapsulation

2.3.1.1 Nanoparticles (NPs)

For more than four decades, nanoparticles (NPs), i.e., colloidal particles < ~100 nm, have been the centre of attention of research in drug delivery. Currently, their clinical translation and application are important pillars in the nanomedicine field. It is because of their size, composition, the nature of their surface, a massive surface area-to-volume ratio, and unique edges for the administration of bioactive payloads that indicate either poor absorption, degradation, or toxicity. These cover molecules which do not meet Lipinski's rule of five (i.e., less than ten H acceptor groups, less than five H donor groups, M_w < 500 Da, logP octanol: water partition coefficient < 5.0) (Lipinski et al., 2001). NPs can contain polysaccharides such as hyaluronic acid (HA), dextran, pectin, arabinogalactans, chitosan (CS), alginate (ALG), and chemical derivatives of them, or proteins such as gelatine, lysozyme, lactoferrin and zein, among others. NPs built from natural polymers and macromolecules have drawn increasing interest, providing the breadth of desirable characteristics, including stability, biocompatibility, and mucoactivity (mucodiffusion or mucoadhesion). Moreover, they can improve the bioavailability and bioaccessibility of low absorption efficiency payloads by increasing their epithelial uptake. Furthermore, by using those mentioned above components, it can be able to produce the vehicles at relatively mild conditions such as aqueous state and room temperature, hence facilitating the maintenance of the bioactivity of delicate biological-type payloads like hormones, nucleic acids, vaccines, antibodies as well as BAPs (Caro-Leon et al., 2018, Luque-Alcaraz et al., 2016).

NPs based on polysaccharides and proteins may also to form and occur during traditional cooking processes of foods, which are referred to as “incidental NPs” (Gao et al., 2021). Additionally, the polymeric NPs may be purposefully fabricated and added to foods as various colloidal dispersions (Zielinska et al., 2020). The NPs intended for oral delivery of BAPs have been prepared via two methods: 1) coacervation (ionic gelation) (Danish et al., 2017, Trapani et al., 2010, Bicak et al., 2021, Chen et al., 2017), and 2) double emulsion and solvent evaporation (Laroui et al., 2010, Xiao et al., 2017). The preparation stages and primary features of each of these protocols are outlined below.

Concerning the coacervation method, the NP systems have been set up from CS (Bicak et al., 2021) and cyclodextrin (CD) (Trapani et al., 2010), tripolyphosphate (TPP) (Danish et al., 2017), and the synthetic methyl acrylate-based copolymers termed Eudragit (Chen et al., 2017). The double emulsion and solvent evaporation approach, CS+ALG (Laroui et al., 2010) and hyaluronic acid (HA)-CS (Xiao et al., 2017) NPs have been studied.

A study conducted by Trapani et al., (2010) investigated glutathione (ECG, also denoted as GSH) encapsulation into CS NPs and CS/CD NPs. Concerning the CD, there were two types of CD were tried: α-CD and sulphobutyl-ether-β-CD – termed or SBE-β-CD. In the CS NPs, encapsulation was performed via blending CS and ECG peptide solutions. Then, tripolyphosphate (TPP) was added to induce spontaneous NP formation via ionic cross-linking between the negative charges on the TPP and the positive charges on the CS. For the entrapment into CS/α-CD or CS/SBE-β-CD NPs, the tripeptide was initially blended with α-CD or SBE-β-CD solutions, and then the CS solution was introduced before finally, TPP was added. In other approaches, the tailored NPs were further coated with another polymer. For instance, a permeation enhancer undecapeptide alongside insulin (a 51 amino acid peptide) encapsulated into Eudragit-coated CS NPs. In this case, the undecapeptide was dissolved using acetic acid, mixed with CS, and cross-linked with TPP to create undecapeptide-insulin-CS NPs. Next, the Eudragit (dissolved in ethanol) was gently introduced into loaded NP dispersion, and the evaporation technique was used to remove ethanol, which then led to coating the NPs (Chen et al., 2017). Moreover, the tripeptide IPP and LKP have also been encapsulated into CS NP systems, however, with different sequences on encapsulant materials addition; in other words, initially, the tripeptide blended with TPP, followed by CS addition (Danish et al., 2017).

These different orders of the addition of the components (see **Figure 2.3**) tend to influence the size, structure, production yields, and encapsulation efficiencies (EE) of the NPs.

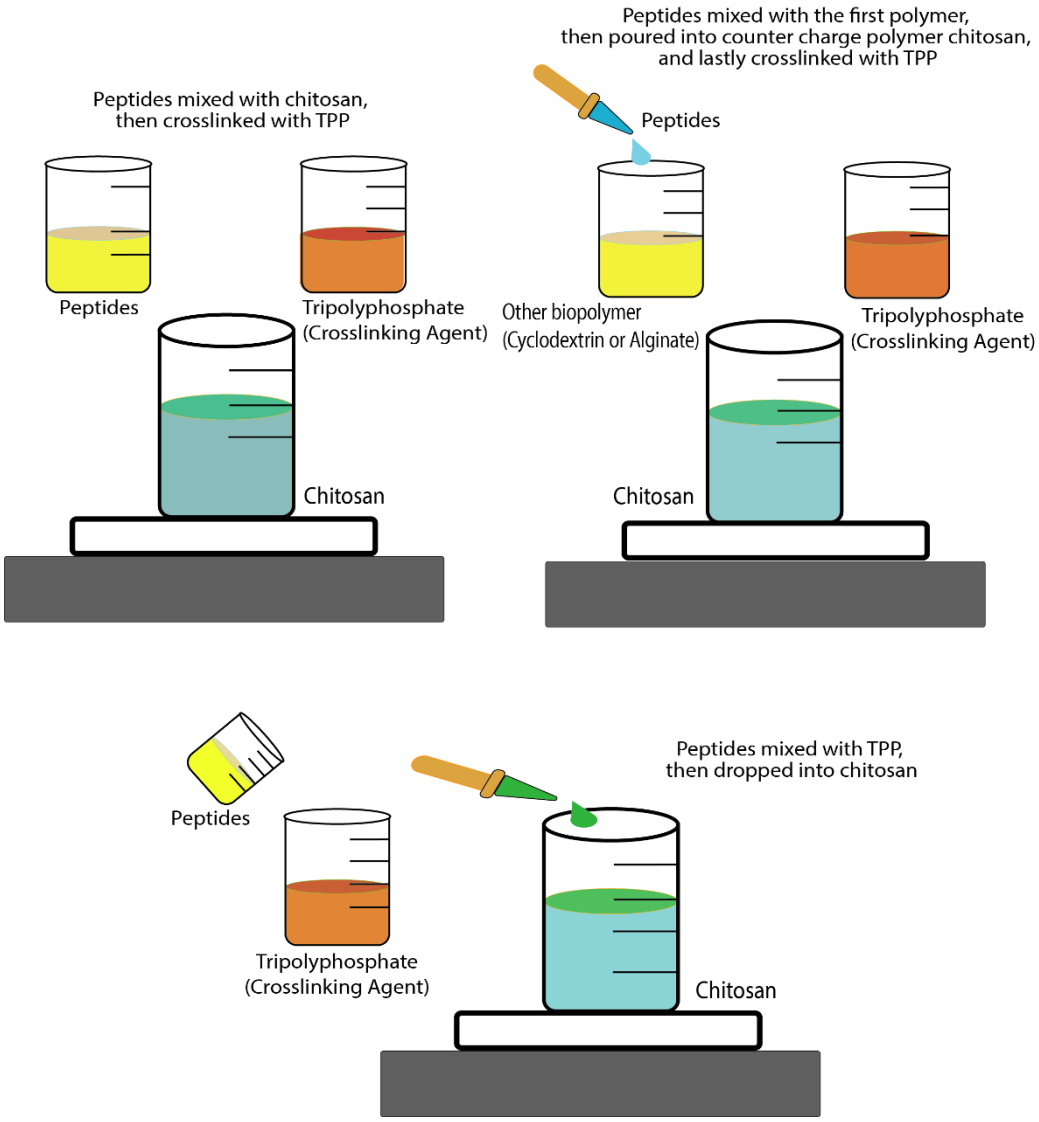


Figure 2.3. Illustration of the three techniques for BAP encapsulations via ionic gelation/coacervation.

Even though the order of mixing of the ingredients (encapsulant materials) is frequently ignored, but it plays a critical role in determining the features of the formulated particles. For example, the EE and size of CS-TPP NPs have been identified to be sensitive. It means that the technique order of mixing could contribute to affecting the EE and size of CS-TPP NPs. Danish et al., (2017) presented that dissolving the peptide into the TPP solution in the beginning, then followed by the addition of CS, fabricating better EE and smaller-sized NPs

compared to the mode of addition studied by Trapani et al., (2010). However, within the scope of CS-CD-TPP-NPs, no definitive proof looks favourable whether it is optimal to add the peptide into either CS or CD solution first. Notably, besides SBE-β-CD having a M_w at least twice as significant as α-CD, CS/SBE-β-CD-TPP NPs showed a smaller size than both CS-TPP NPs and CS/α-CD-TPP. Additionally, the EE of ECG peptide into CS/SBE-β-CD-TPP NPs is more significant than into CS/α-CD-TPP or CS-TPP NPs by a remarkable around fivefold. In theory, it is generally accepted that in ionic gelation, the mixing order depends on each molecule's charge. Dissolving the peptide into the solutions with a similar charge before blending with the counter-charged solution is favoured to avoid undesired premature interactions and aggregation driven by full charge compensation and neutralisation, leading to loss of electrostatic colloidal stabilisation as discussed in **Chapter 1** (section 1.2.2).

Furthermore, the effect of the biopolymer structural properties, for instance, the degree and pattern of acetylation (e.g. CS), block composition (e.g. ALG), degree of esterification (e.g. pectin), as well as the M_w and polydispersity (Đ) of the diverse biopolymer groups, on the size, surface charge, morphology, and peptides EE (discussed later on this Chapter) of the different type of NPs, however has been widely neglected.

With regards to double emulsions and solvent evaporation, they have been used to encapsulate KPV into CS/ALG NPs and hyaluronic acid (HA)-CS NPs (Laroui et al., 2010, Xiao et al., 2017). In fact, most hydrophilic drugs have been encapsulated via water-in-oil-in-water (W/O/W) emulsions in which the core of non-aqueous phase is a combination of solvent/oil mixture + polymer. Then, the solvent is evaporated away to exclude a hardened polymer sheet, coating the internal aqueous phase and its bioactive payload. In the cases of BAPs, the polymers that have been investigated, namely poly(lactic acid) (PLA) or poly(lactide-co-glycolide-acid) (PLGA), which dissolved in dichloromethane, and a final stabilizing layer PVA was incorporated into the dispersion in water. In some cases, this system was freeze-dried and re-dispersed in CS and/or ALG solutions before application. One general limitation of the double emulsion method is the lack of natural, biocompatible W/O emulsifiers.

Eventually, nanotechnology applications in food require a detailed assessment of possible risks to consumers' health and wellness, as documented by the European Food Safety Authority (EFSA) Committee. The EFSA guidance files describe specific standards for nano-specific risk assessment, especially highlighting the particles lower than 500 nm, with a

distribution more than 10% for the size < 250 nm (More et al., 2021, EFSA, 2018). The principal features in this analysis involving the physicochemical characteristics, biokinetics, potential cellular uptake, physiological fate, as well as distribution of NPs. The guidance underscores the relevance of assessing the longevity of particles, such as solubility and dissolution rate, plus aspects such as agglomeration, dispersion, and biological relevance of particle size after reaching the gastrointestinal regions (Schoonjans et al., 2023, Xavier et al., 2021). For food that consisting natural polymers at the nano size level, which undergoes digestion and assimilation without translocation outside the gastrointestinal tract, and no adverse effects are reported, a risk assessment identical to the conventional food products is considered accepted.

2.3.1.2 Liposomes

A liposome is a carrier agent created via phospholipid bilayers that surround a significant proportion of an internal aqueous phase compared to the volume of the bilayers. This sort of carrier agent mimics a cell and its cell membrane. Liposomes have been used to deliver both hydrophobic and hydrophilic drugs and were approved by the Food and Drug Administration (FDA) to deliver doxorubicin (Doxil®) (Thapa and Kim, 2023) in 1995, which is also well known as the first 'nanomedicines' breakthrough during that time. Dissolution of the lipids in an organic solution followed by evaporation of the solvent and rehydration with an aqueous is a conventional technique of liposome fabrication. In addition, the agitation intensity also affects liposome models where mild agitation with slow hydration usually produces multilamellar vehicles (MLVs), whilst more vigorous agitation (frequently with sonication and extrusion) is accustomed to generating unilamellar liposomes.

In BAPs, the hypocholesterolemic tetrapeptides, antihypertensive hexapeptides, and antiproliferative octapeptides have been loaded into liposomes and investigated. There was a case in which the liposomes loaded with BAP were modified further by encapsulating with *Lactobacillus* surface (S-layer) protein as an outer layer to enhance their adhesion (Jiang et al., 2021). Indeed, as mentioned above, the MLVs can be applied to provide extra protective layers to the payload (Uhl et al., 2023).

In situ and pro-loading methods have been used to encapsulate BAPs with liposomes (Ichikawa, 2008). In situ loading shadows are similar to the procedures for liposome preparation, but at the liposome formation, the BAPs are prepared in the aqueous phase. In

this technique, Zhang et al., (2019) encapsulated RLSFNP in cholesterol + soy lecithin liposomes with ethyl ether as a solvent, while Jiang et al., (2021) using 1,2-dipalmitoyl-sn-glycero-3-phosphocholine + cholesterol + octadecylamine liposomes to entrap the LQPE where trichloromethane applied as a solvent.

The pro-loading approach has encapsulated the synthetic octreotide (**Table 2.1**) into tetraether lipid liposomes. Cholesterol, egg phosphatidylcholine (EPC), dipalmitoyl phosphatidylcholine (DPPC), and tetraether lipids from *Archaea spp.* were employed as the lipid materials (Parmentier et al., 2011). The extrusion via 200 and 400 nm membrane filters (after evaporation of the solvent and rehydration of MLVs), was performed to obtained (so-called) as liposomes. Loading was obtained via blending the BAP (octreotide) with the liposome suspension and then freeze-drying and rehydration were carried out.

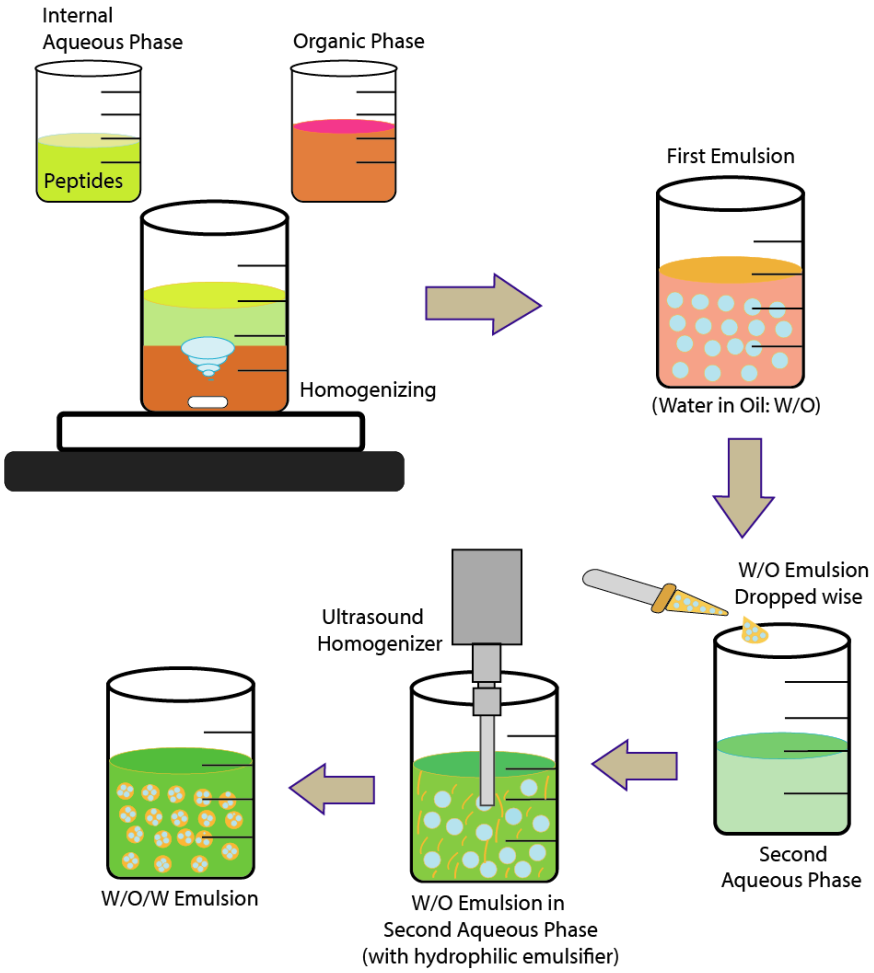


Figure 2.4. An illustration of the approach for encapsulation BAPs using double emulsions + solvent evaporation.

2.3.2 Microencapsulation

Microparticles (MPs) are particles that commonly have means of diameter ranging from 1 to several tens of μm. Even though their greater sizes could cause problems with colloidal stability and sedimentation, several styles have still been explored for BAP encapsulation (McClements, 2018).

2.3.2.1 Microgel particles

Regarding carrier agents of BAPs, coacervation and membrane emulsification are two ways that have been studied to fabricate microgel particles. Then, the most dominant encapsulant wall materials were CS, sodium alginate (SA), and whey protein isolate (WPI). The Guar-CS microgels have encapsulated anxiolytic decapeptide YLGYLEQLLR (Batista et al., 2021). Here, the microgels were prepared by dissolving CS and the BAPs into acetic acid and cross-linked using TPP. Later, the created CS-based microgels were immersed in guar gum solution (Batista et al., 2021). The cold gelation process was also studied to create whey protein microgels for FW and LWMRF BAPs entrapment. Calcium chloride ($CaCl_2$) as a cross-linker blended with pre-heated and cooled whey protein and then followed with immersion into a solution of the BAPs for 24 h (O'Neill et al., 2015a, O'Neill et al., 2015b).

Membrane emulsification and extrusion is another method for producing microgel MPs (Huang et al., 2017). By a W/O emulsion, they have been used to encapsulate the ACE inhibitor VLPVP using SA-coated O-carboxymethyl chitosan (O-CMCS). Initially, the SA and BAPs in acetate shaped the aqueous phase, while paraffin oil, which consists of hexaglycerin penta ester surfactant and petroleum ether, built the oil phase. Then, the water phase is forced into the oil phase via the pores of the membrane to assemble with the first W/O emulsion, and the second W/O emulsion containing $CaCl_2$ is created and merged with the first emulsion. The $CaCl_2$ generates and transfers Ca^{2+} ions to cross-link the SA in the first emulsion creating the gel of water droplets (MPs). The obtained microgel MPs containing BAPs may subsequently be washed and freeze-dried. In this experiment, they also tried extruding SA solution into $CaCl_2$ using a thin nozzle and then coating the particles with O-CMCS. **Figures 2.3** and **2.4** illustrate the ionic gelation/coacervation and double emulsion/solvent evaporation strategies.

2.3.2.2 Microfibers

Microfibers (MFs) have also been applied to encapsulate the dipeptide AW. In this case, the fish sarcoplasmic protein (FSP) was dissolved in hexafluoro-2-propanol (HFIP), the BAPs added, and then MFs formed via the electrospinning technique at room temperature (Stephansen et al., 2014).

However, among the above strategies of encapsulation of BAPs, especially by ionic gelation/coacervation and double emulsion solvent evaporation, there were limited studies on the gastrointestinal stability of the vehicle or encapsulant, both loaded and unloaded. Laroui et al., (2010) used double emulsion and solvent evaporation technique to encapsulate BAPs, which then the obtained loaded NPs embedded in chitosan (CS)+alginate (ALG) hydrogel. However, they examined the gastrointestinal stability of the hydrogel before loading it with NPs. The CS+ALG hydrogel, which ionically cross-linked within the presence of Ca^{2+} and SO_4^{2-} ions, was assessed for its kinetics of swelling to determine its stability in simulated gastric fluid pH 1 to 3 (2 M buffer acetate, 50 μg mL^{-1} pepsin, 5 μg mL^{-1} trypsin) and intestinal fluid pH 4 until 6 (0.1 M buffer phosphate, 5 μg mL^{-1} pepsin, 30 μg mL^{-1} trypsin). As a result, they concluded that the hydrogel was stable at gastric pH 1 - 3 for 24 h, but they shrank at pH 4 and finally collapsed to form a dispersion at pH 5 and 6 after 24 h.

Besides the encapsulation of BAPs, the CS + TPP NPs formed via ionic gelation were assessed for stability in simulated salivary fluid at pH 6.8. The comparison between ALG NPs and pectin NPs (Pec-NPs) revealed CS-NPs to be the least stable, indicated by increasing polydispersity index (PDI) and size (hydrodynamic diameter), in the same time, ζ-potential was getting lower. For instance, before integration with artificial saliva, CS NPs exhibited PDI values below 0.2, then escalated to 0.4 post-mixing and exceeding 0.6 after 20-minute incubation. The size of the CS NPs after 40 minutes of incubation kept increasing gradually. Even though the ζ-potential remained stable throughout the testing period (0 to 120 minutes), they decreased from +25 mV (pre-mixing) to below +10 mV (post-blending with artificial salivary fluid). These changes were associated with pH increasing and then leading to CS deprotonation (i.e. pK_a ~6.1). Moreover, the presence of sulphates, phosphates, and carbonates in the buffer solution could bind to CS's charged groups, causing particle bridging, reduced stability, and the formation of aggregates as well as precipitates (Pistone et al., 2017).

A study from Goycoolea et al., (2009) explored the stability of CS+TPP+ALG NPs loaded with insulin via ionic gelation and examined the efficacy for intranasal delivery of insulin. As a result, the colloidal NPs showed robust stability for a long duration, continuing for 1 h 20 min of incubation in pH 4.3 acetic buffer solution. It was proven by the nonexistence of any discernible changes in their hydrodynamic radius (R_h), as measured using DLS. Under acidic conditions, CS experiences greater protonation, fostering stronger electrostatic interactions between CS and its crosslinking agents, such as TPP and other charged polyanionic molecules. The amplified protonation of the cationic CS aids in the strengthening of these ionic interactions. It is important to note that the stability of NPs formed with ionic gelation, such as CS+TPP NPs, is not exclusively dependent on the ionic strength of the medium, but it is intricately also affected by the molar ratio among the participating molecules (Goycoolea et al., 2009) as introduced in **Chapter 1**.

Regarding emulsion-based encapsulation systems, like water-in-oil-in-water (W/O/W) double emulsion, in which water is the dispersed or called continuous phase and situated on the outermost part of the system, this technique has analogies with the single emulsion oil-in-water (O/W) emulsion. The W/O/W encapsulation system is mainly employed to tackle poor encapsulation efficiency of highly hydrophilic bioactive compounds that tend to leach during encapsulation. The type and concentration of stabilizers used in the system affect its stability, including in the gastrointestinal tract (Iqbal et al., 2015). Undesired flocculation and coalescence of oil droplets, which are probably due to pepsinolysis and the ionic environment effects during digestion, are drawbacks of typical stabilisers used for O/W emulsion formation such as proteins and surfactants (Torres et al., 2019).

Torres et al., (2019) investigated the stability of the O/W emulsion-based encapsulation system during in vitro gastric and intestinal digestion, in which whey protein isolate (WPI) was used as a stabiliser. In this research, the emulsion system was incubated to simulated gastric fluid (SGF) at pH 3 containing pepsin, mimicking the stomach in a fasted state. Afterwards, the encapsulation system was transferred and incubated in simulated intestinal fluid (SIF) at pH 6.8, which contained pancreatin solution and bile salts. The results suggested that the emulsion underwent coalescence and flocculation in the SGF, meaning they have a slightly more stable emulsion droplet distribution in the SIF, with sizes ranging between approximately 1 to 50 µm, when compared to the SIF incubation without in vitro

gastric pre-digestion, the system also had more extended stability. For the latter, the emulsion collapsed within 30 min (becoming very polydisperse) with a notable peak in the size range 100 to 1000 µm. Bile salts could potentially replace the WPI at the interface during intestinal conditions. (The size observation in this study was carried out using confocal laser scanning microscopy - CLSM).

2. 4. Key characteristics of delivery vehicles

Table 2.2 shows several delivery vehicles, their sizes, processes of formation and encapsulation efficiency (EE), and the release behaviour of BAPs. **Figure 2.5** shows their typical scales of size and structures.

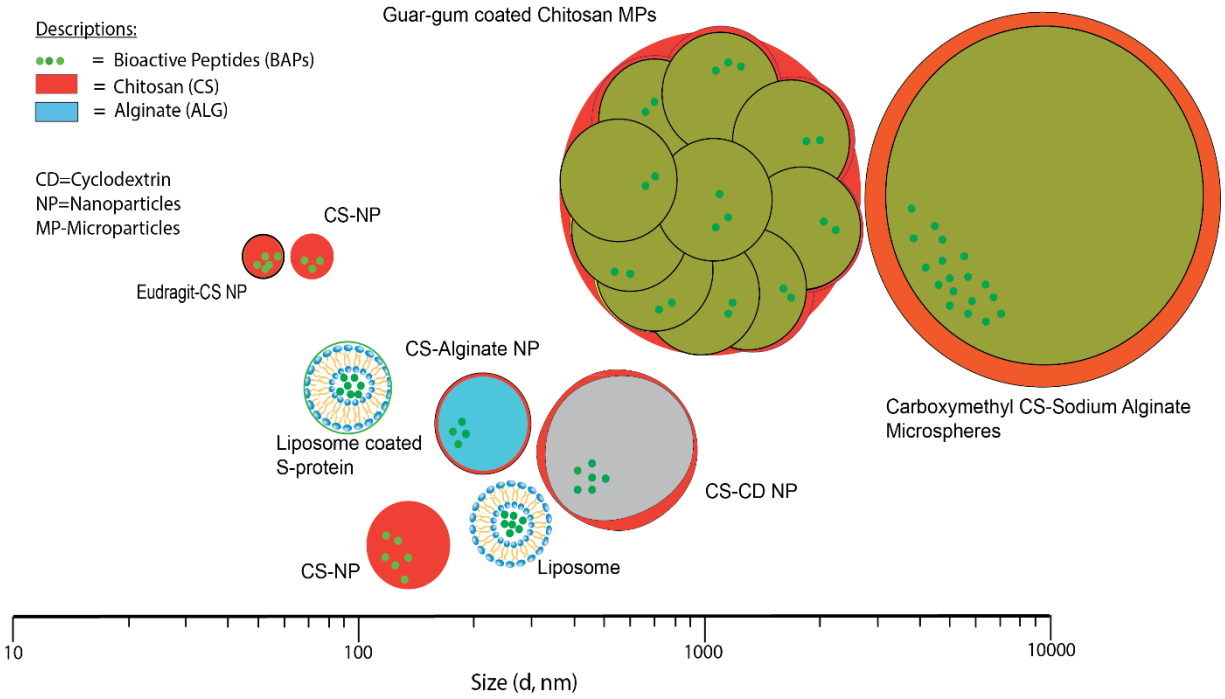


Figure 2.5. Size distribution of NPs and MPs based on biopolymers as delivery vehicles for short-chain BAPs.

2.4.1 Association/entrapment efficiency (EE)

The percentage of BAPs added to a successfully entrapped system within the vehicles is generally called the BAP encapsulation/entrapment efficiency (EE %) (Jiang et al., 2021, Danish et al., 2017, Trapani et al., 2010, Bicak et al., 2021, Zhang et al., 2019). Measuring the amount of BAP lost to the delivery vehicle from the original BAP solution or via extracting the amount of BAP contained within the vehicles post-loading, e.g., by dialysis, centrifugation and

dissolution of the vehicle, are the ways to calculate EE. So far, the most common method to assay for BAP content is HPLC or reverse phase HPLC (RP-HPLC). However, it is frequently challenging to obtain EE values close to 100%; however, delivering a sufficiently high dose of bioactive at the target site is equally important (Park et al., 2019).

To identify the most optimal carrier system, the loaded BAPs in nano- and microparticle carriers require special attention and obstacles, as described earlier. The M_w, solubility, amino acid sequence, hydrophobicity, polarizability, net charge, and ionisation state of the BAPs affect the EE, as outlined in a few comprehensive reviews on therapeutic peptides (Martins et al., 2007, Brown et al., 2019).

On the one side, during their formulation into matrix-type systems such as nanoprecipitates obtained by solvent displacement, they are not retained but released into the aqueous phase. On the other side, upon loading into self-assembled electrostatic polyelectrolyte complexes, the low M_w BAP, which interacts with one of the polyelectrolyte components, may be expelled from the network due to weaker ionic interaction of BAPs compared to other polyelectrolytes that bring exact charges. Determining the association efficiency of low M_w BAPs is like dictating the loading efficiency of small M_w drugs. Therefore, here, for instance, from previous studies in the model of drugs, M_w ranged between 242 and 479 Da (~ 242 until 479 g/mol) have shown that the hydrophobicity and polarizability affect their encapsulation efficiency. Low association efficiency (lower than 12%) was obtained because more hydrophilic compounds with minimal polarizability expressed a greater tendency to be displaced by the chitosan (Fuenzalida et al., 2014). **Table 2.2** presents the association of various types of carrier formulations with the BAPs, demonstrating efficiencies diverse over a wide range between 7 and 95%, hence indicating the complexity of elements involved.

As discussed above, the delivery vehicles that have been developed are relatively wide-ranging. However, their EE and release were not tested for single BAP at diverse vehicle modes: a maximum of two, at most (Jiang et al., 2021, Chen et al., 2017) and rarely three (Trapani et al., 2010), different models of carriers seem to have been investigated for the same BAP. Meanwhile, only one BAP, or occasionally two different BAPs, were tested in most of each type of delivery vehicle (Danish et al., 2017). To consider the intrinsic properties of both delivery vehicles and the BAP, the most effective delivery vehicles for a given low M_w BAP must

be investigated. Thus, the size and structure of the loaded carrier agents may be difficult to compare in terms of the efficiency of various systems and the consequence of the BAP itself. Predominantly, the quantification of BAP composition via EE has used HPLC or RP-HPLC technique. Fluorescence spectroscopy is the sole exception for quantifying BAP (KPV) loaded into W/O/W emulsions (Laroui et al., 2010). Commonly, the more widespread EE values seem lower, except for BAPs of YLGYLEQLLR into CS+TPP+GG microparticles (86.1%) (Batista et al., 2021), and LQPE into liposomes (89.0 %) shown by loading via in situ methods of BAPs into various types of delivery vehicles (Jiang et al., 2021). In these cases, the YLGYLEQLLR should have positive and negative charges at neutral pH, and LQPE has one negative charge.

Furthermore, nanoparticles (NPs) generated from CS-TPP systems, in which three different sequence BAPs, namely, IPP, LKP and YKT, were loaded via an in situ approach, showed EE ranged from 22.6 to 65.1%, influenced by the TPP: CS ratio (Danish et al., 2017, Bicak et al., 2021); the similar carrier had EE merely = 7% for ECG entrapment (Trapani et al., 2010). The explanations for these dissimilarities with different BAPs are not clear, even though it should be emphasised that both YKT and LKP have positive charges at neutral pH, whereas ECG has a negative charge. In addition, by utilising slightly different systems like CS+α-CD+TPP and CS+β-CD+TPP (Trapani et al., 2010) for BAP ECG's entrapment, the EE were 5.6 and 25%, respectively. Before adding the CS, the BAP was mixed first with the CD. Hence, the greater affinity of ECG to β-CD may cause the difference. While encapsulating higher M_w BAP GRKKRRQRRRP with the similar CS+TPP method (Batista et al., 2021), the EE= 51.20 %, i.e., which is higher than the majority of the other CS+TPP systems investigated; therefore, this might factor to increase retention of BAP GRKKRRQRRRP via in situ approach. However, different BAP hydrophobicity's and charges should also be taken into consideration. The later BAP has a relatively more significant composition of amino acids with positive charges during neutral pH. Moreover, there was no change in EE even after the addition of Eudragit to the system post-encapsulation.

For the liposomal NPs, EE has also been quantified, Jiang et al., (2021) via in situ encapsulation, and they provided EE = 89%, both uncoated or coated with SLP. Thus, it seems clear that the dissolution of all the components in a solvent and evaporation before rehydration forced an intimate contact between BAPs and encapsulation components, then increasing EE. (However, this does not exactly mean that rehydration will create a high

retention – see the next section, which discusses BAP release). In addition, NPs created by the double emulsion and solvent evaporation method (Laroui et al., 2010), similarly showed high EE values of around 71%. On the other hand, encapsulation via microgels (pro-loaded) has also been shown to have relatively high EE value ranges. For instance, WPI microbeads loaded with FW and LWMRF using various volume ratios of microbead particles to BAP solutions have an EE maximum of 95.1% (O'Neill et al., 2015b, O'Neill et al., 2015a). The EE increased as a function of increasing ratio; higher EE obtained 56.3% and 95.1% for FW and LWMRF, respectively (at a similar volume ratio), the latter having a positive charge. Furthermore, SAL+O-CMCS beads made via the membrane emulsification method (Huang et al., 2017), for loading BAP VLPVP provide EE = 87.8%, where the loading was via an in situ approach. In this case, the experiments to create the same types of particles via the extrusion method called 'encapsulator' nozzles and needles provided relatively lower EE (maximum values of 65 and 35 %, respectively), indicating that the emulsification approach has superiority in this system.

2.4.2 Size, surface properties and shape (morphology)

Size, surface properties or charge, and shape (morphology) of NPs and MPs are other important attributes that influence EE, release, and interactions of loaded carrier agents with biological interfaces like mucosa or epithelial membranes, thus affecting cellular uptake and intracellular trafficking. The preparation techniques and overall composition can control these attributes to some extent.

Regarding size, it is generally accepted that delivery particles that can cross the cell membrane via passive diffusion are only lipid NPs of size ~30 nm (Kettler et al., 2014). Other studies have shown that particles must be under ~200 nm to diffuse quickly through the intestinal mucus layers to the epithelial cells (Yun et al., 2013, Pearson et al., 2016). Bigger particles rely on active transport, meaning energy-dependent (Yang et al., 2014). Endocytosis, which is commonly receptor-mediated pinocytosis and phagocytosis, is the primary mechanism of cellular particle uptake in eukaryotic cells. Generally, NPs < ~100 nm can be engulfed via pinocytosis, while NPs ~150 – 200 nm are taken up via receptor-mediated endocytosis. In addition, phagocytic mechanisms are working for particles ranging from ~250 nm to 3 μm (Foroozandeh and Aziz, 2018). Regarding the shapes, rod-like NPs with a higher aspect ratio presented more efficiently in penetrating Hela and Caco-2 cell membranes (Salatin et al., 2015).

The NPs and MPs that have been comprehensively identified regarding their size distribution, for instance, include CS NPs and Eudragit-coated CS NPs, whose mean diameters were reported as 57 and 51 nm, respectively (Bicak et al., 2021, Chen et al., 2017). In comparison, CS/CD NPs were the bigger size for this type of NP, as documented at around 500 nm (Trapani et al., 2010). It is concluded that manipulating initial concentration and the solvent environment as controllable attributes is advisable to fabricate CS-based NPs consistently (Sreekumar et al., 2018). The average diameters ranging from ~130 to 218 nm were found in the liposomes loaded with BAPs (Jiang et al., 2021, Parmentier et al., 2011, Zhang et al., 2019). While a diameter of around ~1.8 µm was reported in Guar film-coated CS MPs loaded with BAP (Batista et al., 2021). In addition, the various sizes ranging between ~5.4 and 43.8 µm were documented at carboxymethylated gum/sodium ALG microspheres loaded with BAPs (Huang et al., 2017). All the sizes mentioned above were analysed via dynamic light scattering (DLS) (except carboxymethylated gum/sodium ALG microspheres, which were identified via laser diffraction), which is preferable for particle sizes <1 µm, to determine the distribution of the hydrodynamic radius (R_h). DLS determines the diffusion coefficient of particles based on their Brownian motion in a liquid suspension where smaller particles move rapidly than larger particles that move slowly. This technique is generally employed for the particles < 10 µm. Theoretically, the particle shapes are assumed to be spherical or round, and the apparent particle size (diameter) is inversely related to the diffusion coefficient of particles based on the Stokes-Einstein equation (Pravinata et al., 2016, Seyrek et al., 2011). Thus, in this method, the viscosity and temperature of the buffer or solution are important to determine relevant results (O'Connell et al., 2023). The R_h CS NPs prepared by nanoprecipitation were affected by the dissolution medium during measurement (methanol, water, or acetone) (Luque-Alcaraz et al., 2016). Furthermore, another limiting factor influencing this technique's precision and accuracy is polydispersity (Anaraki et al., 2020).

As discussed earlier, their surface properties significantly affect NP and MP cellular uptake via interaction with the biological interfaces (Adjei et al., 2014). Either transmission electron microscopy (TEM) or cryo-scanning electron microscopy (SEM) can be used as an option. (Okeudo-Cogan et al., 2023) enable the characterisation of the topology of soft surfaces and particle shapes for fixed or frozen samples, where one is aware of the artefacts these methods can produce (Bicak et al., 2021). Some publications from (Jiang et al., 2021,

Trapani et al., 2010, Laroui et al., 2010, Zhang et al., 2019) have found good agreement between the results of such EM approaches and DLS. However, it should be remarked that DLS averages the distribution as intensity (although mathematically, it may offer volume or number distributions) and postulates all particles are spherical; nevertheless, in observing EM images, a number average is obtained, as well as details on particle shape. Moreover, to examine the surface of native particles in an aqueous environment, in principle, atomic force microscopy (AFM) might subjected to the limitations of particle immobilisation on a solid surface and the softness of the surface structure against the AFM cantilever stiffness (Mackie et al., 2017, Chu et al., 2022). Small- angle X-ray scattering (SAXS) and neutron scattering (SANS) can uncover the internal-external structure of particles (Sanver et al., 2020), also hydrodynamic thickness of NP and MP layers can be analysed (Seyrek et al., 2011) related to release and stability. In addition, the surface charge is mainly implied from ζ-potential and electrophoretic mobility analysis.

The regular spherical morphology for liposomes coated with SLP, sodium ALG-O-carboxymethyl CS microspheres and Eudragit-coated CS NPs have been reported after loaded with BAPs (Jiang et al., 2021, Huang et al., 2017, Chen et al., 2017). The surface of microspheres made from sodium ALG-O-carboxymethyl CS, then loaded with BAPs VLPVP was rough, then became smoother as the membrane pore size increased to 5 µm or bigger (Huang et al., 2017).

2.4.3 Stability, release, absorption/permeability, and bioactivity of encapsulated BAPs

To underscore the importance of both BAPs' stability and the efficacy of the encapsulating agent, bioaccessibility, which means the proportion of BAPs released from their delivery system during digestion for absorption in the gastrointestinal tract to manifest their bioactivities, is critical. By increasing their bioaccessibility and stability, encapsulation is also subjected to enhance their bioavailability since several published works indicated that the bioactivities of BAPs are diminished after gastrointestinal digestion and in vivo experiments (Zhao et al., 2019, Liao et al., 2019, Mirzaei et al., 2020). In the pharmaceutical industry, the intention is to improve the bioavailability of therapeutic peptides between 30 and 50% (Shaji and Patole, 2008). This field addresses the intricate interaction of BAPs and their bioaccessibility within the gastrointestinal brush border. **Figure 2.6** illustrates the effect of encapsulation approaches on bioaccessibility of BAPs in the GI tract.

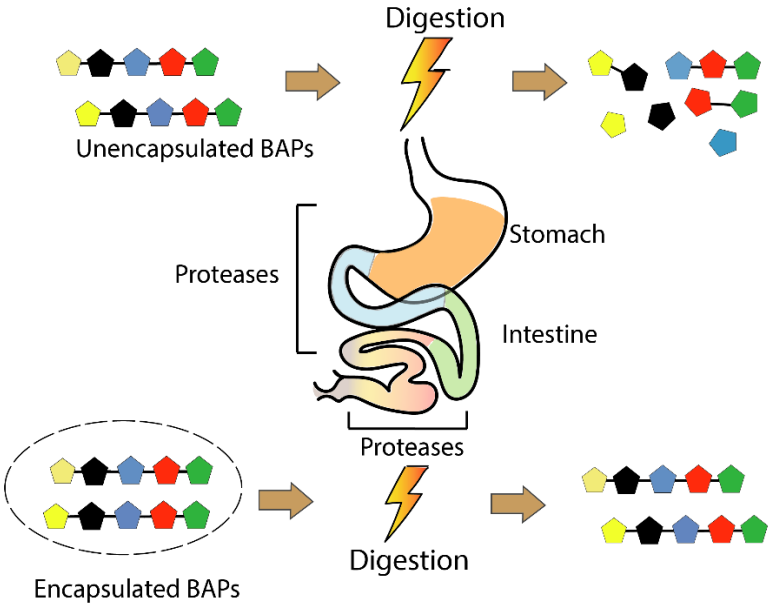


Figure 2.6. The illustration describes the role of encapsulation of BAP during digestion

Stability. The stability of delivery vehicles for BAPs has been examined during simulated gastrointestinal digestion. FSP microfibers were degraded slowly in simulated gastric fluid (SGF) consisting of 0.0032% (w/v) pepsin after 24 h, and it was compared to SGF consisting of a higher composition of pepsin reaching 0.32% (w/v) that resulting fully degraded. Then, during simulated intestinal fluid (SIF) consisting of 0.01% (w/v) of pancreatin, about 50% of the same microfibers had an altered structure after 24 h incubation, and a higher concentration of pancreatin (1% w/v) also degraded the structure altogether (Stephansen et al., 2014). Furthermore, the liposome loaded with BAP LQPE was then treated uncoated and coated with SLP, showing 50% and 68% intact BAP remaining after incubation for 3 h in the artificial gastric juice. The intact BAPs were 55% and 74.5% in the artificial intestinal juice, respectively. In addition, the non-encapsulated BAP was fully hydrolysed after 1 h incubation in artificial gastric or intestinal juice (Jiang et al., 2021). The results of this study demonstrate that encapsulation can increase the gastrointestinal bioaccessibility of BAP by over 50%. These studies demonstrate the encapsulation technique's role, but more systematic studies of gastrointestinal digestion under controlled and comparable conditions may provide different points of view.

Release. The situation is even more fraught with difficulty than trying to rationalise the different EE values when trying to understand the different release characteristics of the vehicles containing the same or different BAPs (see above section 2.4.1). Some studies only

used water as the release medium, which does not mimic the vehicle's fate during digestion. Even though most release experiments have used SGF and/or SIF conditions to investigate % release, those simulations differed throughout all published works in terms of various pH, times, inconsistent enzymes and other digestive components, and different in their concentration and/or specific activity. Although enzymes in the human digestive tract may not hydrolyse some encapsulating materials (for instance, the polysaccharide gums), for others, they are active (such as toward lipids, proteins, and starch-based molecules) (Bicak et al., 2021, Jiang et al., 2021, Danish et al., 2017, Trapani et al., 2010, O'Neill et al., 2015a). Therefore, it would be prudent to test and harmonise conditions as closely as possible in the future (Egger et al., 2016, Minekus et al., 2014). For a few of the entrapment approaches that have been discussed, the release section is not reported. The general approach to quantifying the release is to immerse the carriers (inside the dialysis bag) into a solution containing digestive enzymes or another release solution for some time, then measure the BAPs that diffuse from the bag. The majority of studies indicate a high release after several hours in SGF and/or SIF, whether in NPs, liposomes, or microgels. In some situations, the obtained 100% release with extended times is not similar to typical human digestion fluids. The release is mainly escalated by SGF, then SIF as well, in some cases dramatically so, for instance, ECG in CS+CD+TPP systems (Trapani et al., 2010). The release of BAPs GRKKRRQRRRP, which loaded into CS+TPP NPs, then added an extra layer of Eudragit polymer, gave some slowing release at low pH (Batista et al., 2021), while entrapping BAPs LQPE into liposomes then added an extra layer with SLP also slowed down release to some extent. SLP is expected to act as less permeable, more inert layer placed in the outer of the delivery vehicle. However, the BAPs KPV loaded into PVA NPs then coated with and without extra layers of CS and ALG were subjected to the solution, which seems to represent the digestive condition, but without any enzymes (Laroui et al., 2010).

The other studies found that the O-carboxymethyl CS/SA microspheres loaded with BAPs VLPVP released only 9.6 % during 2 h incubation at pH 1.2, but 87.6% at pH 6.8 after 5 h (Huang et al., 2017), this indicating the delivery vehicles seem promising for gastric protection but not intestinal. Guar film-coated CS MPs protected the BAP (YLGYLEQLLR) during incubation in artificial saliva (pH 6.8) for 4 h, showing a release of less than 2.5% (Batista et

al., 2021). Nevertheless, a consistent situation where delivery vehicle models are examined under the same set of physiological conditions is essential.

As a comparison, the release of peptides of varying M_w (3.4 to 20 kDa) conjugated in poly(ethylene glycol) diacrylate (PEGDA)-peptide hydrogels has been used as an alternative approach (Ross et al., 2012). Where the release of peptides was harnessed via degradation using MMP-2 proteases. It was found that the hydrogel pore sizes influenced the penetration of the MMP-2 protease and the peptide´s M_w, which directly affects hydrogel. To this end, the optimal release of the BAPs was for the PEGDA-10 kDa. Further research is required to examine these situations in matrix-type NPs and MPs where the BAPs are loaded, not as a polymer conjugate, but due to other interactions, where the peptide release is facilitated by the hydrolysis of the particles by proteases, such as a protein-polysaccharide system.

According to these studies, which indicate inconsistent and contradicting results, it cannot be firmly decided what the effects of the BAP sequence, type of encapsulation system, and release medium are on the kinetic of BAP release. Systematic experiments via standardised protocol may assist in explaining in further detail the effect of each of these attributes.

Absorption. The absorption of peptides can be improved by encapsulation. For instance, the BAP ECG encapsulated in CS/α-CD and CS/SBE-β-CD MPs was increased by a factor of 1.4 and 1.2, respectively, in terms of their permeability of the proximal segment of frog duodenum compared to the non-encapsulated one. The permeability increased by 1.3x (CS/α-CD) and 1.8x (CS/SBE-β-CD) in the distal segment (Trapani et al., 2010). The BAP KPV encapsulated with CS/SA NPs has been investigated via fluorescence microscopy and TEM for interaction with membranes of Caco-2 cells (Laroui et al., 2010). By adding hyaluronic acid (HA), it was found that the surface functionalization of the NPs promoted the cellular uptake noticeably higher than NPs without HA (Xiao et al., 2017). Another study showed that the transepithelial transport of LQPE and RLSFNP increased via liposomes (Jiang et al., 2021). At least 2 times higher apparent permeability coefficient of RLSFNP, after being loaded into liposome, as compared to free RLSFNP, was observed (Zhang et al., 2019). Likewise, the permeability of YLGYLEQLLR loaded into CS MPs was 4-fold higher than the free YLGYLEQLLR to across a human adenocarcinoma Caco-2/HT29 colorectal cell line (Batista et al., 2021). The outcomes of this research align with the idea that loading BAP using various approaches

increases its bioavailability. To identify the most optimal systems to enhance their absorption, more mechanistic studies are required to elucidate the optimal carrier systems for given BAPs.

Bioactivity. The activity of ACE inhibitors after nanoencapsulation and release was 84% and 82%, respectively, for IPP. The ACE inhibitory activity of LKP after being loaded into CS-NPs was 85%, and its activity was retained at 83% after incubation in SIF solution (Danish et al., 2017). Microencapsulation of BAP VLPVP into SA-O-carboxymethyl CS-MPs did not significantly reduce the activity against ACE, whereas the unencapsulated and encapsulated BAP had inhibitory activity at 48.2% and 45.2%, respectively (Huang et al., 2017). Therefore, there is the essential fact that the suitable option of the delivery vehicle will not lower the BAP bioactivity after it has been delivered, yet minimal published work has observed in detail the overall process of entrapment, stability, release, and bioactivity from the beginning to the end.

The measurement of the bioactivity of BAPs IPP and LKP after encapsulation in detail involved quantifying the BAP loaded-NPs ability to inhibit angiotensin-converting enzyme (ACE) on the conversion of the *hippuryl-L-histidyl-L-leucine* (*HHL*) (substrate) to the hippuric acid (HPA) (product). This method included identifying the total HPA concentration in the reaction solution by HPLC. Lowering HPA concentration in the reaction solution indicates the higher ACE inhibitory activity. The sonication of the BAP loaded NPs, followed by centrifugation, was performed to measure the BAPs IPP and LKP activities after release. Determination of BAPs in the supernatant was carried out via HPLC, and the BAPs were immediately added into the reaction solution, which consisted of HHL and ACE enzymes. The HPLC-UV/Vis was used to analyse the total HPA in the reaction solution (Danish et al., 2017).

A study by Huang et al., (2017) entrapped an antihypertensive BAP into microspheres, and then the freeze-dried loaded microspheres were immersed into borate buffer and then sonicated for 1 h. The HPLC was used to quantify the amount of BAP release, and the spectrophotometry approach was carried out to determine ACE inhibitory activity using a method described by (Cushman and Cheung, 1971).

Table 2.2. Encapsulation agents, encapsulation methods, encapsulation efficiency (EE), sizes, and kinetic releases for short-chain BAPs

BAPs Payload	Encapsulation wall materials	Encapsulation Methods	Encapsulation efficiency (EE %)	Diameter (nm)	Release	Ref.
YKT	Chitosan MPs (CS: Mw = 50-190 kDa, DA= NR)	Ionic gelation/Coacervation	35	~ 57	26% release at first 8 h, 34% (24 h), 43% (48 h), and 97% (264h/11th day)	(Bicak et al., 2021)
LQPE	Liposome coated SLP	Liposome	89	218.2	liposome-LQPE: 60% after 24 h, SLP-L-LQPE: 40% after 24 h	(Jiang et al., 2021)
YLGYLEQLLR	Guar Film-coated Chitosan MPs (Guar: Mw = NR, CS: Mw = 50-190 kDa, DA = 15-25%)	Ionic gelation/Coacervation	86	1810	<2.5% (4 h)	(Batista et al., 2021)
RLSFNP	Liposome	Liposome	67.50	199	Diffuse through dialysis membrane: 75% (1 h), 98.4% (2h). Cumulative release RLSFNP: 75% (12 h) and 94.92% (24 h).	(Zhang et al., 2019)
IPP	Chitosan NPs (CS: Mw = 110 kDa, DA= 14%)	Ionic gelation/Coacervation	22.6-43.9	113-209	~75% in SGF (120 min); > 90% in SIF (240 min). Over 60% released within the first 2 h in acidic simulated fluid	(Danish et al., 2017)
LKP	Chitosan NPs (CS: Mw = 110 kDa, DA= 14%)	Ionic gelation/Coacervation	40.9-65.1	125-207	~75% in SGF (120 min); ~90% in SIF (240 min). Over 60% released within the first 2 h in acidic simulated fluid	(Danish et al., 2017)
GRKKRRQRRRP	Eudragit (ES)-coated Chitosan NPs (CS: Mw = 100 kDa, DA= 5%)	Ionic gelation/Coacervation	50	50.6 nm	CS NPs: 85% (pH 1.2, 4h), 40% (pH6.8, 1 h). ES-coated CS NPs: 40% (pH 6.8, 1h), 50% (pH 6.8, 4h), 70% (pH 7.4, 1h), almost completely released (pH 7.4, 4 h)	(Chen et al., 2017)
KPV	Chitosan/ALG NPs, and hyaluronic acid (HA)-chitosan/ALG NPs (CS: Mw = NR, DA= NR; ALG: Mw = NR, M/G = NR; HA: Mw = 20 kDa)	Double Emulsions and Solvent Evaporation	NR	273-300	25% at pH 6.2 within 30 min. After 30 minutes, release kinetics is more linier about 35% within 30 h	(Laroui et al., 2010, Xiao et al., 2017)

VLPVP	Carboxymethyl chitosan/Na-ALG microspheres (CMCS: Mw = NR, DS= 35%; ALG: Mw = NR, M/G = NR)	Membrane emulsification combined ionic gelation	64.6-87.8	5390 - 43810	9.59% at pH 1.2 (2 h), and 87.63% at pH 6.8 (5 h)	(Huang et al., 2017)
FW	Whey microbeads	Cold set/Ionic gelation	32-56		56% (6 h), ~80% (Vbead/Vaq <0.2)	(O'Neill et al., 2015a, O'Neill et al., 2015b)
LWMRF	Whey microbeads	Cold set/Ionic gelation	89-95.1	NR	<5% (6 h), ~10% (Vbead/Vaq <0.2)	(O'Neill et al., 2015a, O'Neill et al., 2015b)
AW	FSP microfibers	Electrospinning	NR	100-700 and 1000	61.5% in SGF after 30 min, and max 71.8% in SIF after 15 min	(Stephansen et al., 2014)
FCFWKTCT	Tetraether lipid liposomes	Liposome	13	130-207	NR	(Parmentier et al., 2011)
ECG	Chitosan/CD NPs (CS: Mw = 110 kDa, DA= 14%)	Ionic gelation/Coacervation	7.1-25.1	190-500	pH 1.2: CS/α-CD, 100% (< 200 min); CS/SBE-β-CD, ~25% (<200 min). pH 6.8: CS/α-CD, <60% (< 200 min); CS/SBE-β-CD, 100% (<100 min)	(Trapani et al., 2010)

NR=not reported

2.4.4 Cytotoxicity

When encapsulation agents are to be used in practice, establishing any cytotoxicity of NPs/MPs is paramount. The Caco-2, HT29-MTX, and IEC6 cell lines have been used to mimic gastrointestinal cells, while to mimic liver exposure, HepG2 cells were applied. The 3-(4,5-dimethylthiazol-2-yl)-2,5-diphenyl-2H-tetrazolium bromide (MTT) or 3-(4,5-dimethylthiazol-2-yl)-5-(3-carboxymethoxyphenyl)-2-(4-sulfophenyl)-2H-tetrazolium) (MTS), cell counting kit-8 (CCK-8), and water-soluble tetrazolium salt (WST-1) assays are three standard method used examined the cell viability of NPs/MPs (with or without loaded BAPs.

There were no effects on cell viability (Caco-2 and HepG2) shown by CS-NPs loaded with IPP and LKP at a concentration range between 1 and 10 mM. (Danish et al., 2017) Similarly, there was no effect on cellular death rates of both Caco2-BBE and IEC6 cell lines over 72-80 h exposure with (HA)-CS/SA NPs loaded with BAP KPV (Laroui et al., 2010, Xiao et al., 2017). The Eudragit-CS NPs loaded with BAP GRKKRRQRRRP did not affect the membrane integrity of Caco-2 cells significantly (Chen et al., 2017). In addition, no cytotoxicity effect on

Caco-2 cells was shown by liposome-loaded hexapeptide RLSFNP (Zhang et al., 2019). Moreover, no cytotoxicity effects were depicted by MPs loaded with BAP YLGYLEQLLR, where after incubation with 0.1–5 μg mL^{-1} of BAP on MPs solution, the cell viability maintained around 75-99% (Batista et al., 2021). Thus, there seems to be strong indication of no cytotoxic effects of those types of biopolymer-based NPs, and MPs themselves were negligible, signalling once more the benefit of establishing carrier agents based (mostly) on food-derived materials.

2.5. Summary - Gastrointestinal Delivery Vehicles for BAPs: Challenges and Opportunities

Generally, the release of BAPs from different NPs and MPs described in this review comes across in the range between 60 and 75% in SGF and reaching 90% in SIF. Depending on the actual desired site of action, these rates could be favourable or inconvenient. However, a general trend is that the majority of systems seem to provide sustained (not burst) release in both SGF and SIF, e.g., typically 2 h and 4 h in SGF and SIF, respectively, for full release. For complete digestion and adsorption, food in the human digestive system requires a time between 2 and 6 h. The results might give a chance for pepsin to hydrolyse and change the intact sequences of BAPs before reaching the intestinal brush border since more than half of encapsulated BAPs are released under gastric conditions. Pepsin generally hydrolyses all peptide bonds between aromatic amino acid residues (Schnaith, 1989). It does not guarantee the successful arrival on the BAP at target sites, even up 90% of BAP is released in the intestinal lumen because they still face another proteases such as chymotrypsin, trypsin, carboxypeptidase A, elastase and carboxypeptidase B. Chymotrypsin is usually hydrolysing peptide bonds formed by the carboxyl groups of Tyr (Y), Phe (F), Trp (W), and Leu (L) (Graff et al., 2013). Trypsin is commonly breakdown peptide bonds involving the carboxyl groups of lysine (K) or arginine (R) (Simpson, 2006). Whilst, Carboxypeptidase A particularly hydrolyse C-terminal peptides, with enhance the possibility of hydrolysis rates found when the side-chain R is aromatic or branched aliphatic, like +Tyr (Y), +Phe (F), +Leu (L), +Trp (W), or +Ile (I) (Auld, 2004). Moreover, aminopeptidases and dipeptidases, which are other proteases secreted by the brush border of the small intestine, are likely to attack the BAPs further. Based on this review, The BAPs are very vulnerable to any of the above enzymes if not encapsulated. Then, CS and CS+ALG NPs seem to give a prolonged release of BAPs under gastrointestinal

conditions (see **Table 2.2**). These biopolymers are resistant to human gastric and intestinal enzymes and are not susceptible to protease action. Once again, protecting BAPs during gastric digestion and releasing them on the intestine at a specific rate (fast/sustained/control) to maximise bioavailability is one of the principles of encapsulation bio-actives for food application (Murray et al., 2021).

Creating delivery vehicles in the appropriate size range is another critical challenge. The diameter of pores in the mucus layer, which covers the epithelial cells in the intestine, is around 150 - 200 nm. To enable the vehicles to penetrate this layer freely, carriers of smaller sizes than those pore sizes are essential. It does not seem easy to make biopolymer-based delivery agents with sizes < 200 nm that contain two or three minimum biopolymer layers encircling the BAPs, which is partly a manifestation of the dimension of the natural polymer macromolecules themselves. In contrast, a diameter of less than 60 nm was obtained from partly synthetic Eudragit-CS NPs (Chen et al., 2017), but low toxicity is a strength of purely biopolymer-based NPs. Thus, controlling and minimizing NP size and toxicity may have to be reached by balancing synthetic versus natural biopolymers. NPs must undergo the nano-specific risk assessment stages, as discussed earlier, to that are able to reach the intestine and penetrate through the epithelial cell membrane. They must not only augment the absorption and delivery of particles within the mucosa, the mucosa-adhesive carriers, such as CS, ALG, or their composite on the vehicle surfaces, but also exhibit characteristics of low toxicity, as mentioned before and biodegradability (Goycoolea et al., 2009; Goncalves et al., 2016).

Much more work is required in encapsulating BAPs since a limited number of studies have fully characterized BAP stability during gastrointestinal stimulation fluids and the consequent effects on the bioavailability and bioactivity of any encapsulated BAPs. Particular concern is required for the internal structure of the vehicles, the position of the BAPs, and the influence of that encapsulation on the bioactivities of BAPs. In this regard, there are chances for ongoing investigation and observation of structures composed of more than two biopolymer types, for example, the third one of the biopolymers (or other) type of exterior sheet. For instance, combination of ALG/CS/ALG or CS/ALG/CS possibility. Another promising setting is exploiting a lipid to shield the BAPs inside the biopolymer layers (McClements, 2018). This prevents the BAPs from diffusing into the outer aqueous biopolymer layers due to the created steric hindrance condition.

Most previous studies used buffers during in vitro gastrointestinal simulation to replicate human digestion without added proteases or other attributes (e.g., bile salts, lipases). Very few studies have employed in vivo models. In vitro approaches are preferred due to the expensive costs of in vivo digestion. However, they are challenging to prepare and recapture the physiological context. Some experiments have documented the in vitro static and dynamic digestion simulation models. For instance, Chen et al., (2011) designed a simple model apparatus to simulate an in vitro dynamic physiological digestion process. They investigated the effect of gastric juice ratio, pH, fluid flow, and pepsin concentration on peanut digestion. By this prototype, the variables affecting gastric digestion, such as time, enzyme concentration, food-to-gastric juice ratio, shearing, and hydrodynamic flow, were controllable and adjustable. Kozu et al., (2014) focused on replicating peristalsis effects by designing a Gastric Digestion Simulator (GDS) for in vitro gastric digestion. This prototype detects gastric content changes and food disintegration. Employing two types of Tofu as food representation provides stomach digestion mechanisms. Furthermore Egger et al., (2016) focus on standardising in vitro simulation protocols, bringing attention to the existence of enzymes. Despite human studies being gold standards, in vitro models offer advantages in terms of time, cost-efficiency, ethics, and scalability, especially for screening. They simulate oral, gastric, and small intestinal phases and sometimes sizeable intestinal fermentation, controlling pH, enzymes, time, and salt compositions (Minekus et al., 2014). In addition, few computer models simulate digestion dynamically (Minekus et al., 1995), but many remain static (Zhang et al., 2022). These methods can examine the bioactive peptides (BAPs) in the delivery vehicles or food models.

In summary, much under progress work is needed to find optimal conditions for encapsulation BAPs and simulation digestion models, which enable to protect them adequately during gastrointestinal digestion yet offer sufficient release behaviour, which guarantees the mandatory activity of the BAPs.

Table 2.3. Other essential attributes on encapsulation of BAPs

BAPs payloads	Encapsulation materials	Remarks on essential characteristics	Ref.
YLGYLEQLLR	Guar Film-coated CS MPs	*Absorption/Permeability*: MPs loaded peptide in Caco-2/HT29-MTX: permeability >70% (120 min) and ~50% (60 min). Peptide alone <60% (120 min) and <30% (60 min). *Cytotoxicity:* Cell viability 75-99% (MTT assay) (0-5 μg mL^{-1})	(Batista et al., 2021)
YKT	CS NPs	*Cytotoxicity*: Viability (Control). 100%. 1) 0.1-2.5 mg mL^{-1}: 62.72-79% (after 24 h); 2) 0.1-1.0 mg mL^{-1}: 34-38% (after 48 h).	(Bicak et al., 2021)
LQPE	Liposome coated Lactobacillus S-layer protein (SLP)	*Absorption/Permeability*: All of the transhipment significantly increased. Compared L-LQPE, L-LQPE coated by SLP significantly increases the concentration of LQPE on the Basolateral side with initial concentration of 2 and 6 mmol/L. *Stability*: LQPE Residue. Intestinal juice: 74.5% (SLP-L-LQPE), 55% (L-QPE). Gastric juice: 68% (SLP-L-LQPE), 50% (L-LQPE).	(Jiang et al., 2020)
RLSFNP	Liposome	*Absorption/Permeability*: Both free RLSFNP and RLSFNP liposomes exhibited red fluorescence, indicating cellular uptake. The transport of the hexapeptide RLSFNP in liposome increased significantly in comparison to the peptide alone. *Cytotoxicity*: MTT Results indicated that the RLSFNP display no cytotoxicity in Caco-2 Cells	(Zhang et al., 2019)
IPP	CS NPs	*Cytotoxicity*: IPP loaded CS NPs were tested on Caco-2 and HepG2 cell lines, and no significant decrease of cell viability was found compared to negative control analysed by MTS viability assay. *Bioactivity*: 84% (after encapsulation); 82% (controlled release)	(Danish et al., 2017)
LKP	CS NPs	*Cytotoxicity*: LKP loaded CS NPs were tested on Caco-2 and HepG2 cell lines, and no significant decrease of cell viability was found compared to negative control analysed by MTS viability assay. *Bioactivity*: 85% (After encapsulation); 83% (controlled release)	(Danish et al., 2017)
VLPVP	Carboxymethylated gum/sodium ALG microspheres	*Bioactivity*: 48.2% (before encapsulation); 45.2% (after encapsulation)	(Huang et al., 2017b)
GRKKRRQRRRP	Eudragit (ES)-coated CS NPs	*Cytotoxicity:* Membrane integrity of Caco-2 was not destroyed after treatment with ES-Tat-cNPs and ES-cNPs. There were not toxic toward Caco-2 cell using CCK8 assay (100% of cell viability after treatment)	(Chen et al., 2017)
AW	FSP microfibers	*Stability*: microfiber degraded slowly by low activity SGF until 24 h (compared to after 30 min with higher amount of pepsin); Microfiber has low activity in SIF, only 50% (after 24 h) (compared 100% in the higher amount of pancreatin)	(Stephansen et al., 2014)

FCFWKTCT	Tetraether lipid liposomes	*Bioavailability:* > 750 pg mL^{-1} in plasma, after 100 µg dosage	(Parmentier et al., 2011)
ECG	CS/CD NPs	*Absorption/Permeability***:** CS/α-CD: 1.42 times higher (on proximal segment) and 1.3 times higher (on distal segment). CS/SBE-β-CD: 1.2 times higher (on proximal segment) and 1.8 higher (on distal segment). All of these compared to unencapsulated tripeptide ECG	(Trapani et al., 2010)
KPV	CS/ALG NPs, and hyaluronic acid (HA)-CS/ALG NPs	*Absorption/Permeability*: Qualitative data shown that surface functionalization with HA can promote the cellular uptake efficiency of NPs by targeting cells. *Bioactivity*: HA-KPV-CS NPs can enhance the healing of the wounded colonic epithelial layer. *Cytotoxicity*: Concentration 1 mg mL^{-1} do not cause cellular death of Caco2-BBE and IEC6 cell line over 72-80 h. Cell treated with HA-KPV-NPs had significantly lower TNF-a mRNA expression levels compared with those treated with KPV-NPs	(Xiao et al., 2017, Laroui et al., 2010)

2.6 References

Adjei, I. M., Sharma, B. & Labhasetwar, V. 2014. Nanoparticles: cellular uptake and cytotoxicity. *Adv. Exp. Med. Biol.,* 811**,** 73-91.

Aguilar-Toala, J. E., Quintanar-Guerrero, D., Liceaga, A. M. & Zambrano-Zaragoza, M. L. 2022. Encapsulation of bioactive peptides: a strategy to improve the stability, protect the nutraceutical bioactivity and support their food applications. *RSC Adv.,* 12**,** 6449-6458.

Anaraki, N. I., Sadeghpour, A., Iranshahi, K., Toncelli, C., Cendrowska, U., Stellacci, F., Dommann, A., Wick, P. & Neels, A. 2020. New approach for time-resolved and dynamic investigations on nanoparticles agglomeration. *Nano Research,* 13**,** 2847-2856.

Auld, D. S. 2004. Carboxypeptidase A. *In:* Barrett, A., Woessner, J. & Rawlings, N. (eds.) *Handbook of Proteolytic Enzymes.* Oxford, UK: Elsevier, Academic Press.

Balti, R., Bougatef, A., Sila, A., Guillochon, D., Dhulster, P. & Nedjar-Arroume, N. 2015. Nine novel angiotensin I-converting enzyme (ACE) inhibitory peptides from cuttlefish (*Sepia officinalis*) muscle protein hydrolysates and antihypertensive effect of the potent active peptide in spontaneously hypertensive rats. *Food Chem.,* 170**,** 519-25.

Balti, R., Nedjar-Arroume, N., Bougatef, A., Guillochon, D. & Nasri, M. 2010. Three novel angiotensin I-converting enzyme (ACE) inhibitory peptides from cuttlefish (*Sepia officinalis*) using digestive proteases. *Food Res. Int.,* 43**,** 1136-1143.

Basirico, L., Catalani, E., Morera, P., Cattaneo, S., Stuknyte, M., Bernabucci, U., De Noni, I. & Nardone, A. 2015. Release of angiotensin converting enzyme-inhibitor peptides during in vitro gastrointestinal digestion of Parmigiano Reggiano PDO cheese and their absorption through an in vitro model of intestinal epithelium. *J. Dairy Sci.,* 98**,** 7595-601.

Batista, P., Castro, P. M., Madureira, A. R., Sarmento, B. & Pintado, M. 2021. Preparation, characterization and evaluation of guar films impregnated with relaxing peptide loaded into chitosan microparticles. *Appl. Sci. (Switzerland),* 11**,** 1-13.

Berraquero-Garcia, C., Perez-Galvez, R., Espejo-Carpio, F. J., Guadix, A., Guadix, E. M. & Garcia-Moreno, P. J. 2023. Encapsulation of bioactive peptides by spray-drying and electrospraying. *Foods,* 12.

Bhutia, Y. D. & Ganapathy, V. 2018. Protein Digestion and Absorption. *In:* Said, H. M. (ed.) *Physiology of the Gastrointestinal Tract.* United Kingdom: Academic Press.

Bicak, B., Budama-Kilinc, Y., Kecel-Gunduz, S., Zorlud, T. & Akman, G. 2021. Peptide based nano-drug candidate for cancer treatment: preparation, characterization, in vitro and in silico evaluation. *J. Mol. Struct.,* 1240**,** 130573.

Brown, T. D., Whitehead, K. A. & Mitragotri, S. 2019. Materials for oral delivery of proteins and peptides. *Nat. Rev. Mater.,* 5**,** 127-148.

Byun, H. G. & Kim, S. K. 2001. Purification and characterization of angiotensin I converting enzyme (ACE) inhibitory peptides from Alaska pollack (*Theragra chalcogramma*) skin. *Process Biochem.,* 36**,** 1155–1162.

Cao, S., Wang, Y., Hao, Y., Zhang, W. & Zhou, G. 2020. Antihypertensive effects in vitro and in vivo of novel angiotensin-converting enzyme inhibitory peptides from bovine bone gelatin hydrolysate. *J. Agric. Food Chem.,* 68**,** 759-768.

Caro-Leon, F. J., Arguelles-Monal, W., Carvajal-Millan, E., Lopez-Franco, Y. L., Goycoolea-Valencia, F. M., San Roman Del Barrio, J. & Lizardi-Mendoza, J. 2018. Production and characterization of supercritical CO(2) dried chitosan nanoparticles as novel carrier device. *Carbohyd. Polym.,* 198**,** 556-562.

Cerrato, A., Aita, S. E., Capriotti, A. L., Cavaliere, C., Montone, A. M. I., Montone, C. M. & Lagana, A. 2022. Investigating the short peptidome profile of italian dry-cured ham at different processing times by high-resolution mass spectrometry and chemometrics. *Int. J. Mol. Sci.,* 23.

Chen, J., Gaikwad, V., Holmes, M., Murray, B., Povey, M., Wang, Y. & Zhang, Y. 2011. Development of a simple model device for in vitro gastric digestion investigation. *Food Funct.,* 2**,** 174-82.

Chen, J., Liu, S., Ye, R., Cai, G., Ji, B. & Wu, Y. 2013. Angiotensin-I converting enzyme (ACE) inhibitory tripeptides from rice protein hydrolysate: purification and characterization. *J. Funct. Food,* 5**,** 1684-1692.

Chen, S. X., Guo, F., Deng, T. T., Zhu, S. Q., Liu, W. Y., Zhong, H. J., Yu, H., Luo, R. & Deng, Z. Y. 2017. Eudragit S100-coated chitosan nanoparticles co-loading Tat for enhanced oral colon absorption of insulin. *AAPS Pharmscitech.,* 18**,** 1277-1287.

Chu, J., Metcalfe, P., Linford, H. V., Zhao, S., Goycoolea, F. M., Chen, S., Ye, X., Holmes, M. & Orfila, C. 2022. Short-time acoustic and hydrodynamic cavitation improves dispersibility and functionality of pectin-rich biopolymers from citrus waste. *J. Clean Prod.,* 330**,** 129789.

Contreras, M. D. M., Carrón, R., Montero, M. J., Ramos, M. & Recio, I. 2009. Novel casein-derived peptides with antihypertensive activity. *Int. Dairy J.,* 19**,** 566-573.

Cushman, D. W. & Cheung, H. S. 1971. Spectrophotometric assay and properties of the angiotensin-converting enzyme of rabbit lung. *Biochem. Pharmacol.,* 20**,** 1637-1648.

Dalmasso, G., Charrier-Hisamuddin, L., Nguyen, H. T., Yan, Y., Sitaraman, S. & Merlin, D. 2008. PepT1-mediated tripeptide KPV uptake reduces intestinal inflammation. *Gastroenterology,* 134**,** 166–178.

Danish, M. K., Vozza, G., Byrne, H. J., Frias, J. M. & Ryan, S. M. 2017. Comparative study of the structural and physicochemical properties of two food derived antihypertensive tri-peptides, Isoleucine-Proline-Proline and Leucine-Lysine-Proline encapsulated into a chitosan based nanoparticle system. *Innov. Food Sci. Emerg.,* 44**,** 139-148.

Efsa 2018. Outcome of the public consultation on the draft guidance on risk assessment of the application of nanoscience and nanotechnologies in the food and feed chain: Part 1, human and animal health. *EFSA (European Food Safety Authority) Supporting Publications,* 15.

Egger, L., Ménard, O., Delgado-Andrade, C., Alvito, P., Assunção, R., Balance, S., Barberá, R., Brodkorb, A., Cattenoz, T., Clemente, A., Comi, I., Dupont, D., Garcia-Llatas, G., Lagarda, M. J., Le Feunteun, S., Janssenduijghuijsen, L., Karakaya, S., Lesmes, U., Mackie, A. R., Martins, C., Meynier, A., Miralles, B., Murray, B. S., Pihlanto, A., Picariello, G., Santos, C. N., Simsek, S., Recio, I., Rigby, N., Rioux, L.-E., Stoffers, H., Tavares, A., Tavares, L., Turgeon, S., Ulleberg, E. K.,

Vegarud, G. E., Vergères, G. & Portmann, R. 2016. The harmonized INFOGEST in vitro digestion method: From knowledge to action. *Food Res. Int.,* 88**,** 217-225.

Fahmi, A., Morimura, S., Guo, H. C., Shigematsu, T., Kida, K. & Uemura, Y. 2004. Production of angiotensin I converting enzyme inhibitory peptides from sea bream scales. *Process. Biochem.,* 39**,** 1195-1200.

Fernández-Musoles, R., Salom, J. B., Castelló-Ruiz, M., Contreras, M. D. M., Recio, I. & Manzanares, P. 2013. Bioavailability of antihypertensive lactoferricin B-derived peptides: transepithelial transport and resistance to intestinal and plasma peptidases. *Int. Dairy J.,* 32**,** 169-174.

Fjellestad-Paulsen, A., Hoglund, P., Lundin, S. & Paulsen, O. 1993. Pharmacokinetics of 1-deamino-8-D-arginine vasopressin after various routes of administration in healthy volunteers. *Clin. Endocrinol. (Oxf),* 38**,** 177-82.

Foroozandeh, P. & Aziz, A. A. 2018. Insight into cellular uptake and intracellular trafficking of nanoparticles. *Nanoscale Res. Lett.,* 13**,** 339.

Fuenzalida, J. P., Flores, M. E., Moniz, I., Feijoo, M., Goycoolea, F., Nishide, H. & Moreno-Villoslada, I. 2014. Immobilization of hydrophilic low molecular-weight molecules in nanoparticles of chitosan/poly(sodium 4-styrenesulfonate) assisted by aromatic-aromatic interactions. *J. Phys. Chem. B.,* 118**,** 9782-91.

Fujita, H., Yokoyama, K. & Yoshikawa, M. 2000. Classification and antihypertensive activity of angiotensin I-converting enzyme inhibitory peptides derived from food proteins. *J. Food Sci. ,* 65**,** 564-569.

Fujita, H. & Yoshikawa, M. 1999. LKPNM: a prodrug-type ACE-inhibitory peptide derived from fish protein. *Immunopharmacology,* 44**,** 123–127.

Gao, G., Wang, H., Zhou, J., Rao, P., Ke, L., Lin, J. J., Sun Pan, B., Zhang, Y. & Wang, Q. 2021. Isolation and characterization of bioactive proteoglycan-lipid nanoparticles from freshwater clam (*Corbicula fluminea* Muller) soup. *J. Agric. Food Chem.,* 69**,** 1610-1618.

Geng, X., Tian, G., Zhang, W., Zhao, Y., Zhao, L., Wang, H. & Ng, T. B. 2016. A Tricholoma matsutake peptide with angiotensin converting enzyme inhibitory and antioxidative activities and antihypertensive effects in spontaneously hypertensive rats. *Sci. Rep.,* 6**,** 24130.

Ghassem, M., Arihara, K. & Babji, A. S. 2012. Isolation, purification and characterisation of angiotensin I-converting enzyme-inhibitory peptides derived from catfish (*Clarias batrachus*) muscle protein thermolysin hydrolysates. *Int. J. Food Sci. Tech.,* 47**,** 2444-2451.

Ghassem, M., Arihara, K., Babji, A. S., Said, M. & Ibrahim, S. 2011. Purification and identification of ACE inhibitory peptides from Haruan (*Channa striatus*) myofibrillar protein hydrolysate using HPLC–ESI-TOF MS/MS. *Food Chem.,* 129**,** 1770-1777.

Goncalves, V. S., Gurikov, P., Poejo, J., Matias, A. A., Heinrich, S., Duarte, C. M. & Smirnova, I. 2016. Alginate-based hybrid aerogel microparticles for mucosal drug delivery. *Eur. J. Pharm. Biopharm.,* 107**,** 160-70.

Goycoolea-Valencia, F. M., Lollo, G., Remunan-Lopez, C., Quaglia, F. & Alonso, M. J. 2009. Chitosan-Alginate Blended Nanoparticles as Carriers for the Transmucosal Delivery of Macromolecules. *Biomacromolecules,* 10**,** 1736-1743.

Graff, L., Szilagyi, L. & Venekei, I. 2013. Chymotrypsin. *In:* Barrett, A., Rawlings, N. & Woessner, J. (eds.) *Handbook of Proteolytic Enzymes.* Third ed. Oxford, UK: Elsevier Ltd.

Gu, Y. & Wu, J. 2013. LC-MS/MS coupled with QSAR modeling in characterising of angiotensin I-converting enzyme inhibitory peptides from soybean proteins. *Food Chem.,* 141**,** 2682-90.

Han, R., Maycock, J., Murray, B. S. & Boesch, C. 2019. Identification of angiotensin converting enzyme and dipeptidyl peptidase-IV inhibitory peptides derived from oilseed proteins using two integrated bioinformatic approaches. *Food Res. Int.,* 115**,** 283-291.

Harnedy-Rothwell, P. A., Mclaughlin, C. M., O'keeffe, M. B., Le Gouic, A. V., Allsopp, P. J., Mcsorley, E. M., Sharkey, S., Whooley, J., Mcgovern, B., O'harte, F. P. M. & Fitzgerald, R. J. 2020. Identification and characterisation of peptides from a boarfish (*Capros aper*) protein

hydrolysate displaying in vitro dipeptidyl peptidase-IV (DPP-IV) inhibitory and insulinotropic activity. *Food Res. Int.,* 131**,** 108989.

Huang, G. Q., Xiao, J. X., Hao, L. Q. & Yang, J. 2017. Microencapsulation of an angiotensin i-converting enzyme inhibitory peptide VLPVP by membrane emulsification. *Food Bioprocess Tech.,* 10**,** 2005-2012.

Ichikawa, H. 2008. Application 6 - Design of Nanoparticles for Oral Delivery of Peptide Drugs. *In:* Hosokawa, M., Nogi, K., Naito, M. & Yokoyama, T. (eds.) *Nanoparticle Technology Handbook.* Elsevier Science.

Intarasirisawat, R., Benjakul, S., Wu, J. & Visessanguan, W. 2013. Isolation of antioxidative and ACE inhibitory peptides from protein hydrolysate of skipjack (*Katsuwana pelamis*) roe. *J. Funct. Food,* 5**,** 1854-1862.

Iqbal, M., Zafar, N., Fessi, H. & Elaissari, A. 2015. Double emulsion solvent evaporation techniques used for drug encapsulation. *Int. J. Pharm.,* 496**,** 173-90.

Jiang, X., Pan, D., Zhang, T., Liu, C., Zhang, J., Su, M., Wu, Z., Zeng, X., Sun, Y. & Guo, Y. 2020. Novel milk casein-derived peptides decrease cholesterol micellar solubility and cholesterol intestinal absorption in Caco-2 cells. *J. Dairy Sci.,* 103**,** 3924-3936.

Jiang, X. X., Pan, D. D., Tao, M. X., Zhang, T., Zeng, X. Q., Wu, Z. & Guo, Y. X. 2021. New nanocarrier system for liposomes coated with Lactobacillus acidophilus S-layer protein to improve Leu-Gln-Pro-Glu absorption through the intestinal epithelium. *J. Agr. Food Chem.,* 69**,** 7593-7602.

Kannengiesser, K., Maaser, C., Heidemann, J., Luegering, A., Ross, M., Brzoska, T., Bohm, M., Luger, T. A., Domschke, W. & Kucharzik, T. 2008. Melanocortin-derived tripeptide KPV has anti-inflammatory potential in murine models of inflammatory bowel disease. *Inflamm. Bowel. Dis.,* 14**,** 324-31.

Kettler, K., Veltman, K., Van De Meent, D., Van Wezel, A. & Hendriks, A. J. 2014. Cellular uptake of nanoparticles as determined by particle properties, experimental conditions, and cell type. *Environ. Toxicol. Chem.,* 33**,** 481-92.

Kommineni, N., Sainaga Jyothi, V. G. S., Butreddy, A., Raju, S., Shapira, T., Khan, W., Angsantikul, P. & Domb, A. J. 2023. SNAC for enhanced oral bioavailability: an updated review. *Pharm. Res.,* 40**,** 633-650.

Kozu, H., Nakata, Y., Nakajima, M., Neves, M. A., Uemura, K., Sato, S., Kobayashi, I. & Ichikawa, S. 2014. Development of a human gastric digestion simulator equipped with peristalsis function for the direct observation and analysis of the food digestion process. *Food Sci. Technol. Res.,* 20**,** 225-233.

Lacroix, I. M. & Li-Chan, E. C. 2014. Isolation and characterization of peptides with dipeptidyl peptidase-IV inhibitory activity from pepsin-treated bovine whey proteins. *Peptides,* 54**,** 39-48.

Lacroix, I. M. E., Chen, X. M., Kitts, D. D. & Li-Chan, E. C. Y. 2017. Investigation into the bioavailability of milk protein-derived peptides with dipeptidyl-peptidase IV inhibitory activity using Caco-2 cell monolayers. *Food Funct.,* 8**,** 701-709.

Lacroix, I. M. E., Meng, G., Cheung, I. W. Y. & Li-Chan, E. C. Y. 2016. Do whey protein-derived peptides have dual dipeptidyl-peptidase IV and angiotensin I-converting enzyme inhibitory activities? *J. Funct. Food,* 21**,** 87-96.

Laroui, H., Dalmasso, G., Nguyen, H. T., Yan, Y., Sitaraman, S. V. & Merlin, D. 2010. Drug-loaded nanoparticles targeted to the colon with polysaccharide hydrogel reduce colitis in a mouse model. *Gastroenterology,* 138**,** 843-53.e1-2.

Lau, J. L. & Dunn, M. K. 2018. Therapeutic peptides: historical perspectives, current development trends, and future directions. *Bioorg. Med. Chem.,* 26**,** 2700-2707.

Lee, J. K., Jeon, J.-K. & Byun, H.-G. 2011. Effect of angiotensin I converting enzyme inhibitory peptide purified from skate skin hydrolysate. *Food Chem.,* 125**,** 495-499.

Li-Chan, E. C. Y., Hunag, S., Jao, C. L., Ho, K. P. & Hsu, K. C. 2012. Peptides derived from atlantic salmon skin gelatin as dipeptidyl-peptidase IV inhibitors. *J. Agr. Food Chem.,* 60**,** 973-978.

Li, Y., Wei, G. & Chen, J. 2004. Glutathione: a review on biotechnological production. *Appl. Microbiol. Biotechnol.,* 66**,** 233-42.

Liao, W., Fan, H., Liu, P. & Wu, J. 2019. Identification of angiotensin converting enzyme 2 (ACE2) up-regulating peptides from pea protein hydrolysate. *J. Funct. Food,* 60.

Lin, Y. H., Chen, C. A., Tsai, J. S. & Chen, G. W. 2019. Preparation and identification of novel antihypertensive peptides from the in vitro gastrointestinal digestion of marine cobia skin hydrolysates. *Nutrients,* 11**,** 1351.

Lin, Y. H., Chen, G. W., Yeh, C. H., Song, H. & Tsai, J. S. 2018. Purification and identification of angiotensin I-converting enzyme inhibitory peptides and the antihypertensive effect of *Chlorella sorokiniana* protein hydrolysates. *Nutrients,* 10.

Lipinski, C. A., Lombardo, F., Dominy, B. W. & Feeney, P. J. 2001. Experimental and computational approaches to estimate solubility and permeability in drug discovery and development settings. *Adv. Drug Deliver. Rev. ,* 46**,** 3–26.

Liu, D., Sun, H., Zhang, L., Li, S. & Qin, Z. 2007. High-Level expression of milk-derived antihypertensive peptide in *Escherichia coli* and its bioactivity. *J. Agr. Food Chem.,* 55**,** 5109−5112.

Liu, X., Zhang, M., Shi, Y., Qiao, R., Tang, W. & Sun, Z. 2016. Production of the angiotensin I converting enzyme inhibitory peptides and isolation of four novel peptides from jellyfish (*Rhopilema esculentum*) protein hydrolysate. *J. Sci. Food Agric.,* 96**,** 3240-8.

Lu, J., Sawano, Y., Miyakawa, T., Xue, Y. L., Cai, M. Y., Egashira, Y., Ren, D. F. & Tanokura, M. 2011. One-week antihypertensive effect of Ile-Gln-Pro in spontaneously hypertensive rats. *J. Agric. Food Chem.,* 59**,** 559-63.

Luque-Alcaraz, A. G., Lizardi-Mendoza, J., Goycoolea, F. M., Higuera-Ciapara, I. & Argüelles-Monal, W. 2016. Preparation of chitosan nanoparticles by nanoprecipitation and their ability as a drug nanocarrier. *RSC Adv.,* 6**,** 59250-59256.

Mackie, A. R., Goycoolea, F. M., Menchicchi, B., Caramella, C. M., Saporito, F., Lee, S., Stephansen, K., Chronakis, I. S., Hiorth, M., Adamczak, M., Waldner, M., Nielsen, H. M. & Marcelloni, L. 2017. Innovative methods and applications in mucoadhesion research. *Macromol. Biosci.,* 17.

Mao, X.-Y., Ni, J.-R., Sun, W.-L., Hao, P.-P. & Fan, L. 2007. Value-added utilization of yak milk casein for the production of angiotensin-I-converting enzyme inhibitory peptides. *Food Chem.,* 103**,** 1282-1287.

Marczak, E. D., Usui, H., Fujita, H., Yang, Y., Yokoo, M., Lipkowski, A. W. & Yoshikawa, M. 2003. New antihypertensive peptides isolated from rapeseed. *Peptides,* 24**,** 791-798.

Martins, S., Sarmento, B., Ferreira, D. C. & Souto, E. B. 2007. Lipid-based colloidal carriers for peptide and protein delivery – liposomes versus lipid nanoparticles. *Int. J. Nanomed. ,* 2**,** 595–607.

Mcclements, D. J. 2018. Encapsulation, protection, and delivery of bioactive proteins and peptides using nanoparticle and microparticle systems: a review. *Adv. Colloid Interfac.,* 253**,** 1-22.

Miclo, L., Perrin, E., Driou, A., Papadopoulos, V., Boujrad, N., Vanderesse, R., Boudier, J. F., Desor, D., Linden, G. & Gaillard, J. L. 2001. Characterization of alpha-casozepine, a tryptic peptide from bovine alpha(s1)-casein with benzodiazepine-like activity. *FASEB J.,* 15**,** 1780-2.

Miguel, M., Aleixandre, M. A., Ramos, M. & Lopez-Fandino, R. 2006. Effect of simulated gastrointestinal digestion on the antihypertensive properties of ACE-inhibitory peptides derived from ovalbumin. *J. Agr. Food Chem.,* 54**,** 726−731.

Miguel, M., Davalos, A., Manso, M. A., De La Pena, G., Lasuncion, M. A. & Lopez-Fandino, R. 2008. Transepithelial transport across Caco-2 cell monolayers of antihypertensive egg-derived peptides. PepT1-mediated flux of Tyr-Pro-Ile. *Mol. Nutr. Food Res.,* 52**,** 1507-13.

Minekus, M., Alminger, M., Alvito, P., Ballance, S., Bohn, T., Bourlieu, C., Carriere, F., Boutrou, R., Corredig, M., Dupont, D., Dufour, C., Egger, L., Golding, M., Karakaya, S., Kirkhus, B., Le Feunteun, S., Lesmes, U., Macierzanka, A., Mackie, A., Marze, S., Mcclements, D. J., Menard, O., Recio, I., Santos, C. N., Singh, R. P., Vegarud, G. E., Wickham, M. S., Weitschies, W. & Brodkorb, A. 2014. A standardised static in vitro digestion method suitable for food - an international consensus. *Food Funct.,* 5**,** 1113-24.

Minekus, M., Marteau, P., Havenaar, R. & Huis In't Veld, J. H. J. 1995. A multicompartmental dynamic computer-controlled model simulating the stomach and small intestine. *ATLA,* 23**,** 197-209.

Mirzaei, M., Mirdamadi, S., Safavi, M. & Soleymanzadeh, N. 2020. The stability of antioxidant and ACE-inhibitory peptides as influenced by peptide sequences. *LWT Food,* 130.

Mirzapour-Kouhdasht, A., Mcclements, D. J., Taghizadeh, M. S., Niazi, A. & Garcia-Vaquero, M. 2023. Strategies for oral delivery of bioactive peptides with focus on debittering and masking. *NPJ Sci. Food,* 7**,** 22.

Montone, C. M., Capriotti, A. L., Cavaliere, C., La Barbera, G., Piovesana, S., Zenezini Chiozzi, R. & Lagana, A. 2018. Peptidomic strategy for purification and identification of potential ACE-inhibitory and antioxidant peptides in *Tetradesmus obliquus* microalgae. *Anal. Bioanal. Chem.,* 410**,** 3573-3586.

More, S., Bampidis, V., Benford, D., Bragard, C., Halldorsson, T., Hernandez-Jerez, A., Bennekou, S. H., Koutsoumanis, K., Lambre, C., Machera, K., Naegeli, H., Nielsen, S., Schlatter, J., Schrenk, D., Silano Deceased, V., Turck, D., Younes, M., Castenmiller, J., Chaudhry, Q., Cubadda, F., Franz, R., Gott, D., Mast, J., Mortensen, A., Oomen, A. G., Weigel, S., Barthelemy, E., Rincon, A., Tarazona, J. & Schoonjans, R. 2021. Guidance on technical requirements for regulated food and feed product applications to establish the presence of small particles including nanoparticles. *EFSA J.,* 19**,** e06769.

Murray, B. S., Ettelaie, R., Sarkar, A., Mackie, A. R. & Dickinson, E. 2021. The perfect hydrocolloid stabilizer: Imagination versus reality. *Food Hydrocolloid,* 117.

Nakamura, Y., Yamamoto, N., Sakai, K., Okubo, A., Yamazaki, S. & Takano, T. 1995. Purification and characterization of angiotensin i-converting enzyme inhibitors from sour milk. *J. Dairy Sci.,* 78**,** 777-783.

Ngo, D.-H., Vo, T.-S., Ryu, B. & Kim, S.-K. 2016. Angiotensin- I- converting enzyme (ACE) inhibitory peptides from Pacific cod skin gelatin using ultrafiltration membranes. *Process. Biochem.,* 51**,** 1622-1628.

Nongonierma, A. B., Cadamuro, C., Le Gouic, A., Mudgil, P., Maqsood, S. & Fitzgerald, R. J. 2019. Dipeptidyl peptidase IV (DPP-IV) inhibitory properties of a camel whey protein enriched hydrolysate preparation. *Food Chem.,* 279**,** 70-79.

Nongonierma, A. B. & Fitzgerald, R. J. 2014. Susceptibility of milk protein-derived peptides to dipeptidyl peptidase IV (DPP-IV) hydrolysis. *Food Chem.,* 145**,** 845-52.

O'connell, A., Goycoolea, F. M., Gulotta, A., Holmqvist, P., Schuetz, P. & Mattsson, J. 2023. The structure and dynamics of locust bean gum in aqueous solution. *Food Hydrocolloid,* 138**,** 108446.

O'neill, G. J., Egan, T., Jacquier, J. C., O'sullivan, M. & O'riordan, E.D. 2015a. Kinetics of immobilisation and release of tryptophan, riboflavin and peptides from whey protein microbeads. *Food Chem.,* 180**,** 150-155.

O'neill, G. J., Egan, T., Jacquier, J. C., O'sullivan, M. & O'riordan, E. D. 2015b. Whey microbeads as a matrix for the encapsulation and immobilisation of riboflavin and peptides. *Food Chem,* 160**,** 45-52.

Okeudo-Cogan, M. C., Murray, B. S., Ettelaie, R., Connell, S. D., Radford, S. J., Micklethwaite, S. & Sarkar, A. 2023. Understanding the microstructure of a functional meat analogue: Demystifying interactions between fungal hyphae and egg white protein. *Food Hydrocolloid,* 140.

Park, H., Ha, D. H., Ha, E. S., Kim, J. S., Kim, M. S. & Hwang, S. J. 2019. Effect of stabilizers on encapsulation efficiency and release behavior of exenatide-loaded PLGA microsphere prepared by the W/O/W solvent evaporation method. *Pharmaceutics,* 11.

Parmentier, J., Thewes, B., Gropp, F. & Fricker, G. 2011. Oral peptide delivery by tetraether lipid liposomes. *Int. J. Pharm.,* 415**,** 150-157.

Pearson, J. P., Chater, P. I. & Wilcox, M. D. 2016. The properties of the mucus barrier, a unique gel--how can nanoparticles cross it? *Ther. Deliv.,* 7**,** 229-44.

Pistone, S., Goycoolea, F. M., Young, A., Smistad, G. & Hiorth, M. 2017. Formulation of polysaccharide-based nanoparticles for local administration into the oral cavity. *Eur. J. Pharm. Sci.,* 96**,** 381-389.

Pravinata, L., Akhtar, M., Bentley, P. J., Mahatnirunkul, T. & Murray, B. S. 2016. Preparation of alginate microgels in a simple one step process via the Leeds Jet Homogenizer. *Food Hydrocolloid,* 61**,** 77-84.

Ross, A. E., Tang, M. Y. & Gemeinhart, R. A. 2012. Effects of molecular weight and loading on matrix metalloproteinase-2 mediated release from poly(ethylene glycol) diacrylate hydrogels. *AAPS J,* 14**,** 482-90.

S Vallabha, V. & Tiku, P. K. 2013. Antihypertensive peptides derived from soy protein by fermentation. *Int. J Pept. Res. Ther.,* 20**,** 161-168.

Salatin, S., Dizaj, S. M. & Khosroushahi, A. Y. 2015. Effect of the surface modification, size, and shape on cellular uptake of nanoparticles. *Cell Biol. Int.,* 39**,** 881-890.

Sangsawad, P., Choowongkomon, K., Kitts, D. D., Chen, X.-M., Li-Chan, E. C. Y. & Yongsawatdigul, J. 2018a. Transepithelial transport and structural changes of chicken angiotensin I-converting enzyme (ACE) inhibitory peptides through Caco-2 cell monolayers. *J. Funct. Food,* 45**,** 401-408.

Sangsawad, P., Roytrakul, S., Choowongkomon, K., Kitts, D. D., Chen, X. M., Meng, G., Li-Chan, E. C. Y. & Yongsawatdigul, J. 2018b. Transepithelial transport across Caco-2 cell monolayers of angiotensin converting enzyme (ACE) inhibitory peptides derived from simulated in vitro gastrointestinal digestion of cooked chicken muscles. *Food Chem.,* 251**,** 77-85.

Sangsawad, P., Roytrakul, S. & Yongsawatdigul, J. 2017. Angiotensin converting enzyme (ACE) inhibitory peptides derived from the simulated in vitro gastrointestinal digestion of cooked chicken breast. *J. Funct. Food,* 29**,** 77-83.

Sanver, D., Sadeghpour, A., Rappolt, M., Di Meo, F. & Trouillas, P. 2020. Structure and dynamics of dioleoyl-phosphatidylcholine bilayers under the influence of quercetin and rutin. *Langmuir,* 36**,** 11776-11786.

Schnaith, E. 1989. Determination of the pepsin activity in human gastric juice, using defined oligopeptides as substrates. *Clin. Biochem.,* 22**,** 91-98.

Schoonjans, R., Castenmiller, J., Chaudhry, Q., Cubadda, F., Daskaleros, T., Franz, R., Gott, D., Mast, J., Mortensen, A., Oomen, A. G., Rauscher, H., Weigel, S., Astuto, M. C., Cattaneo, I., Barthelemy, E., Rincon, A. & Tarazona, J. 2023. Regulatory safety assessment of nanoparticles for the food chain in Europe. *Trends Food Sci. Tech.,* 134**,** 98-111.

Seyrek, E., Hierrezuelo, J., Sadeghpour, A., Szilagyi, I. & Borkovec, M. 2011. Molecular mass dependence of adsorbed amount and hydrodynamic thickness of polyelectrolyte layers. *Phys. Chem. Chem. Phys.,* 13**,** 12716-9.

Shaji, J. & Patole, V. 2008. Protein and peptide drug delivery: oral approaches. *Indian J. Pharm. Sci.,* 70**,** 269-277.

Shanmugam, V. P., Kapila, S., Kemgang, T. S., Reddi, S., Kapila, R., Muthukumar, S. & Rajesh, D. 2021. Isolation and characterization of angiotensin converting enzyme inhibitory peptide from buffalo casein. *Int. J. Pept. Res. Ther.,* 27**,** 1481-1491.

Shen, W. & Matsui, T. 2019. Intestinal absorption of small peptides: a review. *Int. J. Food Sci. Tech.,* 54**,** 1942–1948.

Silveira, S. T., Martinez-Maqueda, D., Recio, I. & Hernandez-Ledesma, B. 2013. Dipeptidyl peptidase-IV inhibitory peptides generated by tryptic hydrolysis of a whey protein concentrate rich in beta-lactoglobulin. *Food Chem.,* 141**,** 1072-7.

Simpson, R. J. 2006. Fragmentation of Protein Using Trypsin. *CSH Protoc.,* Oct 1, 2006(5).

Skrzypczak, K., Gustaw, W., Szwajgier, D., Fornal, E. & Wasko, A. 2017. kappa-Casein as a source of short-chain bioactive peptides generated by *Lactobacillus helveticus*. *J. Food Sci. Technol.,* 54**,** 3679-3688.

So, P. B., Rubio, P., Lirio, S., Macabeo, A. P., Huang, H. Y., Corpuz, M. J. & Villaflores, O. B. 2016. In vitro angiotensin I converting enzyme inhibition by a peptide isolated from *Chiropsalmus quadrigatus* Haeckel (box jellyfish) venom hydrolysate. *Toxicon,* 119**,** 77-83.

Sreekumar, S., Goycoolea, F. M., Moerschbacher, B. M. & Rivera-Rodriguez, G. R. 2018. Parameters influencing the size of chitosan-TPP nano- and microparticles. *Sci. Rep.,* 8**,** 4695.

Stephansen, K., Chronakis, I. S. & Jessen, F. 2014. Bioactive electrospun fish sarcoplasmic proteins as a drug delivery system. *Colloid Surface B,* 122**,** 158-165.

Thapa, R. K. & Kim, J. O. 2023. Nanomedicine-based commercial formulations: current developments and future prospects. *J. Pharm. Investig.,* 53**,** 19-33.

Torres, O., Murray, B. S. & Sarkar, A. 2019. Overcoming in vitro gastric destabilisation of emulsion droplets using emulsion microgel particles for targeted intestinal release of fatty acids. *Food Hydrocolloid,* 89**,** 523-533.

Trapani, A., Lopedota, A., Franco, M., Cioffi, N., Ieva, E., Garcia-Fuentes, M. & Alonso, M. J. 2010. A comparative study of chitosan and chitosan/cyclodextrin nanoparticles as potential carriers for the oral delivery of small peptides. *Eur. J. Pharm. Biopharm.,* 75**,** 26-32.

Uenishi, H., Kabuki, T., Seto, Y., Serizawa, A. & Nakajima, H. 2012. Isolation and identification of casein-derived dipeptidyl-peptidase 4 (DPP-4)-inhibitory peptide LPQNIPPL from gouda-type cheese and its effect on plasma glucose in rats. *Int. Dairy J.,* 22**,** 24-30.

Uhl, P., Bajraktari-Sylejmani, G., Witzigmann, D., Bay, C., Zimmermann, S., Burhenne, J., Weiss, J., Haefeli, W. E. & Sauter, M. 2023. A nanocarrier approach for oral peptide delivery: evaluation of cell-penetrating-peptide-modified liposomal formulations in dogs. *Advanced Therapeutics,* 2300021**,** 1-12.

Wang, F.-J., Yin, X.-Y., Regenstein, J. M. & Wang, J.-Z. 2015. Separation and purification of angiotensin-I-converting enzyme (ACE) inhibitory peptides from walnuts (*Juglans regia* L.) meal. *Eur. Food Res. Technol.,* 242**,** 911-918.

Wang, L., Wang, N., Zhang, W., Cheng, X., Yan, Z., Shao, G., Wang, X., Wang, R. & Fu, C. 2022. Therapeutic peptides: current applications and future directions. *Signal Transduct. Target Ther.,* 7**,** 48.

Wu, H., He, H.-L., Chen, X.-L., Sun, C.-Y., Zhang, Y.-Z. & Zhou, B.-C. 2008a. Purification and identification of novel angiotensin-I-converting enzyme inhibitory peptides from shark meat hydrolysate. *Process. Biochem.,* 43**,** 457-461.

Wu, J., Aluko, R. E. & Muir, A. D. 2008b. Purification of angiotensin I-converting enzyme-inhibitory peptides from the enzymatic hydrolysate of defatted canola meal. *Food Chem.,* 111**,** 942-950.

Xavier, M., Parente, I. A., Rodrigues, P. M., Cerqueira, M. A., Pastrana, L. & Gonçalves, C. 2021. Safety and fate of nanomaterials in food: The role of in vitro tests. *Trends Food Sci. Tech.,* 109**,** 593-607.

Xiao, B., Xu, Z., Viennois, E., Zhang, Y., Zhang, Z., Zhang, M., Han, M. K., Kang, Y. & Merlin, D. 2017. Orally targeted delivery of tripeptide KPV via hyaluronic acid-functionalized nanoparticles efficiently alleviates ulcerative colitis. *Mol. Ther.,* 25**,** 1628-1640.

Xie, J., Chen, X., Wu, J., Zhang, Y., Zhou, Y., Zhang, L., Tang, Y. J. & Wei, D. 2018. Antihypertensive effects, molecular docking study, and isothermal titration calorimetry assay of angiotensin I-converting enzyme inhibitory peptides from *Chlorella vulgaris*. *J. Agric. Food Chem.,* 66**,** 1359-1368.

Yamada, A., Sakurai, T., Ochi, D., Mitsuyama, E., Yamauchi, K. & Abe, F. 2015. Antihypertensive effect of the bovine casein-derived peptide Met-Lys-Pro. *Food Chem.,* 172**,** 441-6.

Yan, J., Zhao, J., Yang, R. & Zhao, W. 2019. Bioactive peptides with antidiabetic properties: a review. *Int. J. Food Sci. Tech.,* 54**,** 1909-1919.

Yang, C., Uertz, J., Yohan, D. & Chithrani, B. D. 2014. Peptide modified gold nanoparticles for improved cellular uptake, nuclear transport, and intracellular retention. *Nanoscale,* 6**,** 12026-33.

Yang, R., Zou, Y., Yu, N. & Gu, Z. 2011. Accumulation and identification of angiotensin-converting enzyme inhibitory peptides from wheat germ. *J. Agric. Food Chem.,* 59**,** 3598-605.

Yang, Y., Marczak, E. D., Yokoo, M., Usui, H. & Yoshikawa, M. 2003. Isolation and antihypertensive effect of angiotensin I-converting Enzyme (ACE) inhibitory peptides from spinach rubisco. *J. Agr. Food Chem.,* 51**,** 4897−4902.

Yun, Y., Cho, Y. W. & Park, K. 2013. Nanoparticles for oral delivery: targeted nanoparticles with peptidic ligands for oral protein delivery. *Adv. Drug Deliv. Rev.,* 65**,** 822-32.

Zhang, S., Murray, B. S., Holmes, M., Ettelaie, R. & Sarkar, A. 2022. Gastrointestinal fate and fatty acid release of pickering emulsions stabilized by mixtures of plant protein microgels + cellulose particles: an in vitro static digestion study. *Food Biophys.,* 18**,** 120-132.

Zhang, T., Su, M., Jiang, X. X., Xue, Y. Q., Zhang, J. X., Zeng, X. Q., Wu, Z., Guo, Y. X. & Pan, D. D. 2019. Transepithelial transport route and liposome encapsulation of milk-derived ACE-inhibitory peptide Arg-Leu-Ser-Phe-Asn-Pro. *J. Agr. Food Chem.,* 67**,** 5544-5551.

Zhao, T., Zheng, L., Zhang, Q., Wang, S., Zhao, Q., Su, G. & Zhao, M. 2019. Stability towards the gastrointestinal simulated digestion and bioactivity of PAYCS and its digestive product PAY with cognitive improving properties. *Food Funct.,* 10**,** 2439-2449.

Zhou, X. H. & Po, A. L. W. 1991. Peptide and protein drugs: II. non-parenteral routes of delivery. *Int. J. Pharm.,* 75**,** 117-130.

Zielinska, A., Carreiro, F., Oliveira, A. M., Neves, A., Pires, B., Venkatesh, D. N., Durazzo, A., Lucarini, M., Eder, P., Silva, A. M., Santini, A. & Souto, E. B. 2020. Polymeric nanoparticles: production, characterization, toxicology and ecotoxicology. *Molecules,* 25**,** 3731.

CHAPTER 3
DEVELOPMENT AND CHARACTERISATION OF CHITOSAN-ALGINATE POLYELECTROLYTE COMPLEXES (PECs) FOR ENCAPSULATION BAPs DERIVED FROM FISH

3. 1. Introduction

Among animal-based proteins, marine source and their processing by-products have attracted attention as a significant source of BAPs, revealing bioactivities including antihypertensive, anti-inflammatory, antimicrobial, and antioxidant properties (Nirmal et al., 2022, Gao et al., 2021, Le Gouic et al., 2019, Zamora-Sillero et al., 2018, Halim et al., 2016). Remarkably, fish source seems to outperform antihypertensive BAPs from other origins, with some supplements that contain these BAPs available in the market (Fuentea et al., 2020, Hayes and Tiwari, 2015).

The pentapeptide LKPNM (Leu-Lys-Pro-Asp-Met) is a notable antihypertensive BAP with pronounced bioactivity, which is obtained from the muscle of bonito fish (*Sarda spp.*) by thermolysin hydrolysis. A food supplement containing this BAP is commercially available (Curtis et al., 2002, Fujita and Yoshikawa, 1999), has a patent, with one of its strengths being that LKPNM does not reveal bitterness (Yokoyama et al., 1992). However, it is worth mentioning that research on encapsulation of this particular BAP is currently scarce. There have been several attempts to encapsulate BAPs with sequences < 20 amino acids, especially applying chitosan (CS) as an encapsulant (Danish et al., 2017, Chen et al., 2017, Bicak et al., 2021), or CS combined with alginate (ALG).

CS structure is described in Chapter 1, linear polysaccharides formed by glucosamine (deacetylated units, **D**) and N-acetyl-glucosamine (acetylated units, **A**) (Potaś et al., 2020)(**Fig. 1.1, Chapter 1**). The degree (or fraction) of acetylation (DA) is defined as the ratio of the mole fraction of A residues to the total (A+D). The acetylation pattern is the distribution of A residues in CS, which is usually random by the chemical deacetylation process. However, it is possible to produce block-wise patterned CS via enzymatic technology (Wattjes et al., 2020). The M_w distribution, especially the ratio of the weight average molecular weight to the number average molecular weight (Mn), or the polydispersity index, is another attribute that affects the CS characteristics and utilisation. The intrinsic pK_a (pK_0) of CS, which remains

unaffected by its degree of acetylation (up to DA ~25%) and degree of neutralisation, has been measured as 6.0 ± 0.1 (Rinaudo et al., 1999a, Rinaudo et al., 1999b). Then at pH ≈ 6.0 and lower, relating to a lowest level of protonation of 0.5, the CS dissolves in dilute acidic solutions. In addition, commercial CS demonstrate M_w between ~10 and ~500 kDa and F_A values between ~0.05 and ~0.30 (Luo and Wang, 2014).

CS has been broadly applied in the pharmaceutical, cosmetic, and food industries. As an encapsulation agent, CS has superior characteristics, especially for oral and gastrointestinal delivery, since it is mucoadhesive, biodegradable, biocompatible, easy to modify, and a permeation enhancer. Due to its mucoadhesive ability to facilitate penetration into the intestinal mucus layer, CS increases the bioaccessibility and bioavailability of encapsulated proteins and peptides during gastrointestinal delivery. CS improve absorption via the paracellular route in the intestinal epithelium because it facilitates the opening of the tight junctions (Sonaje et al., 2012). CS forms complexes with polyanions such as alginate (ALG) using electrostatic interactions because its positive charge is maintained at mildly acidic conditions, such as to build polyelectrolyte complexes (PECs) that can aid delivery (Potaś et al., 2020).

ALG is also known as anionic polysaccharide, a linear block co-polymeric biopolymer in structure, which is formed by α-guluronic acid (G) and β-mannuronic acid (M) linked via (1→ 4) bonds as outlined in **Chapter 1**, but also various block lengths (Goycoolea et al., 2009) (see **Fig. 1.2**). The overall M_w of ALG is typically between 60 and 700 kDa. The charged carboxyl groups increase ALG's solubility in water, and they also enable the formation of a gel via lowering the pH (due to COO^- groups being protonated) or via introducing particular divalent cations like Ca^{2+} to form Ca-ALG (Tanaka et al., 1984, Stewart and Swaisgood, 1993). Sodium ALG has been developed as microgel particles by a simple one-step precipitation process to encapsulate the protein lactoferrin (Pravinata et al., 2016).

ALG offers some strengths as an encapsulation agent for gastrointestinal delivery. These cover mucoadhesive attributes, like CS (George and Abraham, 2006, Gombotz and Wee, 1998), biocompatibility, low toxicity and resistance to hydrolysis by most enzymes in the gastric and intestinal tracts. ALG has received GRAS (Generally Recognised as Safe) approval from the FDA and has been used extensively by the food industry. As expressed above, in terms of forming a polyelectrolyte complex (PEC), ALG is an ideal biopolymer to combine with

CS, since it has an anionic charge, and the counterpart brings a cationic charge (**Chapter 1** section 1.2.1). The PEC enables entrapment of BAPs, and then the loaded BAPs are protected and assisted in their delivery. For instance, some published works proven that crosslinking CS and ALG minimises the ALG hydrogel's porosity, and then BAP leaching under gastric conditions was prevented (George and Abraham, 2006, Luo and Wang, 2014, Potaś et al., 2020). CS + ALG systems have been developed to encapsulate the BAP KPV and VLPVP by a double emulsion solvent evaporation and membrane emulsification-ionic gelation approaches, respectively (Xiao et al., 2017, Huang et al., 2017). CS + ALG combinations would seem to make them an ideal candidate model for delivering BAPs, owing to the apparent simplicity and versatility of the resulting PECs. This Chapter describes the development and characterisation a model system in detail, to attempt to interpret the critical factors mitigating their formation, encapsulation efficiency (EE), and BAP release.

3. 2. Materials and Methods

3. 2.1 Materials

Sodium alginate of M_w 8 kDa (ALG8), with a mannuronic (M) to guluronic (G) acid (M/G) ratio = 5.1, and sodium alginate of M_w 21 kDa (ALG21), with M/G ratio = 1.42 were obtained from and characterised by Danisco, (Copenhagen, Denmark), and the samples are part of the same panel of samples used in previous experiment (Goycoolea et al., 2009, Fuenzalida et al., 2016). Chitosan (CS) (batch number 212-160315-03, product code HMC 90/100) with a M_w of 111 kDa (M_w/M_n = 1.2) as analysed via HPSEC-MALS-RI-UV/VIS (*ref*. see appendix), degree of acetylation (DA) = 10 % as characterised by ^{1}H NMR spectroscopy (Hirai et al., 1991), and intrinsic viscosity ([η]) ~ 400 mL g^{-1} (as measured using viscometry in 20% acetic acid-stoichiometric and 85 mM NaCl, 25 °C) and, it was received from Heppe Medical Chitosan GmbH (Halle, Germany).

The synthetic peptide for standards: LKPNM and LKP (≥95% HPLC) were procured from GenScript (Oxford, UK). The bonito fish protein extract (PeptACE®) was purchased from Natural Factors (Washington, USA). Acetonitrile (ACN) (HPLC grade), hydrochloric acid (HCl), sodium chloride (NaCl), and sodium azide (NaN_3) were obtained from Sigma-Aldrich (Gillingham, UK); trifluoroacetic acid (TFA) (HPLC grade 99.5%) was obtained from Alfa Aesar (Heysham, UK). Ultrapure Milli-Q water was provided by a Milli-Q apparatus (Millipore Corp.,

Bedford, MA, USA) and used to make up all solutions unless mentioned otherwise. A Hettich, Ritona 380 R centrifuge (A Hettich, Tuttlingen, Germany) was used to centrifuge (2 mL) all samples across experiments.

3. 2.2 BAP isolation from protein extract

The bonito fish protein extract (PeptACE®), as much as 2 g, was dissolved in water (100 mL) and stirred using a magnetic stirrer (Oxford, UK) at 250 rpm for 60 min at 25 ^{o}C, then centrifuged at 5000 x g for 30 min at 4 ^{o}C. The supernatant was taken and then filtered using Ultracel® ultrafiltration disc with M_w cut off of 3 kDa (Amicon® Bioseparations, Massachusetts, USA). The ultrafiltration (UF) solution was then kept (for 1 week) at 4 ^{o}C before further identification by HPLC (high-performance liquid chromatography). A Shimadzu HPLC with a UFLC-XR system (Kyoto, Japan) was used in reverse-phase (RP) mode. The UF solutions were diluted 10x with water and then filtered using a 0.22 µm hydrophilic PVDF syringe filter before finally loaded into autosampler tubes (1 mL vials). According to the methods adopted from Curtis et al. (2002), Jiang et al. (2017) and Liu et al. (2020), with some modifications, the RP-HPLC was performed. A C-18 column stationary phase (Gemini®, 4.6x250 mm, 5 µm, 110 Å, Darmstadt, Germany) was used for separation. The injection volume was set to 20 µL. The eluents were Milli-Q water (mobile phase A) and ACN (mobile phase B), containing 0.05% TFA, and the flow rate was 1 mL min^{-1}. The gradients of the mobile phase for ACN were 5% (0 – 6 min), 15% (6 – 10 min), 25% (10 – 15 min), and 35% (15 – 21 min). A wavelength (λ) = 219 nm was used to identify the eluent absorbance, and then the results on each retention time were compared to the standards: LKPNM and LKP (GenScript, ≥95% HPLC). Prior to further experimentation, the fraction solutions were stored in a refrigerator.

3. 2.3 Preparation and calibration of the ALG and CS stock solutions

ALG was dissolved in 25 mL of 85 mM NaCl to obtain 10 mg mL^{-1} ALG solution; the pH of this solution was 5.8. The CS was dissolved in the same concentration of NaCl (85 mM), which also had been added with an aliquot of 12 M HCl to provide 1.25x moles of H^+ in comparison to the moles of non-acetylated (ionisable) amino groups. The final concentration of the CS stock solution was 10 mg mL^{-1}. The concentration of NaCl is based on a study from Goycoolea et al. (2009), which was able to maintain the stable particle size of CS + ALG + tripolyphosphate (TPP) nanocomplexes during the formation of CS-TPP nanoparticles (NPs)

(Milkova and Goycoolea, 2020, Sreekumar et al., 2022). The resultant pH of the CS solution was 4.8. Then, sodium azide (0.02% w/v) was added as a preservative for both CS and ALG stock solutions, then subsequently stirred overnight at 25 ^{o}C with a magnetic stirrer. The CS and ALG solutions at a range of dilutions (0, 1.0, 2.0, 3.0, 4.0 and 5.0 mg mL^{-1}) were measured for their densities using a DMA 4500 M density meter (Anton Paar GmbH, Austria) at 25 ^{o}C, and standard curves of the concentration vs density were plotted. All density measurements were performed in triplicate. To calibrate the instrument, solvent (85 mM NaCl) and pure water were initially analysed and to provide further confirmation that density is stable, the density of water at 25 °C (ρ = 0.997 g cm^{-3}) was measured as a reference.

After that, the diluted solutions were loaded into the instrument, each comprising 1 mL dispensed via a 1 mL syringe, ensuring no bubbles were obtained throughout the measurement process. Next, a hydrophilic polyethersulfone (PES) sterile membrane (Millex®, Millipore, Ireland) pore size 0.22 µm, diameter 33 mm was used to filter the remaining CS and ALG solutions and the standard curve was used to convert their densities into their final concentration (O'Connell et al., 2023b). Those filtered solutions were diluted with 85 mM NaCl (also previously filtered through the PES membrane) for subsequent PEC formation to obtain appropriate concentrations. The filtration is important to eliminate extensive undissolved aggregated material and dust in preparation for subsequent light scattering analysis of their mixtures and the solutions. The densities of CS and ALG as a function of their concentration are presented in **Fig. 3.1.** In this study, the preparations of CS (with a M_w of 111 kDa) at concentrations between 0.1 and 0.5 % (w/v) presented ρ between 1.0012 and 1.0029 g/cm³, these were in the same page with the Kumar et al. (2021) study. At the same concentrations (see **Fig. 3.1**), the densities of the ALG solutions were very similar, even though the ALG8 provider was slightly higher than ALG21 in experimental error; for the second time, this was in alignment with Kumar et al. (2021).

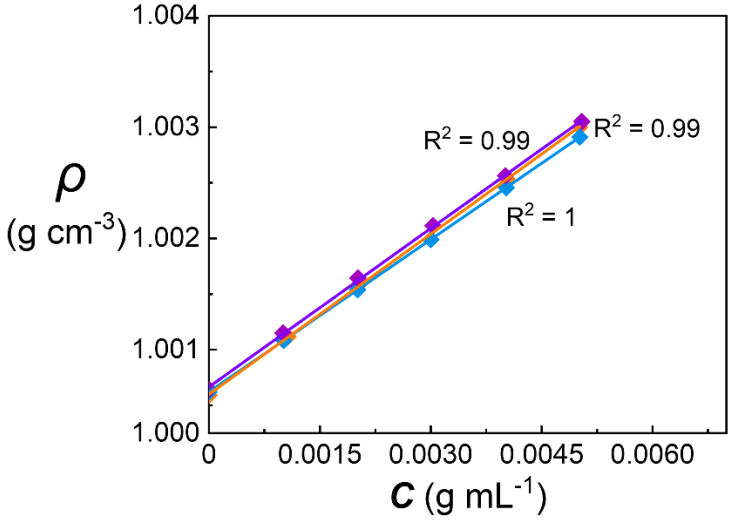


Figure. 3.1 Standard curves for unfiltered solution density (ρ) versus concentration (*C*): CS (orange); ALG21 (blue); ALG8 (purple), with the corresponding linear regression lines.

3.2.4 Molar charge ratio (n^-/n^+) calculation

The molar charge ratio (n^-/n^+) of the biopolymers on mixing is given by:

$$n^-/n^+ = M_{ALG}\cdot N^-_{ALG}/M_{CS}\cdot N^+_{CS} \quad (3.1)$$

Where M_{ALG} = the final molar concentration of ALG, N^-_{ALG} = the number of negative charges per ALG molecule, M_{CS} = the final molar concentration of CS and N^+_{CS} = the number of positive charges per CS molecule. N^-_{ALG} and N^+_{CS} are given by:-

$$N^-_{ALG} = \alpha\cdot M_W ALG/M_W ALG_{mon} \quad (3.2)$$

and

$$N^+_{CS} = (1-\alpha)\cdot(1/100)\cdot(100\text{-}DA)\cdot M_W CS/M_W CS_{mon} \quad (3.3)$$

: M_wALG and M_wCS are the M_w of the ALG and CS, respectively; where α is the degree of dissociation of the ionising groups; $M_w ALG_{mon}$ and $M_w CS_{mon}$ are the M_w of the ALG and CS monomers, respectively. DA is the % degree of acetylation of the CS. Presuming both the ALG carboxylate groups and the CS amino groups are fully charged at the pH at which the polymers are mixed (see later), at −1 and +1, respectively, i.e., α = 1 for COOH and 0 for the NH_3^+ groups, this provides the calculation of N^+_{CS} and N^-_{ALG} if the M_w of the species are known. According to the M_w of the ALG21, ALG8, and CS as 21, 8, and 111 kDa, respectively (as described above), also values of 198 g/mol for ALG_{mon}, and CS_{mon} 166.3 g/mol (the average molar mass of the A

and D of CS residues, factored by DA of CS = 10%), the values of N^{-}_{ALG} for ALG21 and ALG8, and N^{+}_{CS} for CS are 106–, 40.4–, and 601+ respectively. Based on known concentration (2 mg mL^{-1}, converted to M_{ALG} and M_{CS}) of the ALG and CS stock solutions, the different volumes were blended, and then the molar charge ratio (n^{-}/n^{+}) was quantified via **Eq. (3.1)**.

3.2.5 Formation of polyelectrolyte complex (PEC)

A simple one-step mixing technique was carried out for PEC preparation (Goycoolea et al., 2009). According to the charge ratio (n^{-}/n^{+}) calculation indicated above, to give a total volume of 2 mL, the appropriate volumes and concentrations of ALG and CS solutions were mixed. The ALG solution was added to the CS solution using a micropipette. The mixture was then vortexed using Fisherbrand™ Classic Vortex Mixer (Fisher Scientific, Loughborough, UK) at room temperature (20 - 25 °C) for 5 s, subsequently cooled to 4 °C and left for 3 h, then sonicated for 5 min (5 s pulsed ON, 3 s pulsed OFF, amplitude 35% at 20 kHz) using a Sonics® VCX 750 (Sonics & Materials, Inc., Newtown, CT, USA) ultrasonicator which was installed with tapered microtip probe. For loading BAPs into PECs, a final BAP concentration of 1.0 mg mL^{-1} was prepared by dissolving it into water. Subsequently, the BAP solution added into CS solution, before finally mixed with the ALG solution—the PEC preparation outlined in **Figure 3.2.**

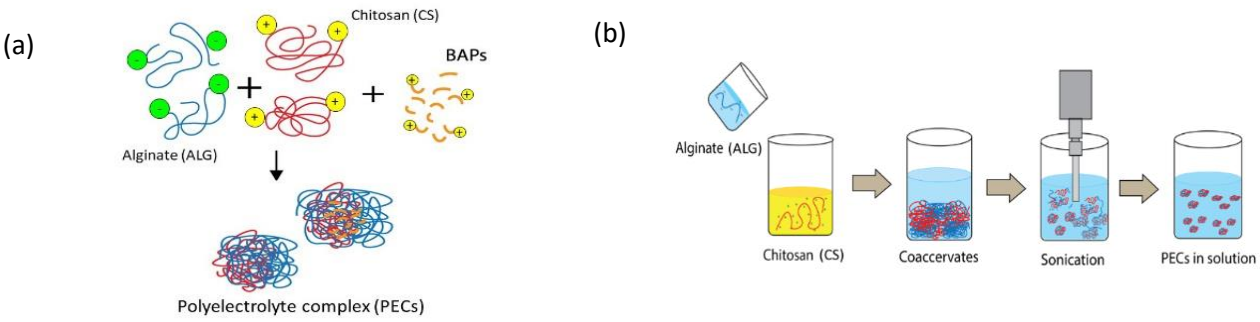


Figure. 3.2. Cartoon of complex formation with or without BAPs (a); schematic illustration of preparation of PECs (b).

3.2.6 Encapsulation efficiency (EE)

The loaded PECs were centrifuged at 20,000 x g for 25 min. Then the supernatant, which consists of free (non-encapsulated) BAP, was determined for concentration using HPLC

as described above (*section 3.2.2*). The percentage of encapsulation efficiency (EE) was calculated as:

$100(C_i\text{-}C_s)/C_i$ (3.4)

(Danish et al., 2017, Bicak et al., 2021) where C_i is the initial BAP concentration in the mixture, and C_s is the BAP concentration in the supernatant analysed using HPLC.

3.2.7 Analysis of viscosity

To indicate differences in the amount of remaining, non-complexed biopolymer, the viscosity (η) analysis of the supernatants from the PECs (both loaded and unloaded) was also performed (Menchicchi et al., 2014), as an approach to qualitatively verifying the extent of complex formation, and the viscosity of supernatants are needed for reliable approximation of R_h using DLS (see *section 3.2.9*). By using the microVISC™ method via RheoSense, each supernatant (300 µL) was loaded into the instrument equipped with a chip with rectangular slit for both the inflow and outflow. The chip, enhanced with sensors, determines the solution's viscosity and flow as a plugger forces it to move through the slit.

3.2.8 The release (R) of BAPs

In vitro release studies were performed at pH 3.0 and 6.8. The PECs loaded with BAPs were centrifuged as described above (*section 3.2.6*), all the pellets were resuspended with water and adjusted to pH 3 and pH 6.8 using 0.1 M HCl and 0.1 M NaOH, respectively. Subsequently, sample were then incubated for 3 h at 37 ^oC (Egger et al., 2016, Zhang et al., 2022). These two pH values and incubation times were applied to mimic the 'typical' gastric and intestinal conditions during human digestion of foods. After the incubation period, the treatments were centrifuged at 20,000 x g for 25 min, and the concentration of BAP in the supernatant was quantified using HPLC. The % release (*R*) was defined as:

$R = 100\ (n^-/n^+_S/C_{BAP})$ (3.5)

Where C_{BAP} = the concentration of BAPs in the treatment (mixture) before incubation (determined by the measured EE), and n^-/n^+_S = the concentration of BAPs released from the treatment on incubation, measured via HPLC analysis of the supernatant.

3.2.9 Measurements of PEC particle sizes

The dynamic light scattering (DLS) was used to analyse mean particle sizes, particle size distributions (PSD) and polydispersity index (PDI). Polymethyl methacrylate (PMMA) semi-micro, UV-transparent cuvettes with a path length of 10 mm (VWR International, UK) were filled with sample suspensions and then measured with a Zetasizer Ultra (Malvern Panalytical). The analysis was carried out by setting the refractive index of the dispersant 1.33 (water) and the cuvette mode of ZEN0040 on the instrument. Samples were analysed using backscattered light (wavelength 633 nm) at a detection angle of 173° and equilibrated for 120 s at 25 °C to analyse the average hydrodynamic radius (R_h), on the assumption that the particles are spherical and follow the Stokes-Einstein relationship:

$$R_h = \frac{k_B T}{3 \pi \eta D} \qquad (3.6)$$

: where, Boltzmann's constant is represented by k_B, absolute temperature (298.15 K) represented by T, and D = diffusion coefficient as measured by the instrument (Anderson et al., 2013; Stetefeld et al., 2016). Mixed-mode phase analysis light scattering (M3-PALS) was also used to measure their electrophoretic mobility (μ), so that the ζ-potential of the particles could be calculated. Samples were diluted 50 times (5 mL of 10 mM NaCl for 100 μL of sample at pH ~ 7) and vortexed. NaCl concentration (10 mM) was used at a low value to fix the ionic strength and avoid particle aggregation or complex dissolution. Then, the folded capillary zeta cell DTS1070 was loaded with 0.8 mL of sample, and subsequently, Zetasizer Ultra (Malvern Panalytical) equipped with a 4 mW He/Ne laser beam (λ = 633 nm) was used for analysis at 25 °C. The Smoluchowski approximation was used to calculate the ζ-potential:

$$\zeta = \frac{4\pi \eta \mu}{\varepsilon.\varepsilon_0} \qquad (3.7)$$

:in which ε_0 represents the permittivity of free space (8.854 x 10^{-12} F m^{-1}), ε_r represents the relative dielectric constant of the solvent (10 mM NaCl and water ≈ 78.5), and $\mu = v/E$, where v is the velocity of a particle in an electric field of strength E (Doroszkowski, 1999, Zhang et al., 2021). In several samples, the Eppendorf tubes containing a small amount of glycerol were used to hold PEC solutions of both loaded and unloaded, and then centrifuged at 20,000 x g for 25 min. Subsequently, the supernatants poured out, while the pellets were resuspended with filtered 85 mM NaCl and mixed via pipetting to re-measure PEC particle size.

3. 2.10 Small angle X-ray scattering (SAXS)

Small angle X-ray scattering (SAXS) was used on unloaded PECs analysis at 25 ^{o}C. SAXS measurements were performed using the SAXSpace small-angle X-ray camera from Anton Paar (Graz, Austria). Briefly, the X-ray beam was collimated into a line focus, length of 20 mm and width of 0.5 mm. The distance of the sample to the detector was 317 mm, determined via utilisation of silver behenate powder. Each sample was loaded into a 1.5 mm diameter quartz capillary tube and exposed to the beam (wavelength 0.154 nm) for 3600 s, operating at 40 kV and 50 mA. The instrument system was additionally run in high-intensity mode, offering a minimum accessible scattering vector magnitude q_{min} = 0.12 nm^{-1} (where $q = 4\pi/\lambda \sin(\theta)$, and 2θ represents the scattering angle). Further details of the instrument and its operation are available elsewhere (Apostolidis et al., 2023).

3. 2.11 Transmission electron microscopy (TEM)

To observe the size and morphology of selected loaded PECs, transmission electron microscopy (TEM) was used. A copper TEM grid placed on filter paper was dropped with the liquid sample, then left to dry at room temperature, covered with the transparent container. Then, tweezers placed the grid carefully into the TEM specimen holder and were clamped. A FEI Titan3 Themis G2 S/TEM (Massachusetts, USA) operated at 300 kV with an energy spread of $\approx$ 0.25 eV and fitted with a Gatan OneView 4K CMOS digital camera was used to observe the samples.

3. 2.12 Statistical analysis

The data are shown in average values and their associated standard deviations, which were repeated three times, except for the HPLC analysis, which was repeated two times. SPSS Statistics 29.0 (IBM, Chicago, IL) was used for the data analysis. The treatment's efficacy was processed via one-way analysis of variance (ANOVA), followed by the Tukey's test for their significance. A threshold of $p < 0.05$ was applied for the statistical significance analysis.

3.3 Results and Discussion

3.3.1 Fish BAPs fractionation and identification

There are two predominant peptides in the ultrafiltrate of the PeptACE sample as revealed by the HPLC chromatograms (**Figure. 3.3**), indicated by sharp and high-intensity

peaks at retention times ranging from 105 to 117 s, and 218 to 225 s. The peaks were confirmed by those of the two synthetic peptides, LKPNM and LKP, which corresponds to previous publications (Curtis et al., 2002, Fuentea et al., 2020, Fujita and Yoshikawa, 1999), when injected with similar treatment at concentrations ranging from 0 to 0.25 mM. Probably owing to its lower M_w and higher solubility in the hydrophilic mobile phase, the LKP eluted just before LKPNM.

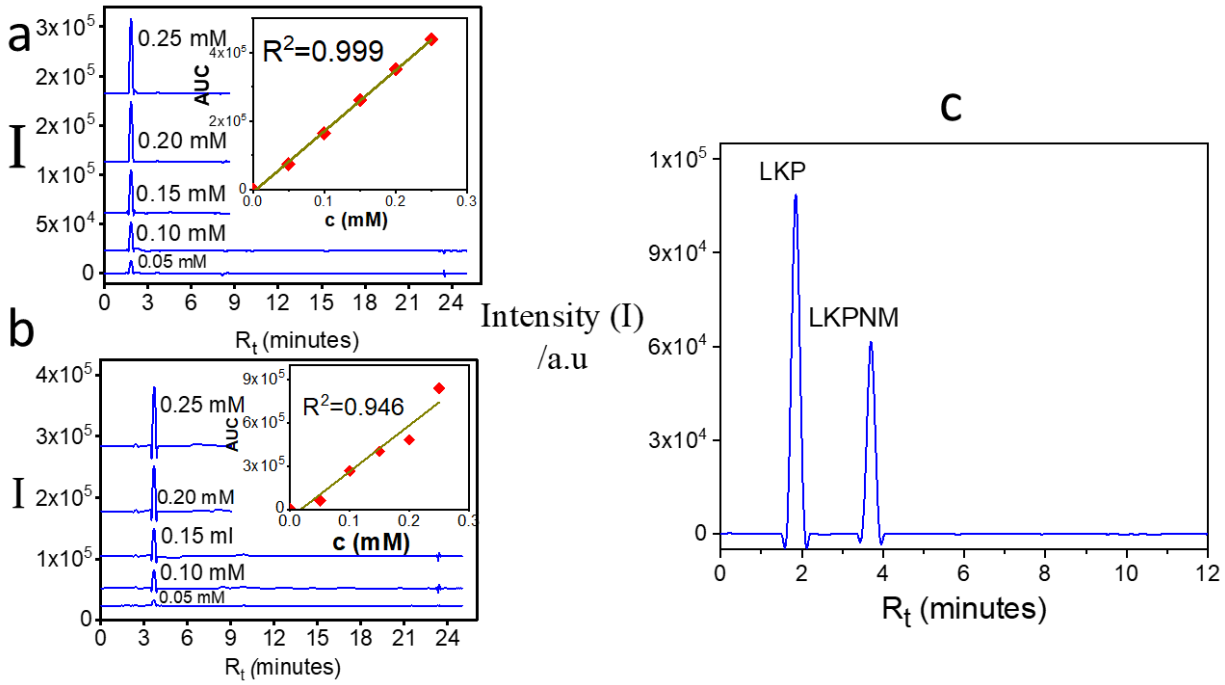


Figure 3.3 Chromatograms of standard curves for synthetic LKPNM (a), synthetic LKP (b), and chromatogram UF fraction (≤ 3kDa) fish BAPs calculated from area under the curves (AUC) (c).

As indicated earlier, hydrolysis of LKPNM may lead to the existence of LKP (Fujita et al., 2000, Fujita and Yoshikawa, 1999), in which it was presented that two peptides: LKP and NM, were obtained from LKPNM. Remarkably, compared to the parent sequence LKPNM, LKP exhibited an eight-fold higher antihypertensive activity, with an IC_{50} of 0.32 µM, whilst NM exhibited no biological activity. Despite assertions claiming the presence of six short fish peptides on the sample, no additional BAPs were observed (Guan et al., 2001). A work published by Curtis et al. (2002) mentioned that by LC-MS analysis, the BAPs in the PeptACE® exhibited 95% similarity with synthetic LKPNM. PeptACE® is expected to comprise 85% LKPNM

BAP with IC_{50} of 50.2 µg mL^{-1} (2.40 µM). The LKPNM has an isoelectric point ranging from 9.6 to 10.5 and is entirely soluble in water (Curtis et al., 2002, Fujita and Yoshikawa, 1999).

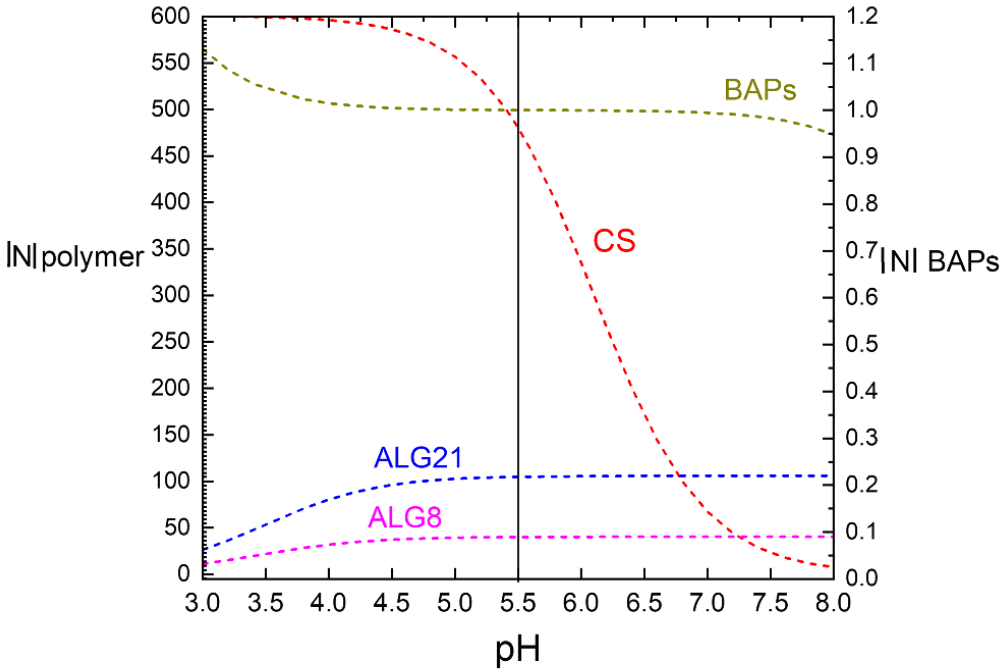


Figure. 3.4. The magnitude of the net charge |N| on single molecules of the polymers and the BAPs as a function of pH. Left hand ordinate: |N| (+ve) for CS (red short, dashed line); |N| (-ve) for ALG21 (blue short, dashed line); |N| (-ve) for ALG8 (magenta short, dashed line). Right hand ordinate: |N| for the LKPNM or LKP BAPs. (Calculation explained in the text). The vertical dashed line indicates the pH (5.5) of PEC formation.

The theoretical plots of the net charge on the BAPs, alginates (ALG), and chitosan (CS) as function of pH is showed in **Figure 3.4**, considering the different values according to the pK_a of the different ionizing groups (a = (K_α/([H^+] + K_α)). The pK_a values for the $-NH_2$, terminal COOH group, and LYS side-chain NH_2 of the BAPs (LKP or LKPNM) were taken as 9.3, 2.2, and 10.2, respectively (Belitz and Grosch, 1999). The value of the pK_o CS NH_2 groups was interpreted as 6.0 (see *3.1 Introduction*), and the ALG mannuronic (M) and guluronic (G) COOH groups are 3.38 and 3.65, respectively (**Chapter 1**). As described above, the number of NH_2 and COOH groups on the CS and ALG molecules was calculated. In the case of ALG8 and ALG21, the M/G ratio was taken into account because of their slightly different pK_a's. At the pH of PEC

formation (5.5), compared to the charge on ALG8 and ALG21 molecules, the charge on the CS is dominant, approximately 11 and 4 times more prominent (and opposite in sign), respectively. As explained below, the net charge (~ +1) on both BAPs is minuscule in comparison, but due to their lower M_w, the molar concentration of +ve charges becomes significant. CS loses approximately 20% of its full charge between pH 3.0 and 5.5, then should have lost almost all its charge by pH 8. The ALG lose approximately 70% of their negative charge between pH 3.0 and pH 5.5

3.3.2 Physical properties of CS + ALG PECs

The measured hydrodynamic radius (R_h) and ζ–potential of PECs formed as a function of the molar charge ratio n^-/n^+, between n^-/n^+= 0.1 (excess CS) and n^-/n^+ 10 (excess ALG) for CS + ALG8 and CS + ALG21 are show in **Figure 3.5**. (Note that the viscosities of the background solutions were used to calculate those R_h values, analysed after the PECs were centrifuged off – see **Fig. 3.7** below, whereas for the ζ measurements, the samples were highly diluted into water). One critical parameter influencing the formation and stability of such PECs is n^-/n^+, while published works focusing on this seem to be scarce. Only few studies such as conducted by Becheran-Maron et al. (2004), Sæther et al. (2008), and Yilmaz et al. (2019) seem have endeavoured to control the n^-/n^+ in CS + ALG PECs formation. Full charge neutralisation occurs at a non-stoichiometric n^+/n^- (charge ratio) of 0.70 ± 0.2 (*i.e.,* $n^-/n^+ \sim 1.43$) according to Becheran-Maron et al., (2004). As charge ratio n^-/n^+ approaches 1, the electrostatic attraction intensifies, leading to the formation of coacervates or larger aggregates. At the same time, ζ swaps from negative to positive. At $n^-/n^+ > 1$, R_h decreases again and the ζ values tend to level off at -30 and -42 mV for the ALG8 and ALG 21 systems, respectively. For $n^-/n^+ < 1$ and as $n^-/n^+ \rightarrow 1$, R_h is reduced slightly (from ca. 800 to 300 ± 50 nm), with the CS + ALG8 system presenting smaller R_h than the CS + ALG21 system, within experimental error. But all the R_h > 10 µm, particularly just beyond $n^-/n^+ = 1$. In contrast the ζ-potentials of the two systems are generally similar between n^-/n^+ = 0.1 and 1. For $n^-/n^+ > 1$ where the charge inversion occurs. It is necessary to mention that the polydispersity index (PDI) of the sizes is also more extensive at the higher values of n^-/n^+. It is agrees with Yilmaz et al. (2019), published work that recorded smaller R_h when CS was in excess rather than ALG. Also notable is that the range of n^-/n^+ at which the sharp climb in R_h occurs and the charge flipping for $n^-/n^+ > 1$ is shifted to slightly

higher n^-/n^+ for the lower M_w ALG8, and the highest R_h (at $n^-/n^+ = 10$) for CS + ALG8 system is also noticeably greater than for the CS + ALG21, these last sizes being around 10 and 2 μm, respectively. Hence, compared than those formed with the higher M_w ALG, the lower M_w ALG when in excess ($n^-/n^+ > 1$), appears to give more expanded and lower charged PECs, perhaps indicating that the ALG21 is more 'efficient' than ALG8 in being able to pull CS chains together to form the PECs at the equal n^-/n^+. Note that there should be less molecules of ALG21 than ALG8 available at the similar n^-/n^+. However, it makes sense that the higher M_w ALG is more efficient as an agent of cross-linking if the connection between the two types of polymers is a co-operative process depending upon multiple points of attraction between the different polymers.

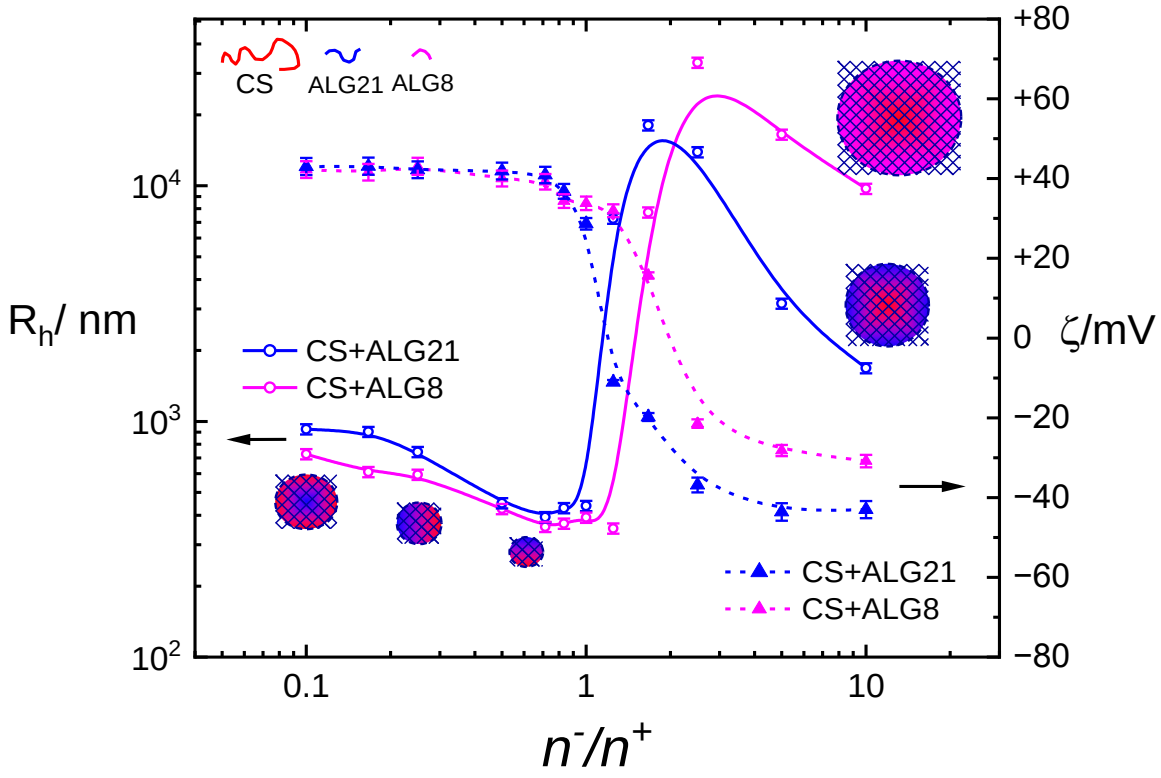


Figure. 3.5 Hydrodynamic radius (R_h) and ζ-potential of unloaded PECs as a function of molar charge ratio n^-/n^+ at a total polymer concentration of 2 mg mL^{-1}. Shading on the round shape in figure indicating biopolymers constructing the PECs. Red dominant meaning excess CS, blue and magenta dominant indicating excess ALG21 and ALG8 respectively.

Based on Vold et al. (2006), the persistence length of ALG, at 12 nm, is typically larger than that of this sort of CS: ca. 5 nm (Rinaudo et al., 1993, Schatz et al., 2004), in other words, ALG is stiffer than CS, so that ALG might be expected to have a disproportionate effect on the size of the complexes of the two molecules, even though the CS M_w is so much higher.

Figure 3.6 compares the values of the radius of gyration (R_g) as determined by SLS (at scattering angles between 30 ° and 130°) with the R_h determined via DLS for freshly prepared PECs at n^-/n^+ = 0.5 and 10 of CS + ALG21. The spherical particles scattering model was applied to fit the angular dependency of scattered intensities from SLS data. An asymmetric size distribution for different PECs with a skewness towards large dimensions and the average radius of gyration (R_g) for each sample were provided from the analysis (size distributions and SLS data fitting are presented in the Appendix). The R_g values are considerably and consistently lower than R_h for both n^-/n^+, which is an interesting result. This suggests that the core of the structures in both cases is somewhat similar, whilst the outer layers differ – R_h being much more sensitive to the presence of long, less dense 'hairy' layers at the surface might indicate this. Therefore, minor divergence between R_g and R_h in n^-/n^+ = 0.5, once more indicates a tighter structure when CS is in excess rather than ALG in excess or n^-/n^+ = 10. Representative documented R_g:R_h ratios for spherical nanoparticles (NPs) are 0.775, and for macromolecules between 1 and 2, ratios higher than 2 usually reveal anisotropy in the molecules, i.e., elongated structures such as rod-like conformations. The highly swollen macromolecules or microgels are typically represented by the ratio < 0.7 (Schmidt et al., 1979).

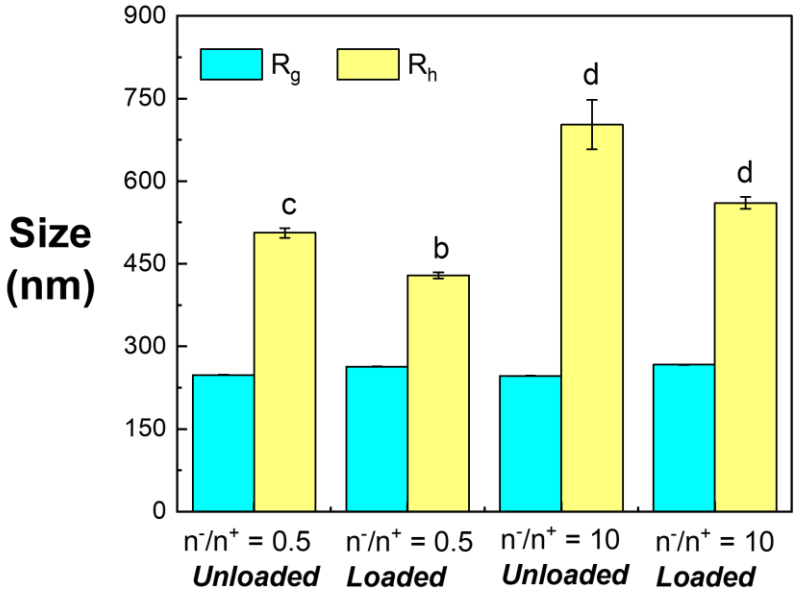


Figure. 3. 6. Measured PEC sizes via SLS (R_g, cyan) and DLS (R_h, light yellow) for the CS + ALG21 systems at $n^-/n^+ = 0.5$ and 10, both loaded and unloaded with BAPs. (Bars with different letters are values that are statistically different from one another, at $p < 0.05$)

The results in **Figure 3.7a** and **3.7b,** which show the viscosities (η) of the supernatants when centrifuging off the PECs, as a function of the mass fraction (*f*) of ALG in the system, indicate that cross-linking via ALG21 is more efficient, as also mentioned previously (**Figure 3.5**). Higher levels of polymer have become trapped within the PECs indicated by the measured viscosity (η) being further away (lower) than the theoretical additive line (which assumes no interaction between the polymers in dilute solution). (A similar dilute solution viscosity approach was used in a previous publication to analyse the degree of interaction between polysaccharides of varying structure and conformation (Goycoolea et al., 1995) and between CS and other polysaccharides with soluble mucin (Menchicchi et al., 2015, Menchicchi et al., 2014)). In the case of the CS + ALG8 system, it is seen that η is closer to the additive line overall (**Figure 3.7a**). The CS + ALG21 is larger (1.7x larger) than CS + ALG8 for quantitatively the integrated area between the curve which describes the data points and the additive straight line (see **Figure 3.7c** and **3.7d**). When η higher than the theoretical additive line, e.g. in case of CS + ALG8 between f = 0.7 and 1, that might be due simply to the inaccuracy of the measurement at low η, it might be because non-homogeneous blending or inadequate separation of molecules in the centrifugation step, because the η of the CS was considerably

higher than that of the ALG8 stock solution. Therefore, minimal deviation in CS content could have an enormous impact on the total η. Likewise, this situation also happens in the CS + ALG21 systems at $f > 0.92$.

The SAXS patterns and corresponding Kratky plots before and after complexation are shown in **Figure 3.8**. For clarity, the intensities on the Y-axis of both curves are shown in arbitrary units and shifted vertically. The scattering intensities (I) demonstrate a slow decay by scattering vectors (q), accompanied by a monotonous increase of $I \times q^2$ in Kratky plot for the pure CS and ALG polyelectrolyte solutions. The characteristic suggests the presence of homogeneous solutions of stretched chains of polyelectrolytes. At the studied pH, the stretching is enforced by the biopolymers' high charge along the chain under the condition. On the contrary, a much higher angular dependency is observed (the intensity versus q decays faster compared to the pure polyelectrolytes, after mixing the two biopolymers and upon formation of PECs.

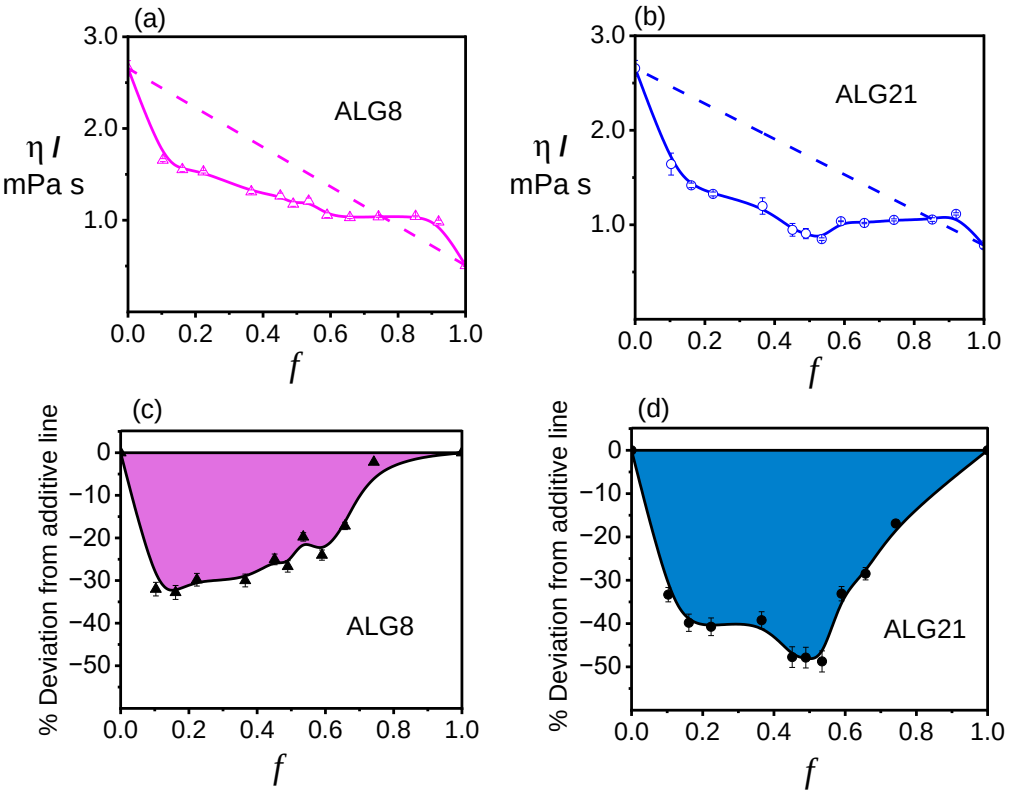


Figure. 3.7. Viscosity (η) of the supernatants of centrifuged CS + ALG mixtures as a function of the original mass fraction of ALG (*f*) in the systems for (a) CS + ALG 8 kDa and (b) CS + ALG 21 kDa at 25 °C. The dashed lines in (a) and (b) are the theoretical η of the biopolymer mixtures assuming simple additivity of the η of the pure components. (Thus, η at $f = 0$ and 1 are the values of CS and ALG stock solutions at 2 mg mL^{-1}, respectively). Figures (c) and (d) show the % difference of the measured η from the additive line for CS + ALG8 and CS + ALG21, respectively.

The intensities decline until q=0.5 nm^{-1} (which relates to the length >12 nm); however, the rate of these decreases depends on the M_w and type of polyelectrolytes (PEs). A close look at Kratky plots helps understand the chain arrangement for different PECs. The Kratky plot shows a plateau at low q for the PEC of ALG8 at $n^-/n^+ = 1$, which verifies a Gaussian chain (random coil) behaviour (Takeshita et al., 2019). The Kratky plot behaviour of ideal Gaussian chains represented by the dashed lines in **Figure 3.8b**, and with the experimental data for CS + ALG8 PEC at $n^-/n^+ = 1$, the line is perfectly aligned. On the contrary, the decrease in versus q at q<0.5 nm^{-1} was shown in the complexes of ALG21 at both ratios ($n^-/n^+ = 1$ and $n^-/n^+ = 0.2$). This deviation from Gaussian chain behaviour indicates more collapsed chain configurations and possibly the formation of larger clusters in PEC samples. The deviation is more pronounced for CS + ALG8 PEC when $n^-/n^+ = 1$ (see blue curve in **Figure 3.8b**). At higher q values (q>0.5 nm-1), it is noteworthy that all SAXS curves behave similarly, suggesting that when focusing into smaller scales (length scales below 12 nm), chains appear swollen.

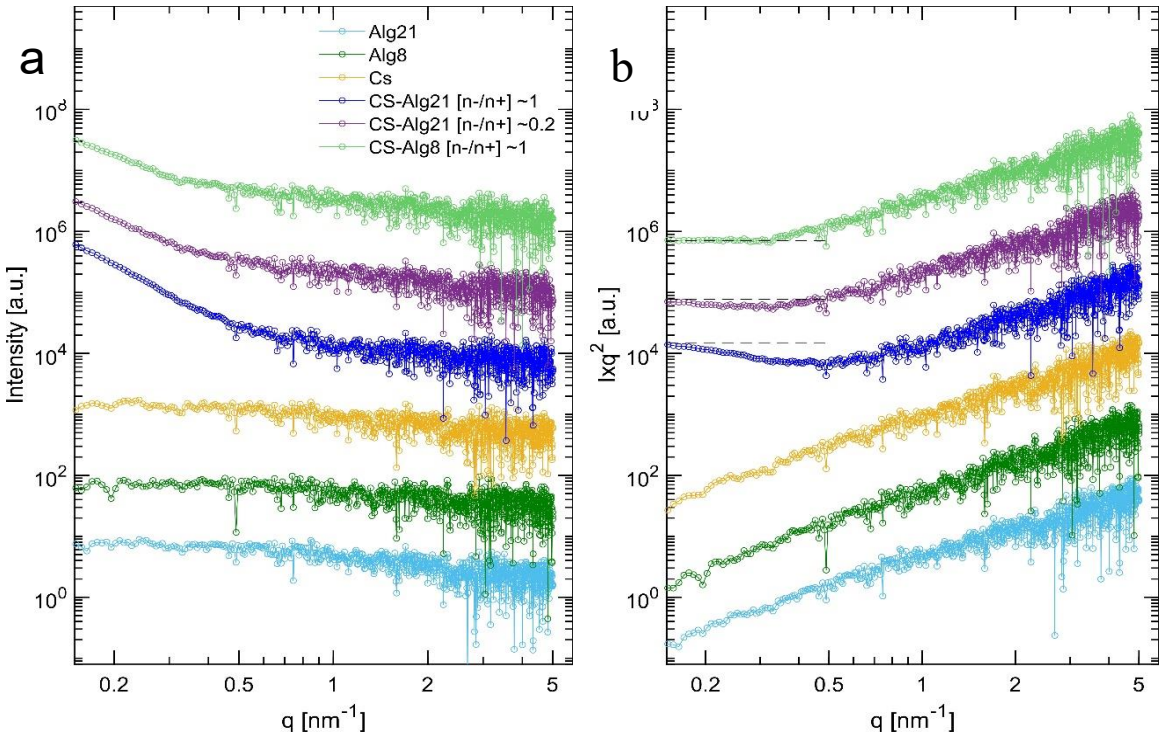


Figure. 3.8. Small-angle X-ray scattering (SAXS) patterns (a) and corresponding Kratky plots (b) are presented for 2 mg mL^{-1} CS, ALG, and their PECs at two different n^-/n^+ molar charge ratios. The Kratky plots demonstrate swollen chain behaviour for pure polyelectrolytes, whereas Gaussian and collapsed chains/clustered structures are observed for PECs of ALG8 and ALG21, respectively. The scattering profiles were acquired at 85 mM NaCl and 25 °C. The horizontal dashed lines in Kratky plots provide a guide for the Gaussian (random coil) chain behaviour at low q values.

3.3.3 Physical properties of CS + ALG PECs loaded with BAPs

Two n^-/n^+ = 0.5 and 10 for ALG21 were chosen to test the effects of the addition of BAPs to the systems and given the sensitivity (particularly around n^-/n^+ = 1) of the properties of the unloaded PECs to n^-/n^+. Additionally, these two n^-/n^+ values are projected to create complexes of highly different sizes (presuming similar characteristics as in **Figure 3.5**), i.e., sub-micron and > 1 μm, that could have different release profiles and applications, whilst their aggregation should be prevented by the higher ζ values. As described in the Methods (*section 3.2*), LKPNM and LKP from the ultrafiltration fractions of fish BAPs were encapsulated into PECs, and the BAPs were added to the CS solution before mixing with ALG. Thus, two net positively charged molecules are contained in the starting solution: the BAPs and CS. The results are summarised in **Table 3.1**.

Table 3.1. Comparison of measured properties of CS + ALG21 PECs with and without BAP loading. n^-/n^+ = molar charge ratio; R_h hydrodynamic radius; ζ = zeta potential; PDI = polydispersity index; EE = encapsulation efficiency.

PEC systems	n^-/n^+	R_h (nm)	ζ (mV)	PDI	PEC yield (%)	EE (%)
No BAPs	0.5	402 ± 13^{a}	$+36.0 \pm 2.1^{a}$	0.25 ± 0.02^{a}	8.6 ± 0.7^{bc}	-
with BAPs	0.5	322 ± 2^{a}	$+33.9 \pm 1.3^{b}$	0.19 ± 0.01^{a}	13.5 ± 1.1^{ab}	85 ± 0.1^{a}
No BAPs	10	843 ± 88^{b}	-23.0 ± 1.3^{c}	0.49 ± 0.06^{b}	3.0 ± 1.4^{c}	-
with BAPs	10	436 ± 54^{a}	-14.6 ± 2.3^{d}	0.42 ± 0.04^{b}	6.9 ± 5.8^{bc}	80.6 ± 0.5^{b}

Letters in the same column with different notations indicate differences with significance >95% ($p < 0.05$).

A significant reduction in R_h and PDI was observed at both n^-/n^+ = 0.5 and 10, after loading with the BAPs, suggesting that the BAP contributed to the cross-linking and led to more compact structures. When the PECs were formed in the presence of the BAPs, the yield of PECs also increased significantly, strengthening the supposition that the BAPs participated in PEC establishment. Concurrently, it is noticeable that the value of ζ attained was smaller in magnitude: less +ve for n^-/n^+ = 0.5 (excess CS) and less –ve for n^-/n^+ =10 (excess ALG) when the BAP was included in the complexes. This might suggest that the BAP has a greater role in the cross-linking, especially at the surface of the PEC, and the CS dominates over any structural effect due to the BAP in combination with excess CS. Similar growth in the yields of PEC

assembly (> ~50%) was noticed in CS + ALG NPs containing low M_w ALG when loading them with insulin (Goycoolea et al., 2009).

The molar charge ratio of –ve species (ALG21) to +ve charged species when the moles of charge carried by the encapsulated BAPs is included is shown in **Figure 3.9**, compared to when the charge from the BAPs is disregarded. Although per BAP molecule there is only one net +ve charge, compared to CS that has 601 per molecule, as n^-/n^+ approaches 10 it is seen that the contribution of the BAPs to n^-/n^+ does become significant, i.e, in the CS- depleted but ALG21-rich complexes, because noticeably higher molar concentration of the BAPs. This further supports the hypothesis that, in the latter system, the BAPs might play a significant role to the integrity and structure of the created PECs.

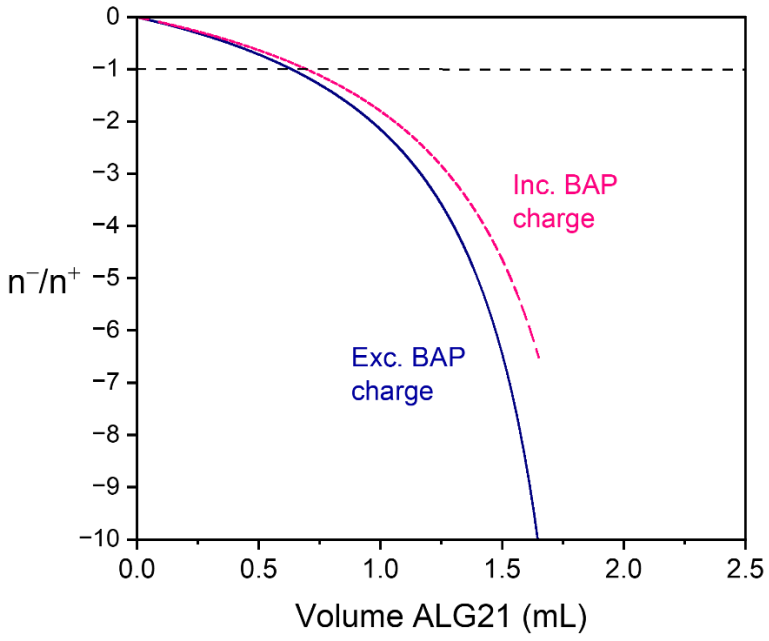


Figure. 3.9. The signed molar charge ratio $-(n^-/n^+)$ for the CS + ALG21 PECs calculated excluding (back full curve) and including (red dashed curve) the contribution of charges from encapsulated BAPs as a function of the volume of 2 mg mL^{-1} stock ALG21 solution added into the system. The horizontal dashed line indicates $n^-/n^+ = 1$, i.e., overall charge compensation of the systems.

For both systems, the encapsulation efficiency (EE) was similar and high, ≈ 85 % for $n^-/n^+ = 0.5$ and 80.6 % for $n^-/n^+ = 10$, hence a little higher for the more compact PECs (within experimental error). EE (of IPP and LKP) between 22.6% - 43.9% and 40.9% - 65.1%, respectively (Danish et al., 2017). Bicak et al., (2021) reported that the EE of tripeptide YKT

into CS 'macroparticles' (MP) was approximately 35%. Moreover, the EE of around 86% was obtained when using guar-gum MPs coated with CS to encapsulate the decapeptide YLGYLEQLLR (Batista et al., 2021). Thus, the CS + ALG system reported in this work seems promising, in term of providing equivalent or higher EE than these other systems.

The influence of re-suspension of CS + ALG21 PECs, both loaded and unloaded, was also investigated for their R_h, ζ-potential, and PDI to monitor for PEC stability to dilution and re-dispersion. The findings are presented in **Figure 3.10**, explained as the ratio of the values for the freshly prepared to the resuspended. The ratios were close to 1 for $n^-/n^+ = 0.5$ (excess CS), indicating no significant differences. In contrast, the ratio was significantly > 1 for $n^-/n^+ = 10$ (excess ALG), especially for the R_h and ζ values, suggesting that the PECs with excess ALG were more unstable, taking into consideration that these PECs were considerably larger and therefore probably less compact from the beginning. This was further confirmed by comparing the η of the supernatants after centrifugation. A greater proportion of the polymer was incorporated into the PECs when BAPs were present, but especially when CS was in excess, as indicated by the fact that η was lower for the loaded PEC, as seen in **Figure 3.11**.

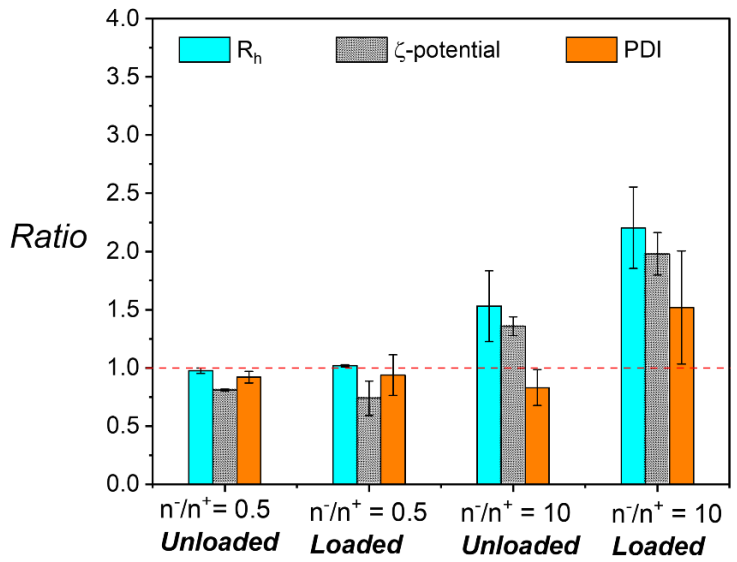


Figure. 3.10. Ratio between freshly prepared and re-suspended values of R_h, ζ, and PDI of both loaded and unloaded CS + ALG21 PECs, at $n^-/n^+ = 0.5$ and 10.

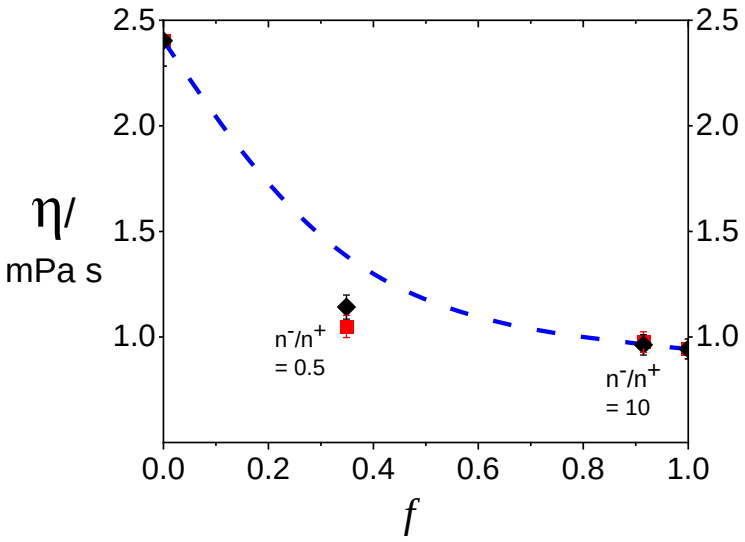


Figure. 3.11. Viscosity (η) at 25 °C of the supernatants of centrifuged CS + ALG21 mixtures as a function of the original mass fraction of ALG21 (*f*) in the system. The dashed curve represents the data for the unloaded system, taken from **Figure. 7b.** The red squares indicate the η values for the PECs loaded with BAPs, the black diamonds correspond to unloaded (but re-suspended) PECs.

3.3.4 Microscopic evidence of morphology of PECs loaded with BAPs

Transmission electron microscopy (TEM) was used to examine the morphology of the smaller PECs with the highest BAP loading (i.e., excess CS, at $n^-/n^+ = 0.5$ with ALG21) – see **Figure. 3.12**. The TEM images showed particles ranging from less than 20 nm to over 500 nm, with some larger particles exceeding 1 µm, whereas the size measured via DLS was approximately 322 nm. Within these structures smaller objects (< 20 nm) were consistently observed, but some of these structures appeared to consist of aggregates, in some regions which also seemed to form larger clusters. Those smaller objects were presumed to be aggregates of the encapsulated BAP. As shown in previous studies focused on polysaccharide and protein systems (Glantz et al., 2010, Nilsson, 2013, Hakansson et al., 2012, O'Connell et al., 2023a), this is in overall agreement with the low R_g:R_h ratios discussed above (**Figure. 3.5**.), and future fractionation studies using asymmetric flow field-flow fractionation can shed more light on the presence of aggregates. Spherical-like PEC structures are formed as suggested in most other microscopic observations of PEC-type structures with encapsulated peptides (Jiang et al., 2021, Chen et al., 2017, Huang et al., 2017). Huang et al. (2017) examined the

pentapeptide VLPVP encapsulated into sodium ALG-O-carboxymethyl CS microspheres and found that the surface of the microspheres manifested roughness after BAPs loading. However, it is unclear if the roughness was because of BAP aggregates after loading, as noticed in **Figure. 3.12**. Because the samples are dehydrated, which can induce dense aggregation of the particles, very inconclusive SEM measurements were obtained on the samples (results are not shown).

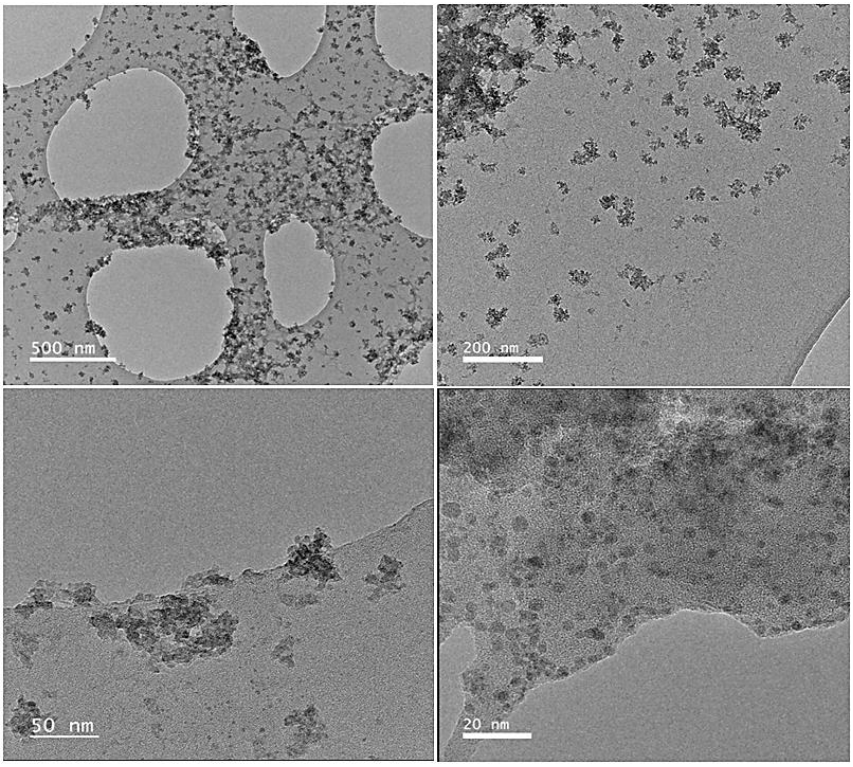


Figure. 3.12. TEM analysis of PECs for CS + ALG21 at n^-/n^+ = 0.5 after loading with fish BAPs.

3.3.5 Studies of BAP release from PECs due to pH change

In the final experiment chapter, this thesis intend to test the stability and release characteristics of the above loaded PECs to digestive conditions. This, of course, involves the addition of enzymes, but also various salts and pH changes from low (gastric) pH to neutral (intestinal) pH conditions. Since electrostatic interactions is the basis of PEC formation, first this thesis tested the effect of pH and salt, i.e., without including digestive enzymes. Although digestive enzymes will not hydrolyse the CS or ALG, they might impact the BAPs, which also seem to influence the PEC structure when encapsulated at this level, as already described. At the same time, it seemed important to try and separate the effects of enzymes, salts, and pH

in the first instance, as it is well known that pH and salt will affect the electrostatic interactions thought to be holding the PECs together.

In separate experiments, the CS + ALG21 PECs for $n^-/n^+ = 0.5$ (excess CS) and $n^-/n^+ = 10$ (excess ALG21) were incubated for 3 h at 37 °C at pH 3 (representative of gastric pH) and pH 6.8 (representative of intestinal pH). These two pH values and incubation times were applied to mimic 'typical' physical gastric and intestinal conditions during human digestion of foods (Egger et al., 2016, Zhang et al., 2022). After the suspensions were centrifuged, the amounts of BAPs released in the supernatants were quantified via RP-HPLC according to the **Method** (*section 3.2*). The BAP release was less than 8% at pH 3 and less than 18% at pH 6.8, as depicted in the results (**Figure. 3.13**). The charge states of the CS, ALG and BAPs are probably causing the higher release at pH 6.8. Both the CS and the BAP carry significantly higher positive charge at pH 3 than at pH 6.8 (see **Figure. 3.4**) bringing to stronger interactions with the ALG, that is in the PECs anticipated to hold the oppositely charged polymers more closely together and diminish any diffusive loss of BAP by perhaps with reduced pore size. Concurrently, the BAP itself will be more strongly bound to the ALG chains within the PEC structure.

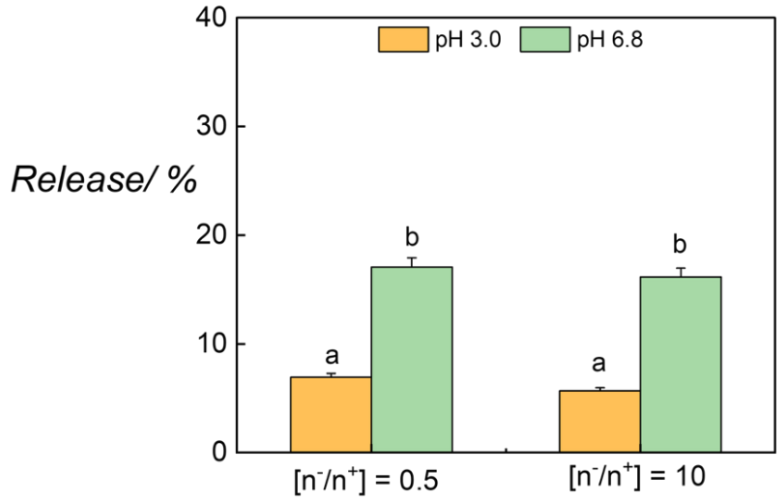


Figure. 3. 13. The % release of BAPs from CS + ALG21 PECs for $n^-/n^+ = 0.5$ (excess CS) and $n^-/n^+ = 10$ (excess ALG21) after 3 h at 37 °C at pH 3.0 and pH 6.8. Bars with different letters are statistically different from one another, at $p < 0.05$.

As observed in this chapter, the release of short-chain BAPs during simulated gastrointestinal digestion is an important observation across various carrier systems. Compared to previous studies, release kinetics tend to be mitigated when using composite or hybrid wall materials as outlined in **Table 2.2** (**Chapter 2**). The interactions of the BAPs with the polymers have been considered, but the n^-/n^+ consideration was absent in these other studies.

3. 4. Conclusions

The robust structural integrity of CS+ALG polymeric electrolyte complexes (PECs), particularly those formed at a molar charge ratio (n^-/n^+) < 1, has been shown by this study. The stability is elevated in PECs with both excess CS and excess ALG in NaCl solution. More compact and stable PECs are produced for higher M_w ALG molecules (21 kDa versus 8 kDa). The successful incorporation of the low M_w bioactive peptides (BAPs), as well as their integration into and additional stabilisation of the PEC structure, was indicated by a reduction in their hydrodynamic radius (R_h), with minimal impact on their ζ-potential and polydispersity. Strong association between the oppositely charged BAP and ALG molecules is possible because the encapsulation efficiency was high, and release was low in gastric and intestinal pH conditions. Thus, a promising encapsulation technique for future industrial development, offering a sustainable approach for incorporating BAPs into gastrointestinal delivery vehicles, is possible by the simple one-step process of mixing CS, ALG and BAPs at an appropriate charge ratio (n^-/n^+).

3.5 References

Anderson, W., Kozak, D., Coleman, V. A., Jamting, A. K., & Trau, M. 2013. A comparative study of submicron particle sizing platforms: accuracy, precision and resolution analysis of polydisperse particle size distributions. *J Colloid Interface Sci, 405*, 322-330.

Apostolidis, E., Stergiou, A., Kioupis, D., Sadeghpour, A., Paximada, P., Kakali, G. & Mandala, I. 2023. Production of nanoparticles from resistant starch via a simple three-step physical treatment. *Food Hydrocolloids,* 137**,** 108412.

Batista, P., Castro, P. M., Madureira, A. R., Sarmento, B. & Pintado, M. 2021. Preparation, characterization and evaluation of guar films impregnated with relaxing peptide loaded into chitosan microparticles. *Appl. Sci. (Switzerland),* 11**,** 1-13.

Becheran-Maron, L., Peniche, C. & Arguelles-Monal, W. 2004. Study of the interpolyelectrolyte reaction between chitosan and alginate: influence of alginate composition and chitosan molecular weight. *Int J Biol Macromol,* 34**,** 127-33.

Belitz, H. D. & Grosch, W. 1999. *Food Chemistry,* Berlin, Germany, Springer-Verlag.

Bicak, B., Budama-Kilinc, Y., Kecel-Gunduz, S., Zorlud, T. & Akman, G. 2021. Peptide based nano-drug candidate for cancer treatment: preparation, characterization, in vitro and in silico evaluation. *J. Mol. Struct.,* 1240**,** 130573.

Chen, S. X., Guo, F., Deng, T. T., Zhu, S. Q., Liu, W. Y., Zhong, H. J., Yu, H., Luo, R. & Deng, Z. Y. 2017. Eudragit S100-coated chitosan nanoparticles co-loading Tat for enhanced oral colon absorption of insulin. *AAPS Pharmscitech.,* 18**,** 1277-1287.

Curtis, J. M., Dennis, D., Waddell, D. S., Macgillivray, T. & Ewart, H. S. 2002. Determination of angiotensin-converting enzyme inhibitory peptide Leu-Lys-Pro-Asn-Met (LKPNM) in bonito muscle hydrolysates by LC−MS/MS. *Journal of Agricultural and Food Chemistry,* 50**,** 3919−3925.

Danish, M. K., Vozza, G., Byrne, H. J., Frias, J. M. & Ryan, S. M. 2017. Comparative study of the structural and physicochemical properties of two food derived antihypertensive tri-peptides, Isoleucine-Proline-Proline and Leucine-Lysine-Proline encapsulated into a chitosan based nanoparticle system. *Innov. Food Sci. Emerg.,* 44**,** 139-148.

Doroszkowski, A. 1999. The physical chemistry of dispersion. *In:* Lambourne, R. & Strivens, T. A. (eds.) *Paint and Surface Coatings: Theory and Practice.* Second Edition ed. Cambridge, England: Woodhead Publishing Limited.

Egger, L., Ménard, O., Delgado-Andrade, C., Alvito, P., Assunção, R., Balance, S., Barberá, R., Brodkorb, A., Cattenoz, T., Clemente, A., Comi, I., Dupont, D., Garcia-Llatas, G., Lagarda, M. J., Le Feunteun, S., Janssenduijghuijsen, L., Karakaya, S., Lesmes, U., Mackie, A. R., Martins, C., Meynier, A., Miralles, B., Murray, B. S., Pihlanto, A., Picariello, G., Santos, C. N., Simsek, S., Recio, I., Rigby, N., Rioux, L.-E., Stoffers, H., Tavares, A., Tavares, L., Turgeon, S., Ulleberg, E. K., Vegarud, G. E., Vergères, G. & Portmann, R. 2016. The harmonized INFOGEST in vitro digestion method: From knowledge to action. *Food Res. Int.,* 88**,** 217-225.

Fuentea, B. D. L., Tornosa, A., Príncepa, A., Lorenzob, J. M., Pateirob, M., Berradaa, H., Barbaa, F. J., Ruiza, M.-J. & Martí-Quijal, F. J. 2020. Scaling-up processes: Patents and commercial applications. *In:* Lorenzo, J. M. & Barba, F. J. (eds.) *Aquaculture and By-Products: Challenges and Opportunities in the Use of Alternative Protein Sources and Bioactive Compounds.* Academic Press.

Fuenzalida, J. P., Nareddy, P. K., Moreno-Villoslada, I., Moerschbacher, B. M., Swamy, M. J., Pan, S., Ostermeier, M. & Goycoolea, F. M. 2016. On the role of alginate structure in complexing with lysozyme and application for enzyme delivery. *Food Hydrocolloids,* 53**,** 239-248.

Fujita, H., Yokoyama, K. & Yoshikawa, M. 2000. Classification and antihypertensive activity of angiotensin I-converting enzyme inhibitory peptides derived from food proteins. *J. Food Sci. ,* 65**,** 564-569.

Fujita, H. & Yoshikawa, M. 1999. LKPNM: a prodrug-type ACE-inhibitory peptide derived from fish protein. *Immunopharmacology,* 44**,** 123–127.

Gao, R., Yu, Q., Shen, Y., Chu, Q., Chen, G., Fen, S., Yang, M., Yuan, L., Mcclements, D. J. & Sun, Q. 2021. Production, bioactive properties, and potential applications of fish protein hydrolysates: Developments and challenges. *Trends in Food Science & Technology,* 110**,** 687-699.

George, M. & Abraham, T. E. 2006. Polyionic hydrocolloids for the intestinal delivery of protein drugs: alginate and chitosan--a review. *J Control Release,* 114**,** 1-14.

Glantz, M., Hakansson, A., Lindmark Mansson, H., Paulsson, M. & Nilsson, L. 2010. Revealing the size, conformation, and shape of casein micelles and aggregates with asymmetrical flow field-flow fractionation and multiangle light scattering. *Langmuir,* 26**,** 12585-91.

Gombotz, W. R. & Wee, S. F. 1998. Protein release from alginate matrices. *Advanced Drug Delivery Reviews,* 31**,** 267–285.

Goycoolea-Valencia, F. M., Morris, E. R. & Gidley, M. J. 1995. Screening for synergistic interactions in dilute polysaccharide solutions. *Carbohydrate Polymers,* 28**,** 351-358.

Goycoolea, F. M., Lollo, G., Remunan-Lopez, C., Quaglia, F. & Alonso, M. J. 2009. Chitosan-alginate blended nanoparticles as carriers for the transmucosal delivery of macromolecules *Biomacromolecules,* 10**,** 1736–1743.

Guan, Z., Tjoeng, F. S., Li, W., Mandrell, K., Liu, M. & Chen, X. 2001. *Anti-hypertensive Peptides*. United States patent application PCT/US01/07479.

Hakansson, A., Ulmius, M. & Nilsson, L. 2012. Asymmetrical flow field-flow fractionation enables the characterization of molecular and supramolecular properties of cereal beta-glucan dispersions. *Carbohydr Polym,* 87**,** 518-523.

Halim, N. R. A., Yusof, H. M. & Sarbon, N. M. 2016. Functional and bioactive properties of fish protein hydolysates and peptides: A comprehensive review. *Trends in Food Science & Technology,* 51**,** 24-33.

Hayes, M. & Tiwari, B. K. 2015. Bioactive carbohydrates and peptides in foods: an overview of sources, downstream processing steps and associated bioactivities. *International Journal of Molecular Sciences,* 16**,** 22485-22508.

Hirai, A., Odani, H. & Nakajima, A. 1991. Determination of degree of deacetylation of chitosan by ^{1}H NMR spectroscopy. *Polymer Bulletin***,** 87-94.

Huang, G.-Q., Xiao, J.-X., Hao, L.-Q. & Yang, J. 2017. Microencapsulation of an angiotensin I-converting enzyme inhibitory peptide VLPVP by membrane emulsification. *Food Bioprocess Tech.,* 10**,** 2005-2012.

Jiang, X. X., Pan, D. D., Tao, M. X., Zhang, T., Zeng, X. Q., Wu, Z. & Guo, Y. X. 2021. New nanocarrier system for liposomes coated with Lactobacillus acidophilus S-layer protein to improve Leu-Gln-Pro-Glu absorption through the intestinal epithelium. *J. Agr. Food Chem.,* 69**,** 7593-7602.

Kumar, P., Hajdu, C., Toth, A. & Horvath, D. 2021. Flow-driven surface instabilities of tubular chitosan hydrogel. *Chemphyschem,* 22**,** 488-492.

Le Gouic, A. V., Harnedy, P. A. & Fitzgerald, R. J. 2019. Bioactive peptides from fish protein by-products. *Bioactive Molecules in Food.*

Luo, Y. & Wang, Q. 2014. Recent development of chitosan-based polyelectrolyte complexes with natural polysaccharides for drug delivery. *Int J Biol Macromol,* 64**,** 353-67.

Menchicchi, B., Fuenzalida, J. P., Bobbili, K. B., Hensel, A., Swamy, M. J. & Goycoolea, F. M. 2014. Structure of chitosan determines its interactions with mucin. *Biomacromolecules,* 15**,** 3550-8.

Menchicchi, B., Fuenzalida, J. P., Hensel, A., Swamy, M. J., David, L., Rochas, C. & Goycoolea, F. M. 2015. Biophysical analysis of the molecular interactions between polysaccharides and mucin. *Biomacromolecules,* 16**,** 924-35.

Milkova, V. & Goycoolea, F. M. 2020. Encapsulation of caffeine in polysaccharide oil-core nanocapsules. *Colloid and Polymer Science,* 298**,** 1035-1041.

Nilsson, L. 2013. Separation and characterization of food macromolecules using field-flow fractionation: A review. *Food Hydrocolloids,* 30**,** 1-11.

Nirmal, N. P., Santivarangkna, C., Rajput, M. S., Benjakul, S. & Maqsood, S. 2022. Valorization of fish byproducts: Sources to end-product applications of bioactive protein hydrolysate. *Compr Rev Food Sci Food Saf,* 21**,** 1803-1842.

O'connell, A., Gonzalez-Espinosa, Y., Goycoolea, F. M., Schuetz, P. & Mattsson, J. 2023a. Characterisation of locust bean gum with asymmetric flow field-flow fractionation (AF4) and light scattering. *Carbohydr Polym,* 322**,** 121286.

O'connell, A., Goycoolea, F. M., Gulotta, A., Holmqvist, P., Schuetz, P. & Mattsson, J. 2023b. The structure and dynamics of locust bean gum in aqueous solution. *Food Hydrocolloid,* 138**,** 108446.

Potaś, J., Szymańska, E. & Winnicka, K. 2020. Challenges in developing of chitosan – Based polyelectrolyte complexes as a platform for mucosal and skin drug delivery. *European Polymer Journal,* 140**,** 110020.

Pravinata, L., Akhtar, M., Bentley, P. J., Mahatnirunkul, T. & Murray, B. S. 2016. Preparation of alginate microgels in a simple one step process via the Leeds Jet Homogenizer. *Food Hydrocolloid,* 61**,** 77-84.

Rinaudo, M., Milas, M. & Le Dung, P. 1993. Characterization of chitosan. Influence of ionic strength and degree of acetylation on chain expansion. *International Journal of Biological Macromolecules,* 15**,** 281–285.

Rinaudo, M., Pavlov, G. & Desbrie`Res, J. 1999a. Influence of acetic acid concentration on the solubilization of chitosan. *Polymer,* 40**,** 7029–7032.

Rinaudo, M., Pavlov, G. & Desbrières, J. 1999b. Solubilization of chitosan in strong acid medium. *Int. J. Polym. Anal. Charac.,* 5**,** 267-276.

Sæther, H. V., Holme, H. K., Maurstad, G., Smidsrød, O. & Stokke, B. T. 2008. Polyelectrolyte complex formation using alginate and chitosan. *Carbohydrate Polymers,* 74**,** 813-821.

Schatz, C., Domard, A., Viton, C., Pichot, C. & Delair, T. 2004. Versatile and efficient formation of colloids of biopolymer-based polyelectrolyte complexes. *Biomacromolecules,* 5**,** 1882–1892.

Schmidt, M., Nerger, D. & Burchard, W. 1979. Quasi-elastic light scattering from branched polymers: 1. Polyvinylacetate and polyvinylacetate—microgels prepared by emulsion polymerization. *Polymer,* 20**,** 582-588.

Sonaje, K., Chuang, E. Y., Lin, K. J., Yen, T. C., Su, F. Y., Tseng, M. T. & Sung, H. W. 2012. Opening of epithelial tight junctions and enhancement of paracellular permeation by chitosan: microscopic, ultrastructural, and computed-tomographic observations. *Mol Pharm,* 9**,** 1271-9.

Sreekumar, S., Wattjes, J., Niehues, A., Mengoni, T., Mendes, A. C., Morris, E. R., Goycoolea, F. M. & Moerschbacher, B. M. 2022. Biotechnologically produced chitosans with nonrandom acetylation patterns differ from conventional chitosans in properties and activities. *Nat. Commun.,* 13**,** 7125.

Stetefeld, J., Mckenna, S. A. & Patel, T. R. 2016. Dynamic light scattering: a practical guide and applications in biomedical sciences. *Biophys Rev,* 8**,** 409-427.

Stewart, W. W. & Swaisgood, H. E. 1993. Characterization of calcium alginate pore diameter by size-exclusion chromatography using protein standards. *Enzyme and Microbial Technology,* 15**,** 922-927.

Takeshita, S., Sadeghpour, A., Malfait, W. J., Konishi, A., Otake, K. & Yoda, S. 2019. Formation of Nanofibrous Structure in Biopolymer Aerogel during Supercritical CO(2) Processing: The Case of Chitosan Aerogel. *Biomacromolecules,* 20**,** 2051-2057.

Tanaka, H., Matsumura, M. & Veliky, I. A. 1984. Diffusion characteristics of substrates in Ca-alginate gel beads. *Biotechnol Bioeng,* 26**,** 53-8.

Vold, I. M. N., Kristiansen, K. A. & Bjørn, E. C. 2006. A study of the chain stiffness and extension of alginates, in vitro epimerized alginates, and periodate-oxidized alginates using size-exclusion chromatography combined with light scattering and viscosity detectors. *Biomacromolecules,* 7**,** 2136–2146.

Wattjes, J., Sreekumar, S., Richter, C., Cord-Landwehr, S., Singh, R., El Gueddari, N. E. & Moerschbacher, B. M. 2020. Patterns matter part 1: Chitosan polymers with non-random patterns of acetylation. *Reactive and Functional Polymers,* 151.

Xiao, B., Xu, Z., Viennois, E., Zhang, Y., Zhang, Z., Zhang, M., Han, M. K., Kang, Y. & Merlin, D. 2017. Orally targeted delivery of tripeptide KPV via hyaluronic acid-functionalized nanoparticles efficiently alleviates ulcerative colitis. *Mol. Ther.,* 25**,** 1628-1640.

Yilmaz, T., Maldonado, L., Turasan, H. & Kokini, J. 2019. Thermodynamic mechanism of particulation of sodium alginate and chitosan polyelectrolyte complexes as a function of charge ratio and order of addition. *Journal of Food Engineering,* 254**,** 42-50.

Yokoyama, K., Chiba, H. & Yoshikawa, M. 1992. Peptide inhibitors for angiotensin I-converting enzyme from thermolysin digest of dried bonito. *Biosci Biotechnol Biochem,* 56**,** 1541-5.

Zamora-Sillero, J., Gharsallaoui, A. & Prentice, C. 2018. Peptides from fish by-product protein hydrolysates and its functional properties: an overview. *Mar Biotechnol (NY),* 20**,** 118-130.

Zhang, S., Murray, B. S., Holmes, M., Ettelaie, R. & Sarkar, A. 2022. Gastrointestinal fate and fatty acid release of pickering emulsions stabilized by mixtures of plant protein microgels + cellulose particles: an in vitro static digestion study. *Food Biophys.,* 18**,** 120-132.

Zhang, S., Murray, B. S., Suriyachay, N., Holmes, M., Ettelaie, R. & Sarkar, A. 2021. Synergistic interactions of plant protein microgels and cellulose nanocrystals at the interface and their inhibition of the gastric digestion of pickering emulsions. *Langmuir,* 37**,** 827-840.

CHAPTER 4
CHITOSAN-ALGINATE PECs LOADED WITH FISH BAPs: AN IN VITRO DIGESTION STUDY

4.1 Introduction

Oral administration of peptides or bioactive peptides (BAPs) via gastrointestinal route has shown low bioavailability due to chemical, enzymatic, and physical barriers (Amigo and Hernandez-Ledesma, 2020, Sun et al., 2020, Bourganis et al., 2017). Some approaches have been studied to overcome this limitation and improve the bioavailability of peptides, including using protease inhibitors (Wagner et al., 2018, Bernkop-Schnurch, 1998), chemical modification of peptides (Buckley et al., 2016), use of permeation enhancers (Kim et al., 2022), or using delivery vehicles (Aguilar-Toala et al., 2022, Atma et al., 2024). BAP encapsulation with a colloidal vehicle is one of technique to protect BAPs from early denaturation without changing their native structures and conformation. Several colloidal carriers have been applied for peptides whether polymeric-based or lipid based (Perry and McClements, 2020, McClements, 2018a). Currently, the development of vehicles based on natural biodegradable colloidal polymers is an area of active research, despite the advancements in synthetic alternatives (Li et al., 2023). For example, a polyelectrolyte complexes (PEC). Encapsulation of peptide within PECs is a technique that offers low cost and facile processing of encapsulation, without additional treatment, heat processing, while also avoiding any organic solvent that could likely diminish the bioactivity of BAPs. **Chapter 3** demonstrated the feasibility of encapsulation of fish BAPs into alginate (ALG) and chitosan (CS) PECs which demonstrated relatively high encapsulation efficiency. The present chapter investigates the *in vitro* bioactivity and digestibility of those PECs.

PECs prepared using CS+ALG are the most popular and extensively investigated nanocarriers (Park et al., 2019b, Nikolova et al., 2021) that are also used for peptides encapsulation and delivery (Luo and Wang, 2014, Zhao et al., 2019a). ALG and CS are also well known for their effect on decreasing the digestion rate of a range of nutrients in the gastrointestinal tract (Brownlee, 2011). Previous studies mentioned that encapsulation of bioactive substances using ALG+CS PECs reduces proteases penetration into the core of PEC

systems, leading to reduced digestibility of polypeptides (Reis et al., 2008, Zhang et al., 2011). The combination CS + ALG has examined for encapsulation fish BAPs (**Chapter 3**), haemoglobin (Ribeiro et al., 2005), insulin (Sarmento et al., 2007b, Reis et al., 2008, Collado-González et al., 2020), peanut's peptide (Han et al., 2022), stone fish BAPs (Auwal et al., 2024). Based on these studies, the stability and release of encapsulated BAPs during digestion are mostly dependent on the conformational stability of complexes in the surrounding environment or solution.

Some studies found that encapsulating bioactive compounds inside ALG+CS PECs was lowering the initial release of the payload in the gastric condition but releasing it in intestinal pH (Sarmento et al., 2007b, Reis et al., 2008, Yoksan and Towongphaichayonte, 2024). According to Wasupalli & Verma (2018), CS+ALG PEC was stable in the pH range of 4.5 to 6.5 due to the formation of a fibrous structure (Wasupalli and Verma, 2018). An increasing pH to the intestinal condition (i.e ~ 6.5 – 7.0) might affect the stability of CS+ALG PECs after loading, which could then lead to substantial release of the loaded BAPs. Our initial study found that the antihypertensive fish BAPs (isoelectric point = 9.6 to 10.5) loaded into ALG+CS PECs were released less than 8% at gastric pH 3, and less than 18% at intestinal pH 6.8 after 3 hours of incubation (Atma et al., 2025). For the latter, we predicted this might be the consequence of CS's deprotonation at pH 6.8, hence allowing much BAPs release into the medium (Potaś et al., 2020). Yet, as we mentioned in the beginning, pH is not the only aspect affecting PEC's or any encapsulant's stability during digestion (Sarkar et al., 2017, Torres et al., 2019). During its physiological transition, the particles could release the encapsulated active molecules in several ways. Apart from pH, the environmental ionic strength and enzymatic composition should be considered before examining the release caused by very complicated human gastrointestinal tract.

To understand the function of PECs in gastrointestinal condition, the stability of loaded PECs and the release of fish BAPs should be tested in simulated gastric and intestinal fluids. There are salts naturally existing in gastric and intestinal fluids with stronger ionic strength than ionisable peptide or BAPs (Minekus et al., 2014, Lehninger et al., 2004), so that might be able to replace BAPs position during ionic interaction within PECs. Also, pepsin, trypsin, and chymotrypsin that predominantly found in human gastrointestinal among other enzymes. A study conducted by Castel-Molieres et al., (2017) corroborates that the n^-/n^+ of ALG+CS

affects the swelling ability of PECs in a solution, causing peptide release (Castel-Molieres et al., 2017). Nevertheless, there is no report in the literature concerning the stability of BAPs loaded into PECs during gastric or intestinal digestion.

This Chapter investigated the stability of two systems ALG+CS PECs loaded with fish BAPs, with excess ALG ($n^-/n^+ > 1$) and excess CS ($n^-/n^+ <1$), during storage and during static gastric and intestinal digestions. The in vitro gastrointestinal fluids were prepared to mimic human gastric and intestinal fluid compositions without enzymes and with enzymes. The International Network on Food Digestion (INFOGEST) protocol as one of the most appropriate methods to simulate gastric and intestinal fluids was used to prepare the mimicking fluids (Egger et al., 2016, Zhang et al., 2022). Then, the biophysical stability of the systems by measuring their sizes (R_h), ζ-potential, and polydispersity were performed. Total fish BAPs and the bioactivity after release were also quantified. Moreover, the interaction and stability of PECs under controlled pH conditions as well as stability of BAP alone against proteases were tested.

4.2 Materials and Methods

4.2.1 Materials

Sodium alginate (ALG), M_w 21 kDa, with a mannuronic (M) to guluronic (G) acid (M/G) ratio = 1.42, chitosan (CS) with a M_w of 111 kDa, degree of acetylation (DA)=10%, and bonito fish protein extract (PeptACE®) were obtained from the producer/suppliers as detailed in **Chapter 3**. Acetonitrile (ACN) HPLC grade (Oxford, UK) and trifluoroacetic acid (TFA) (HPLC grade 99.5%) from Alfa Aesar (Massachusetts, United States). Sodium azide (NaN_3) (Sigma-Aldrich, Missouri, United States) was used as preservative, *Hippuryl-His-Leu* (HHL) hydrate (purity ≥ 98%, HPLC), angiotensin converting enzyme (ACE) from rabbit lung (≥ 2.0 units mg^{-1}), and boric acid were procured from Sigma (St. Louis, MO, United States), and captopril (purity 98,91%) was purchased from ApexBio (Houston, Texas, United States). Sodium chloride (NaCl) and glycerol (analytical grade) was obtained from Fisher Scientific (Loughborough, UK). Hydrochloric acid and sodium hydroxide were obtained from Sigma-Aldrich (Missouri, United States). All reagents and chemicals for preparing gastric and intestinal fluids were used and purchased exactly following International Network on Food Digestion (INFOGEST) protocol with individual enzymes (Brodkorb, et al. 2019), they were covering KCl (Merck, Germany), KH_2PO_4 (J.T Baker, US), $NaHCO_3$ (Merck, Germany), NaCl

(Merck, Germany), $MgCl_2(H_2O)_6$ (Merck, Germany), $(NH_4)_2CO_3$ (Sigma-Aldrich, US), $CaCl_2(H_2O)_2$ (Sigma-Aldrich, US), porcine pepsin EC 3.4.23.1 (Sigma-Aldrich, US), porcine trypsin EC 3.4.21.4 (Sigma-Aldrich, US), bovine chymotrypsin EC 3.4.21.1 (Sigma-Aldrich, US), pefabloc SC (Sigma-Aldrich, US), and pepstatin A (Sigma-Aldrich, US). All aqueous solutions were prepared using ultrapure Milli-Q water from BioPak with resistivity 18.2 MΩ at 25 ^oC.

4.2.2 Methods

4.2.2.1 Preparation ALG, CS and polyelectrolyte complexes (PECs) loaded and unloaded with fish BAPs

Each 0.2% (m/v) ALG and CS solutions were prepared from the stocks by diluting them using filtered 85 mM NaCl as adopted from previous research (Goycoolea et al., 2009). An ultrafiltration (using MWCO membrane 3 kDa) freeze-dried fish BAPs dissolved with distilled water, then added into CS solution at pH 5.5. After that, the ALG solution added with molar mass equivalent n^-/n^+ 10 times higher (excess ALG) and two times lower (excess CS) than CS. The fish BAPs added as much as 1 mg mL^{-1} final concentration in the mixture solution. Next, the mixed solution homogenized using vortex for 5 s and then incubated for around 3 h at 4 ^oC. The PECs without BAPs also prepared with similar condition. Then the self-assembly of the coacervate occurs and subsequently sonicated for 5 min (5 seconds pulsed ON, 3 seconds pulsed OFF), amplitude 35%, 20 kHz via a Sonics® VCX 750 (Sonics & Materials, Inc., Newtown, CT, United States) ultrasonicator coupled with a tapered microtip probe. This process is to break down large coacervate into small PECs, then they were stored in the fridge before further analysis.

4.2.2.2 Stability PECs

The freshly prepared both loaded and unloaded PECs as described above were incubated under 4 conditions: uncontrolled pH meaning no adjustment step (initial pH 5.5), and with controlled pH in buffers, namely pH 4, 5, and 6. Adjusting pH was carried out by dropping 0.1 M HCl or 0.1 M NaOH in to freshly prepared PECs. The incubation was performed at room temperature, and every 7 days their hydrodynamic radius (R_h), ζ-potential, and polydispersity index (PDI) were measured until 28 days of incubation, following which they were compared with the initial measurements (just after immersion into buffers).

4.2.2.3 Gastric and intestinal fluids preparation

Gastric and intestinal were prepared following the INFOGEST protocol adopted from Brodkorb et al., (2019), Minekus et al., (2014), and Zhang et al., (2021b) with pepsin (gastric) and trypsin and chymotrypsin (intestinal). Firstly, each salt was dissolved in water, based on their needed stock concentrations. Secondly, salt solutions were mixed according to the volumes detailed in **Table 4.1**. Next, the gastric or intestinal solutions were mixed in a 50 mL Falcon tube at room temperature using a Fisherbrand™ Classic Vortex Mixer (Loughborough, UK). Finally, the mixed solutions were stored in the freezer at -20°C before being used for further experiments.

Table 4.1 Volume and concentration stock solutions for gastric and intestinal fluids

Salt compositions	**Stock Concentration**		**Gastric (pH 3)**		**Intestinal (pH 7)**	
	(g L^{-1})	[M]	*Volume added* (mL)	Final Conc. [mM]	*Volume added* (mL)	Final Conc. [mM]
KCl	37.3	0.5	6.9	6.9	6.8	6.8
KH_2PO_4	68	0.5	0.9	0.9	0.8	0.8
$NaHCO_3$	84	1	12.5	25	42.5	85
NaCl	117	2	11.8	47.2	9.6	38.4
$MgCl_2(H_2O)_6$	30.5	0.5	0.4	0.1	1.1	0.33
$(NH_4)_2CO_3$	48	0.5	0.5	0.5	-	-
Total Volume			33		60.8	

On the day of experiment, the gastric and intestinal fluids were thawed, then added with $CaCl_2$ final concentration 0.15 mM and 0.6 mM respectively followed by adding pepsin (2000 U mL^{-1}) into gastric fluid and trypsin (100 U mL^{-1}) and chymotrypsin (25 U mL^{-1}) into intestinal fluids. Lastly, the gastric and intestinal fluids adjusted to pH 3 and 7, respectively, using 0.1 M HCl or 0.1 M NaOH before being used as static gastric and intestinal simulation digestion media.

The ionic strength calculation was calculated from the formula based on Debye-Huckel theory as describe below:

$$\mathrm{Is} = \frac{1}{2}.\sum_{\mathrm{i}}^{1} C_i.{Z_i}^2 \qquad (4.1)$$

Where I_s is ionic strength, C_i is concentration each ion in solution, and Z_i is charge of i-th ion.

Table 4.2. The ionic strength of salts on the gastric fluid

							Ionic strength		
Salts	**C_i (mM)**	**Ions**			**(+ve)**	**(-ve)**	**Cationic**	**Anionic**	**Total**
KCl	6.9	K^+	Cl^-		1	1	6.9	6.9	6.9
KH_2PO_4	0.9	K^+	$H_2PO_4^-$		1	1	0.9	0.9	0.9
$NaHCO_3$	25	Na^+	HCO_3^-		1	1	25	25	25
NaCl	47.2	Na^+	Cl^-		1	1	47.2	47.2	47.2
$MgCl_2(H_2O)_6$	0.1	Mg^{2+}	$2Cl^-$	$6H_2O$	2	1	0.4	0.1	0.25
$(NH_4)_2CO_3$	0.5	$2NH_4^+$	CO_3^{2-}		1	2	0.5	2	1.25
$CaCl_2(H_2O)_2$	0.075	Ca^{2+}	$2Cl^-$	H_2O	2	1	0.3	0.075	0.1875
							81.2	82.175	**81.687**

Table 4.3. The ionic strength of salts on the intestinal fluid

							Ionic strength		
Salts	**C_i (mM)**	**Ions**			**(+ve)**	**(-ve)**	**Cationic**	**Anionic**	**Total**
KCl	6.8	K^+	Cl^-		1	1	6.8	6.8	6.8
KH_2PO_4	0.8	K^+	$H_2PO_2^-$		1	1	0.8	0.8	0.8
$NaHCO_3$	85	Na+	HCO_3^-		1	1	85	85	85
NaCl	38.4	Na+	Cl^-		1	1	38.4	38.4	38.4
$MgCl_2(H_2O)_6$	0.33	Mg^{2+}	$2Cl^-$	$6H_2O$	2	1	1.32	0.33	0.825
$CaCl_2(H_2O)_2$	0.3	Ca^{2+}	$2Cl^-$	H_2O	2	1	1.2	0.3	0.75
							133.52	131.63	**132.575**

4.2.2.4 In vitro static digestion and release study

A 1 mL freshly prepared PECs loaded with fish BAPs was transferred into a new Eppendorf tube which initially had been filled with five drops (≈ 100 – 150 µL) of glycerol using a 1 mL syringe needle, then followed by centrifugation using Thermoscientific (Heraeus Fresco 21 Centrifuge, Osterode, Germany) at 20,000 x g for 25 minutes at 4 °C. Then the supernatant (***S1***) was separated, and the pellet was resuspended with 400 µL of new 85 mM NaCl solution using a micropipette until all the pellets dispersed homogeneously. The resuspended solution

was added into gastric or intestinal fluids with the composition described above (without enzymes and with enzymes) with a volume ratio PEC solution: digestion fluid following (Zhang et al., 2021b), i.e., 1:1 (v/v), and then incubated for 2 - 3 h in a shaking incubator (Incu Shake-MAXI,SciQuip, Newtown, UK), at 37 °C, 100 rpm. Every 30 min, the incubation was stopped by adding enzyme inhibitors:pepstatin A (250 µL, 1.0 µM) for gastric and pefabloc SC (500 µL, 5 mM) for intestinal, and then centrifuged at 20,000 x g for 25 min, and the supernatant was collected (***S2***) and stored at -20 ^{o}C. The loaded PECs were separated immediately (without delay) after mixing with digestion fluids, representing the 0-minute sampling. Finally, BAPs which was released in supernatants ***S1*** and ***S2*** quantified with Liquid Chromatography (LC). The release (%) of BAPs during static simulation digestion quantified as follows:

$$\text{Release (\%)} = 100\ (CS2/\ C_{BAPs} - CS1) \qquad (4.2)$$

where C_{BAPs} is the concentration of BAPs in the initial mixture before resuspension, *CS1* is the concentration of BAPs in supernatant 1 (from resuspension), and *CS2* is the concentration of BAPs in supernatant 2 during incubation/simulation.

4.2.2.5 In vitro enzymatic stability of fish BAPs

In vitro hydrolysis of fish BAPs was conducted by mixing of BAPs (1 mg mL^{-1}) with pepsin (at pH 3), trypsin, and chymotrypsin (at pH 7) with final activity of enzymes 2,000 U mL^{-1}, 100 U mL^{-1}, and 25 U mL^{-1} respectively then incubated for 0 - 2 h at 37 ^{o}C. Afterward, the hydrolysis reaction stopped by adding pepstatin A (final concentration 1 µM) to BAPs with pepsin, and pefabloc SC (final concentration 100 mM) to BAPs with trypsin or with chymotrypsin. The mixing solution subsequently loaded into ultrafiltration membrane molecular weight (M_w) cut-off < 3 kDa, and the filtered solution stored at -20 ^{o}C before being analysed with HPLC (*Section 4.2.2.7*) for BAPs identification and with ELISA plate reader (multiscan) for their activity against ACE (*Section 4.2.2.9*).

4.2.2.6 Fourier transform infrared spectroscopy (FT-IR)

Before measuring freeze-dried samples: CS, ALG, fish BAPs and PECs both loaded and unloaded, the FT-IR spectrometer measured the background spectrum without any sample in the path. This spectrum will account for the instrument and environmental contributions to the signal. Then, freeze-dried samples were placed in the sample cell, covered, and secured with an attenuated total reflectance (ATR) crystal accessory. The spectrum of transmittance

of the sample powder as a function of wavenumber (cm^{-1}), measured with a resolution of 4 cm^{-1} and a scan range from 4000 to 550 cm^{-1} (Niaz et al., 2021, Oh et al., 2023). After each sample change, the sample cell and ATR crystal were cleaned with isopropyl alcohol (IPA).

4.2.2.7 Ultra-high-performance liquid chromatography (UHPLC)

Liquid chromatography (LC) was carried out by a method adopted from Liu et al., (2020), Jiang et al., (2017), and Curtis et al., (2002) with some modifications. Briefly, reversed phase ultra-high-performance liquid chromatography (UHPLC) equipped with a quaternary pump (operated with only 2 lines: water and organic solvent) and coupled with a Diode Array Detector (DAD) (Agilent, Infinity II, Germany) was used. The stationary phase was a C-18 column with specifications of 4.6x250 mm, 5 µm, and 110 Å (length, diameter, and particle size, respectively) (Supelco®, Gemini, Darmstadt, Germany). The mobile phases were Milli-Q water (**mobile phase A**) and acetonitrile (ACN) spiked with 0.05% trifluoroacetate (TFA) (**mobile phase B).**

Before loading into UHPLC, the samples were filtered by a 0.22 µm Kinesis KX mixed cellulose esters (MCE) membrane with very low protein binding (Cole-Parmer®, Cambridgeshire, UK), followed by an autosampler injection setup of 20 µL. The UHPLC was run with a flow rate of 1 mL min^{-1}, system pressure <250 bar, and column temperature of 25 °C for 20 min. The mobile phase gradients were as follows: 100% mobile phase A (0-1 min); 95% mobile phase A5, % mobile phase B (1-6 min); 85% mobile phase A, 15% mobile phase B (6-10 min); 75% mobile phase A, 25% mobile phase B (10-15 min); and 65% mobile phase A, 35% mobile phase B (15-20 min). The eluents were monitored at an ultraviolet (UV) wavelength (λ) = 219 nm, and their area under the curve (AUC) at retention times similar with synthetic LKPNM and LKP were collected. Quantification was performed based on AUC of standard purified fish BAPs at concentrations ranging from 0 to 2.5 mg mL^{-1}.

4.2.2.8 Hydrodynamic radius (Rh), ζ-potential, and polydispersity index (PDI)

The R_h, ζ-potential and PDI were measured using Zetasizer Ultra (Malvern Panalytical, UK) according to the method and calculation approaches as described in **Chapter 3**.

4.2.2.9 In vitro angiotensin converting enzyme (ACE) inhibition assay

ACE inhibitory activity was measured using methods described by Ben Henda et al., (2013) and Han et al., (2021) with slight modifications, employing *Hippuryl-His-Leu* (*HHL*) as a

substrate (Cushman and Cheung, 1971). ACE (60 mU mL^{-1}) in a buffer (50 mM borate buffer + 300 mM NaCl, pH 8.3) was added with 30 µL, followed by incubation for 5 minutes at 37 °C. Then, 20 µL of the same buffer was added, and the mixture was incubated for another 5 minutes at 37 °C. Subsequently, 15 µL of the inhibitors (BAPs at concentrations ranging from 0 to 0.25 mg mL^{-1}, or release BAPs from supernatant ***S2*** after simulation, or captopril at concentrations ranging from 0 to 0.1 mM, or blank) was added, followed by the addition of 50 µL of 5 mM HHL. The mixture was incubated for 30 minutes at 37 °C to initiate the conversion and inhibition reaction. In this step, ACE converts *HHL* to hippuric acid (HPA), but the presence of an inhibitor inhibits the reaction. After incubation, 100 µL of 1 M HCl was added to stop the reaction, and the absorbance was measured at λ 235 nm using a Tecan Spark10M plate reader (Zurich, Switzerland). All ACE inhibition mixtures and measurements were performed in UV-transparent 96-well microplates (Greiner Bio-one, Kremsmünster, Austria). The ACE inhibition activity (%) was quantified using the following formula:

$$\text{ACE inhibiton (\%)} = [\, 1 - (A_i / A_b)] \times 100 \qquad (4.3)$$

Where Ai represents the absorbance of the reaction with the inhibitor (BAPs, release BAPs, or captopril) and A_b denotes the absorbance of the reaction with the blank solutions.

4.2.3 Statistical analysis

Data collection was conducted with three replications for most measurements, except for the HPLC analysis, which was performed with two repetitions. The resulting data were subjected to analysis of variance (ANOVA) at a 95% confidence level using SPSS Statistics 29.0 software (IBM, Chicago, IL) to ensure the reliability and accuracy of the statistical analysis. Where significant differences among treatments were detected, a Tukey post-hoc test was subsequently employed to identify specific differences between the treatment groups.

4.3 Results and Discussion

4.3.2 CS+ALG polyelectrolyte complexes (PECs) and interaction with BAPs

Figure 4.1 presents the FT-IR transmittance (in %) of CS, ALG, fish BAPs individual powder and CS+ALG, CS+ALG+BAPs after complexation using FT-IR spectra analysis at mid-IR spectrum i.e 4000 – 550 cm^{-1}. As shown in **Fig. 4.1a**, the peaks from CS and ALG indicating their polysaccharide structures, such as the broad peaks at ~3370 and ~3260 cm^{-1} which are attributed to their polymeric ν(O-H) stretching vibrations, and a band at ~2896 to 2910 cm^{-1} assigned to ν(C-H) stretching, and the fingerprint region bands at ~1059 and ~1032 cm^{-1} are assigned to C–C, C–O as well as C–O–C bonds stretching vibrations of the carbohydrate ring. The figure also displays the different bands of single CS and ALG at wavenumber ~1500 to ~1750 cm^{-1}, where CS's spectrum does not show any sharp band but only small peaks near ~1626 cm^{-1} assigned to acetamido protein groups, namely, amide I at ~1650 cm^{-1} due to ν (C=O)-related stretching, and amide II at ~1580 cm^{-1} due to δ(N-H)- related deformation. As expected, these bands are very weak, as they are ascribed to residual GlcNAc residues in chitosan. On the other hand, the ALG exhibited a peak of strong intensity at ~1598 and ~1395 cm^{-1} , ascribed to carbonyl (COO^-) groups, which come from symmetric and asymmetric COO^- stretching vibrations, respectively (Lawrie et al., 2007). In addition, the BAPs revealed high-intensity peaks at 1635, 1540, and 1395 cm^{-1} that most probably correspond with stretching and vibration of amides I, II, and III respectively like normally identified on proteins or peptides (Nandiyanto et al., 2019, Pawlowski et al., 2023).

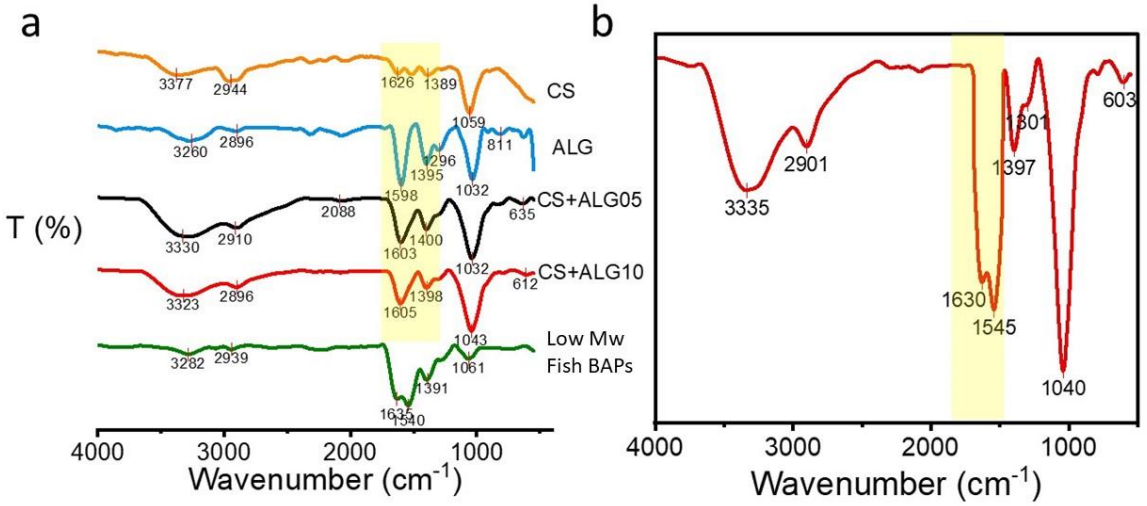


Figure 4.1. FT-IR spectra of freeze-dried CS, ALG, CS+ALG PEC (n^-/n^+ = 0.5 or excess CS and n^-/n^+ = 10 or excess ALG), and BAPs (**a**); and CS+ALG PEC (n^-/n^+ = 0.5) loaded with BAPs (**b**).

Upon complexation in CS+ALG PECs, the band corresponding to ν(O-H) stretching vibrations present on both polysaccharides appears broadened thus indicating that the hydrogen bonds between the absorbed water molecules and the CS+ALG PECs are enhanced. Then, importantly, at wavenumber 1598 cm^{-1}, the peaks of PECs are not as sharp as of a single ALG citing to the interaction of COO^- groups of ALG with ionic groups of CS (NH_3^+). Some studies found that shifted to a less intense peak from COO^- groups of ALG suggesting crosslinking and strong ionic interaction with the counter charge molecules or ions (Lawrie et al., 2007, Yan et al., 2000). Study conducted by Lawrie et al. (2007) found that ALG+CS PEC precipitate displayed IR spectrums with peaks at ~1606 and ~1416 cm^{-1} related with large amount amine and carboxyl groups being deprotonated. They suggest that the presence of ionic forms on both molecules during the formation of ALG+CS PEC at pH 4.8, the presence of ionic forms on both molecules, and mixing them promote the formation of a strongly ionic interaction and associated complex (Lawrie et al., 2007). Li et al. (2009) also indicated in their study that band at ~1610 with two others at ~1414 and ~1298 cm^{-1} suggesting most of ALG in the PECs was deprotonated (Li et al., 2009).

The FT-IR patterns for unloaded systems and loaded ones with low concentrations appear to be very similar in the middle range (at ~1635 and ~1540 cm^{-1}) suggesting that the complexation leads to an overlap of signals from BAPs with the ones from ALG+CS. However, when the concentration of BAPs increases to values above 2 mg mL^{-1}, the peak intensities associated with BAPs become sharply visible at ~1630 and ~1545 cm^{-1} as depicted in **Fig. 4.1b,** remarking the complexation BAPs within ALG+CS. The interaction of BAPs is most probably via ionic interaction between positively charged amine groups of BAPs from lysine and N-terminals, with the negatively charged carboxyl groups of ALG. Additionally, the complexation of ALG+CS+BAPs also shows strong intensity at ~1040 cm^{-1} the known carbohydrate fingerprint region given by C–C, C–O, and C–O–C stretching on the PECs as well as confirming no changes on their structures.

4.3.3 Stability of CS+ALG PECs with BAPs

4.3.3.1 Incubation at different pH

The stability of PECs ALG+CS before and after loading with BAPs was compared at different pH at room temperature by hydrodynamic size (R_h) and ζ-potential measurements for 28 days of incubation, as shown in **Figure 4.2**. The R_h of PECs with excess CS ($n^-/n^+ = 0.5$)

remain stable for both unloaded and loaded, while it increases with excess ALG ($n^-/n^+ = 10$), indicative of its reduced stability. The increase in size for the latter case seems to appear more rapidly at low pH. At pH 6 and uncontrolled conditions, it seems that no differences between PECs size and ζ-potential was observed for unloaded and loaded PECs at excess ALG. And both reach a maximum of ≈2 µm after 28 days of incubation (twice as large than their initial sizes). Of note, at acidic pHs (4 and 5) the PECs with excess ALG have dissimilar size trend changing between unloaded and loaded. For the unloaded PECs, the R_h values increased slightly during incubation until 1.5 – 2 times greater than initial sizes. At the same time, the size of loaded PECs at pH 4 and 5 tend to increase moderately reaching a maximum of 3 times bigger than their starting sizes. This contrasted with the similar trends observed between these formulations at pH 6 and uncontrol condition.

The ζ-potential of both PEC systems, with excess CS and excess ALG, became less positive and less negative, respectively, upon incubation at different pH conditions, thus indicating lower stability of the PEC particles. The loaded PECs have even further reduced their absolute ζ-potential compared to unloaded ones after incubation in both CS+ALG PECs, excess CS and ALG. The reason behind this, might be some rearrangement of the ALG that shifted their occurrence from the inside to the surface area of PEC particles, while CS diffused to the core of PEC or BAPs moieties, thus contributing to the total charge on the outer layer of complexes that were initially dominated by CS. The opposite condition seems at play for PEC with excess ALG, where CS may have migrated to the outer layer of PEC and gave the contribution to the total charge of PECs. For instance, in the case of incubation at pH 5, PECs have significant ζ-potential changes compared to others. We can speculate that ALG moves to the surface higher than other pH condition. The phenomena of CS diffusion also happened in the research conducted by Chen et al., (2006a) which was creating ALG+CS PECs microcapsules, then finally they used double layers, crosslinked with genipin to restrict, and block CS diffusion (Chen et al., 2006a).

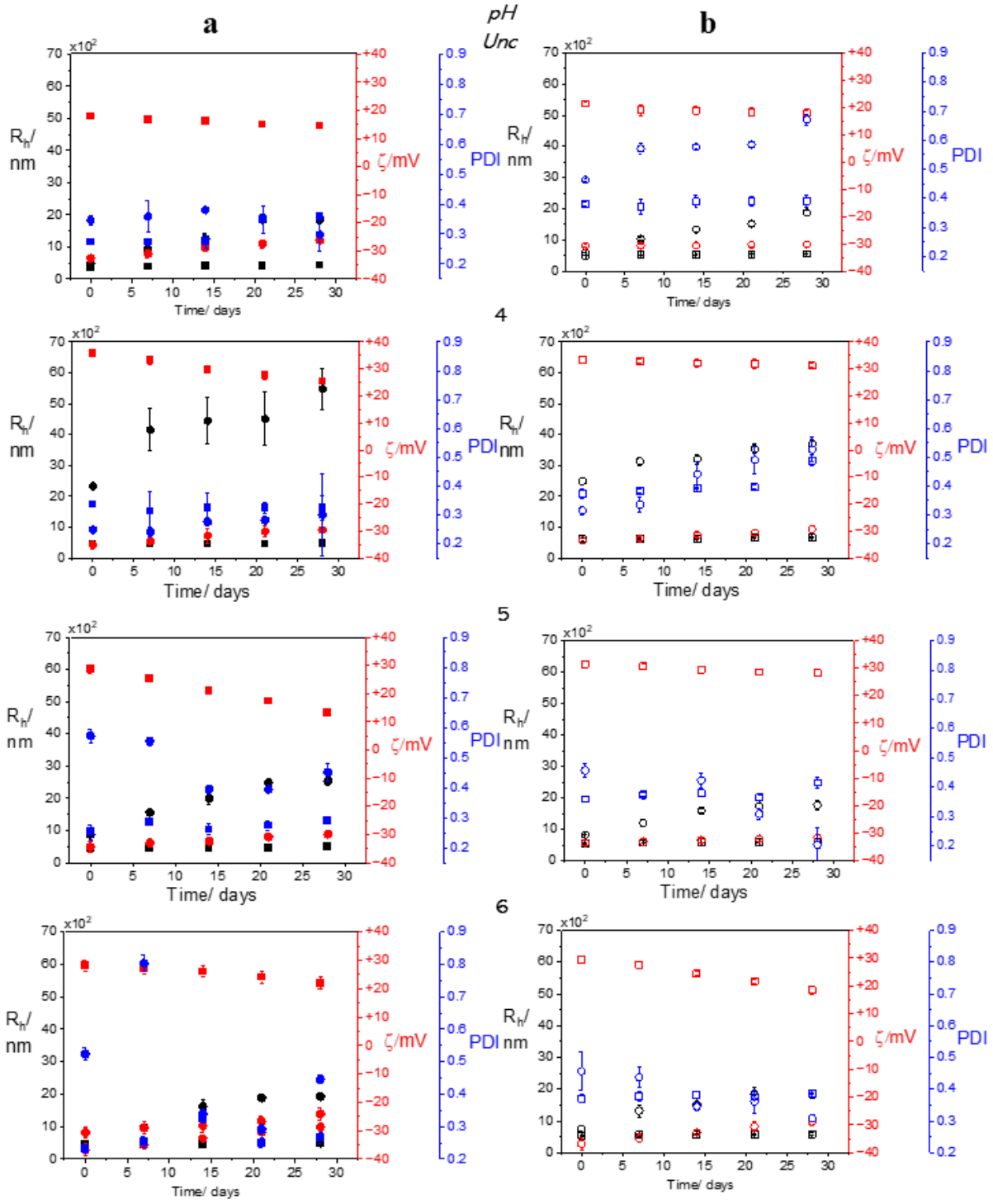


Figure 4.2. Hydrodynamic radius (R_h) (black), z-potential (red), and PDI (blue) of CS+ALG PECs (n^-/n^+ = 10, circles; and n^-/n^+ = 0.5, boxes) loaded with BAP (filled symbols, left panels) (a), or unloaded (open symbols, right panels) (b), during incubation at different pH conditions (as per central legends: uncontrolled, 4, 5, and 6) and varying time intervals

The PEC's loaded BAPs have lower polydispersity than unloaded ones as consistent with our previous experiments reported in **Chapter 3**. In general, the loaded PECs also showed stagnant polydispersity index (PDI) over the time of incubation, whilst the unloaded PECs presented an increasing PDI during incubation and reached a maximum after 28 days incubation. According to **Fig. 4.2**, it is clearly shown that unloaded PECs at excess ALG have higher PDI values than other systems and they are moderately increased during the incubation especially the system with uncontrolled pH. However, the PDI of PECs is stable if the pH for incubations has been controlled, with attention to that, we agreed that controlling the pH of PECs in a buffer solution during storage is critical to maintain the dispersity of PECs ALG+CS both loaded and unloaded.

4.3.3. In vitro digestion

The stability of PECs upon incubation on simulated gastric and intestinal fluids used in *in vitro* digestion studies have been analysed and their results are presented in **Figures 4.3**

Figure 4.3 summarises all the results of the digestion studies in terms of the % release (%R) of the fish BAPs and the corresponding changes in the PECs size and surface charge. **Figure. 4.3a** shows %R *vs*. time. A monotonic increase in %R can be noted under all conditions, so after 3 h, all the BAP has been released. However, %R is faster under SIF conditions than SGF conditions, particularly, for the excess ALG system. For example, after 1 h digestion, %R is already ~100% for the latter, whilst for the other three systems, it is still < ~40%. The systems at pH 7, have the less (positive) charge on the excess CS and less (negative) on the excess ALG systems. Fish BAPs may be released from the PEC particles via one or more of the following mechanisms: diffusion (involving swelling or not), erosion from the surface inwards, or general disintegration. The results, therefore, lend the question of whether is there any correlation between the results of %R (**Figure**. **4.3a**) and R_h (**Figure. 4.3b**) that could account for any of the release mechanisms at play?

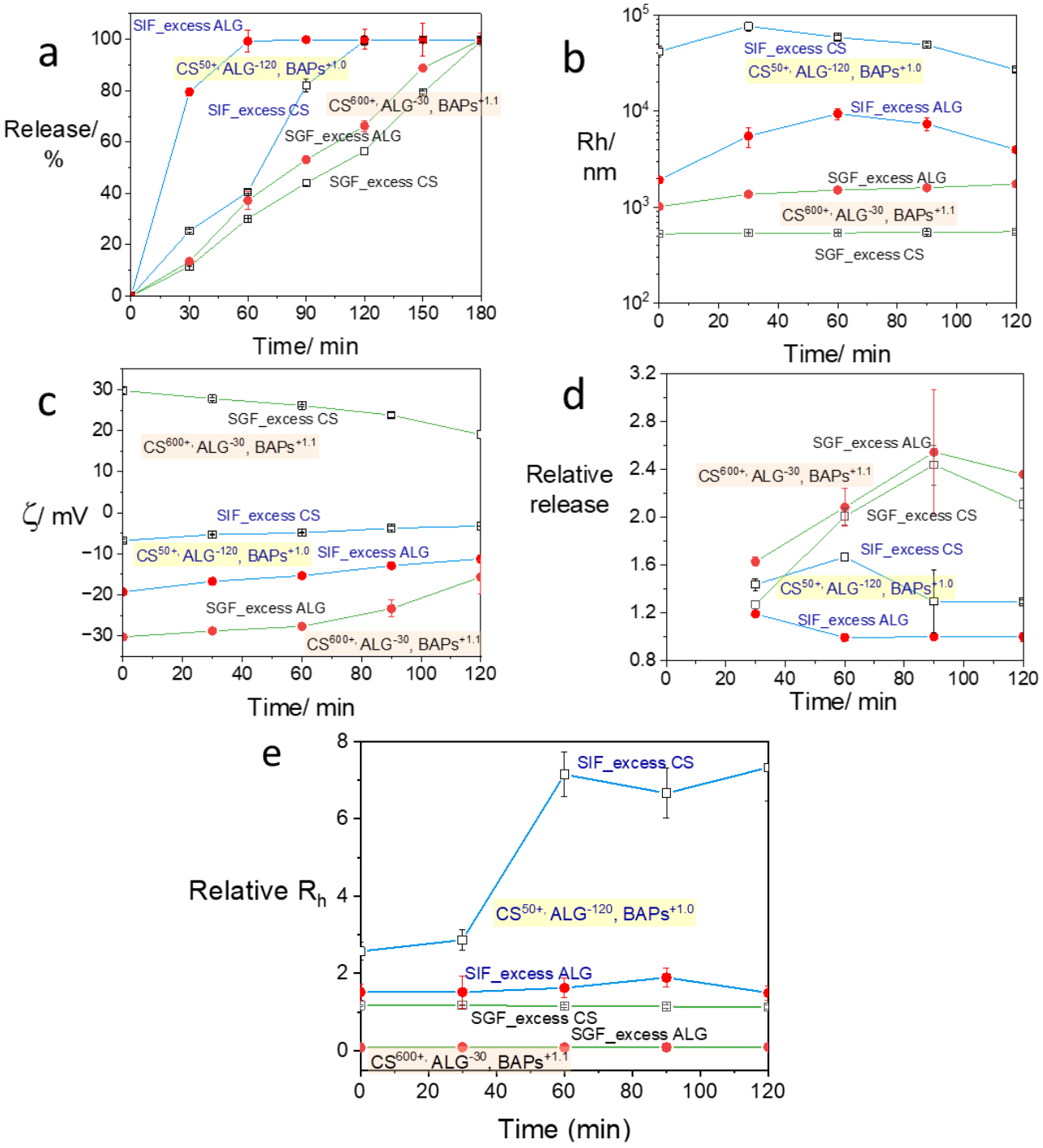


Figure 4.3 Evolution of BAPs release (%R) (a), R_h (b), and ζ-potential (c) of loaded PECs during *in vitro* digestion, and relative release (% release with enzymes:% release without enzymes) (d), as well as relative R_h (R_h with enzymes:R_h without enzymes) (e). The excess CS systems ($n^-/n^+ = 0.5$) are shown by open (black boxes) symbols and the excess ALG system ($n^-/n^+ = 10$) are shown by filled (red circles) symbols both throughout. Note that the corresponding charges on the constituent molecules at the gastric and intestinal digestion conditions are as follows: Gastric (SGF), pH 3 (orange): CS600+, ALG-30, FP (fish BAPs) +1.1. The intestinal (SIF), pH 7, (yellow): CS50+, ALG-120, FP+1.0.

Figure. 4.3b also shows that the initial sizes/R_h of the complexes in SGF are smaller than in SIF, but there is no substantial change in R_h with time (NB: all other measurements were only conducted for 120 min and not 180 min, as in **Figure. 4.3a**). The R_h for the excess CS system is unchanged (with experimental error) over 2 h, despite the %R rising steadily to ~60%. Like with the %R data, the excess ALG system under SGF behaves similarly, although the initial PEC size is larger, and there is a slight increase in size with time. However, these data do not suggest that the significant %R seen in **Figure. 4.3a** is due to the falling apart of the PEC structure, which might be expected to be accompanied by a reduction in R_h. Instead, the evolution of the sizes of the PECs under SIF conditions is significantly different in that (i) the initial PEC sizes are much larger at the start of the digestion compared to in SGF conditions, and (ii) there are more significant changes in R_h with digestion time. The excess ALG systems show an increase to significantly larger R_h after 1 h, followed by a decrease in R_h, though after 2 h, the R_h value is still larger than at the start. In contrast, the excess CS system in SIF conditions is the only one to show a significant and consistent decrease in R_h after 30 min, though starting at the largest particle size of all (and there is an increase in R_h between 0 and 30 min before the decrease occurs). These more drastic changes in PEC size under SIF conditions, i.e., pH 7, correspond to the faster and more extensive %R shown for these conditions in **Figure. 4.3a**, as compared to SGF ones. This scenario seems consistent with the notion that the higher %R is related to a more extensive disruption of the PEC structure.

The decrease in R_h for excess CS in SIF could clearly be interpreted as the disintegration of the PECs, whilst any large increase in R_h (for example, with excess ALG) may point to changes in the composition of the PECs such that are less stable and so start to aggregate. Whether these differences between SGF and SIF are related to the much higher (12 x) +ve charge on the CS molecules at pH 3 versus pH 7 is unclear, but this is the main molecular difference between the two systems (NB: ALG negative charge is 4x larger at pH 7 cf. pH 3, but these are much smaller molecules than the CS). Regarding the mechanism of any breakdown or re-structuring of the PECs, it might be thought that the corresponding changes in ζ-potential might provide more clues as discussed next – these are shown in **Figure. 4.3c**.

Figure. 4.3c shows that, for all four systems, the absolute magnitude of ζ–potential (+ve or –ve) decreases with digestion time, though the changes are modest. The most stable system in terms of smaller, more constant particle size and which gives the slowest release,

i.e., excess CS in SGF, shows a gradual decrease in ζ–potential from +30 to +20 mV. The system which gave the fastest release and the largest swing in R_h, i.e., excess ALG in SIF, showed a similar steady decrease in ζ–potential from -20 to -10 mV. The other two systems, excess CS in SIF and excess ALG in SGF, gave similar sorts of changes in ζ–potential, though the latter started at a negative ζ–potential of much higher magnitude (ca. -30 mV versus – 7 mV, respectively). It is interesting in itself that ζ–potential was -ve for both: the PECs from excess CS ($n^-/n^+ = 0.5$) in SIF, where the +ve charge on CS is minimal (50+); also, for the PECs from excess ALG in SGF, where the charge on the CS is a maximum (600+) but the CS concentration is lowest ($n^-/n^+ = 10$). This result suggests that ALG chains dominate the outer layers of the PECs. Only for the system of excess CS in SGF, where the CS charge is a maximum, are the PECs positively surface charged (and remain so throughout the digestion), suggesting that CS might dominate the electric behaviour of the surface in this system.

Possibly the positive surface charge on the PECs repels or attract the enzymes. Note that the reported isoelectric pH (pI) values of the constituent enzymes are: for SGF, pepsin = 2.7 – 2.9 (Herriott et al., 1939, Patrickios and Yamasaki, 1995) for SIF, trypsin = 10.1 to 10.5 (Miguez et al., 2023) and chymotrypsin = 9.1 (Woitovich Valetti et al., 2012). These values mean that pepsin will be slightly net negatively charged under SGF conditions (pH 3) whilst trypsin and chymotrypsin will be net positively charged under SIF conditions (pH 7). Thus, the enzymes may interact electrostatically with their oppositely charged biopolymers in the PECs, both within and at the surface of the PECs. Hence, it may affect the enzyme activity for the fish BAPs and the stability of the complexes and/or their net surface charge and, therefore, ζ. This condition does not seem to have been considered in previous studies of enzymatic digestion of such complexes. At this stage, it can be concluded that the presence of the biopolymers does not appear to interfere with the bioactivity of the free fish BAPs (**see Figure 4.4**).

Overall, the changes in R_h on their own does not suggest significant structural re-arrangement of the PECs during the in vitro gastric or intestinal digestion conditions, even though there is a complete release of the fish BAPs. The earlier work (**Chapter 3**) suggested that the initial structure of the PECs themselves was affected by the inclusion of the fish BAPs when the complexes were formed since the PECs were smaller when the fish BAPs were included. This situation was attributed to the positive charge on the fish BAPs expected at

both pH values: +1.1 and +1.0 at pH 3 (SGF) and 7 (SIF), respectively. Although the fish BAPs are tiny in M_w compared to the ALG and CS, their molar concentration is relatively high, so they might also act as a cross-linking agent between the ALG chains. If this is the case, one might expect that any digestion of some of the fish BAPs by the enzymes might affect the structure and integrity of the PECs and the subsequent release of the fish BAPs. The digestion results of the free fish BAPs shown in **Figure 4.7** clearly show that the fish BAPs are susceptible to SGF (pepsin) and SIF (trypsin and chymotrypsin) degradation. Therefore, it is interesting to compare the %R in the presence of the enzymes to that in their absence in SGF or SIF fluids of the same composition under identical conditions (pH, ionic strength, temperature, etc.) but lacking the added enzymes.

Figure 4.3d shows the *relative* release behaviour, i.e., %R in the presence of enzymes divided by the %R in the absence of enzymes, referred to as "Rel%R", versus digestion time. The absolute %R values in the absence of enzymes are given in the *Appendix* – note there is still some release, assumed to be due to changes induced by the change in pH from that in which the PECs were originally formed (pH 5.5) as well as the added salts as part of the simulated SGF and SIF conditions. **Figure. 4.3d** shows that under SGF conditions, both for the excess ALG and excess CS systems, there is significantly greater %R when the enzymes are present, i.e., Rel%R >> 1, the value increasing with increasing digestion time. In contrast, under SIF conditions, Rel%R > 1 (within experimental error). Thus, although the absolute %R is faster in SIF than SGF (**Figure. 4.3a**), this is probably not a result of the enzymes themselves but the other SIF conditions (cf. **Figure. 4.3d**). The opposite appears to be true under SGF conditions, i.e., it seems likely that the %R is more due to SGF enzymes (i.e., pepsin) than the change in pH and ionic composition.

As with the absolute values of %R, comparing corresponding the relative size (R_h) changes of the PECs with and without enzymes is also interesting. **Figure. 4.3e** shows R_h with enzymes (from **Figure. 4.3b**) divided by R_h without enzymes, termed $RelR_h$ (NB: again, the absolute values of R_h without enzymes are given in *Appendix Fig. A2*). In SGF, R_h is unaffected by adding the enzymes ($RelR_h$ = 1) for excess CS in this case. R_h is lower for excess ALG but also more or less constant over the digestion time. These results, therefore, suggest that although the enzymes induce greater release of the fish BAPs for the excess CS system (see **Figure. 4.3d**), this is not connected with the enzymes themselves inducing any additional change in the sizes of the complexes. The SGF enzyme (pepsin) does, however, seem to be

responsible for an initial and considerable shrinkage of the PECs right at the start of the SGF digestion. The reasons for this are not clear. In SIF condition for the excess ALG system is like the excess CS system in SGF condition where $RelR_h$ is almost invariant over time and > 1. The main outlier is the excess CS system in SIF, which shows a much higher R_h in the presence of the enzymes ($RelR_h$ >> 1). Note that in absolute terms, this system had the largest particle size at the start (see **Figure 4.3b**), so whatever the exact effect of the SIF enzymes on the internal PEC structure, the stability of this system in terms of particle size seems to get worse when the enzymes are present. Again, however, as with the absolute values of %R and R_h, it is challenging to reconcile completely the different $RelR_h$ (**Figure 4.3e**) with the corresponding Rel%R data (**Figure 4.3d**).

In summary, the differences between the responses of the PECs under SGF and SIF conditions are complex. Both the excess CS and ALG PECs appear to confer some protection to the fish BAPs digestion, in terms of slowing it down and more so in the case of gastric conditions. It is harder at this stage to explain what happens to the PECs during the release. As R_h increases, this does not necessarily correspond to a disintegration or decrease in the size of the PECs. Changes in the composition and/or distribution of the remaining CS and ALG within them may cause the PECs to aggregate or swell, as evidenced by the increase in R_h sometimes observed. Aggregation or swelling cannot be distinguished in this respect. Similarly, the corresponding changes in ζ–potential cannot be unambiguously interpreted – structural rearrangements and release of CS and ALG components may occur. However, released species may also adsorb to the surface of the new structures forming, which may maintain or moderate the net surface charge and, therefore, ζ–potential. This situation would require a different suite of techniques to visualize the location of the constituting components within the PECs during digestion at very high resolution, but this is beyond the scope of the current study.

The *Appendix Fig A2* shows side by side the change hydrodynamic radius (R_h) during in vitro digestion with/without enzymes. Based on the findings shown in *Appendix Fig. A2a* and *A2b*, all systems in the absence of enzymes show stable R_h over 2 h of incubation in gastric fluid except the PECs with excess CS (n^-/n^+ 0.5) and loaded with BAPs. Whilst the change in size of PECs in intestinal fluids with and without enzymes are shown in *Appendix Fig A2c* and *A2d*. The ζ-potential of PECs with excess CS and excess ALG exhibits positive and negative

values, respectively, during gastric incubation. A slight decrease in absolute values of ζ-potential is observed over incubation, possibly due to exposure to the ionic strength of the gastric conditions (see *Appendix Fig. A3a* and *A3b*). The polydispersity index (PDI) of PECs during gastric and intestinal digestion (*Appendix Fig. A4*) both unloaded and loaded are completely different.

4.3.4 Bioactivity

4.3.4.1 Bioactivity after release

The bioactivity of BAPs to inhibit ACE is shown by their ability to compete with ACE, reducing the conversion of hippuryl-histidyl-leucine (HHL) into hippuric acid (HPA). A lower amount of HPA produced indicates stronger ACE inhibition by BAPs. **Figure 4.4** reveals the ACE inhibitory activity after gastric and intestinal digestion of CS+ALG PECs of excess CS (n^-/n^+ = 0.5) or excess ALG (n^-/n^+ 10). The ACE inhibition activity after release in gastric conditions follows a very similar pattern to the release studies (*Appendix Fig. A6*) in which reaches a maximum of ∼40% with enzymes and a ∼30% in absence of enzymes after 3 h incubation. In more detail, ACE inhibition with pepsin increases steadily, while without it, only 10% activity is measured after 2 h, followed by a sudden increase to >∼20% inhibition after 3 h (**Figure 4.4b**).

By contrast, the ACE inhibitory bioactivity after release of BAPs from PECs during intestinal digestion shows different behaviour between excess CS (n^-/n^+ 0.5) and excess ALG (n^-/n^+ 10) PECs compared to gastric conditions. The BAPs activity from CS-rich (n^-/n^+ 0.5) PECs appears to reach its maximum much more slowly than ALG-rich (n^-/n^+ 10) PECs, within the first one hour of incubation, in both cases with and without enzymes. In contrast, for excess ALG (n^-/n^+ 10) PECs with encapsulated BAP, the release is observed just after 30 min incubation. **Figure 4.4** also exhibits no bioactivity values from the unloaded PECs used as control in all the experiments. The most important feature of the ACE inhibition and the release studies is that the inhibition activity follows the same pattern as the amount of release in both gastric and intestinal media, with and without enzymes. This indicates that the PECs as a system to encapsulate the BAPs had no influence on their bioactivity apart from controlling their release.

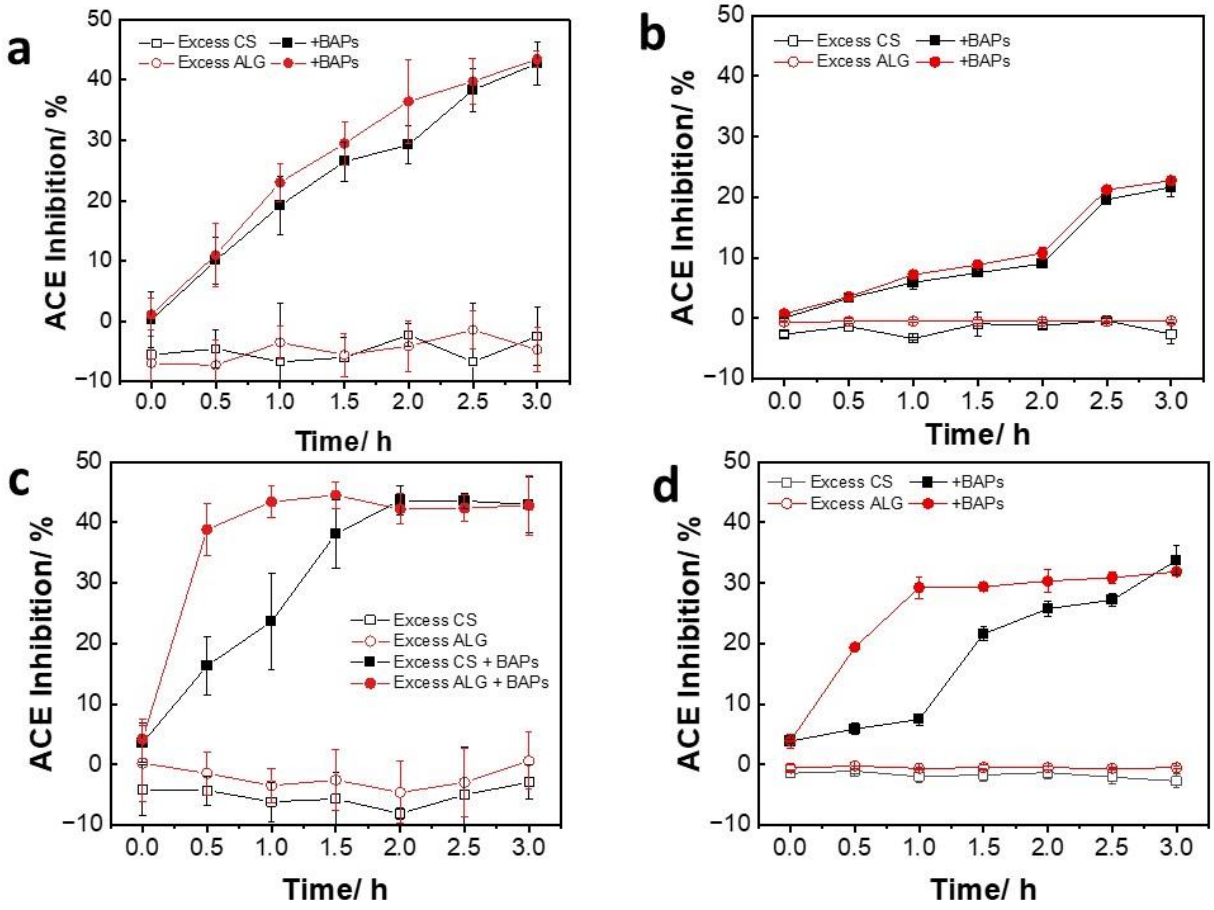


Figure 4.4. The bioactivity ACE inhibition with time of BAPs upon release during gastric (top) and intestinal (bottom) digestion with enzymes (left) and without enzymes (right) of CS + ALG PECs of excess CS ($n^-/n^+ = 0.5$) PEC and excess ALG ($n^-/n^+ = 10$) PEC. The bioactivity assay was performed on both BAP-loaded (filled symbols) and unloaded (open symbols) PECs.

Our findings are in good agreement with previous studies on BAPs encapsulated in CS and ALG complexes, all of which show slow release under gastric conditions while a fast release in intestinal fluids. A study using enzymes conducted by Han et al. (2022) found that, peanut peptide encapsulated within CS+ALG PECs released ~30.69% in the gastric fluid but 100% in intestinal fluid, within the first 2 h (Han et al., 2022). In this case, they were using n-trimethy chitosan as the wall material. A study conducted by Abruzzo et al., (2021) without enzymes stated that the peptide encapsulated with CS+ALG NPs released nearly 80% at pH 7.4 after 2 h (Abruzzo et al., 2021). In addition, a study by Thongcumsuk et al., (2023) using enzymes indicated that a negligible amount of peptide was released in gastric fluid after 2 h, but around 27.24% in intestinal fluid after 6 h (Thongcumsuk et al., 2023). The ionic strength of gastric and intestinal fluids is one of key factors at play that affects release of BAPs. Based on Table 4.2 and 4.3 (In the *Method section 4.2.2.3*), it follows that the total ionic strength in

intestinal fluid is 1.6 times stronger than gastric fluid. This fact is in keeping with the idea that the CS+ALG PEC, being governed by self-assembly electrostatic interactions, as the ionic strength increases, these interactions are weakened by screening of the charges on both polyelectrolytes, thus favouring the release of the BAPs payload which is faster on intestinal than on gastric conditions. In line with this proposal, increase in the ionic strength from 0 to 150 mM of NaCl, has been seen to trigger the release an enzyme (β-lactamase) loaded in ALG + lysozyme PECs (Fuenzalida et al., 2016).

4.3.5 Enzymatic stability BAPs

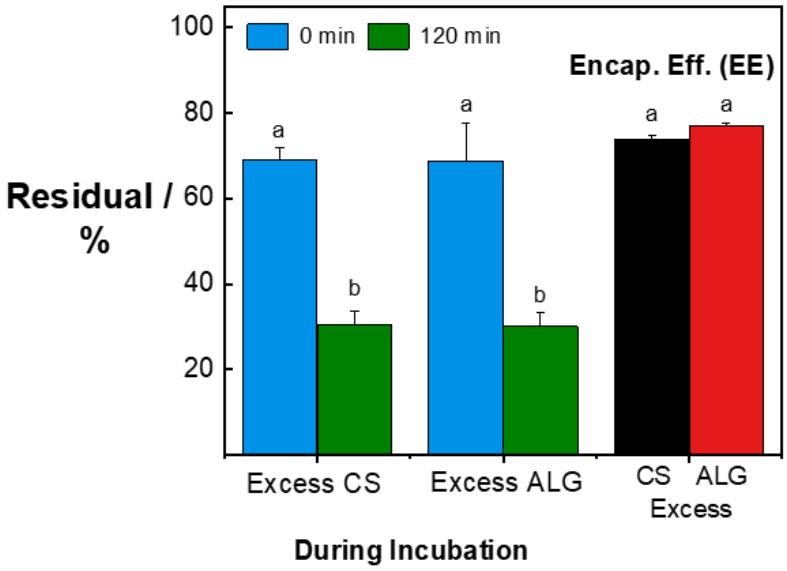


Figure 4.5 Residual BAPs in % (initial loaded concentration 1 mg mL^{-1} = 100%) in CS+ALG PECs taken at the beginning (0 min), and after 120 min of incubation in gastric fluid compared with their encapsulation efficiency

Figure 4.5 presents the percentage of BAPs that are entrapped inside the PECs, where in the early time of incubation, i.e. 0 min, the BAPs remain high and do not significantly differ from encapsulation efficiency (EE). However, after 2 h incubation, the BAPs inside the PEC left is ~30%, as this finding confirmed with previous results where BAPs released in gastric with enzyme ~60% after 2 h (**Figure. 4.3**). This validation was performed by measuring BAPs in the PEC by isolating them with PECs and then immersing them into a pH 12 solution where CS lost their charge; simultaneously, the ALG and BAPs were negatively charged.

Furthermore, to understand the kinetic of proteases action against the fish BAPs, an *in vitro* analysis of free fish BAPs incubated with enzymes during certain time at gastrointestinal pH conditions was performed. The PECs loaded with BAPs (1 mg mL^{-1}) incubated with enzymes with series of time (30 – 120 min). Then the residual BAPs in the supernatant analysed via UHPLC, then the area under the curve (AUC) quantified based on the standard curve of fish BAP concentrations. As depicted in **Figure. 4.6**, the fish BAPs are minimally hydrolysed in presence of pepsin at pH 3, but vulnerable when facing trypsin and chymotrypsin at pH 7. The low M_w fish BAPs seem stable during the first 30-minute incubation with pepsin, then the concentration BAPs reduced 40% after 1 h, and prolong incubation until 2 h does not change quantity of residual of fish BAPs. In other hand, intact sequences of fish BAPs almost completely degraded during incubation period of times, with exception with trypsin for 30 min which only decreased by 30%.

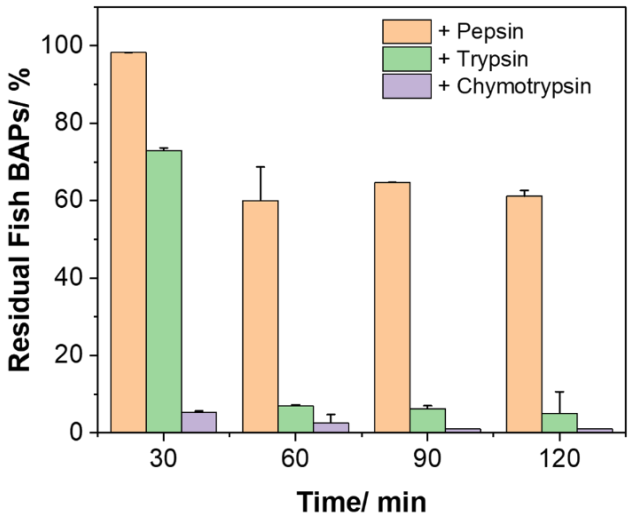


Figure 4.6. Residual fish BAP (initial concentration = 1 mg mL^{-1}) after incubated with pepsin (2000 U mL^{-1} at pH 3), trypsin (100 U mL^{-1} at pH 7), chymotrypsin (25 U mL^{-1} at pH 7) quantified with HPLC at different time interval.

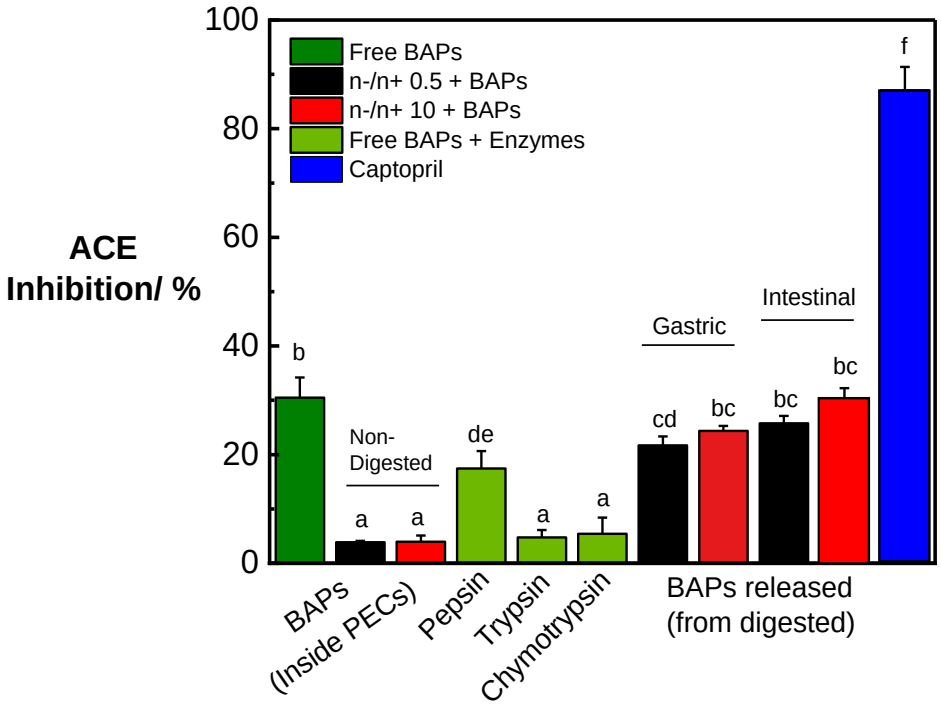


Figure 4.7. ACE inhibition of free fish BAPs (concentration 1 mg mL^{-1}), captopril (0.1 mM), BAPs after loaded into ALG + CS and BAPs release from ALG + CS after 120 min incubation in gastric and intestinal fluids.

Figure. 4.7 compares the bioactivity of captopril with that of BAPs before and after loading as well as after release. The ACE inhibition of non-encapsulated BAPs was also carried out after incubation with pepsin, trypsin, and chymotrypsin. Captopril is an antihypertensive agent that has been used as a drug via the ACE inhibition mechanism. The bioactivity of encapsulated BAPs (i.e., BAPs inside PECs) was quantified by incubating a solution containing BAP-loaded PECs with the substrate and ACE. In this assay, the components of the PECs (CS and ALG) were considered background, and their contribution was accounted for by subtracting the results obtained from unloaded PECs. In contrast, the bioactivity of BAPs after release was quantified using the supernatant obtained by centrifuging the loaded-PECs after 2 hours of incubation. In this case, individual CS and ALG solutions were again used as background controls.

As per our prediction, the ACE inhibition activity of captopril is significantly higher than fish BAPs even with the lowest concentration than others. While the bioactivity of BAPs is three times lower than the antihypertensive drug, where around 30% at a concentration of 0.1%. The ACE inhibition of BAPs after loading into PECs, whether in excess CS or excess ALG, seems to become extremely low compared to captopril or free BAPs. Interestingly, the BAPs activity after release from both PECs after 2 h incubation in the intestinal fluid were identical to free BAPs

A study conducted by Danish et al. (2022) encapsulated ACE inhibitor tripeptide Leucine-Lysine-Proline (LKP) and Isoleucine-Proline-Proline (IPP) into CS and Zein nanoparticles (NPs) and they found the ACE inhibitory activity of the released peptides was similar to native ones (Danish et al., 2022). Alvarado et al., (2019) in turn, performed research concerning the encapsulation of low molecular weight (< 3 kDa) ACE inhibitor whey peptides which were using sodium alginate complexed with collagen, gum arabic, and gelatin respectively, and then studied their release in simulated static gastric and intestinal fluids. They observed that the encapsulation preserves the inhibitory activity of peptides against ACE, while ACE inhibition increases upon release in gastric and intestinal fluids (Alvarado et al., 2019).

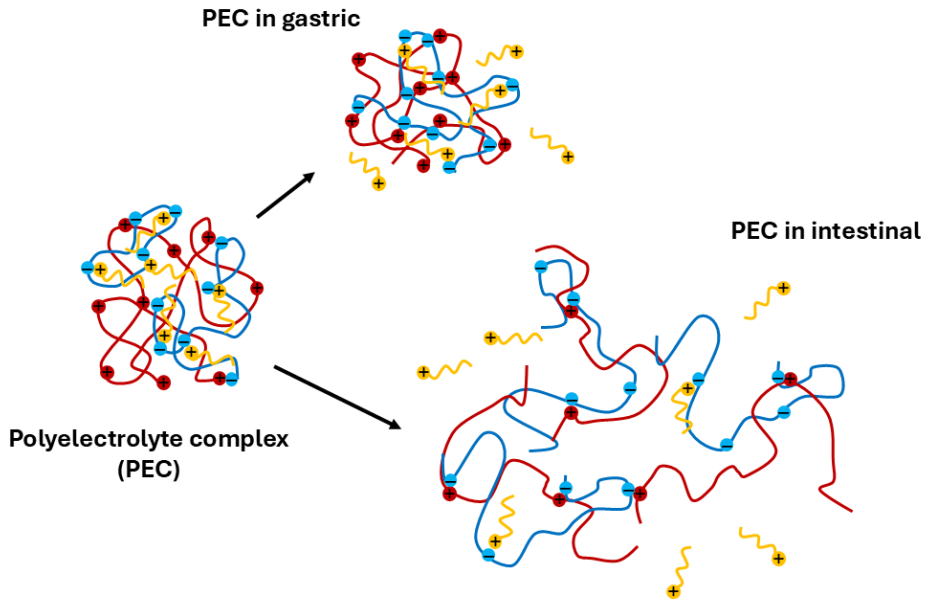


Figure 4.8 Schematic illustration showing the proposed structure of PEC and the released BAP after digestion.

4.4 Conclusion

In conclusion, the FT-IR analysis confirmed CS and ALG BAPs complexation. Then, the PEC stability over 28 days at room temperature was lower at acidic pH (∼4-5) compared to pH 6. The PECs with excess ALG ($n^-/n^+ = 10$), whether unloaded or loaded, have better stability in gastric fluid than intestinal fluid and PECs with excess CS ($n^-/n^+ = 0.5$) are stable to gastric digestion but not intestinal. There were no correlations between the release of BAPs from PECs and their hydrodynamic radius (R_h). The PECs protect the BAPs from gastrointestinal protease hydrolysis and maintain their ACE activity until reaching the intestines. However, the digestive enzymes (namely pepsin, trypsin, chymotrypsin) induce greater BAP release than under the same conditions without enzymes. And under intestinal conditions 100% release of BAPs occurs after 1 h with excess ALG and after 2 h with excess CS. The results anticipate the potential application of CS+ALG PECs as encapsulation vehicles to associate BAPs and increase their oral bioaccessibility.

4.5 References

Abruzzo, A., Giordani, B., Miti, A., Vitali, B., Zuccheri, G., Cerchiara, T., Luppi, B. & Bigucci, F. 2021. Mucoadhesive and mucopenetrating chitosan nanoparticles for glycopeptide antibiotic administration. *Int J Pharm,* 606**,** 120874.

Aguilar-Toala, J. E., Quintanar-Guerrero, D., Liceaga, A. M. & Zambrano-Zaragoza, M. L. 2022. Encapsulation of bioactive peptides: a strategy to improve the stability, protect the nutraceutical bioactivity and support their food applications. *RSC Adv.,* 12**,** 6449-6458.

Alvarado, Y., Muro, C., Illescas, J., Diaz, M. D. C. & Riera, F. 2019. Encapsulation of Antihypertensive Peptides from Whey Proteins and Their Releasing in Gastrointestinal Conditions. *Biomolecules,* 9.

Amigo, L. & Hernandez-Ledesma, B. 2020. Current Evidence on the Bioavailability of Food Bioactive Peptides. *Molecules,* 25**,** 1-36.

Atma, Y., Murray, B. S., Sadeghpour, A. & Goycoolea, F. M. 2024. Encapsulation of short-chain bioactive peptides (BAPs) for gastrointestinal delivery: a review. *Food Funct,* 15**,** 3959-3979.

Atma, Y., Sadeghpour, A., Murray, B. S. & Goycoolea, F. M. 2025. Chitosan-alginate polyelectrolyte complexes for encapsulation of low molecular weight fish bioactive peptides. *Food Hydrocolloids,* 160.

Auwal, S. M., Ghanisma, S. B. M. & Saari, N. 2024. Improved systolic blood pressure (SBP)-lowering effect of stone fish-derived angiotensin-I converting enzyme (ACE)-inhibitory peptide entrapped in chitosan-coated alginate nanocomposites. *Food Bioscience,* 60**,** 104349.

Ben Henda, Y., Labidi, A., Arnaudin, I., Bridiau, N., Delatouche, R., Maugard, T., Piot, J. M., Sannier, F., Thiery, V. & Bordenave-Juchereau, S. 2013. Measuring angiotensin-I converting enzyme inhibitory activity by micro plate assays: comparison using marine cryptides and tentative threshold determinations with captopril and losartan. *J Agric Food Chem,* 61**,** 10685-90.

Bernkop-Schnurch, A. 1998. The use of inhibitory agents to overcome the enzymatic barrier to perorally administered therapeutic peptides and proteins. *Journal of Controlled Release,* 52**,** 1-16.

Bourganis, V., Karamanidou, T., Kammona, O. & Kiparissides, C. 2017. Polyelectrolyte Complexes as Prospective Carriers for the Oral Delivery of Protein Therapeutics. *Eur. J. Pharm. Biopharm.,* 111**,** 44-60.

Brodkorb, A., Egger, L., Alminger, M., Alvito, P., Assuncao, R., Ballance, S., Bohn, T., Bourlieu-Lacanal, C., Boutrou, R., Carriere, F., Clemente, A., Corredig, M., Dupont, D., Dufour, C., Edwards, C., Golding, M., Karakaya, S., Kirkhus, B., Le Feunteun, S., Lesmes, U., Macierzanka, A., Mackie, A. R., Martins, C., Marze, S., Mcclements, D. J., Menard, O., Minekus, M., Portmann, R., Santos, C. N., Souchon, I., Singh, R. P., Vegarud, G. E., Wickham, M. S. J., Weitschies, W. & Recio, I. 2019. INFOGEST static in vitro simulation of gastrointestinal food digestion. *Nat Protoc,* 14**,** 991-1014.

Brownlee, I. A. 2011. The physiological roles of dietary fibre. *Food Hydrocolloids,* 25**,** 238-250.

Buckley, S. T., Hubalek, F. & Rahbek, U. L. 2016. Chemically modified peptides and proteins - critical considerations for oral delivery. *Tissue Barriers,* 4**,** e1156805.

Castel-Molieres, M., Conzatti, G., Torrisani, J., Rouilly, A., Cavalie, S., Carrere, N. & Tourrette, A. 2017. Influence of Homogenization Technique and Blend Ratio on Chitosan/Alginate Polyelectrolyte Complex Properties. *Journal of Medical and Biological Engineering,* 38**,** 10-21.

Chen, H., Ouyang, W., Lawuyi, B. & Prakash, S. 2006a. Genipin Cross-Linked Alginate-Chitosan Microcapsules: Membrane Characterization and Optimization of Cross-Linking Reaction. *Biomacromolecules,* 7**,** 2091-2098.

Collado-González, M., Ferreri, M. C., Freitas, A. R., Santos, A. C., Ferreira, N. R., Carissimi, G., Sequeira, J. a. D., Díaz Baños, F. G., Villora, G., Veiga, F. & Ribeiro, A. 2020. Complex Polysaccharide-Based Nanocomposites for Oral Insulin Delivery. *Marine Drugs,* 18.

Curtis, J. M., Dennis, D., Waddell, D. S., Macgillivray, T. & Ewart, H. S. 2002. Determination of angiotensin-converting enzyme inhibitory peptide Leu-Lys-Pro-Asn-Met (LKPNM) in bonito muscle hydrolysates by LC−MS/MS. *Journal of Agricultural and Food Chemistry,* 50**,** 3919−3925.

Cushman, D. W. & Cheung, H. S. 1971. Spectrophotometric assay and properties of the angiotensin-converting enzyme of rabbit lung. *Biochem. Pharmacol.,* 20**,** 1637-1648.

Danish, M.K., Gleeson, J. P., Brayden, D. J., Byrne, H. J., Frias, J. M. & Ryan, S. M. 2022. Formulation, Characterisation and Evaluation of the Antihypertensive Peptides, Isoleucine-Proline-Proline and Leucine-Lysine-Proline in Chitosan Nanoparticles Coated with Zein for Oral Drug Delivery. *Int J Mol Sci,* 23.

Egger, L., Ménard, O., Delgado-Andrade, C., Alvito, P., Assunção, R., Balance, S., Barberá, R., Brodkorb, A., Cattenoz, T., Clemente, A., Comi, I., Dupont, D., Garcia-Llatas, G., Lagarda, M. J., Le Feunteun, S., Janssenduijghuijsen, L., Karakaya, S., Lesmes, U., Mackie, A. R., Martins, C., Meynier, A., Miralles, B., Murray, B. S., Pihlanto, A., Picariello, G., Santos, C. N., Simsek, S., Recio, I., Rigby, N., Rioux, L.-E., Stoffers, H., Tavares, A., Tavares, L., Turgeon, S., Ulleberg, E. K., Vegarud, G. E., Vergères, G. & Portmann, R. 2016. The harmonized INFOGEST in vitro digestion method: From knowledge to action. *Food Res. Int.,* 88**,** 217-225.

Fuenzalida, J. P., Nareddy, P. K., Moreno-Villoslada, I., Moerschbacher, B. M., Swamy, M. J., Pan, S., Ostermeier, M. & Goycoolea, F. M. 2016. On the role of alginate structure in complexing with lysozyme and application for enzyme delivery. *Food Hydrocolloids,* 53**,** 239-248.

Goycoolea-Valencia, F. M., Lollo, G., Remunan-Lopez, C., Quaglia, F. & Alonso, M. J. 2009. Chitosan-Alginate Blended Nanoparticles as Carriers for the Transmucosal Delivery of Macromolecules. *Biomacromolecules,* 10**,** 1736-1743.

Han, C., Fang, L., Song, S. & Min, W. 2022. Polysaccharides-based delivery system for efficient encapsulation and controlled release of food-derived active peptides. *Carbohydr Polym,* 291**,** 119580.

Han, R., Hernandez Alvarez, A. J., Maycock, J., Murray, B. S. & Boesch, C. 2021. Comparison of alcalase- and pepsin-treated oilseed protein hydrolysates - experimental validation of

predicted antioxidant, antihypertensive and antidiabetic properties. *Curr. Res. Food Sci.,* 4**,** 141-149.

Herriott, R. M., Desreux, V. & Northrop, J. H. 1939. Electrophoresis of pepsin. *J Gen Physiol,* 23**,** 439-47.

Jiang, B., Zhang, X., Yuan, Y., Qu, Y. & Feng, Z. 2017. Separation of antioxidant peptides from pepsin hydrolysate of whey protein isolate by ATPS of EOPO co-polymer (UCON)/phosphate. *Sci Rep,* 7**,** 13320.

Kim, J. C., Park, E. J. & Na, D. H. 2022. Gastrointestinal Permeation Enhancers for the Development of Oral Peptide Pharmaceuticals. *Pharmaceuticals (Basel),* 15.

Lawrie, G., Keen, I., Drew, B., Chandler-Temple, A., Rintoul, L., Fredericks, P. & Grøndahl, L. 2007. Interactions between Alginate and Chitosan Biopolymers Characterized Using FTIR and XPS. *Biomacromolecules,* 8**,** 2533-2541.

Lehninger, A. L., Nelson, D. L. & Cox, M. M. 2004. *Lehninger - Principles of Biochemistry* New York, USA, W H Freeman & Co.

Li, S., Zhao, Q., Wang, S., Bai, Y., Guo, K., Liu, P., Hu, X. & Li, T. 2023. A novel starch-based microparticle with polyelectrolyte complexes and its slow digestion mechanism. *Food Hydrocolloids,* 135.

Li, X., Xie, H., Lin, J., Xie, W. & Ma, X. 2009. Characterization and biodegradation of chitosan–alginate polyelectrolyte complexes. *Polymer Degradation and Stability,* 94**,** 1-6.

Liu, Q., Yang, M., Zhao, B. & Yang, F. 2020. Isolation of antioxidant peptides from yak casein hydrolysate. *RSC Adv,* 10**,** 19844-19851.

Luo, Y. & Wang, Q. 2014. Recent development of chitosan-based polyelectrolyte complexes with natural polysaccharides for drug delivery. *Int J Biol Macromol,* 64**,** 353-67.

Mcclements, D. J. 2018. Encapsulation, protection, and delivery of bioactive proteins and peptides using nanoparticle and microparticle systems: A review. *Adv Colloid Interface Sci,* 253**,** 1-22.

Miguez, J. P., Fernandez-Lafuente, R., Tavano, O. L. & Mendes, A. A. 2023. The Immobilization and Stabilization of Trypsin from the Porcine Pancreas on Chitosan and Its Catalytic Performance in Protein Hydrolysis. *Catalysts,* 13.

Minekus, M., Alminger, M., Alvito, P., Ballance, S., Bohn, T., Bourlieu, C., Carriere, F., Boutrou, R., Corredig, M., Dupont, D., Dufour, C., Egger, L., Golding, M., Karakaya, S., Kirkhus, B., Le Feunteun, S., Lesmes, U., Macierzanka, A., Mackie, A., Marze, S., Mcclements, D. J., Menard, O., Recio, I., Santos, C. N., Singh, R. P., Vegarud, G. E., Wickham, M. S., Weitschies, W. & Brodkorb, A. 2014. A standardised static in vitro digestion method suitable for food - an international consensus. *Food Funct.,* 5**,** 1113-24.

Nandiyanto, A. B. D., Oktiani, R. & Ragadhita, R. 2019. How to Read and Interpret FTIR Spectroscope of Organic Material. *Indonesian Journal of Science and Technology,* 4.

Niaz, T., Sarkar, A., Mackie, A. & Imran, M. 2021. Impact of albumin corona on mucoadhesion and antimicrobial activity of carvacrol loaded chitosan nano-delivery systems under simulated gastro-intestinal conditions. *Int J Biol Macromol,* 169**,** 171-182.

Nikolova, D., Simeonov, M., Tzachev, C., Apostolov, A., Christov, L. & Vassileva, E. 2021. Polyelectrolyte complexes of chitosan and sodium alginate as a drug delivery system for diclofenac sodium. *Polymer International,* 71**,** 668-678.

Oh, J. X., Murray, B. S., Mackie, A. R., Ettelaie, R., Sadeghpour, A. & Frison, R. 2023. gamma-Cyclodextrin Metal-Organic Frameworks: Do Solvents Make a Difference? *Molecules,* 28.

Park, H., Ha, D. H., Ha, E. S., Kim, J. S., Kim, M. S. & Hwang, S. J. 2019a. Effect of stabilizers on encapsulation efficiency and release behavior of exenatide-loaded PLGA microsphere prepared by the W/O/W solvent evaporation method. *Pharmaceutics,* 11.

Park, J. W., Park, K. H. & Seo, S. 2019b. Natural polyelectrolyte complex-based pH-dependent delivery carriers using alginate and chitosan. *Journal of Applied Polymer Science,* 136**,** 48143.

Patrickios, C. S. & Yamasaki, E. N. 1995. Polypeptide amino acid composition and isoelectric point. II. Comparison between experiment and theory. *Anal Biochem,* 231**,** 82-91.

Pawlowski, L., Mania, S., Banach-Kopec, A., Bartmanski, M., Ronowska, A., Jurak, K., Mielewczyk-Gryn, A., Karska, N., Rodziewicz-Motowidlo, S. & Zielinski, A. 2023. Osteoblast and bacterial cell response on RGD peptide-functionalized chitosan coatings electrophoretically deposited from different suspensions on Ti13Nb13Zr alloy. *J Biomed Mater Res B Appl Biomater,* 111**,** 1800-1812.

Perry, S. L. & Mcclements, D. J. 2020. Recent Advances in Encapsulation, Protection, and Oral Delivery of Bioactive Proteins and Peptides using Colloidal Systems. *Molecules,* 25**,** 1-26.

Potaś, J., Szymańska, E. & Winnicka, K. 2020. Challenges in developing of chitosan – Based polyelectrolyte complexes as a platform for mucosal and skin drug delivery. *European Polymer Journal,* 140**,** 110020.

Reis, C. P., Ribeiro, A. J., Veiga, F., Neufeld, R. J. & Damge, C. 2008. Polyelectrolyte biomaterial interactions provide nanoparticulate carrier for oral insulin delivery. *Drug Deliv,* 15**,** 127-39.

Ribeiro, A. J., Silva, C., Ferreira, D. & Veiga, F. 2005. Chitosan-reinforced alginate microspheres obtained through the emulsification/internal gelation technique. *Eur J Pharm Sci,* 25**,** 31-40.

Sarkar, A., Zhang, S., Murray, B., Russell, J. A. & Boxal, S. 2017. Modulating in vitro gastric digestion of emulsions using composite whey protein-cellulose nanocrystal interfaces. *Colloids Surf B Biointerfaces,* 158**,** 137-146.

Sarmento, B., Ribeiro, A., Veiga, F., Sampaio, P., Neufeld, R. & Ferreira, D. 2007a. Alginate/Chitosan nanoparticles are effective for oral insulin delivery. *Pharmaceutical Research,* 24**,** 2198-2206.

Sarmento, B., Ribeiro, A. J., Veiga, F., Ferreira, D. C. & Neufeld, R. J. 2007b. Insulin-loaded nanoparticles are prepared by alginate ionotropic pre-gelation followed by chitosan polyelectrolyte complexation. *J Nanosci Nanotechnol,* 7**,** 2833-41.

Sun, X., Acquah, C., Aluko, R. E. & Udenigwe, C. C. 2020. Considering Food Matrix and Gastrointestinal Effects in Enhancing Bioactive Peptide Absorption and Bioavailability. *J. Funct. Foods,* 64**,** 103680.

Thongcumsuk, B., Woraprayote, W., Janyaphisan, T., Cheunkar, S. & Oaew, S. 2023. Microencapsulation and Peptide identification of purified bioactive fraction from spirulina protein hydrolysates with dipeptidyl peptidase IV (DPP-IV) inhibitory activity. *Food Bioscience,* 56.

Torres, O., Murray, B. S. & Sarkar, A. 2019. Overcoming in vitro gastric destabilisation of emulsion droplets using emulsion microgel particles for targeted intestinal release of fatty acids. *Food Hydrocolloid,* 89**,** 523-533.

Wagner, A. M., Gran, M. P. & Peppas, N. A. 2018. Designing the new generation of intelligent biocompatible carriers for protein and peptide delivery. *Acta Pharm. Sin. B,* 8**,** 147-164.

Wasupalli, G. K. & Verma, D. 2018. Molecular interactions in self-assembled nano-structures of chitosan-sodium alginate based polyelectrolyte complexes. *Int J Biol Macromol,* 114**,** 10-17.

Woitovich Valetti, N., Lombardi, J., Boeris, V. & Picó, G. 2012. Precipitation of chymotrypsin from fresh bovine pancreas using ι-carrageenan. *Process Biochemistry,* 47**,** 2570-2574.

Yan, X., Khor, E. & Lim, L. Y. 2000. PEC Films Prepared from Chitosan-Alginate Coaccervate. *Chem. Pharm. Bull. ,* 48**,** 941-946.

Yoksan, R. & Towongphaichayonte, P. 2024. Vitexin-loaded poly(ethylene glycol) methyl ether-grafted chitosan/alginate nanoparticles: preparation, physicochemical properties and in vitro release behaviors. *J Sci Food Agric,* 104**,** 956-966.

Zhang, S., Murray, B. S., Holmes, M., Ettelaie, R. & Sarkar, A. 2022. Gastrointestinal fate and fatty acid release of pickering emulsions stabilized by mixtures of plant protein microgels + cellulose particles: an in vitro static digestion study. *Food Biophys.,* 18**,** 120-132.

Zhang, S., Murray, B. S., Suriyachay, N., Holmes, M., Ettelaie, R. & Sarkar, A. 2021b. Synergistic interactions of plant protein microgels and cellulose nanocrystals at the interface and their inhibition of the gastric digestion of pickering emulsions. *Langmuir,* 37**,** 827-840.

Zhang, Y., Wei, W., Lv, P., Wang, L. & Ma, G. 2011. Preparation and evaluation of alginate-chitosan microspheres for oral delivery of insulin. *Eur J Pharm Biopharm,* 77**,** 11-9.

Zhao, L., Skwarczynski, M. & Toth, I. 2019a. Polyelectrolyte-based platforms for the delivery of peptides and proteins. *ACS Biomater. Sci. Eng,* 5**,** 4937–4950.

CHAPTER 5
GENERAL DISCUSSION

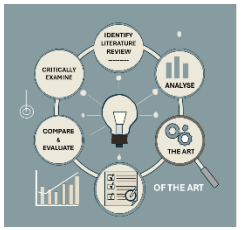
5.1 Introduction

This thesis provides fundamental aspects on the development of polysaccharide polyelectrolyte complexes (PECs) for gastrointestinal delivery of bioactive peptides (BAPs). The fundamental aspects start from selecting the polycationic and polyanionic wall materials and the BAPs for loading, then constructing the unloaded PECs, and finally encapsulating the BAPs into the PECs. This followed by a thorough characterisation of the constituent polyelectrolytes, BAPs and the PECs using a panel of biophysical techniques. **Chapter 2 has** discussed the criteria for selection of representative BAPs, which are food origin with high bioactivity assessed as a low half-maximum inhibitory concentration (IC_{50}). Besides that, the preparation and isolation of BAP should not be time-consuming. The fish BAPs from Bonito fish were selected based on those criteria. This chapter reviews the current research trends on the encapsulation of short-chain BAPs. Thus, it was found that encapsulation of BAPs with the oppositely charged polysaccharides chitosan (CS) and alginate (ALG) micro/nanoparticles should prevent the burst release of BAPs in intestinal condition. The release under gastric conditions should be minimal. In addition, CS and ALG are two natural polymers with supportive physicochemical and functional properties as delivery vehicles for foods, nutraceuticals, supplements, and biomedicinal applications.

In **Chapter 3**, PECs were crafted by electrostatic self-assembly via setting n^-/n^+ (molar charge ratio) of ALG to CS. The n^-/n^+ is an essential variable that determines PEC formation and stability. However, prior to this, two ALG with low M_w were selected. The ALG M_w 8 and 21 kDa were selected as counter ion of CS because low M_w ALG generates smaller PECs, confirmed with preliminary data (data not shown). The size of the resulting PEC is important to consider because fish BAPs have $M_w < 3$ kDa. To remove all potential aggregates of dissolved CS and ALG, they were filtered, and subsequently, their densities were measured and plotted as a function of concentration. Then, n^-/n^+ was varied from 0.1 to 10, and the calculation of n^-/n^+ was explained in detail in **Chapter 3**. PEC formation was conducted at a low salt (NaCl) concentration of 85 mM (Goycoolea et al., 2009) at pH 5.5, where CS has a positive charge and ALG has a negative one. According to the value of n^-/n^+, a wide range of PECs in terms of size (hydrodynamic radius/R_h) and stability (ζ-potential) were obtained. After this initial

screening n^-/n^+ conditions of excess CS and excess ALG for both ALG M_w (8 and 21 kDa) were chosen, and again, the size and stability of PECs were mainly considered. Later, the two formulations (excess CS and excess ALG) from CS + ALG 21 kDa were loaded with fish BAPs followed by measurements of PEC size, stability, and polydispersity via dynamic light scattering and encapsulation efficiency with liquid chromatography (HPLC) - UV detection. At the same time, the viscosities of the remaining (uncomplexed) non-PEC biopolymers in solution were also measured as an indirect way of confirming the degree of PEC formation. Subsequently, the CS + ALG21 kDa PECs was pursued for further investigation of BAP release under gastrointestinal conditions. The last part of **Chapter 3** addressed fish BAPs release from PECs during incubation at gastric and intestinal pH.

Chapter 4 mainly examines the behaviour of loaded PECs, and the BAPs released during *in vitro* gastric and intestinal fluid simulated conditions. The *in vitro* digestion set closely resembles the human gastric and intestinal composition following the standardised INFOGEST protocol (Brodkorb et al., 2019, Egger et al., 2016, Minekus et al., 2014). However, two states were studied: without enzymes (only salt and pH adjustment) and with enzymes (+ salts and pH adjustment). These two states were chosen to understand and compare the effect of salts with and without proteases in human gastric and intestinal systems to the PECs as a delivery platform for BAPs. The ionic strength of the solution determines the PEC stability (Delair, 2011, Berger et al., 2004). Over the 2-3 h incubation, the trends of hydrodynamic radius/R_h, ζ-potential, polydispersity, and size distribution were measured. At the same time, the released of BAPs were also identified. Identification of release BAPs is based on the amount (as analysed with HPLC-UV), and bioactivity (ACE inhibitory activity) of BAPs that escape the PEC throughout incubation. Several analyses have been performed to assess the result of the release trend from HPLC data. In addition, the stability of PECs, both loaded and unloaded PECs with fish BAPs, was also investigated during storage at different pH and room temperatures for 28 days. The latter is to predict and estimate the self-life of PECs in a solution before proceeding further to the next phase of research development. The overall structure of the thesis is illustrated in **Figure 5.1.**

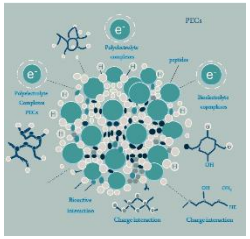


Chapter 2

State of the art current research encapsulation BAPs

Keywords:
short-chain BAPs, encapsulation, gastrointestinal delivery

Results:
- Diverse vehicle size, mostly in submicron
- CS+ALG showed lower release in gastric & slower release in intestinal

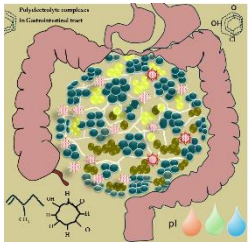


Chapter 3

PECs formation & encapsulation BAPs into PECs

Variables:
M_w ALG, n^-/n^+ (charge ratio), pH, BAPs loading

Results:
- Higher M_w ALG provide smaller and compact PECs than lower M_w ALG
- $n^-/n^+ < 1$ or > 1, better stability
- After loading with BAP, PECs become smaller
- pH intestinal, BAPs release more



Chapter 4

In vitro digestion: PECs-loaded BAPs

Variables:
Salts, enzymes (proteases), bioactivity measurement

Results:
- Intestinal salt composition gives maximum release
- Proteases induce faster release than without enzymes
- The BAPs remain active after release

Figure 5.1 Schematic framework of this thesis

According to high-performance liquid chromatography (HPLC-UV) analysis, the ultrafiltration fraction (UF) (UF membrane = <3 kDa) of fish BAPs contains two dominant peptide sequences, namely LKPNM and LKP. These BAPs have M_w 0.6 kDa (601.76 g/mol) and 0.35 kDa (356.46 g/mol), respectively. Both BAPs have angiotensin-converting enzyme (ACE) inhibitory activity, and they have a similar net charge at different pH and the same isoelectric point (pI). The charge similarity significantly controls pH for their encapsulation via polyelectrolyte complexes (PECs). The details of the chromatogram of UF of fish BAPs are shown in **Chapter 3**. *In silico* analysis predicts that these BAPs are resistant to gastric pepsin but hydrolysed by trypsin and chymotrypsin in the intestine. This hydrolysis is confirmed by the *in vitro* experiment, indicating the absence of peaks at their retention time. **Chapter 4** shows the *in vitro* studies of fish BAPs: LKPNM and LKP.

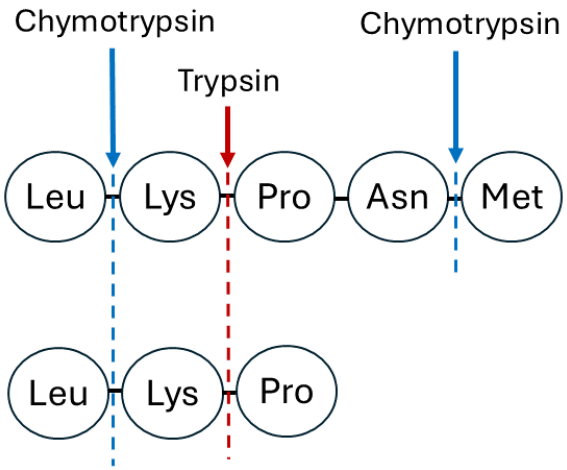


Figure 5.2 schematic hydrolysis of LKPNM and LKP by trypsin and chymotrypsin via in silico analysis

The cleaving sites of fractionated fish BAPs by key proteases in the human digestion system targets three peptide bonds for LKPNM and two sites for LKP (**Figure 5.2**). This hydrolysis produces amino acids and some shorter peptides. However, the products do not indicate any bioactivities, especially as ACE inhibitors after hydrolysis, whether by amino acids or peptides, based on BAP bioactivity databases (Minkiewicz et al., 2019). Importantly, **Chapter 4** have been showed that the bioactivity of BAPs released from PECs during digestion is not compromised by the residual PEC (CS and ALG) material in the mixture.

5.2 Comparison of Encapsulation Efficiency (EE) with Similar Studies

Table 5.1 EE of BAPs and other bio-active payloads with CS+ALG PEC compared with other studies

Delivery Vehicles	Bio-actives load	Loading Concentration (mg mL^{-1})	Encapsulation Efficiency (EE) (%)	References
PEC CS + ALG	< 3 kDa fish BAPs (LKPNM, LKP)	1.0	80.6 – 85	This thesis
CS/Cyclodextrin (CD) NPs	ECG	0.38	7.1 – 25.1	Trapani et al. (2010)
Carboxymethyl CS/Na-ALG microspheres	VLPVP	1.25 – 3.75	64.6 – 87.8	Huang et al. (2017)
Guar gum film-coated CS MPs	YLGYLEQLLR	0.125	86	Batista et al. (2021)
Eudragit (ES)-coated CS NPs	GRKKRRQRRRP	0.4	50	Chen et al. (2017)
CS + ALG PEC	Ovalbumin	0.5	80.2	Cegnar et al. (2011)
CS + ALG PEC	Doxorubicin (DOX)	0.2	65.7	Park et al. (2019)
	Rhodamine 6G (R6G)	0.006	50.6	
CS + ALG PEC	Sodium diclofenac	1.0	29 – 89	Nikolova et al. (2021)
CS + ALG Hydrogels	Rice bran BAPs: KHNRGDEF	NR	68.9	Liu et al. (2025)
CS + ALG NPs	Stone fish BAPs: ALGPQFY	NR	74.5	Auwal et al. (2024)
CS + ALG NPs	Rapeseed-derived peptides (RPPs)	1.0	90.7 – 91.4	Wang et al. (2024)

NR=not reported details

Table 5.1 compares the EE values obtained from this study with other published studies that use CS + ALG or CS + other polymers to encapsulate BAPs or low M_w bio-actives. Based on this comparison, it can be noticed that the EE of fish BAPs using PECs seems promising because it seems to provide one of the highest EE. The method of encapsulating fish BAPs into CS + ALG was via mixing at room temperature 1 mg mL^{-1} (final concentration) of fish BAPs into CS solution, then adding with ALG (volumes of mixing were based on n^-/n^+ calculation). This concentration of BAPs addition (at the initial encapsulation process) is similar to studies conducted by Wang et al. (2024) on the encapsulation of rapeseed-derived peptides (RPPs) into CS + ALG NPs, and sodium diclofenac, M_w 318 g/mol, into CS + ALG PEC (Nikolova

et al., 2021). Furthermore, the concentration of fish-coated BAPs is within the range of encapsulation BAPs or bio-active molecules from previously published work. The protocol to obtain the PECs is simple, reproducible, and scalable, as it does not require equipment of any sophistication, high shearing, nor the use of solvents or corrosive chemicals. Also, the protocol is amenable for downscaling to technologies such as microfluidics that enable to work with very small volumes (*i.e.*, with very expensive biologics such as therapeutic genes, hormones, growth factors), as shown in recent studies to obtain monodispersed emulsions or lipid nanoparticles (Roces et al., 2020, Chu et al., 2007).

5.3 Cumulative Release BAPs from PECs

Cumulative release of BAPs refers to the incremental fraction released of the total loaded peptide from PEC as a function of time. This parameter has been the focus of studies concerning the delivery system or vehicle of bioactive compounds such as BAPs. Some studies have investigated the cumulative release of BAPs from their delivery vehicles. However, the incubation conditions were mainly caused by setting the pH, representing the gastric and intestinal fluids (Liu et al., 2025), and mostly ignored the composition of salts (Wang et al., 2024), and proteases (Batista et al., 2021, Chen et al., 2017, Trapani et al., 2010) for simulated human digestion conditions. This thesis examined the release of BAPs at gastric and intestinal pH conditions, as shown in **Chapter 3**, indicating minimal release (<∼20% after 2 h incubation). Then, in **Chapter 4**, the conditions were set closely to represent gastric and intestinal fluids by adding salts, proteases, and pH settings. These conditions provide different results from the situation of just by setting the pH. Therefore, it is concluded that both salts and proteases influence triggering the BAPs release from PECs. **Figure 5.3** depicts the **total** (cumulative) BAPs released from PECs during incubation on gastric and intestinal fluids, in which the fluid compositions follow the INFOGEST protocol.

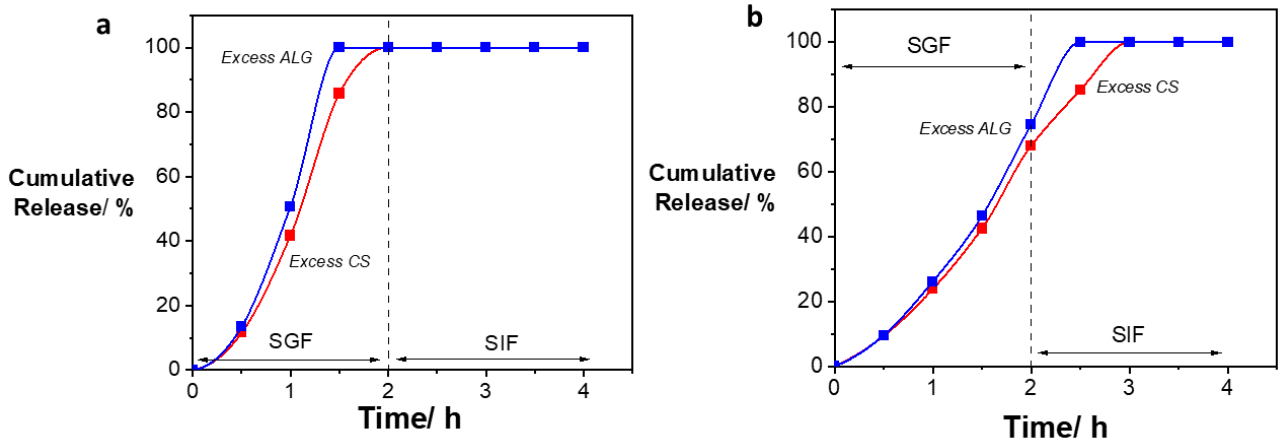


Figure 5.3 Cumulative release (%) of fish BAPs from CS+ALG PECs at gastrointestinal fluids with enzymes (a) and without enzymes (b)

These results give insight into the fact that PECs with excess CS do not have such a large disparity with those of excess ALG in terms of cumulative release of BAPs. For example, in SGF with enzymes, the trends describe an exponential increase for both systems, reaching >∼85% (excess CS) and ∼100% (excess ALG) after 1.5 h. The corresponding release profile of BAPs in conditions without enzymes is linear at the beginning of SGF (0 – 1.5 h) for both systems. Then for PECs of excess ALG at 2.5 h and excess CS at 3 h in SIF are released entirely. Generally, the BAPs are retained by the PECs in SGF and then fully released in SIF. Enzymes (proteases) stimulate the BAP's release a little faster, whereas SGF without enzymes gives ≈70% release after 2 h, while with enzymes, it reveals complete release.

5.4 Size and Stability PECs During Digestion

The size (R_h) and stability of CS+ALG PECs during digestion were investigated by DLS during conditions without enzymes, as discussed in **Chapter 4**. These parameters are critical to examine the characteristics of the carrier agent in the process of digestion. In gastric conditions, the PEC's hydrodynamic radius (R_h) seems constant after 2 h incubation for the system with excess CS (n^-/n^+ 0.5) but slightly increased for the PEC with excess ALG (n^-/n^+ 10). On the contrary, the R_h of PECs during intestinal simulation digestion became larger at the initial time incubations for both PECs:excess CS (getting maximum after 30 min incubation) and excess ALG (reaching maximum after 60 min), afterwards, the R_h values decreased again. According to all these facts, PECs appear to maintain their sizes and overall structural integrity

during gastric digestion, but not during intestinal digestion. The apparent instability of PECs in intestinal digestion conditions was also confirmed by the dramatic change in the ζ-potential. While, for PECs in gastric conditions, especially with excess CS, the ζ-potential value after 2 h incubation was still categorized as stable (≈ +20 mV).

A study by Nikolova et al. (2021) found that the PECs based on CS + ALG become larger, and the degree of swelling increases, during incubation at pH 7.4 due to deprotonation of CS´s amino groups. As a result, the electrostatic interaction between polycationic CS and polyanionic ALG is weakened, causing complex dissociation. Hence, it makes sense that the release of bioactive peptides (BAPs) is vastly higher in the intestinal than in the gastric conditions, as discussed above and in **Chapter 4.** Altogether, these results, allow to anticipate that the gastrointestinal bioaccesibility of BAPs is enhanced by their encapsulation in CS+ALG PECs. The full potential of these formulations to also enhance the systemic absorption and hence, the bioavailability of the BAPs is yet to be investigated.

Some studies about CS+ALG PECs have been published; however, the focus was mostly on aspects of complex formation, bioactive encapsulation, and stability against different pH. There are only limited studies centred on the size and stability of CS+ALG PECs during gastric and intestinal digestion, which considered not only the effect of pH-swing, but also salt concentrations and compositions as well as enzyme existence.

5.5 References

Auwal, S. M., Ghanisma, S. B. M. & Saari, N. 2024. Improved systolic blood pressure (SBP)-lowering effect of stone fish-derived angiotensin-I converting enzyme (ACE)-inhibitory peptide entrapped in chitosan-coated alginate nanocomposites. *Food Bioscience,* 60**,** 104349.

Batista, P., Castro, P. M., Madureira, A. R., Sarmento, B. & Pintado, M. 2021. Preparation, characterization and evaluation of guar films impregnated with relaxing peptide loaded into chitosan microparticles. *Appl. Sci. (Switzerland),* 11**,** 1-13.

Berger, J., Reist, M., Mayer, J. M., Felt, O. & Gurny, R. 2004. Structure and interactions in chitosan hydrogels formed by complexation or aggregation for biomedical applications. *Eur J Pharm Biopharm,* 57**,** 35-52.

Brodkorb, A., Egger, L., Alminger, M., Alvito, P., Assuncao, R., Ballance, S., Bohn, T., Bourlieu-Lacanal, C., Boutrou, R., Carriere, F., Clemente, A., Corredig, M., Dupont, D., Dufour, C., Edwards, C., Golding, M., Karakaya, S., Kirkhus, B., Le Feunteun, S., Lesmes, U., Macierzanka, A., Mackie, A. R., Martins, C., Marze, S., Mcclements, D. J., Menard, O., Minekus, M., Portmann, R., Santos, C. N., Souchon, I., Singh, R. P., Vegarud, G. E., Wickham, M. S. J., Weitschies, W. & Recio, I. 2019. INFOGEST static in vitro simulation of gastrointestinal food digestion. *Nat Protoc,* 14**,** 991-1014.

Cegnar, M., Miklavzin, A. & Kerc, J. 2011. Freeze-Drying and Release Characteristics of Polyelectrolyte Nanocarriers for the Mucosal Delivery of Ovalbumin. *Acta Chim. Slov.,* 58**,** 241–250.

Chen, S. X., Guo, F., Deng, T. T., Zhu, S. Q., Liu, W. Y., Zhong, H. J., Yu, H., Luo, R. & Deng, Z. Y. 2017. Eudragit S100-coated chitosan nanoparticles co-loading Tat for enhanced oral colon absorption of insulin. *AAPS Pharmscitech.,* 18**,** 1277-1287.

Chu, L. Y., Utada, A. S., Shah, R. K., Kim, J. W. & Weitz, D. A. 2007. Controllable monodisperse multiple emulsions. *Angew Chem Int Ed Engl,* 46**,** 8970-4.

Delair, T. 2011. Colloidal polyelectrolyte complexes of chitosan and dextran sulfate towards versatile nanocarriers of bioactive molecules. *Eur J Pharm Biopharm,* 78**,** 10-8.

Egger, L., Ménard, O., Delgado-Andrade, C., Alvito, P., Assunção, R., Balance, S., Barberá, R., Brodkorb, A., Cattenoz, T., Clemente, A., Comi, I., Dupont, D., Garcia-Llatas, G., Lagarda, M. J., Le Feunteun, S., Janssenduijghuijsen, L., Karakaya, S., Lesmes, U., Mackie, A. R., Martins, C., Meynier, A., Miralles, B., Murray, B. S., Pihlanto, A., Picariello, G., Santos, C. N., Simsek, S., Recio, I., Rigby, N., Rioux, L.-E., Stoffers, H., Tavares, A., Tavares, L., Turgeon, S., Ulleberg, E. K., Vegarud, G. E., Vergères, G. & Portmann, R. 2016. The harmonized INFOGEST in vitro digestion method: From knowledge to action. *Food Res. Int.,* 88**,** 217-225.

Goycoolea, F. M., Lollo, G., Remunan-Lopez, C., Quaglia, F. & Alonso, M. J. 2009. Chitosan-alginate blended nanoparticles as carriers for the transmucosal delivery of macromolecules *Biomacromolecules,* 10**,** 1736–1743.

Huang, G.-Q., Xiao, J.-X., Hao, L.-Q. & Yang, J. 2017. Microencapsulation of an angiotensin I-converting enzyme inhibitory peptide VLPVP by membrane emulsification. *Food Bioprocess Tech.,* 10**,** 2005-2012.

Liu, X., Liu, L., Huang, F., Meng, Y., Chen, Y., Wang, J., Wang, S., Luo, Y., Li, J. & Liang, Y. 2025. pH-sensitive chitosan/sodium alginate/calcium chloride hydrogel beads for potential oral delivery of rice bran bioactive peptides. *Food Chem,* 470**,** 142618.

Minekus, M., Alminger, M., Alvito, P., Ballance, S., Bohn, T., Bourlieu, C., Carriere, F., Boutrou, R., Corredig, M., Dupont, D., Dufour, C., Egger, L., Golding, M., Karakaya, S., Kirkhus, B., Le Feunteun, S., Lesmes, U., Macierzanka, A., Mackie, A., Marze, S., Mcclements, D. J., Menard, O., Recio, I., Santos, C. N., Singh, R. P., Vegarud, G. E., Wickham, M. S., Weitschies, W. & Brodkorb, A. 2014. A standardised static in vitro digestion method suitable for food - an international consensus. *Food Funct.,* 5**,** 1113-24.

Minkiewicz, P., Iwaniak, A. & Darewicz, M. 2019. BIOPEP-UWM Database of Bioactive Peptides: Current Opportunities. *Int J Mol Sci,* 20**,** 5978.

Nikolova, D., Simeonov, M., Tzachev, C., Apostolov, A., Christov, L. & Vassileva, E. 2021. Polyelectrolyte complexes of chitosan and sodium alginate as a drug delivery system for diclofenac sodium. *Polymer International,* 71**,** 668-678.

Park, J. W., Park, K. H. & Seo, S. 2019. Natural polyelectrolyte complex-based pH-dependent delivery carriers using alginate and chitosan. *Journal of Applied Polymer Science,* 136**,** 48143.

Roces, C. B., Lou, G., Jain, N., Abraham, S., Thomas, A., Halbert, G. W. & Perrie, Y. 2020. Manufacturing Considerations for the Development of Lipid Nanoparticles Using Microfluidics. *Pharmaceutics,* 12.

Trapani, A., Lopedota, A., Franco, M., Cioffi, N., Ieva, E., Garcia-Fuentes, M. & Alonso, M. J. 2010. A comparative study of chitosan and chitosan/cyclodextrin nanoparticles as potential carriers for the oral delivery of small peptides. *Eur. J. Pharm. Biopharm.,* 75**,** 26-32.

Wang, Q., Dong, X., Castaneda-Reyes, E. D., Wu, Y., Zhang, S., Wu, Z., Wang, Z., Dai, L., Xu, B. & Xu, F. 2024. Chitosan and sodium alginate nanocarrier system: Controlling the release of rapeseed-derived peptides and improving their therapeutic efficiency of anti-diabetes. *Int J Biol Macromol,* 265**,** 130713.

CHAPTER 6
CONCLUSIONS AND POTENTIAL FUTURE WORK

6.1 Conclusions

1. Delivery vehicles made from two undigestible polysaccharide, chitosan (CS) and alginate (ALG), showed slow release of BAPs compared to other systems. (**Chapter 2**).
2. One-step polyelectrolyte complexes (PECs) formation can be tailored using CS and ALG by setting their charge n^-/n^+ and determining the obtained size and stability. Higher M_w ALG (21 kDa) gave a smaller and more compact structure than lower M_w ALG (8 kDa). Introducing BAPs during complexation resulted in smaller PECs than unloaded ones, and the BAPs were not as quickly released at gastric and intestinal pH after 2 h incubation (**Chapter 3**).
3. PECs from excess CS are more stable during resuspension (**Chapter 3**) and during storage at pH 4 – 6 than excess ALG (comparison was carried out with ALG M_w 21 kDa) (**Chapter 4**). When the PECs are introduced into the simulation digestion fluids (salts + enzymes), the release patterns are different compared to only controlling pH. The BAPs release faster when PECs are immersed in a solution containing salts and enzymes (proteases). The presence of proteases induces a slightly higher release than only salts + pH. In addition, the PECs can hold some short BAPs in gastric fluids but not in the intestine (**Chapter 4**).
4. There is no correlation between the release of BAPs from PECs during in vitro gastrointestinal digestion and their hydrodynamic radius (R_h) (**Chapter 5**)

6.2 Potential Future Work

1. To create PECs with no BAP release in SGF (salts + enzymes) since the cumulative release at SGF during 2 h incubation is high.
2. To control PEC formation and minimise the aggregation since the polydispersity index of the obtained PECs is high, as confirmed by transmission electron microscopy (TEM) observation.
3. To examine the mucoadhesive or mucodiffusive behaviour of the CS+ALG PECs, which currently cannot be addressed using in vitro digestion approaches. The previous works

on transmucosal delivery of biologics (e.g., insulin) using CS+ALG+TPP nanoparticles (Goycoolea et al. 2009), allow to anticipate that the developed CS+ALG PECs will also be effective for the gastrointestinal delivery of BAPs to enhance their bioavailability.

APPENDICES

Chitosan M_w distribution analysis

An AF2000 Multiflow system from Postnova Analytics (Postnova Analytics GmbH, Landsberg, Germany) in SEC mode was used to analyse the M_w distribution of CS by following a protocol from Gonzalez-Espinosa et al. (2019). Three TSK gel columns (G6000PW, G5000PW, and G2500PW) and a guard column at 30 °C were used to analyse. The preparation of CS solution (1 mg mL^{-1}) was carried out by dissolving (overnight) in a 0.3 M acetic acid/0.2 M sodium acetate solvent at pH 4.5. Subsequently, the solution was filtered via a 22 µm regenerated cellulose syringe filter (Millex®, Millipore, Ireland). A similar solvent was filtered using a 0.1 µm mixed cellulose esters membrane and used as the mobile phase. A crossflow rate of 3 mL min^{-1} was set as flow conditions, and for optimal sample characterisation, a programmed time delay exponential decay was applied. The refractive index increment (dn/dc) for CS was set at 0.19 mL g^{-1} with a refractive index (RI) of 1.3. A Nova SEC software was used for data processing (Sajid et al., 2023).

References:

González-Espinosa Y., Sabagh B., Moldenhauer E., Clarke P., Goycoolea F.M. (2019). Characterisation of chitosan molecular weight distribution by multi-detection asymmetric flow-field flow fractionation (AF4) and SEC. *Int. J. Biol. Macromol.*136,911–919. https://doi.org/10.1016j.ijbiomac.2019.06.122

Sajid A., Castronovo M., Goycoolea FM. (2023) On the Fractionation and Physicochemical Characterisation of Self-Assembled Chitosan–DNA Polyelectrolyte Complexes. *Polymers*. 2023; 15(9):2115. https://doi.org/10.3390/polym15092115.

Table A1. Measured values of the viscosities (η) of supernatants of PEC preparations, used for calculation (via eq. (3.6) in the text) of the hydrodynamic radii (R_h) of the PECs from the diffusion coefficients (*D*) of the PECs measured via DLS. Values are shown for the two different combinations of CS + ALG8 and CS + ALG21 at the different molar charge ratios n^-/n^+.

	CS + ALG8			**CS + ALG21**		
n^-/n^+	η/ mPa s	D x 10^{25} / m^2 s^{-1}	R_h/ nm	η / mPa s	D x 10^{25} / m^2 s^{-1}	R_h/ nm
0.1	1.7	3.63	364	1.6	2.87	463
0.2	1.6	4.61	305	1.4	3.41	452
0.3	1.5	4.81	297	1.3	4.44	371
0.5	1.3	7.84	213	1.2	8.11	225
0.7	1.3	9.68	179	0.9	11.75	197
0.8	1.2	10.08	184	0.9	11.23	215
1.0	1.2	9.25	196	0.8	11.76	219
1.3	1.1	11.78	176	1.0	0.58	3632
1.7	1.0	0.55	3855	1.0	0.24	9033
2.5	1.0	0.13	16650	1.1	0.30	6950
5.0	1.0	0.25	8250	1.1	1.31	1582
10.0	1.0	0.46	4860	1.1	2.33	842

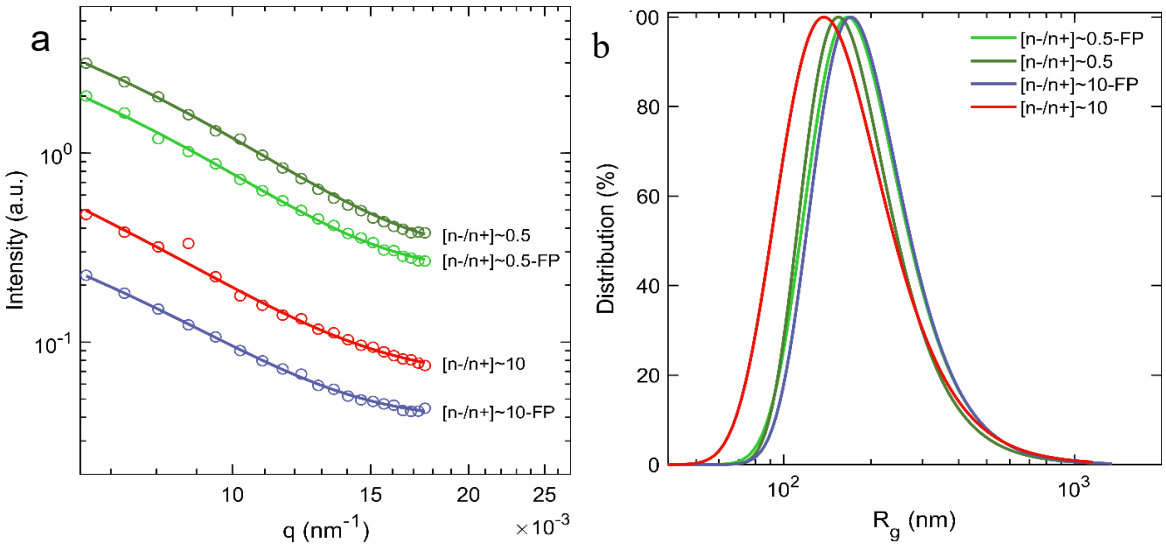


Fig. A1. a) The experimental (circles) and fitted (lines) static light scattering of PECs for CS + ALG21 with and without fish peptide (FP) at different charge ratios. b) The distribution of radius of gyration of PEC obtained from the fitting of experimental data using the spherical particles model.

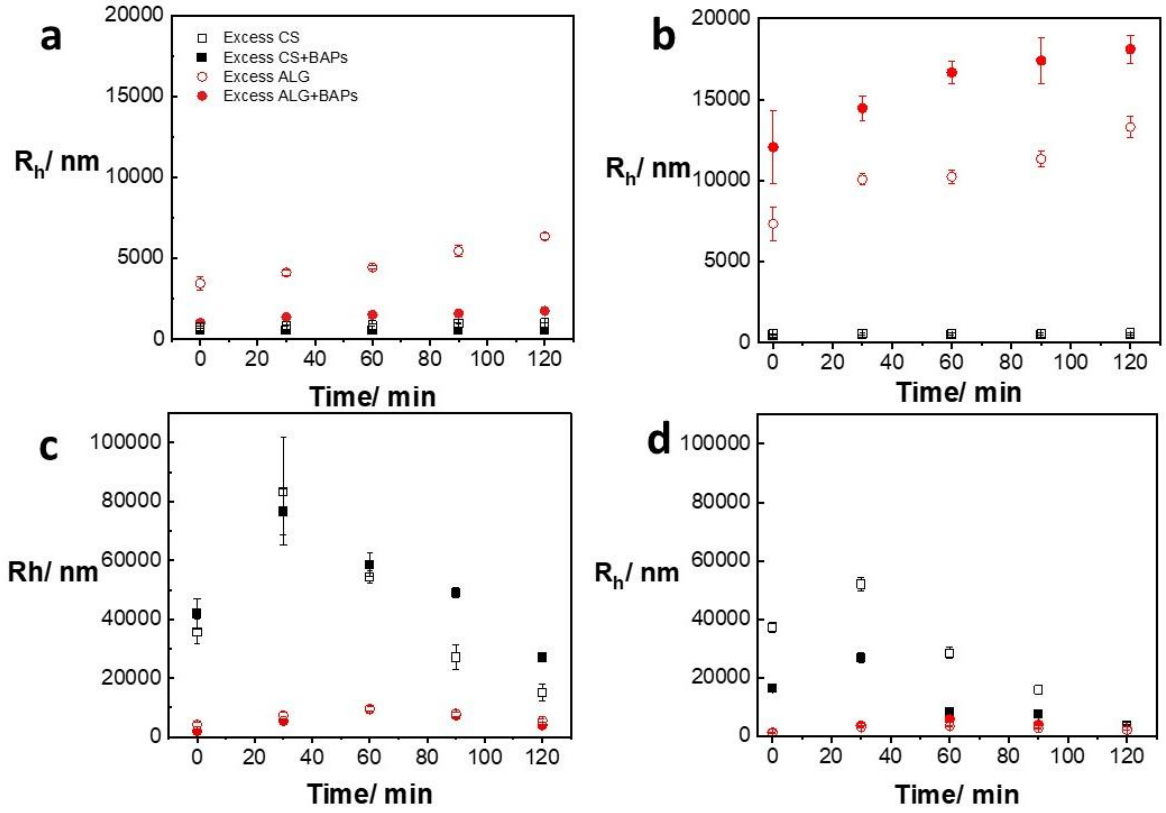


Fig A2. Hydrodynamic radius (R_h) of ALG+CS, loaded (filled symbols) and unloaded (open symbols) with excess CS (n^-/n^+ 0.5) (black) and excess ALG (n^-/n^+ 10) (red), measured during gastric fluid (top) and during intestinal fluid (bottom) with enzymes (left) and without enzymes (right).

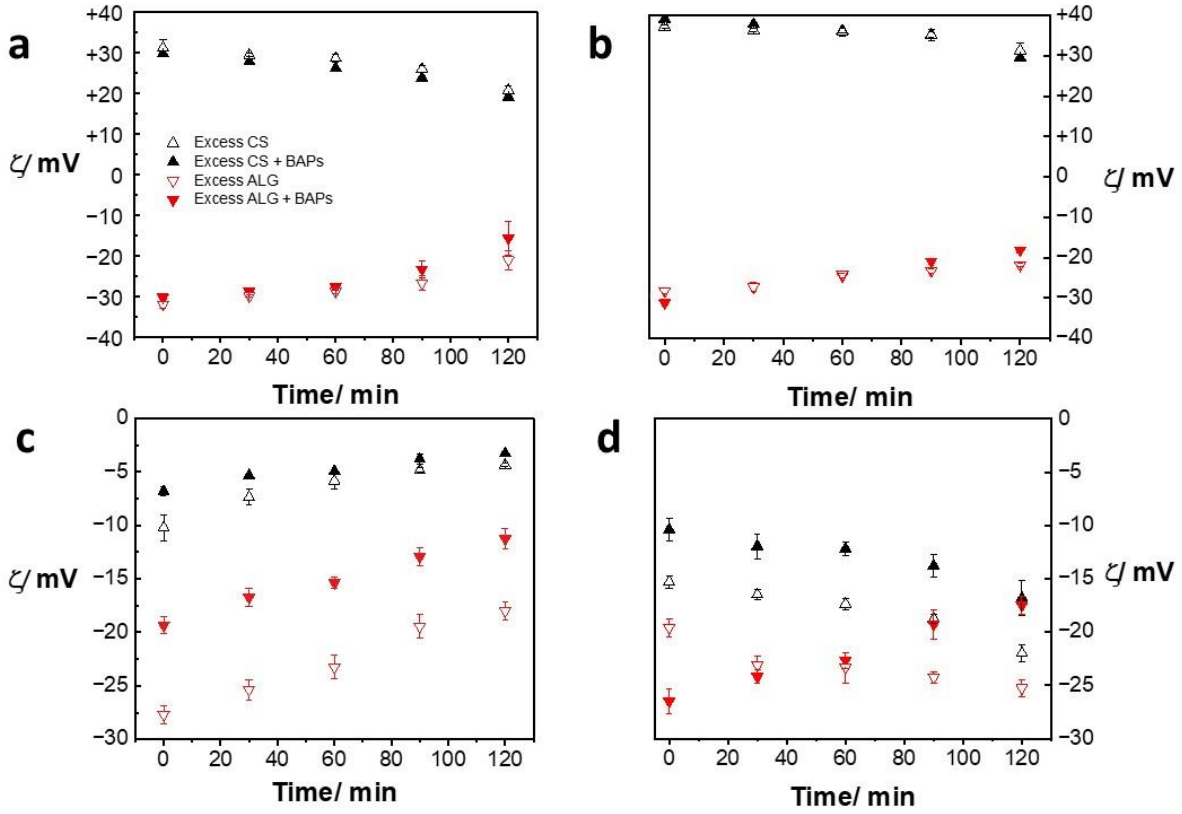


Fig. A3. ζ-potential of ALG+CS, loaded (filled symbols) and unloaded (open symbols) with excess CS (n^-/n^+ 0.5) (black) and excess ALG (n^-/n^+ 10) (red), measured during gastric fluid (top) and during intestinal fluid (bottom) with enzymes (left) and without enzymes (right).

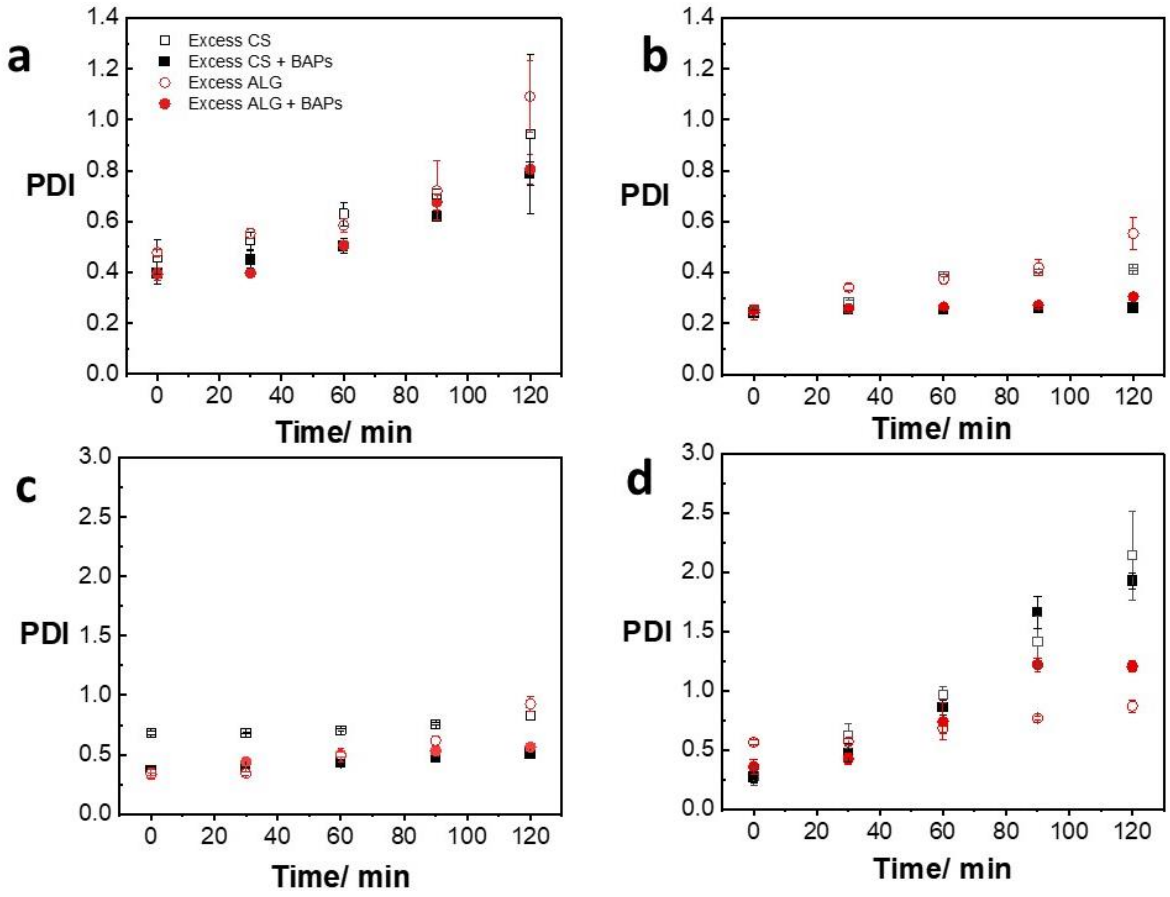


Fig. A4. Polydispersity indexes (PDI) of PECs ALG+CS, loaded (filled symbols) and unloaded (open symbols) with excess CS (n^-/n^+ 0.5) (black) and excess ALG (n^-/n^+ 10) (/(red), measured during gastric fluid (top) and during intestinal fluid (bottom) with enzymes (left) and without enzymes (right).

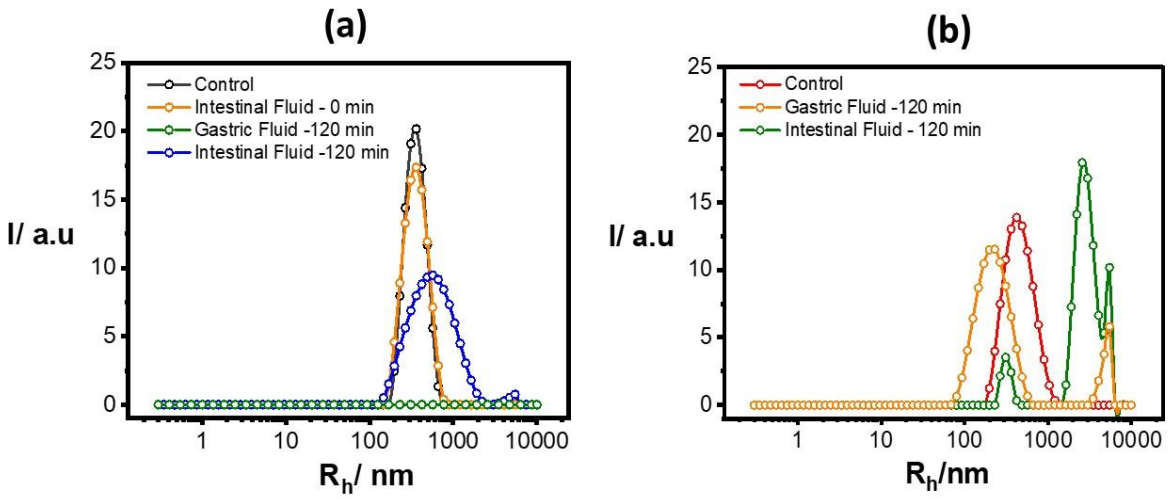


Fig. A5. Size distribution after gastric and intestinal simulation digestion (without enzymes) of loaded polyelectrolyte complexes (PECs) ($n^-/n^+ \approx 0.5$ excess CS (a) and $n^-/n^+ \approx 10$ excess ALG (b).

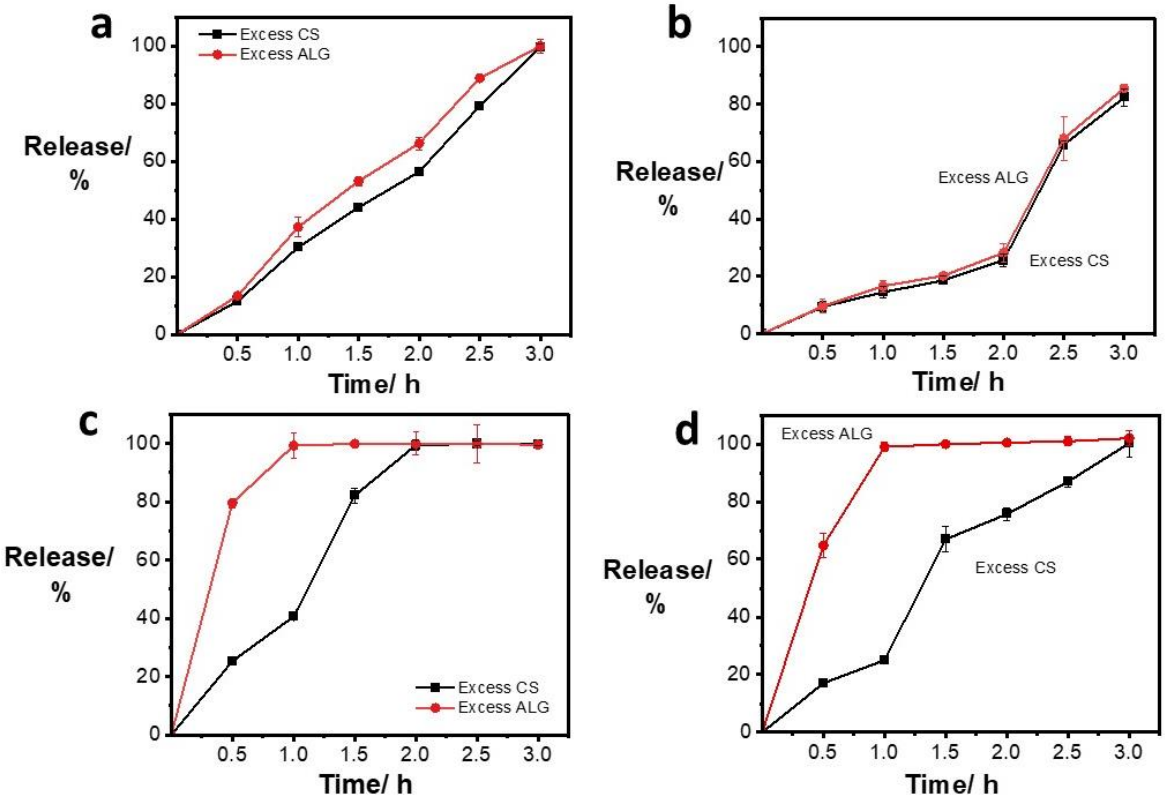


Fig. A6. Percentage of fish BAPs release from PECs during gastric (top) and intestinal (bottom) static digestion with enzyme (left) and without enzymes (right).

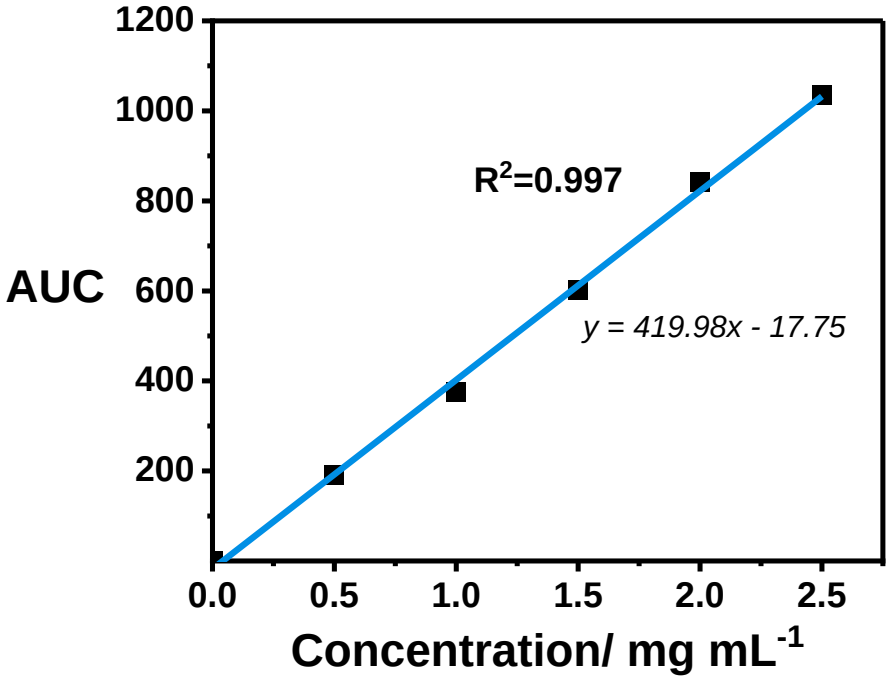


Fig. A7. Standard curve generated from chromatographic analysis of fish-derived BAPs, plotting concentration against area under the curve (AUC)